TECHNICAL REPORT
NATICK/TR-02/019

AD_____

# PICO WIRELESS INTEGRATED NETWORK SENSORS (PicoWINS):
# INVESTIGATING THE FEASIBILITY OF WIRELESS TACTICAL TAGS

by
W. M. Merrill
K. Sohrabi
G. J. Pottie
W. Kaiser
H. L. N. Liu
and
J. Leong

Sensoria Corporation
Culver City, CA 90230

July 2002

Final Report
June 1999 - October 2001

Prepared for
**U.S. Army Soldier and Biological Chemical Command
Soldier Systems Center
Natick, Massachusetts 01760-5020**

# REPORT DOCUMENTATION PAGE

| 1. REPORT DATE (DD-MM-YYYY) 10-07-2002 | 2. REPORT TYPE Final Report | 3. DATES COVERED (From - To) June 1999 - October 2001 |
|---|---|---|

**4. TITLE AND SUBTITLE**
PICO WIRELESS INTEGRATED NETWORK SENSORS (PicoWINS): INVESTIGATING THE FEASIBILITY OF WIRELESS TACTICAL TAGS

**5a. CONTRACT NUMBER**
C-DAAD16-99-C-1024

**5b. GRANT NUMBER**

**5c. PROGRAM ELEMENT NUMBER**

**6. AUTHOR(S)**
W. M. Merrill, K. Sohrabi, G. J. Pottie, W. Kaiser, H. L. N. Liu and J. Leong

**5d. PROJECT NUMBER**

**5e. TASK NUMBER**

**5f. WORK UNIT NUMBER**

**7. PERFORMING ORGANIZATION NAME(S) AND ADDRESS(ES)**
Sensoria Corporation
200 Corporate Pointe Suite 100
Culver City, CA 90230

**8. PERFORMING ORGANIZATION REPORT NUMBER**

**9. SPONSORING/MONITORING AGENCY NAME(S) AND ADDRESS(ES)**
Sponsor: Defense Advanced Research Projects Agency (DARPA)
Advanced Technology Office (Thomas Altshuler)
3701 North Fairfax Drive
Arlington, VA 22203-1714

**10. SPONSOR/MONITOR'S ACRONYM(S)**

**11. SPONSOR/MONITOR'S REPORT NUMBER(S)**
NATICK/TR-02/019

**12. DISTRIBUTION/AVAILABILITY STATEMENT**
Approved for public release; distribution is unlimited.

**13. SUPPLEMENTARY NOTES**
Monitor: US Army Soldier and Biological Chemical Command, Soldier Systems Center,
ATTN: AMSSB-RSS-A(N) (T. Gilroy), Natick, MA 01760-5020

**14. ABSTRACT**
This report documents the results of the PicoWINS investigation of the feasibility of tactical tags as a landmine replacement system. Specifically it provides a description of a tag prototype system, and of the design issues required to create a viable low power, autonomous wireless sensor system. Focus within this analysis was given to the radio frequency propagation limits for tag operation, including tag-to-tag links, tag-to-gateway links, and tag-to-munition links for homing ammunition. Within this context, a full propagation study as a function of height, range, and frequency was conducted in nineteen outdoor environments. Also explored were algorithms for locating the tags, and for optimizing the individual tags communication range. Each of the system components needed to create a tactical tag system are explored in detail, with focus given to the electromagnetic limitations imposed by the propagation environment, tag size, and tag power.

**15. SUBJECT TERMS**
COMMUNICATION LINKS     PROTOTYPE     LANDMINE ALTERNATIVES
POSITION TRACKING     SENSORS     FEASIBILITY STUDIES
RF(RADIO FREQUENCY)     RF TAGS     LOCATION AID DEVICES
WIRELESS SENSORS     LOW POWER     WINS(WIRELESS INTEGRATED NETWORK SENSORS)

| 16. SECURITY CLASSIFICATION OF: | | | 17. LIMITATION OF ABSTRACT | 18. NUMBER OF PAGES | 19a. NAME OF RESPONSIBLE PERSON Thomas Gilroy |
|---|---|---|---|---|---|
| a. REPORT UNCLASSIFIED | b. ABSTRACT UNCLASSIFIED | c. THIS PAGE UNCLASSIFIED | SAR | 188 | 19b. TELEPHONE NUMBER (Include area code) 508-233-5855 |

**TABLE OF CONTENTS**

# LIST OF FIGURES

vii

# LIST OF TABLES

# PREFACE

This report provides the details of the PicoWINS tactical tag land mine replacement feasibility investigation and the Propagation Study to Quantify Short-Range Surface-to-Surface Communication Links conducted at Sensoria Corporation as an addendum to the PicoWINS contract. The tactical tag concept is to use low volume wireless battery operated sensors to seed a field. These sensors then affix to a target passing through the field, notify wirelessly through a Multihop network their location and state (speed, etc..) a remote controller, and potentially act as a homing beacon for incoming artillery. Sensoria Corporation's effort within the PicoWINS (Pico Wireless Integrated Network Sensors) has been to assess the feasibility of constructing and operating these tags. Within that analysis substantial effort has been focused on assessing propagation within tag specific scenarios, as detailed in this report.

The study described herein includes an assessment of the viability of compact wireless tags which affix to targets, and the technology limits of such a technology. A short description of a prototype tag is provided followed by discussion of a tag location scenario, a complete analytic and empirical propagation study, and discussion of a prototype tag antenna concept. Particular focus is given to short range wireless propagation near the ground, particularly in three Industrial, Scientific, and Medical (ISM) bands, focusing on the frequencies: 902-928MHz, 2400-2426MHz, and 5725-5751MHz. Experimental propagation loss is presented for nineteen environments falling into six classifications, at varying heights, distances, and polarizations. These frequencies and short ranges are relevant to a large number of ad-hoc communication applications currently under development in the academic, commercial, and defense communities. Comparison with a two-ray propagation model is shown as well as a detailed justification for the applicability of this model, with the two ray prediction in general providing a lower bound on the data recorded at antenna heights of 5cm. Additionally limited numerical modeling of the impact of surface roughness is provided.

The PicoWINS program demonstrated the feasibility of the tactical tags concept, and provides as detailed in this report a description of how these tags may be implemented and the central concerns involved in creating this technology.

# PICO WIRELESS INTEGRATED NETWORK SENSORS (PicoWINS): INVESTIGATING THE FEASIBILITY OF WIRELESS TACTICAL TAGS

## SUMMARY

New battlefield surveillance capabilities are required for security and the protection of distributed assets. These new surveillance capabilities must detect the opponent, identify the opponent, and provide a severe hindrance to the opponent's operations. A new approach is based on the deployment of compact, low power, devices that sense presence and motion. In addition, these devices will locate and track the opponent. Most importantly, unlike conventional distributed sensors, these compact devices will be scattered in large quantity and will adhere to personnel and vehicles. A new wireless integrated network sensor (WINS) technology, PicoWINS, will be developed that employs flexible, thin film substrate packages, new communication and networking strategies, new sensing methods. PicoWINS are conformal and may be embedded in many packages. PicoWINS may be launched by artillery in canisters and scattered widely.

PicoWINS nodes are a marked departure from previous technologies. PicoWINS will attach to boots, vehicle tires and treads, and detect proximity, touch, sound, and light. PicoWINS will incorporate new microelectronics for low power. These devices will exploit new methods, developed for PicoWINS, that will provide cooperative sensing and communication in a power constrained and low cost system. Communication physical layers will include both RF and acoustic methods. Also, PicoWINS will carry processing systems adapted to security. Finally, PicoWINS will be interoperable with large scale WINS networks and will link via redundant Gateways to standard network services.

A frontier in global network extension is the connectivity of the Internet to deeply distributed, processors, sensors, and controls. Revolutionary opportunities are ahead for low cost devices that are deeply and widely distributed in environments and integrated into equipment to provide continuous, global, sensing and monitoring of the battlefield, area and facility security, environmental status, and globally distributed assets. Due to the restrictions and cost of conventional wireline networking, low power wireless networking between nodes is essential for achieving the deep and dense deployment required for these applications.

WINS technology has been developed for local area applications and recently for globally distributed, satellite network linked GlobalWINS. This report describes the work within the PicoWINS program, to explore the fundamental limits on the most ubiquitous tier of the WINS hierarchy, PicoWINS devices that are thin, conformal, micropower, autonomous devices. Within this program prototype wireless networked

sensors were built, algorithms were designed for locating each of these nodes, and a complete description of the electromagnetic propagation and antenna requirements for a PicoWINS scenario was provided. This report details the possibilities of tag manufacture, identifies a tag location solution, and provides an in depth look at the propagation environment these tags must operate in, and means to optimize the PicoWINS tags within that environment.

# DEVELOPMENT OF PICOWINS TAGS: SYSTEM INTEGRATION AND ASSEMBLY OF PICOWINS TAGS FOR MULTIHOP NETWORKS.

Within this program a new PicoWINS Tag was designed to enable implementation of combined sensing, communication, and networking. The PicoWINS tactical Tag must provide:

1) Wireless networking to enable verification of Tag operation and notification of Tag attachment

2) Wireless geolocation capability

3) Sensing to enable detection of attachment

4) Compact packaging and electromagnetics

5) Micropower intelligent systems

This device will support wireless multihop Tag-to-Tag communication, thereby increasing the level of network robustness. Multihop communication provides redundant communication pathways and drastically reduces required communication power, by reducing the required communication range.

The new PicoWINS Node prototype package is shown in Figure 1. This device has been fabricated with conventional printed circuit board systems, rather than the PicoWINS flexible package, for this early prototype verification.

The PicoWINS prototype contains:

1) Bidirectional communication

2) A MEMS microaccelerometer for attachment detection

3) A micropower control system

4) The PicoWINS prototype is programmable to allow for development of operational algorithms for verification of Tag attachment.

Design of sensors and semiconductor systems is constrained to permit this device to be implemented with an integrated solution in the next phase of development. This new node permits the development and testing of complex tactical Tag operations, within the constraints and using the algorithms described in the following sections.
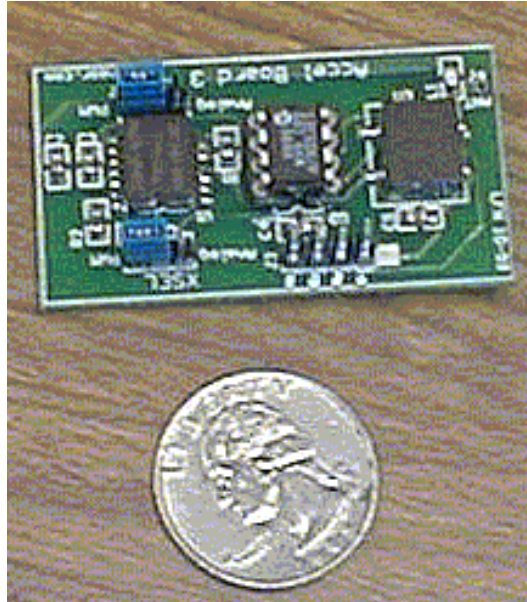
**Figure 1** **The PicoWINS prototype tactical Tag containing sensors, sensor interface, computation, and wireless communication systems. This tactical Tag supports multihop communication. This device was implemented and tested and used for development purposes. The scale of this device is larger than the expected optimized deployment prototype. It is implemented at this scale for the purpose of development. Finally, after the design is optimized, a compact, flexible substrate system could be fabricated.**

# TACTICAL TAG GEOLOCATION

In a wireless network of tactical Tags the relative position of every Tag, and hence any acquired target, is of fundamental importance. However, due to the Tag network's lack of infrastructure, size and cost constraints, and variety of deployment environments, available technologies are not sufficient to solve this problem. Prior geolocation systems have been developed using a substantial infrastructure, such as in GPS, the emergency cell phone location FCC mandate, and local area ranging systems (for example the recently developed Pinpoint Technologies 3D-iD system). Each of these systems require a substantial infrastructure (satellites, cellular base-stations, and a central workstation with hardwired antennas-respectively) in order to locate a lower cost asset. All of these systems are based on the most robust presently available electromagnetic location scheme of measuring a signals time of arrival (or its subset time difference of arrival), however none of the systems are ideal to locate a network of tactical Tags, due to their infrastructure requirements. A wireless network of tactical Tags should operate independently of other systems, and in addition only requires the relative location of every Tag within the network. However, as in the above mentioned geolocation systems, the clock speed on every Tag (or local asset) will not be precise enough to allow accurate direct ranging from a signal's time of arrival. As a result a methodology similar to those prior technologies must be developed which does not require a fixed, large-scale infrastructure.

Geolocation for tactical Tags may rely on a hierarchical network architecture that separates the tactical Tag network into multiple tiers. The lowest (and most ubiquitous) layer consists of the Tags, while the next layer consists of less numerous, and more complex Gateways. Geolocation technology may be developed for the more complex Gateways by leveraging their higher clock speed, and increased size and power, then the Tag's location algorithm would leverage that of each Gateway. To initially locate the Gateways with a minimum of processor speed and complexity, an active, zero-delay, or fixed delay transponder may be developed. This system would leverage the stability of the clock on a single Gateway by measuring the round-trip time, and hence range, between two Gateways. Now, with geolocation set for the Gateways, ranging of the Tags may proceed. (The zero-delay transponder concept and system design was developed in the PicoWINS program.)

The geolocation of Tags presents unique challenges. These include:

Currently, all available RF geolocation systems require high-speed and low drift clocks and correllator systems. The power and volume requirements for these systems exceed the target volume (0.5 cm$^3$) for Tags by a factor of 10 to 100.

Further, conventional systems will require that the RF signal from the Tag be received by multiple Gateways. This requirement is severe for Tags distributed in the

field where direct transmission may not be permitted and where, instead, multihop communication may be required.

In view of these constraints, it has been proposed in the PicoWINS program to develop a Tag geolocation system that does not rely on precision timing at the Tag or direct Tag-to-Gateway communication.

Tag geolocation relies on the "coincidence method" developed in the PicoWINS program (see Figures 2 – 5). The PicoWINS coincidence geolocation method relies on a network operating with synchronized Gateway Nodes that produce a set of time-sequenced RF signal codes. Remote PicoWINS Tags receive these codes and must detect only a *coincidence* in the arrival time of the codes. The recognition of a coincidence requires far less accuracy for timing than would otherwise be required. The detection of a coincidence may be transmitted via multihop messaging to Gateways or other assets. The Gateways are capable of sweeping their code transmission time delay values. This causes the point of coincidence (the point in space at which the signals from three nodes arrive simultaneously) to move in space. Thus, the Gateways may effectively sweep an area, examining for Tags that are static or moving, hidden or visible.

This technique for Tag geolocation only requires direct one-way communication from the Gateways to the Tag. The Tag is capable of detecting the coincidence. Later notification that a coincidence was observed (at a particular, approximate, past time) can be transmitted to the Gateways. Since the Gateways control the location of the coincidence in space and move this point of coincidence in time, the Gateway network can geolocate the Tag merely by knowing at what approximate time the coincidence has appeared. The requirement on timing is not constrained by geolocation timing, but, rather by identification of the particular message in the PicoWINS messaging network.. In this case, timing constraints are substantially relaxed. Since messaging timing is relaxed, the Tag then communicates the detection of a coincidence via multi-hop links to the Gateways. This methodology enables the geolocation of any tactical Tag within the network, by building the required location infrastructure into the existing Gateways and Tags, extending the work done in prior position location technologies. The following Figures describe the coincidence method:
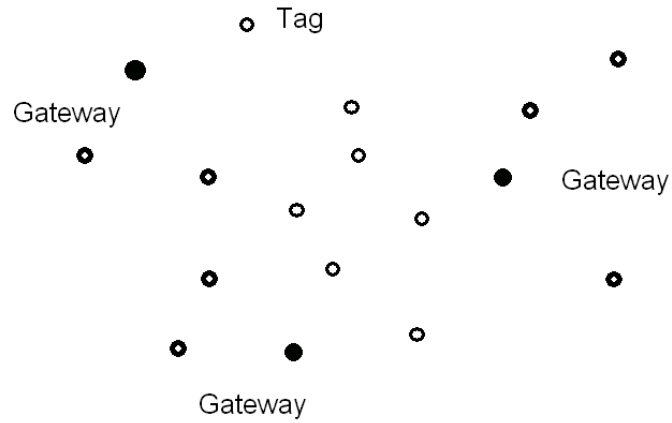
**Figure 2. This figure displays a distribution of Tags and Gateways. The Tags may be mobile. Gateways are capable of providing accurate ranging to enable their geolocation. Gateways will transmit signals, as shown in the following figures, that allow a Tag to identify its location within the Gateway network.**
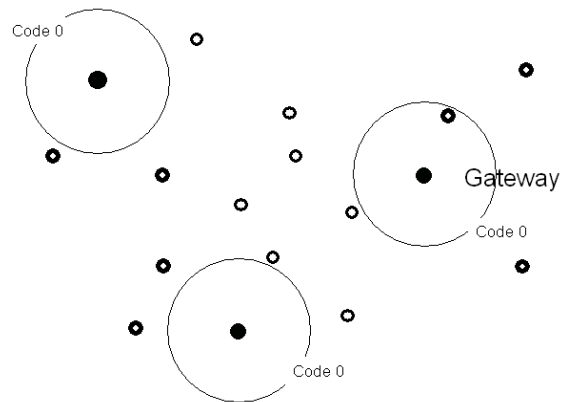


**Figure 3. This figure depicts the network at the point in time when a signal (pseudonoise (PN) code) has been transmitted by all Gateways at the same instant. This PN code is received by all Tags.**
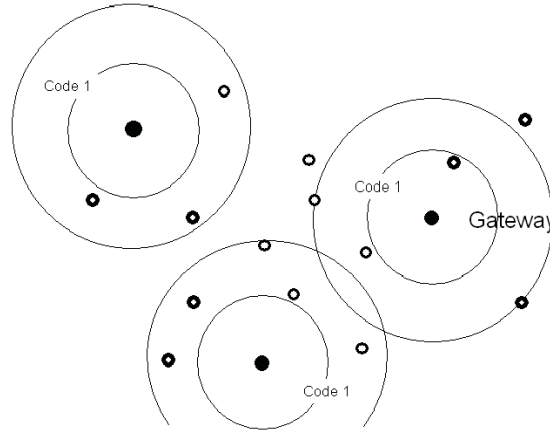
**Figure 4. This figure depicts the network at the point in time when a second PN appears.**
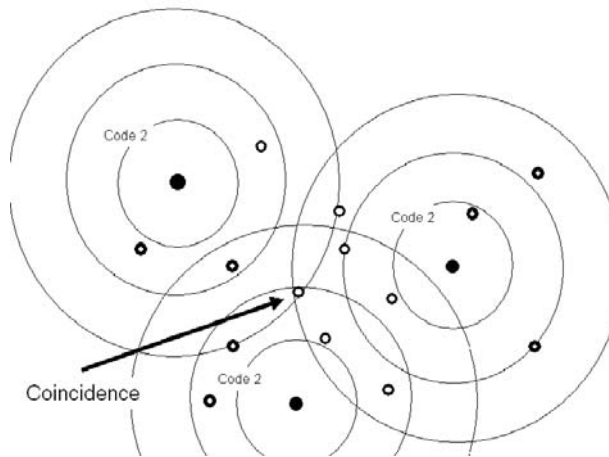


**Figure 5. This figure depicts the point in time where three PN codes have been transmitted. In this special case one of the Tags has received three PN sequences nearly simultaneously. The Tag identifies this (with a relatively simple, dedicated, geolocation system). Later, the Tag may notify the network that it has detected the coincidence. Most importantly, the timing of the three Gateway signals may be arranged such that the point of coincidence may be made to sweep through the entire area, allowing the mapping of all Tags.**

# THEORY OF SHORT RANGE WIRELESS PROPAGATION

Robust, distributed wireless communication is becoming a fundamental and inevitable requirement for the next generation of wireless networks for tactical sensors including, anti-vehicular mines, anti-personnel land mine replacements, antisubmarine and anti-torpedo networks, IFF systems, asset management, personal area networks, wire replacement services, and other applications. Wireless data communication between personnel, between personnel and weapons systems, and between weapon systems will be a lifeline for command and control. In addition, as the number of commercial inter-networked appliances and sensors increases short-range wireless propagation in variety of environments becomes a crucial issue. Wireless networks for defense applications, Bluetooth[TM,] IEEE 802.11, HomeRF, etc.. are becoming more prevalent to network small, embedded systems with limited power capabilities. In addition these systems are deployed in a wide variety of environments with substantially different propagation characteristics. This report presents a summary of experimental data collection on wireless propagation at ranges and outdoor locations appropriate to these systems in addition to a simple description of the dominant phenomena, with particular focus on peer-to-peer systems randomly deployed outdoors.

The focus of prior modeling and empirical propagation studies was at longer ranges than the maximum 100-200m ranges expected for low power ground based local autonomous networks. This white paper is intended to provide information to fill in the gap in empirical data, which can be used by the defense community, and academic community in general, to optimize compact, embedded, wireless sensors. An extensive body of literature exists on long-range propagation at frequencies up to approximately 2 GHz. Seminal papers by Sommerfeld [1] and Norton [2] among others, as detailed in the overview by Wait [3], explored the idea of a trapped wave propagating along the surface of the earth, both theoretically and experimentally. The focus of these papers however reflects the dominant communication means of the time, generally directed at UHF frequencies and below. Prior to the explosive growth of cellular communications most studies of propagation above 1GHz focused on point-to-point satellite or similar line of sight links. Recently a large number of papers have appeared quantifying propagation fall off and multi-path in cellular systems [4,5]. These studies generally directed toward wireless phone providers focus on the base-station to mobile link at distance of at least a few hundred meters with most considering frequencies below 2 GHz. In addition the intent of these studies is to implement high data rate channels in mobile systems (3G and 4G cellular systems) not specific to low power peer-to-peer embedded systems. This paper is intended to fill in where these cellular and other RF communication studies have stopped, by extending to higher frequencies and by considering the local environment and lower heights as ranges become smaller than those relevant for a picocell cellular system.

A few studies do exist looking at parts of the frequency ranges we are considering. For example papers by Patwari[6] and Sohrabi[7] consider local propagation. However these systems were limited by the non-portable nature of their measurement system and provide an initial sampling of the variability of propagation results seen in surface-to-

9

surface links. These papers provide a basis upon which this paper expands by including a more extensive environmental variation study, incorporating polarization considerations, as well providing measurements in all three ISM bands.

At the frequencies considered in this study (900MHz to 5.8GHz) most propagation effects in the local environment are well modeled with ray tracing physical analogies. Contributions from surface waves or lateral waves propagating along a ground or vegetation interface are not substantial due to the permittivity of the surfaces and the scale of the vegetation variation. However, particularly near a finite conductivity ground a fourth power propagation fall is observed for both horizontal and vertical polarization. This fall is explainable in a ray-tracing analog in terms of the destructive interference of a direct ray and a ground-bounce ray. The reflection coefficient for a smooth surface is –1 for both polarizations at an incidence of 90 degrees from the surface normal. The perfect electric conducting (PEC) surface limit represents a discontinuity in the reflection coefficient for parallel (vertical) polarization. The limit of the parallel reflection coefficient as the incidence angle approaches 90 degrees is –1 for a lossy conductor while the parallel reflection coefficient value at exactly 90 degrees is +1 corresponding to the PEC case at any angle of incidence. Thus unlike the change in antenna input impedance due to the proximity of a conducting surface (which detunes a horizontally polarized antenna near a finite conductivity surface and approximately doubles the effective antenna aperture size of a vertically polarized antenna) the fourth power propagation fall off seen at near grazing angles affects both polarizations. Thus a two-ray model (direct and ground bounce ray) of propagation near the ground provides a first order approximation to the path loss, at least in environments in which large scatterers are not nearby and once the antenna's gain (including radiation efficiency and directivity) is considered separately. One of the intents of this paper is to compare the accuracy of this simple intuitive physical model, and describe the deviation from it based on ground roughness, distributed scattering, and distance considered with empirically collected data.

In a ray tracing analogy each ray is described independently in terms of its geometric path, with the caveat that the radiating antenna's far field power is radiated over a spherical surface. This follows the Friis transmission formula as shown equation (1)[8]

$$\frac{P_r}{P_t} = e_t e_r \left(\frac{\lambda}{4\pi R}\right)^2 D_t D_r \left|\hat{\rho}_t \cdot \hat{\rho}_r\right|^2 \qquad (1).$$

e represents the antenna efficiency, $\rho$ its polarization, and D its angularly dependent directivity for the transmit (t) and receive (r) antennas. From this equation it is easily seen that larger propagation loss is expected for the same distance at higher frequencies as increasing the frequency equates to increasing the electrical path length (i.e. scaling all distances with the wavelength). This loss can be offset if the antenna aperture is held constant as the frequency is reduced (assuming the antenna is matched) since the electrical antenna size grows, the directivity can be larger in certain directions, however generally constant electrical sized antenna apertures are assumed for comparisons. Equation (1) provides a fundamental propagation description as a function of frequency

in an antenna's far field assuming constant electrical sized antennas. In the data presented in this paper this scaling rule is held to as all measurements are performed with matched monopole antennas (an offset feed point provides a matched antenna without a ground plane) which are approximately a half-wavelength long and provide similar directivity.

The propagation loss between the transmit (Tx) and receive (Rx) points over a flat surface can be written as a sum of two rays by assuming isotropic, matched, co-polarized antennas for each ray in equation (1) yielding:

$$\frac{P_{rx}}{P_{tx}} = \left(\frac{\lambda}{4\pi}\right)^2 \left| \frac{e^{jkr_1}}{r_1} + R(\theta)\frac{e^{jkr_2}}{r_2} \right|^2 \tag{2}$$

The angle of reflection for the ground bounce ( ) is dictated by the ray's path defining each ground bounce ray's reflection coefficient R. Given the ground's reflection coefficient (which for a flat ground is based on its permittivity and permeability) and the transmit antenna, and receive antenna locations the propagation loss between the transmit and receive antennas can be defined. Equation (2) does not include the effect of scattering, however it provides a first order approximation of signal propagation near the ground.

This report focuses on the propagation loss observed in short range near the ground RF communication links. As a result portable equipment, which provides only received signal strength indication (RSSI) without phase or delay spread information is used. In high-speed links the multipath delay spread is of significant interest in that it provides a straightforward description of multipath interferences limit on the signal modulation rate (i.e. inter-symbol interference). However as the focus of this paper is on short-range links appropriate for lower data rate systems more portable, lower cost equipment providing signal amplitude only was utilized. In most short-range environments the signal delay spread due to multi-path components is too small to adversely affect low data rate signaling schemes. For example in [15] at 1.92MHz in twelve indoor and outdoor environments the longest delay spread observed was 200ns, with most providing less than 50ns of delay spread. This spread is an order of magnitude less than the chipping rate for most data rates used by battery operated applications considered in this paper (for example 50ns per chip for a 20Mbps coding rate). As a result within this analysis only amplitude information is collected, with the influence of multi-path scattering demonstrated on the received signal strength, but not on the signal's temporal dispersion. To obtain amplitude information a continuous wave portable data collection system was utilized to collect the received signal strength.

### ANALYTICAL JUSTIFICAITON OF THE TWO RAY MODEL

The analysis of electromagnetic waves propagating over a lossy earth has a long history stretching back to the turn of the last century [3]. One of the first simplifications in this analysis is to consider the surface of the earth as a lossy half-space. Further modifications include accounting for the earth's curvature and reflection off the

ionosphere. However, in considering microwave radiation in either the 2.4GHz or 5.8GHz bands at distances of less than a few kilometers these modifications are unnecessary. Rather than the earth's curvature the representation of the earth as a perfectly smooth homogenous lossy medium will be the most likely cause of inconsistencies when compared with actual measurements. Nevertheless, for the analysis here this approximation will be utilized to provide a window on the basic physics.

THE VERTICAL ELECTRIC DIPOLE (VED)

To investigate radiation in the presence of the earth, first consider a vertical (z oriented) infinitesimal dipole. Then, following the asymptotic analysis of [16] the potential of the field above a lossy half-space ($z>0$) may be approximated as:

$$\psi_0 \cong \frac{e^{-jk_0 R_0}}{R_0} + \left[ \frac{C-\Delta}{C+\Delta} - \frac{1}{p\left(1+\dfrac{C}{\Delta}\right)^3} - \frac{3}{2p^2\left(1+\dfrac{C}{\Delta}\right)^5} + \cdots \right] \frac{e^{-jkR_1}}{R_1}. \tag{1}$$

In this equation the dipole is considered a height $h$ above the ground half-space, which has relative permittivity $\varepsilon_r$ and conductivity $\sigma$. In addition the following variable definitions are used:

$$
\begin{aligned}
R_1 &= \sqrt{\rho^2 + (z-h)^2} \\
R_2 &= \sqrt{\rho^2 + (z+h)^2} \\
R &= \sqrt{\rho^2 + z^2} \\
C &= \frac{h-z}{R_1} \\
\Delta &= \frac{\eta_1}{\eta_0}\left(1 - \frac{\eta_1^2}{\eta_0^2}\sqrt{1-C^2}\right) \\
p &= \frac{kR}{2}\left(\frac{1}{\dfrac{\sigma}{\varepsilon_0 \omega} + j\varepsilon_r}\right)
\end{aligned}
\tag{2}
$$

-z is the distance of the observation point above the ground and $\rho$ is the radial distance along the ground from the dipole. Equation (1) contains both 1/r and $1/r^2$

behavior. In the far field the electric field is directly proportional to the potential. Thus the dominant r dependence of the potential shows up in the field. Only in the case when the first term on the left hand side (containing $R_0$) and the first term within the parenthesis cancel one another will the $1/r^2$ ($1/r^4$ in power) behavior dominate the far field. This occurs when R>>h and Δ>>C. In other words, in the far field with R>>h close to the ground when C<<1, or when the impedance contrast between the two half-spaces is large but not huge. The factor (C-Δ)/(C+Δ) corresponds to the plane wave reflection coefficient of the lossy ground. Thus, the first two terms of equations (1) can be considered as the geometrical optics incident and reflected fields. However, it should be kept in mind that 1/r2 electric field attenuation (1/r4 propagation loss) may result from the residual left over by incomplete cancellation of the 1/r terms as well as from there complete cancellation leaving the $1/r^2$ terms. Thus as will be explored further in the next section the $1/r^4$ propagation loss is describable simply with the geometrical optics (1/r) terms.

At radio frequencies the $1/r^2$ electric field component ($1/r^4$ in power) behavior has been shown experimentally to dominate propagation along the ground and as a result this behavior has been historically called a ground wave or Norton surface wave. At microwave frequencies the relative permittivity and loss tangent for soil are generally not as high as at radio frequencies. As a result in order to investigate the dominance of the $r^{-4}$ propagation for this infinitesimal vertical dipole the electric field radiated from the dipole using realistic soil permittivity values is calculated. Further separation of the contribution of individual terms of equation (1) will wait until the next section were an alternate analysis will extend beyond simply the vertical electric dipole. There the appropriateness of modeling the field behavior at microwave frequencies unlike at much lower frequencies using only the geometrical optics terms (the 1/r terms of eq. 1) will be demonstrated. The electric field above the ground (z<0) is related to the potential through:

$$E_\rho = \frac{\partial^2 \psi_0}{\partial \rho \partial z}. \tag{3}$$

$$E_z = \left( k_0^2 + \frac{\partial^2}{\partial z^2} \right) \psi_0. \tag{4}$$

$$E_\phi = 0 \tag{5}$$

In order to evaluate the derivatives in equation (3) and (4) it is convenient to use a forward difference approximation evaluated numerically. This is done to plot the z and ρ components of the electric field in Figure 6. In this figure and all which follow the magnitude of the electric field is plotted in dB, with the relative normalization being

consistent between figures 5 to 8 and then a different consistent normalization for figures 9 to 17.
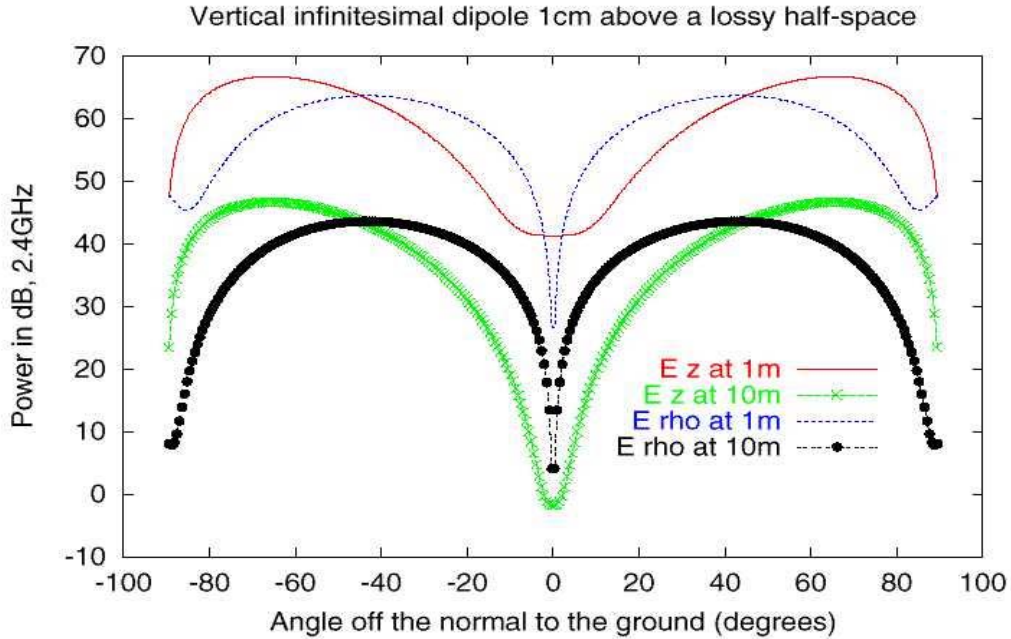


**Figure 6: The magnitude of the electric field components due to an infinitesimal vertical electric dipole over dry soil.**

In figure 6 representative values for soil's permittivity of $\varepsilon_r$=3 and $\sigma$=0.01S/m are used. The fields in this figure are plotted at distances of one meter and ten meters for a dipole located 1cm above the earth. It is easily seen from this figure through the 20dB difference between the 1m and 10m plots the 1/r fall off of the field over almost the entire angular range. It is only within about 5 degrees of the ground that the plots tend towards $1/r^2$ behavior (1/r$^4$ or a 40db in power difference). In addition it is interesting to note the 1/r radiation, particularly from the z component of the electric field peaks at relatively close to grazing. This indicates the high directivity needed by any antenna in order to couple only into the $1/r^2$ ground wave along the horizon, without providing telltale radiation above the horizon.

The soil permittivity used to plot figure 6 ($\varepsilon_r$=3 and $\sigma$=0.01S/m) represents the lowest end of data measured in [13]. The relative real part of the permittivity of soil at 2.4GHz ranges from about 3 up to about 20 for various density and moisture content [13]. Increasing the moisture content from 0% to 20% of the soil's dry weight increased the permittivity in this range. The conductivity of these soils at 2.4GHz ranged from about .01 mho/m up to about .5 mho/m (tan$\delta$ from about 0.025 to 0.2). Again increasing with soil moisture content. For comparison with figure 6, the z and $\rho$ components of the electric field at one meter and ten meters for a dipole 1cm above the ground is shown in figure 7 for soil with

$\varepsilon_r$=20 and $\sigma$=0.5S/m. The high value represents soil with moisture added up to 20% of the soils dry weight, and represents the highest value measured in [13] at 2.4GHz. The variation in soil permittivity from 2.4GHz to 5.8GHz is generally seen mainly in an increase in the conductivity by a factor on the order of two.
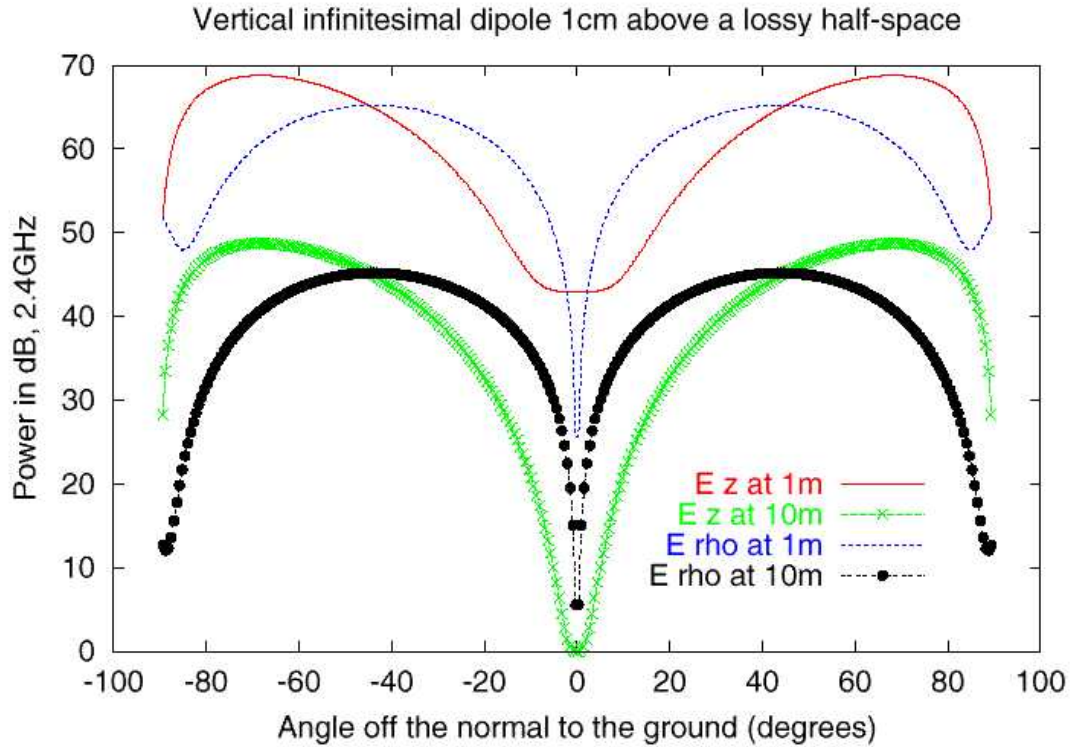


**Figure 7: The magnitude of the electric field components due to an infinitesimal vertical electric dipole over moist soil.**

Comparison of figures 6 and 7 shows that fall off steeper than $1/r^2$ in power only shows up at 2.4GHz within about 5 degrees off the ground for almost any soil. Similar comparisons were conducted at distances exceeding 10m and a similar pattern emerged. At 2.4GHz by 10m the field is well within its far field behavior since this distance is eighty wavelengths from the dipole. From figures 6 and 7 it can be seen that the $1/r^4$ in power behavior appears to show up along the surface of the earth at 2.4GHz. However in order to couple radiation predominantly into this attenuated wave, requires a highly directive antenna. The horizontal electric dipole will provide a different picture although substantial change is not expected.

One method of increasing the directivity of the antenna towards the horizon is to adjust the height of the vertical dipole above the lossy earth. A vertical dipole a half-wavelength above the ground (6.25cm) is shown in figure 8. This figure is plotted for soil with $\varepsilon_r$=3 and $\sigma$=0.01S/m. The peak directivity in this case is increased from

about 70 degrees off the normal to about 80 degrees. However, by 10 meters this is still a predominantly $1/r^2$ in power effect. Within an environment such as a forest or city, which will scatter this beam back towards the ground, this may increase the power propagating along the surface and reduce the total power radiated towards the sky (by increasing the effective path length and hence attenuation as the field is scattered before it heads towards the sky). In addition by comparing figures 6 and 8 a few dB are gained at the grazing angle, however the predominant radiation is $1/r^2$ in power and off grazing.
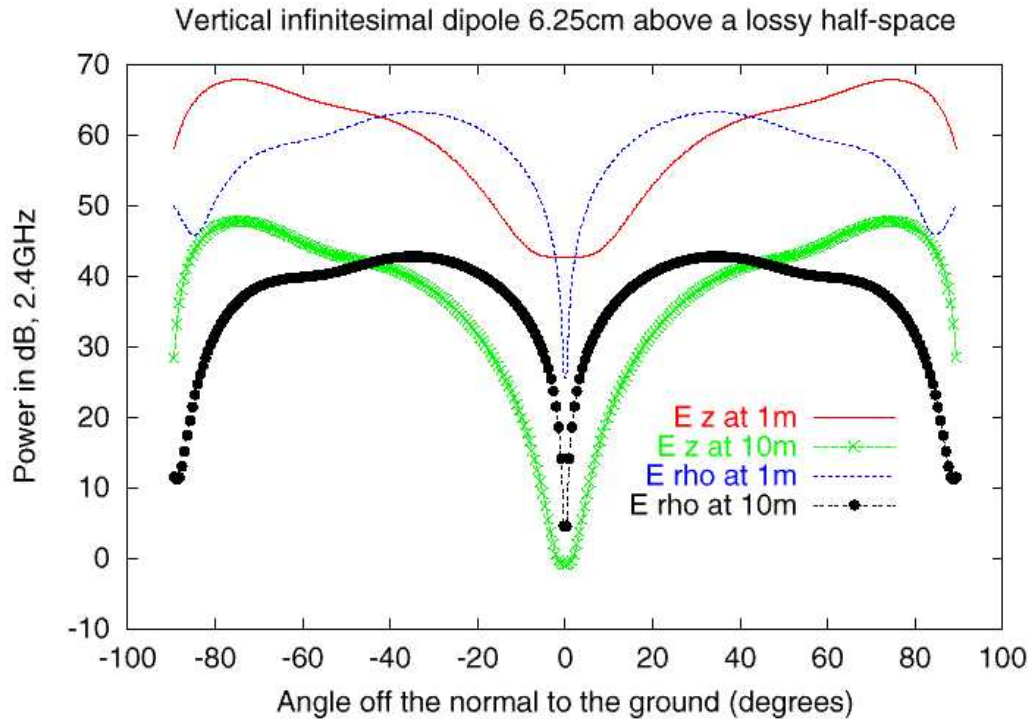


**Figure 8: The magnitude of the electric field components due to an infinitesimal vertical electric dipole over dry soil.**

The spacing of 6.25cm in figure 8 would be optimum for broadside radiation from a vertical dipole above a perfectly conducting half-space. However the lossy, low conductivity nature of the soil modifies the reflection coefficient off the ground so that slight improvements over figure 8 are possible. In general though, these figures demonstrate the effect of the earth on radiation at 2.4GHz. The $1/r^4$ in power fall off along the air soil interface is still present, however only present within about 5 degrees of grazing. As a result, in order to couple energy predominantly into this ground wave an antenna needs a beam width within this range of five degrees in the presence of the soil. Generally to obtain efficient stealthy (from an airborne detector) communication will require an optimized antenna operating in the presence of the ground with a high

16

directivity. From the perspective of total power flow however the $1/r^2$ ground wave ($1/r^4$ for power) appears to be the worst case, with power especially from below 10m not attenuated quite this much.

Investigating the vertical infinitesimal electric dipole provides a preliminary account of radiation in the presence of a lossy half-space. In fact this preliminary investigation demonstrates that including only the geometric optics terms in an asymptotic analysis of a non-plane wave source are sufficient to provide a description of the $r^{-4}$ power fall off seen in measurements. However for a complete description of the physical phenomena, since the half-space breaks the symmetry of the medium, both horizontal and vertical dipoles must be considered. In addition to provide completeness magnetic as well as electric dipoles must be considered.

### HORIZONTAL AND VERTICAL ELECTRIC AND MAGNETIC DIPOLES

The radiation of any antenna within a layered environment can be understood in terms of four basic radiating elements: a vertical electric dipole (VED), a horizontal electric dipole (HED), a vertical magnetic dipole (VMD), and a horizontal magnetic dipole (HMD). The radiation from any three dimensional source in a layered environment can be built up from these elements. Understanding their interaction within a layered environment describes the basic physics of propagation within that environment. In a homogeneous space only the electric and magnetic dipole are required, however as a result of the broken symmetry of a layered geometry, all four radiators must be included to describe propagation in a one dimensionally inhomogeneous, or layered structure such as a lossy earth half-space. For any layered media the field components may be written using Sommerfeld integrals following [17]. This analysis is used rather than the previous analysis following [16], as it provides a more straightforward presentation of the field in terms of the geometric optics incident and reflected fields, which will be shown to be appropriate in describing the fundamental physics involved at 2.4GHz and 5.8GHz. The resulting fields in region 1 above a layered media, separating the transverse electric (TE) or $H_z$ and transverse magnetic (TM) or $E_z$ response follow.

For the VED:

$$H_{1z} = 0$$

$$E_{1z} = \frac{-Il}{8\pi\omega\varepsilon_1} \int_{-\infty}^{\infty} \frac{k_\rho^3}{k_{1z}} H_0^{(1)}(k_\rho\rho)\left[e^{ik_{1z}|z|} + \widetilde{R}_{12}^{TM} e^{ik_{1z}z+2ik_{1z}d}\right]dk_\rho \tag{6}$$

For the VMD:

$$H_{1z} = \frac{-iIA}{8\pi} \int_{-\infty}^{\infty} \frac{k_\rho^3}{k_{1z}} H_0^{(1)}(k_\rho \rho) \left[ e^{ik_{1z}|z|} + \widetilde{R}_{12}^{TE} e^{ik_{1z}z + 2ik_{1z}d} \right] dk_\rho$$

(7)

$$E_{1z} = 0$$

For the HED:

$$E_{1z} = \frac{iIl}{8\pi\omega\varepsilon_1} \cos\phi \int_{-\infty}^{\infty} k_\rho^2 H_1^{(1)}(k_\rho \rho) \left[ \pm e^{ik_{1z}|z|} - \widetilde{R}_{12}^{TM} e^{ik_{1z}z + 2ik_{1z}d} \right] dk_\rho$$

(8)

$$H_{1z} = \frac{iIl}{8\pi} \sin\phi \int_{-\infty}^{\infty} \frac{k_\rho^2}{k_{1z}} H_1^{(1)}(k_\rho \rho) \left[ e^{ik_{1z}|z|} + \widetilde{R}_{12}^{TE} e^{ik_{1z}z + 2ik_{1z}d} \right] dk_\rho$$

For the HMD:

$$E_{1z} = \frac{-IA}{8\pi} \cos\phi \int_{-\infty}^{\infty} k_\rho^2 H_1^{(1)}(k_\rho \rho) \left[ \pm e^{ik_{1z}|z|} - \widetilde{R}_{12}^{TE} e^{ik_{1z}z + 2ik_{1z}d} \right] dk_\rho$$

(9)

$$H_{1z} = \frac{\omega\mu IA}{8\pi} \sin\phi \int_{-\infty}^{\infty} \frac{k_\rho^2}{k_{1z}} H_1^{(1)}(k_\rho \rho) \left[ e^{ik_{1z}|z|} + \widetilde{R}_{12}^{TM} e^{ik_{1z}z + 2ik_{1z}d} \right] dk_\rho$$

With

$$k_{iz} = \sqrt{k_i^2 - k_\rho^2}$$

In the first equation of both (8) and (9) the positive sign corresponds to z>0 while the negative sign corresponds to z<0. $H_n^{(1)}$ is the Hankel function of the first kind and R is the TE or TM reflection coefficient from the layered media. Equations (6) to (9) are general for the field above any layered (one dimensionally inhomogeneous) medium. They correspond to the fields due to an electric infinitesimal dipole of current I and length l, or a magnetic infinitesimal dipole of current I in an area A.

In order to look at the fundamental field behavior predicted by these equations these integrals can be asymptotically evaluated in the limit that the observation distance is

18

electrically large. Following [17] the fields in region 1 above the layered media from each of these dipoles may be split into three components.

$$E = E^{inc} + E^{RS} + E^{RB}$$
$$H = H^{inc} + H^{RS} + H^{RB}$$

(10)

The first term corresponds to the incident field due to the dipole, the second to the field directly reflected off the layered medium, and the third to a contribution from evaluating the integration across the branch cuts at $k_{2z}$. In the asymptotic limit the first term corresponds to the geometric optics incident field and the second to the geometric optics reflected field, while the third terms encompasses surface wave and leaky wave, or lateral wave phenomena sees with multi-layered media.

Extending the analysis in [17] and using the method of stationary phase to evaluate the geometrical optics contributions to the field, and the method of steepest descent to evaluate the branch point or ground wave contributions the asymptotic fields are found for each dipole. The incident and reflected asymptotic fields are general to any layered medium for which the TE and TM reflection coefficients are known, however to evaluate the branch cut contribution a half-space was assumed.

For the VED:

$$E^{inc} \approx \frac{-Il}{4i\pi\omega\varepsilon_1 r} k_1^2 \sin^2\theta\, e^{ik_1 r}$$

$$E^{RS} \approx \frac{-Il}{4i\pi\omega\varepsilon_1 r_I} k_1^2 \widetilde{R}_{12}^{TM}(\theta_I)\sin^2\theta_I\, e^{ik_1 r_I}$$

(11)

$$E^{RB} \approx \frac{-Il\varepsilon_2\sqrt{i}}{2\pi\omega\sqrt{\rho}}\left[\frac{i}{\rho+\frac{ik_2(z+2d)}{\sqrt{k_2^2-k_1^2}}}\right]^{\frac{3}{2}} \frac{ik_2}{\varepsilon_2^2-\varepsilon_1^2} e^{ik_2\rho-\sqrt{k_2^2-k_1^2}(z+2d)}$$

With

$$r = \sqrt{\rho^2 + z^2} \quad r_I = \sqrt{\rho^2 + (z+2d)^2} \ .$$

d is the height off the dipole above the layered medium.

For the VMD:

$$H^{inc} \approx \frac{-IA}{4\pi r}k_1^2 \sin^2\theta\, e^{ik_1 r}$$

$$H^{RS} \approx \frac{-IA}{4\pi r_I}k_1^2 \widetilde{R}_{12}^{TE}(\theta_I)\sin^2\theta_I\, e^{ik_1 r_I} \tag{12}$$

$$H^{RB} \approx \frac{-IA\sqrt{i}}{2\pi\sqrt{\rho}}\left[\frac{i}{\rho + \dfrac{ik_2(z+2d)}{\sqrt{k_2^2-k_1^2}}}\right]^{\frac{3}{2}} \frac{ik_2^3}{k_2^2-k_1^2}e^{ik_2\rho - \sqrt{k_2^2-k_1^2}(z+2d)}$$

For the HED:

$$E^{inc} \approx \frac{-iIl}{4\pi\omega\varepsilon_1 r}\cos\phi\, k_1^2 \sin\theta\cos\theta\, e^{ik_1 r}, \quad H^{inc}\approx \frac{Il}{4\pi r}\sin\phi\, k_1^2 \sin^2\theta\, e^{ik_1 r}$$

$$E^{RS} \approx \frac{iIl}{4\pi\omega\varepsilon_1 r_I}\cos\phi\, k_1^2 \widetilde{R}_{12}^{TM}(\theta_I)\sin\theta_I\cos\theta_I\, e^{ik_1 r_I}, \quad H^{RS}\approx \frac{Il}{4\pi r_I}k_1^2 \widetilde{R}_{12}^{TE}(\theta_I)\sin^2\theta_I\, e^{ik_1 r_I}$$

$$E^{RB} \approx \frac{-iIl\varepsilon_2\sqrt{i}}{2\pi\omega\sqrt{\rho}}\cos\phi\left[\frac{i}{\rho + \dfrac{ik_2(z+2d)}{\sqrt{k_2^2-k_1^2}}}\right]^{\frac{3}{2}} \frac{\sqrt{k_2^2-k_1^2}}{\varepsilon_2^2-\varepsilon_1^2}e^{ik_2\rho - \sqrt{k_2^2-k_1^2}(z+2d)}$$

$$H^{RB} \approx \frac{Il\sqrt{i}}{2\pi\sqrt{\rho}}\sin\phi\left[\frac{i}{\rho + \dfrac{ik_2(z+2d)}{\sqrt{k_2^2-k_1^2}}}\right]^{\frac{3}{2}} \frac{k_2^2}{k_2^2-k_1^2}e^{ik_2\rho - \sqrt{k_2^2-k_1^2}(z+2d)}$$

$$\tag{13}$$

For the VMD:

$$E^{inc} \approx \frac{-i\omega\mu IA}{4\pi r}\sin\phi\, k_1^2 \sin^2\theta c\, e^{ik_1 r}, \quad H^{inc} \approx \frac{IA}{4\pi r}\cos\phi\, k_1^2 \sin^2\theta\, e^{ik_1 r}$$

$$E^{RS} \approx \frac{-i\omega\mu IA}{4\pi r_I}\sin\phi\, k_1^2 \widetilde{R}_{12}^{TM}(\theta_I)\sin^2\theta_I\, e^{ik_1 r_I}, \quad H^{RS} \approx \frac{-IA}{4\pi r_I}\cos\phi\, k_1^2 \widetilde{R}_{12}^{TE}(\theta_I)\sin\theta_I \cos\theta_I\, e^{ik_1 r_I}$$

$$E^{RB} \approx \frac{\omega\mu IA\varepsilon_1\varepsilon_2\sqrt{i}}{2\pi\sqrt{\rho}}\sin\phi\left[\frac{i}{\rho+\dfrac{ik_2(z+2d)}{\sqrt{k_2^2-k_1^2}}}\right]^{\frac{3}{2}}\frac{1}{\varepsilon_2^2-\varepsilon_1^2}e^{ik_2\rho-\sqrt{k_2^2-k_1^2}\,(z+2d)} \qquad (14)$$

$$H^{RB} \approx \frac{-\omega\mu IA\sqrt{i}}{2\pi i\sqrt{\rho}}\cos\phi\left[\frac{i}{\rho+\dfrac{ik_2(z+2d)}{\sqrt{k_2^2-k_1^2}}}\right]^{\frac{3}{2}}\frac{k_2^2}{\sqrt{k_2^2-k_1^2}}e^{ik_2\rho-\sqrt{k_2^2-k_1^2}\,(z+2d)}$$

The incident and reflected terms can be easily seen to cancel for grazing incidence for all the dipoles since both the TE and TM reflection coefficients off a layered media at grazing incidence ($\theta=\pi/2$ radians or 90 degrees) are $-1$. The reflection coefficients off of a half-space are:

$$R_{12}^{TE}(\theta_I) = \frac{\mu_2 k_1\cos\theta_I - \mu_2\sqrt{k_2^2-k_1^2}\sin\theta_I}{\mu_2 k_1\cos\theta_I + \mu_2\sqrt{k_2^2-k_1^2}\sin\theta_I} \qquad (15)$$

$$R_{12}^{TM}(\theta_I) = \frac{\varepsilon_2 k_1\cos\theta_I - \varepsilon_2\sqrt{k_2^2-k_1^2}\sin\theta_I}{\varepsilon_2 k_1\cos\theta_I + \varepsilon_2\sqrt{k_2^2-k_1^2}\sin\theta_I} \qquad (16)$$

In order to investigate the validity of including only the geometric optics terms in the stationary phase evaluation of the Sommerfeld integrals (corresponding to the 1/r terms in the asymptotic expansion of the fields in [16]) the evaluation of the VED as shown in [16] is compared with the analysis of [17]. This is demonstrated in figures 9 and 10. These figures compare Wait's solution from equations (1) and (4) [16], with the asymptotic solution of the Sommerfeld integral of equation (11) yielding the geometric optics (GO) terms and the branch cut contribution [17]. Figure 9 compares the two solutions (normalized to the same

value) as a function of θ, the angle to the observation point from the dipole measured off the z-axis. This figure is plotted for an observation point ten meters from the dipole. Figure 10 compares the two solutions as a function of the distance from the dipole along grazing incidence, for θ=89.95 degrees. These two figures were plotted for a dipole height of 2cm. The height of the observation point is a function of θ and the distance from the dipole r, as z=r sinθ. The dipole is at z=0, ground is at z=-d. Compared in these figures are fields with a lossy earth of high permittivity ε=20 and conductivity σ=0.5 S/m and the fields above a lossy earth of low permittivity ε=3 and σ=0.01 S/m. These figures demonstrate that the two solutions match well, at least away from θ=0 corresponding to the observation region right above the dipole for which the far-field radiated from the VED has a null. In these plots the branch cut contribution ($E^{RB}$) of equation (11) is insignificant as compared to the geometric optics incident and reflected terms at all angles. Even for the low permittivity earth $\text{Re}[\sqrt{k_2^2 - k_1^2}] = 71.1 m^{-1}$ so as the observation point or the height of the dipole increases to a few cm the contribution of this term drops out. In fact even at d=0, z=0, this term provides only a negligible influence at 2.4GHz. The comparison of the asymptotic, geometric optics, and branch cut contributions corresponds to predictions in [18] that experiments demonstrate that the Norton wave can be neglected in the microwave region and a geometrical optics approach is sufficient to model the physics of the flat earth model.

.
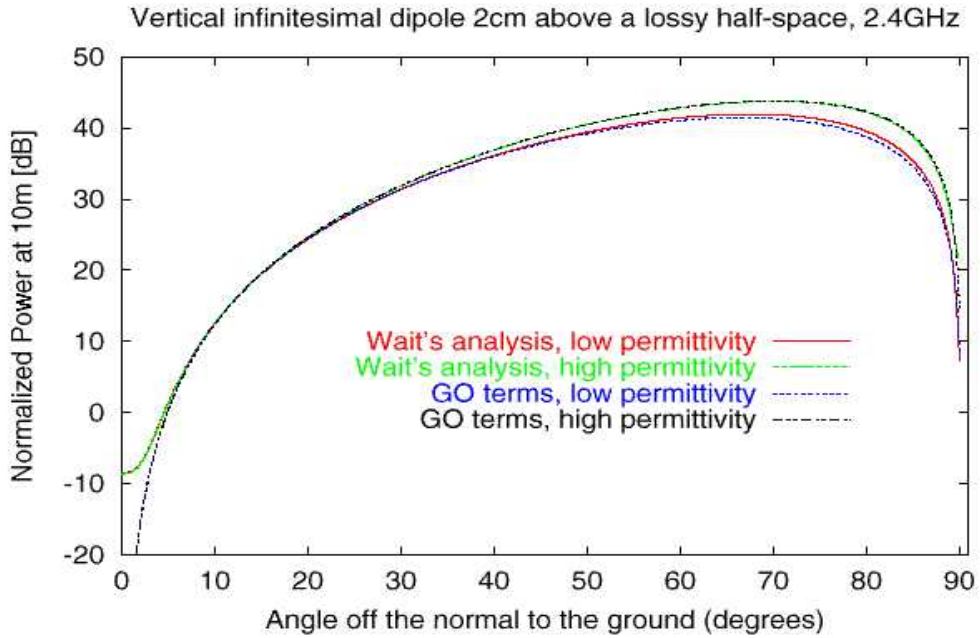


**Figure 9: Electric Field along z for a VED.**
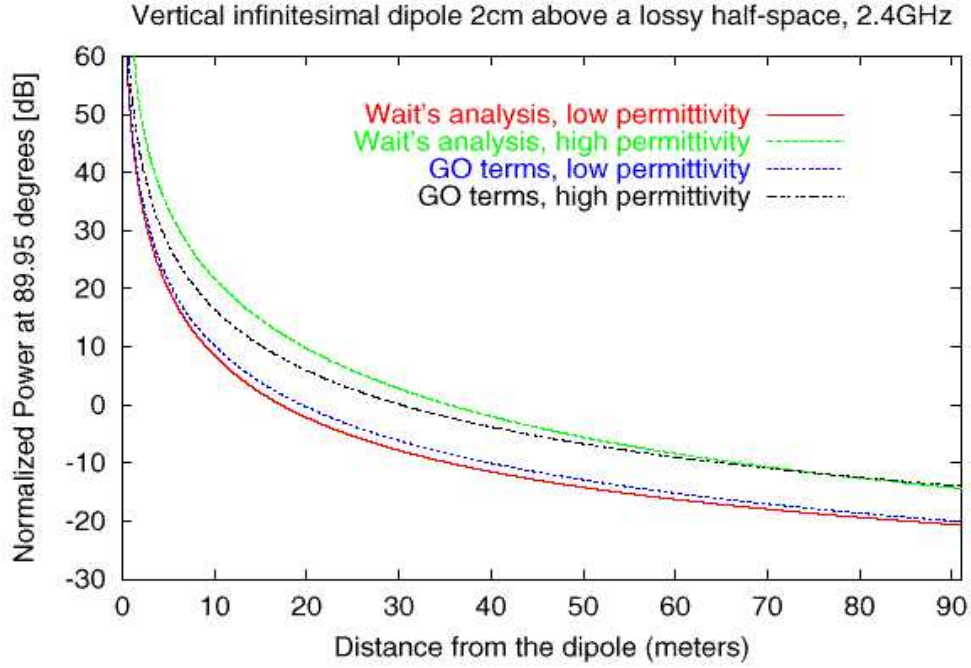
**Figure 10: Electric Field along z for a VED, versus r.**

The interaction of the incident and reflected geometrical optics fields of equations (11) to (14) are strongly dependent on the plane wave reflection coefficients of equations (15) and (16). Particularly along the ground when z=-d, so r=$r_I$ and cosθ=cosθ$_I$ and the incident (inc) and reflected (RS) terms add with a phase determined by the reflection coefficient R. The difference between the fields due to the horizontal and vertical dipoles may then be understood in terms of only the TE and TM reflection coefficients. Plotted in figure 11 are the real part of the TE and TM reflection coefficients for the low permittivity earth (ε=3 σ=.01S/m) and the high permittivity earth (ε=20 σ=.5S/m). The real part is much larger than the imaginary part and so gives an indication of the interference between the incident and reflected signals. The existence of the Brewster's angle for which the reflection coefficient drops to zero is easily seen in the TM components of this figure. As the dielectric constant of the earth increases the Brewster angle approaches 90 degrees and the TM reflection coefficient looks like a square pulse (+1 for incidence at angles of (-90,90) and −1 at the exact angle of 90 or -90 degrees). On the other hand the TE reflection coefficient in this limit is −1 at any angle. The negative TM reflection coefficient at less than 90 degrees results in the cancellation of the incident and reflected fields along the ground surface. For the PEC or infinite permittivity ground the field from a VED adds in phase with its image (with the reflected field) up to 90 degrees at which the field is on the PEC and hence by definition zero. However, as the permittivity (or conductivity) drops from zero the incident and reflected field cancel for the VED or TM fields below 90-degree incidence. Thus the appearance of a power fall

23

off of $1/r^4$ along the ground may be understood a result of the non-infinite permittivity of the ground resulting in cancellation of both TE and TM fields at grazing. Since for any non unity permittivity the reflection coefficient approaching grazing drops to –1, this will lead to cancellation of the GO incident and reflected fields. As one approaches grazing the cancellation is not complete until an incidence of 90 degrees and this cancellation can lead to a fall off more rapid than the $1/r^2$ (in power) fall off seen in the individual GO terms. To describe the fields over the lossy earth the fall off for the VED, HED, VMD, and HMD is presented.

Reflection coefficient of a lossy half-space
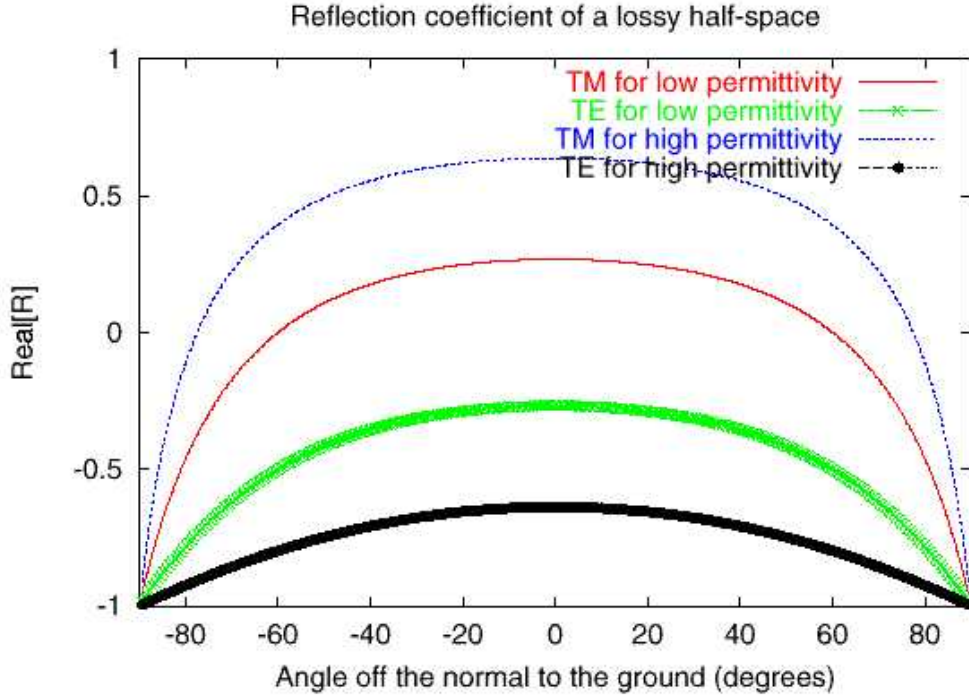


**Figure 11: Real part of the reflection coefficient off a lossy earth half-space.**

The geometric optics terms dominate the response of the infinitesimal dipole over a lossy ground at both 2.4GHz and 5.8GHz. Thus to compare the horizontal and vertical electric and magnetic dipoles these terms may be focused on. In order to provide comparable response from the terms of equations (11) to (14) the normalized power in terms of $|E|^2$ and $|\eta H|^2$ are plotted in dB. To compare the fields from the magnetic and electric dipoles in addition the normalization was used that IA=Il/k. This provides consistency between the VED and the VMD, and between the HMD and the HED. However, since only the z components of the fields are plotted (as all the other components may be found from these through Maxwell's equations) the relative power levels of the horizontal versus vertical dipoles are not normalized to the same level.

24

Shown in figure 12 are the responses of the dipoles when they are 2cm above the earth half-space, at an angle of θ=89.95 degrees (observation point slightly higher than 2cm, for example observing at a height of 2.9cm at 10m). This figure is plotted along φ=45 degrees, or 45 degrees off the axis of the horizontal dipoles. All of the terms in this figure demonstrate an approximately $1/r^3$ to $1/r^4$ fall off in power. In addition the dominance of the $E_z$ component for the HMD and $H_z$ component for the HED are seen. That is the cross coupling from TE to TM fields of the HMD and TM to TE of the HED is seen to be of minimal influence in this high permittivity (ε=20, σ=.5) earth case.
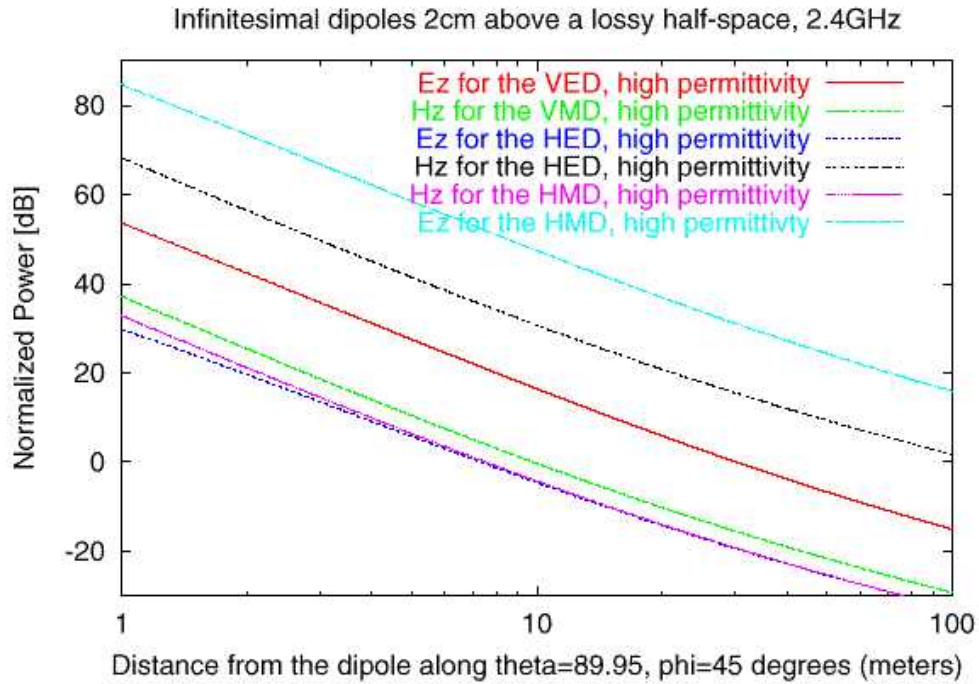


**Figure 12: Dipole response over a lossy earth versus distance at an observation angle of 89.95 degrees, and oriented 45 degrees from the horizontal dipoles.**

For comparison with figure 12 the same field components above a low permittivity earth with (ε=3 σ=.01) are shown in figure 13. In this figure the same general behavior is observed except for the $H_z$ component due to the HMD. For the HMD in this low permittivity case up until about 2 meters the coupling into the TE component (which would not occur without the ground) dominates the primary TM radiated field. Since the TE component of the HMD field falls off more quickly than the TE component, up to about 5 m, although close to the dipole it dominates the field strength in this low

25

permittivity case, it indicates that the TM component is more useful for propagation beyond a few meters. In terms of antennas this means that if a horizontal patch antenna (which can be represented with a superposition of HMDs) is the radiating antenna, a similarly polarized antenna should be used for the receiver.
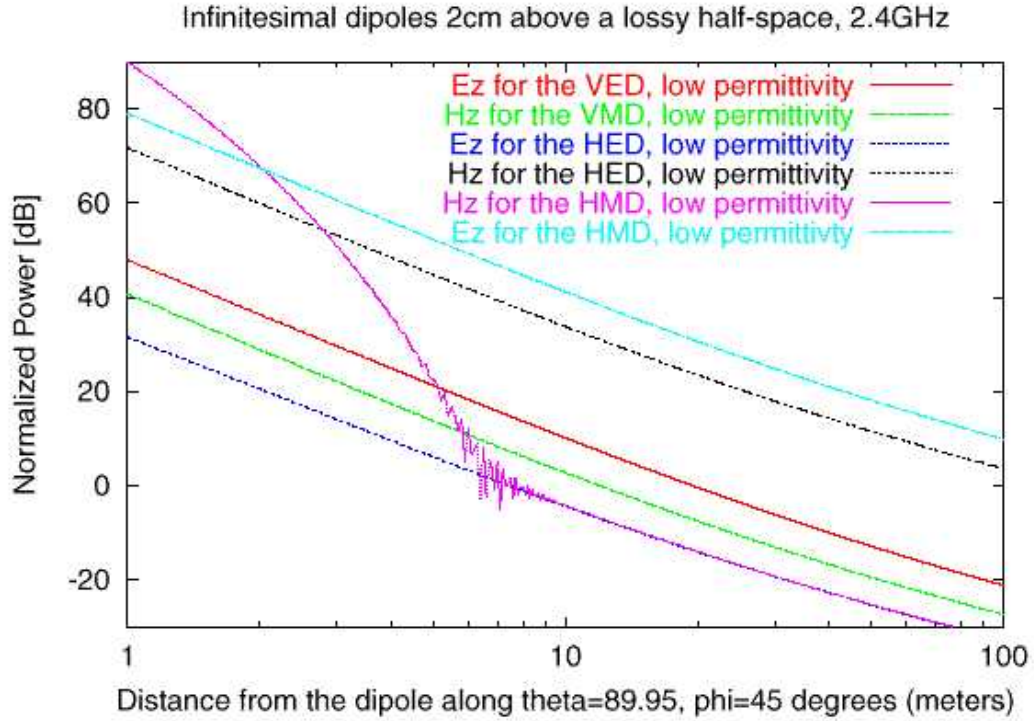


**Figure 13: Dipole response over a lossy earth versus distance at an observation angle of 89.95 degrees, and oriented 45 degrees from the horizontal dipoles**

To more fully explore the effect of the dipole, and observation point height (d=h) above the ground the fields due to the HED, VED, HMD, and VMD, above the same low and high permittivity earth are plotted in figures 14, 15, 16, and 17. These figures are all plotted for an observation distance of 10m, and observation angle φ=45 degrees. Figures 14 and 15 show the fields as a function of antenna height when θ=89.95 degrees so that the observation height is slightly higher than the dipole height as the dipole height increase. Figures 16 and 17 on the other hand show the field with the observation point along the ground (z=-d) as a function of increasing antenna height. In all of these figures raising the dipole even slightly off the ground is seen to have a substantial effect on the radiated power levels. While in all cases raising the dipoles beyond 20cm does not provide much improvement in the radiated power levels. In fact beyond this height

26

fluctuations resulting from phase changes in the path length of the received and transmitted field cause substantial variation in the received power levels. In figures 16 and 17 a higher maximum field is seen at the ground than above the ground in figures 14 and 15. This may be explained since in these plots, as d increases above 10cm or so $\theta$ and $\theta_I$ are no longer along grazing, the incident and reflected GO terms no longer necessarily cancel. At these heights the path lengths of the incident and reflected components are not the same and hence result, in this case, in higher power levels along the ground.
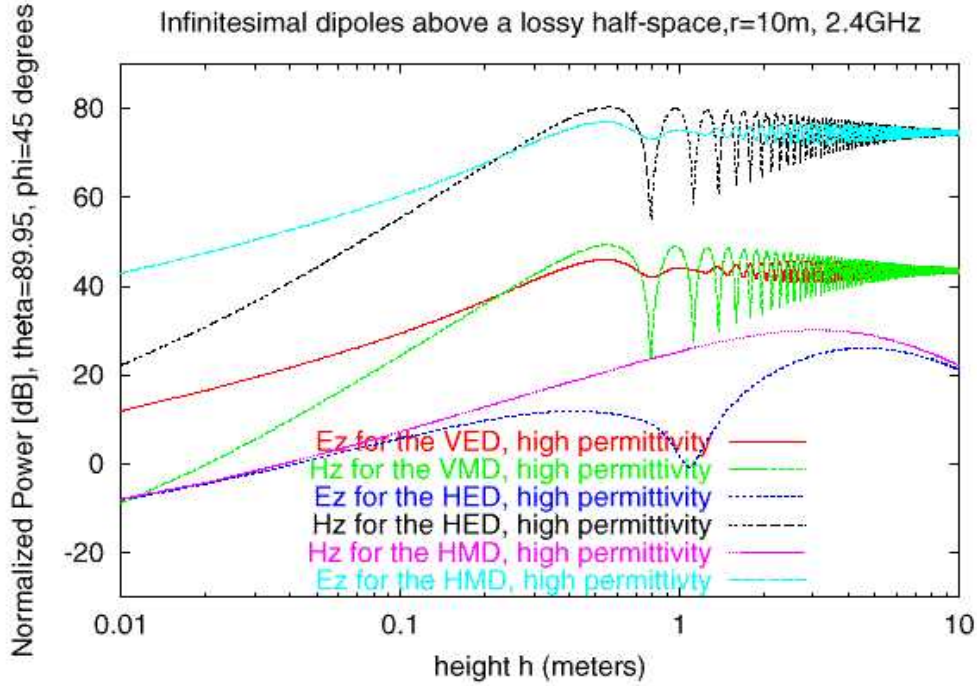


**Figure 14: Dipole fields as a function of dipole height at ten meters.**
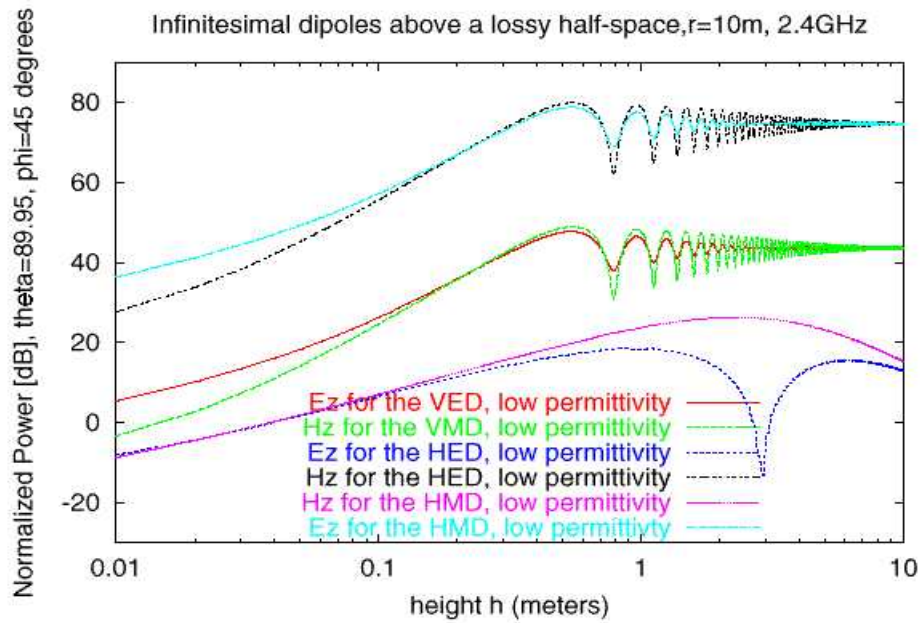
**Figure 15: Dipole fields as a function of dipole height.**
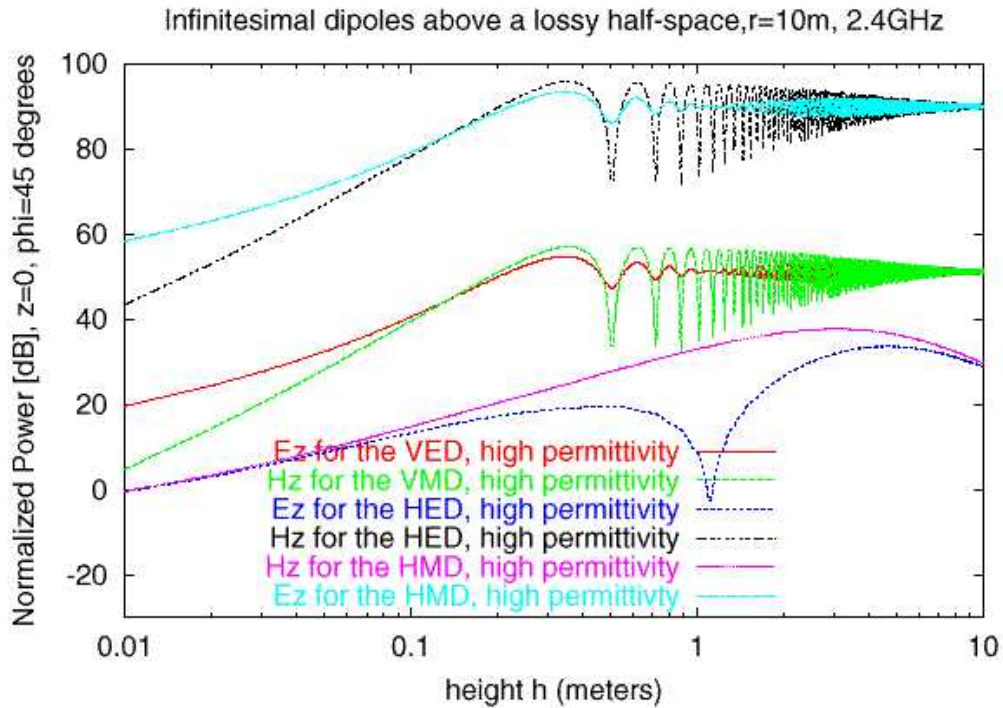


**Figure 16: Dipole fields along the ground as a function of dipole height.**

28
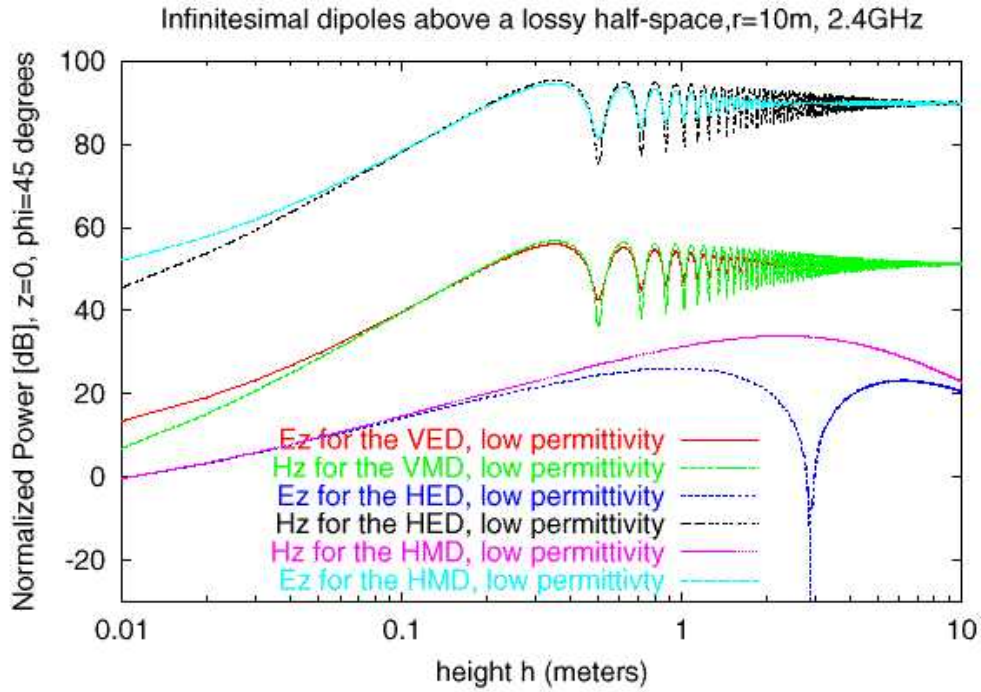
**Figure 17: Dipole fields along the ground as a function of dipole height.**

The pattern due to each of the dipole components at a distance of 10m and a dipole height of 2cm as a function of observation angle is shown in figures 18 and 19. The figures demonstrate the intensity level of each dipole both along and away from the ground for the high and low permittivity grounds. It is interesting to note in these figures the improved radiation near grazing (θ approaching 90 degrees) of the HMD and VED over the HED and VMD respectively.

29

Infinitesimal dipoles 2cm above a lossy half-space, 2.4GHz
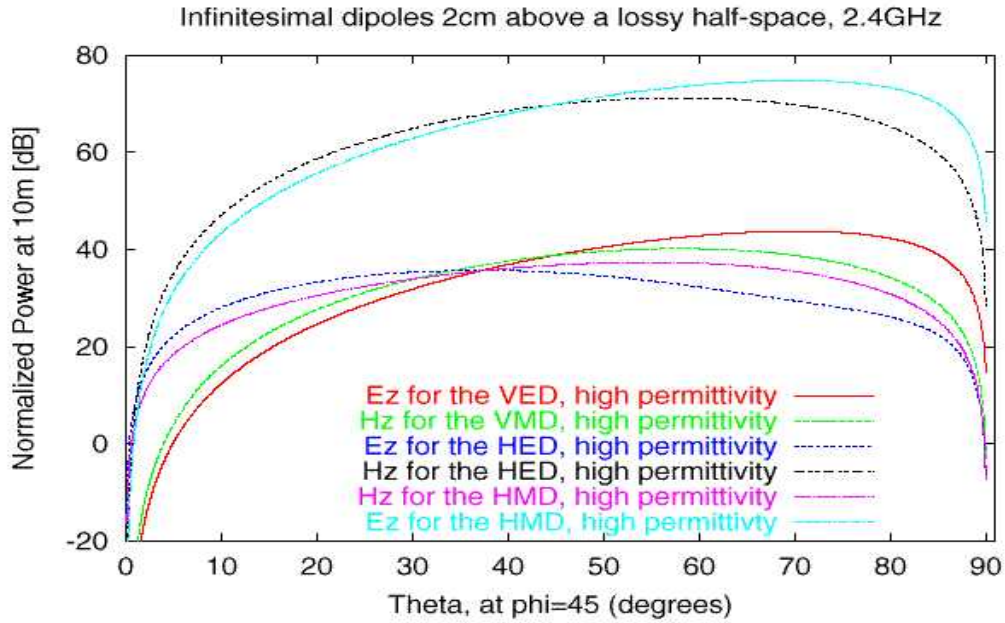


**Figure 18: Dipole fields as a function of observation angle.**

Infinitesimal dipoles 2cm above a lossy half-space, 2.4GHz
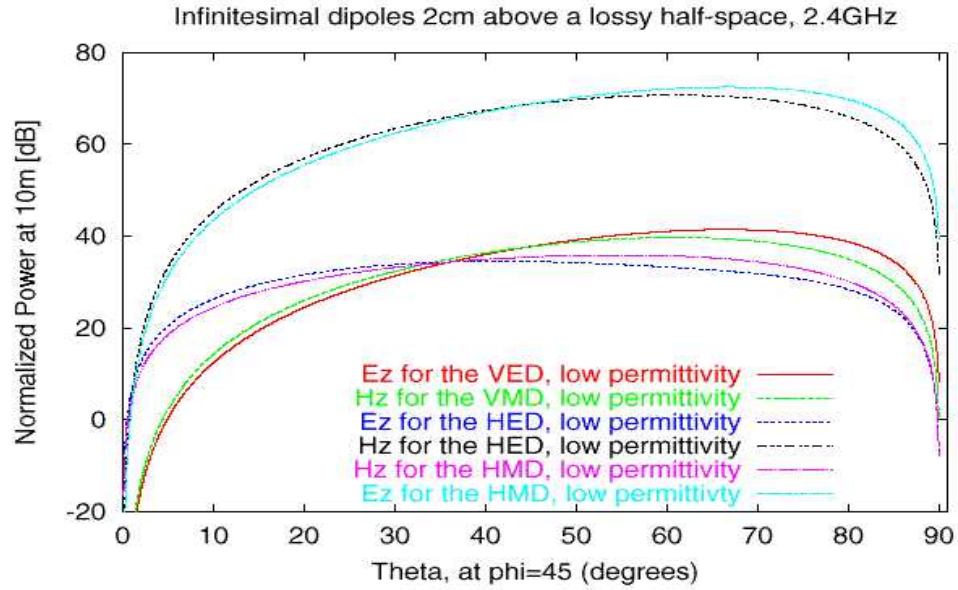


**Figure 19: Dipole radiated power as a function of observation angle.**

Through comparing the analytic solution for the vertical and horizontal electric and magnetic dipoles the predicted response over a flat lossy earth has been shown. The fall off at 2.4GHz for each dipole element has been demonstrated to be between $1/r^3$ and $1/r^4$ (in power) with some fluctuations as the permittivity of the soil is changed. Generally this slope held constant for the primary fields radiated form each component however.

To improve the radiation characteristics along the ground raising the dipole and/or observation point by even a few centimeters was seen to make a substantial difference. In addition, in comparing the radiating elements, for propagation along the ground, the VED and HMD, or antennas that may be constructed out of a superposition of these dipoles, seem to provide the highest fields near grazing.

In conclusion the physical nature of an antenna radiating over a lossy earth was accurately modeled at 2.4GHz and 5.8GHz as a sum of geometric optics terms corresponding to incident and reflected rays. The attenuation of the radiated power due to these components was explored as function of observation angle, antenna height, and distance from the source in the range of 1 to 100 meters. The importance of raising the antenna off the surface of the earth, even by a few centimeters, and the characteristics of the four canonical radiating elements over a layered medium was demonstrated.

# PROPAGATION MODELING SOFTWARE

In addition to comparison with a simple two ray physical model, Commercial ray tracing software incorporating multiple reflections off individual scatterers and surfaces was also utilized to investigate scattering off rough surfaces. Specifically, Remcom's Wireless Insight software was utilized to compare with the influence of surface roughness seen in the measured data, particularly to analyze the expected impact of the environments surface roughness as a function of frequency.

## SURFACE VARIATION EFFECTS ON PROPAGATION

Remcom's Wireless Insite is a simulation tool designed to model the effects of buildings and terrains on the propagation of electromagnetic waves. In the past month, this software has been used to model the physical characteristics of the rough terrain. Specifically, the effects of surface variation were investigated on the path loss of electromagnetic signals.

Several simulation runs were made with different surface variation of the terrain to observe the effects on signal propagation. The software allowed modeling of terrains with different degrees of variation by subdividing the terrains into different number of facets. Associated with each facet are values that can be assigned for the surface heights. For the purpose of this analysis, the heights were set with continuous random variations from 0 to 0.05 meters. The number of subdivisions in the terrain is directly related to the degree of variation. For comparison, terrains were created with 5 by 5, 10 by 10, 50 by 50, and 100 by 100 subdivisions on a 1 kilometer by 1 kilometer square area, with the 100 by 100 subdivided terrain having the greatest surface variation.

Three frequencies in the three ISM bands, 904MHz, 2402MHz, and 5726MHz, each with bandwidths of 5Mhz, are used in the simulations. An ideal vertical-dipole antenna pattern is used with the antennas set at heights of 15 centimeters at both the transmitting and receiving ends. The ground type of the terrain has been modeled at each frequency with a relative permittivity of 4 and conductivity 0.001 S/m in the ray tracing software (corresponding to the software's model of dry earth).

The transmitter and receiver locations for each simulation run are fixed at one of two particular orientations in the terrain, as shown in figures 20 and 21. Two separate runs were made (labeled run #1 and run #2 in the figures) at 904Mhz, 2402Mhz, and 5726Mhz for each orientation, giving two simulation runs at orientation A and two simulation runs at orientation B for each waveform. Each run is distinct in that the random seeds used to generate the random surface heights are different. Consequently, the surface roughness of the terrains in the four runs (two at each orientation) for each waveform is unique. However, for a particular run and orientation, the random seeds used to generate the surface heights are the same for the three different frequencies being examined. For example, the surface variation in the terrains is identical for simulation run #1 with orientation A at 904MHz, 2402Mhz, and 5726Mhz. Albeit, different from the surface variation for simulation run #2. The intent of the different simulations is to investigate how random surface variations affect path loss.
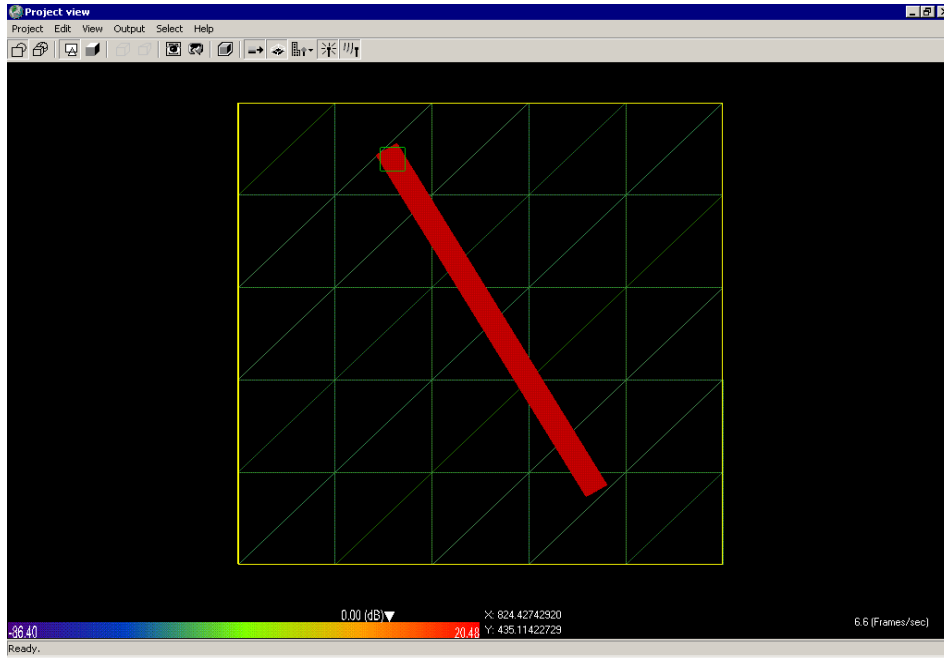
**Figure 20: Orientation A. Modeled with fixed transmitter and receiver locations. The red lines indicate the fixed receiver routes. The green square at the beginning of the route is the transmitter location. The yellow box encloses the terrain area.**
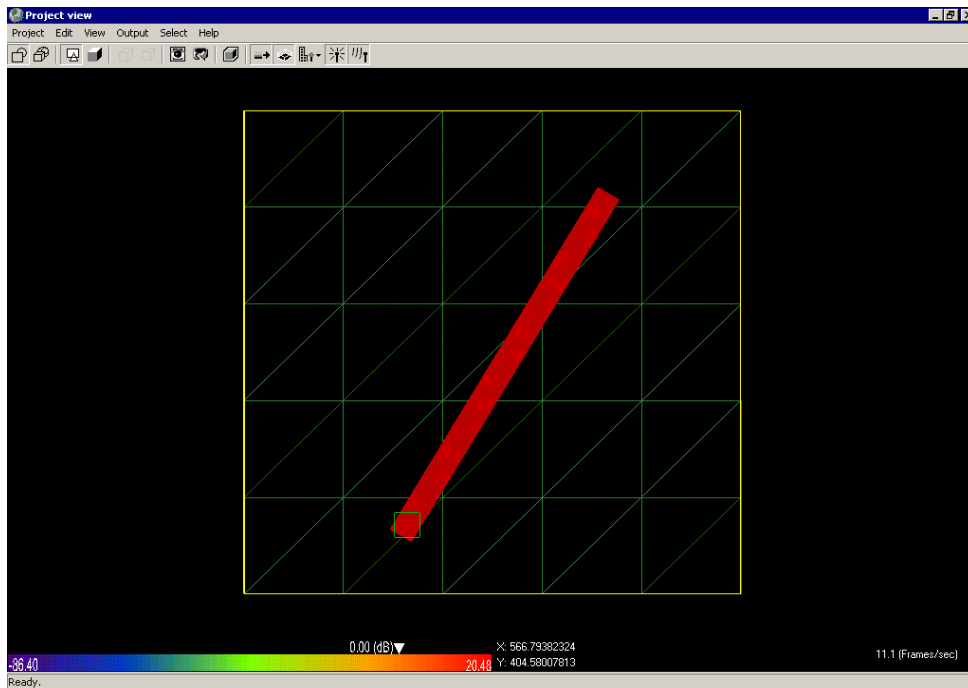


**Figure 21: Orientation B.**

Figures 22 to 33 are plots showing path loss versus distance for all three ISM waveforms. In all plots the path loss over a flat surface (with no surface variation) is also shown. Figures

24 and 25 demonstrate the increased scattering effects at 5726MHz with increasing variation in the terrain. The trend lines in these graphs deviate more from the no variation line as the variation in the terrains increases. The deviations from the no variation graph for the 5726Mhz waveform can be as much as ±3.0 dB. These observations are evident in all the simulation runs. In addition, we observe from the power levels in the graphs that the average signal strength is smaller as we increase the variation in the terrains. Moreover, at closer distances less scattering is observed in the terrains with less variation (10 by 10 cells) compared to the terrains with greater surface variations (100 by 100 cells). This phenomenon is easily understood since there are less surface variation (i.e. the land is fairly flat) at closer receiver and transmitter separation distances in the 10 by 10 terrain, since the distances between the surface variation (or vertices in context to the terrain file) are large relative to the 100 by 100 variation terrains. Lastly, the graphs reveal that at longer distances the signal strength is approximately 3dB smaller in terrains with variations than the terrains with no variation. Similar observations can also be made for the 904MHz and 2402MHz waveforms.

**5726 MHz:**

**Path Loss Vs Distance at 5726Mhz, 10x10 Variation**
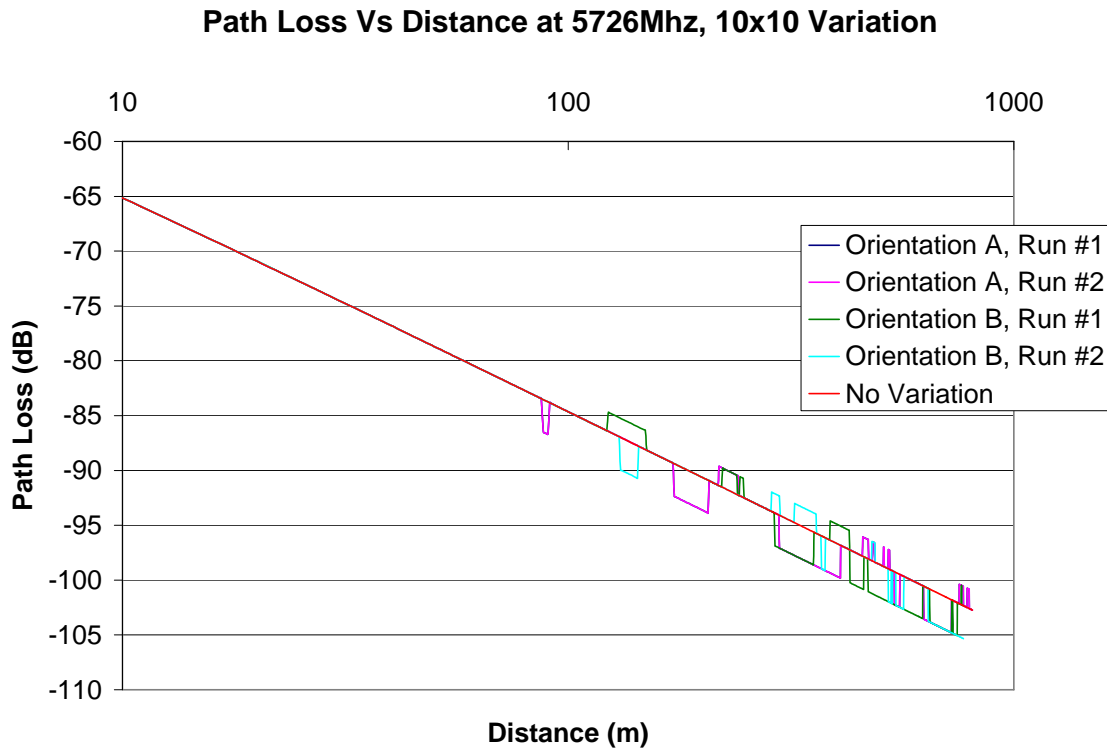


**Figure 22: 5x5 variation at 5726MHz.**

**Path Loss Vs Distance at 5726Mhz, 10x10 Variation**
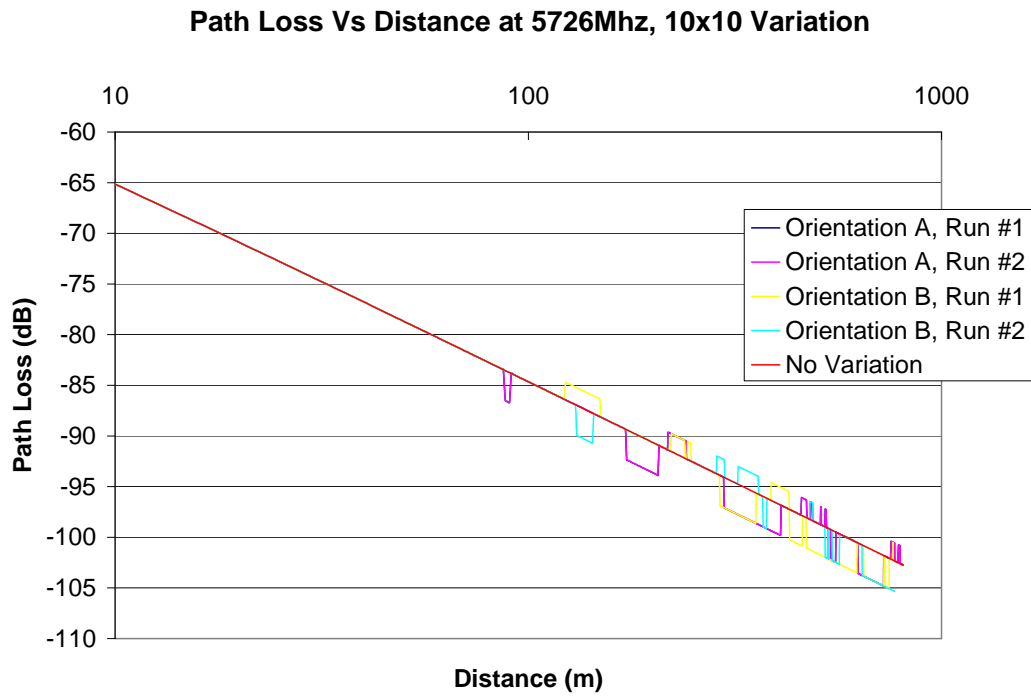


**Figure 23: 10x10 Variation at 5726MHz**

**Path Loss Vs Distance at 5726Mhz, 50x50 Variation**
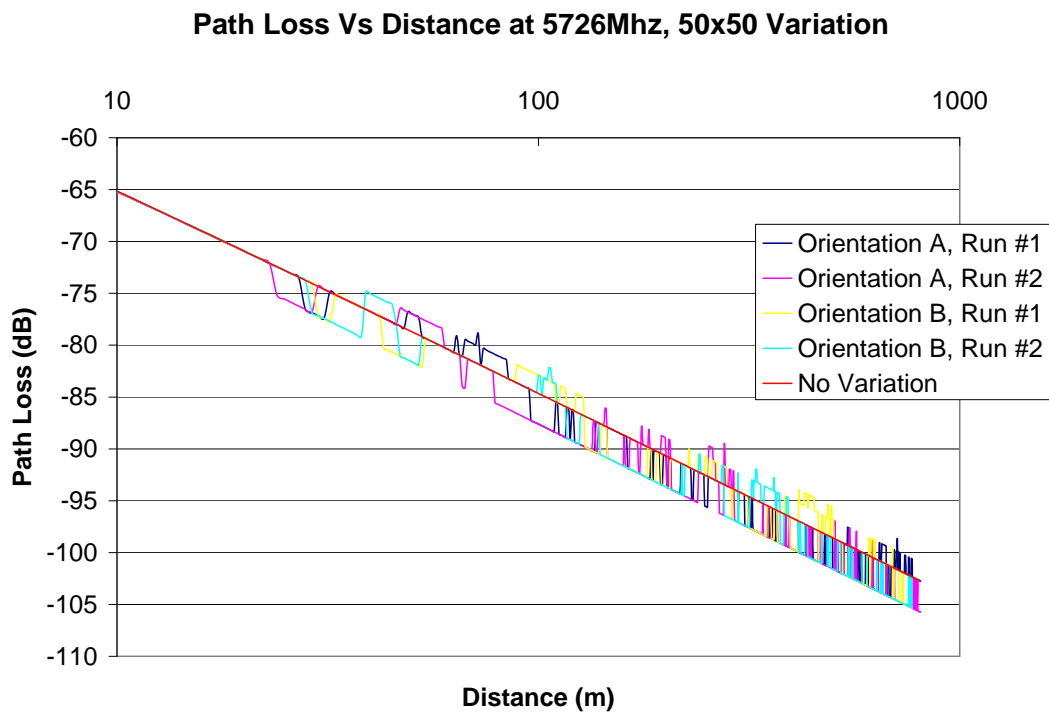


**Figure 24: 50x50 variation at 5726MHz.**

**Path Loss Vs Distance at 5726Mhz, 100x100 Variation**
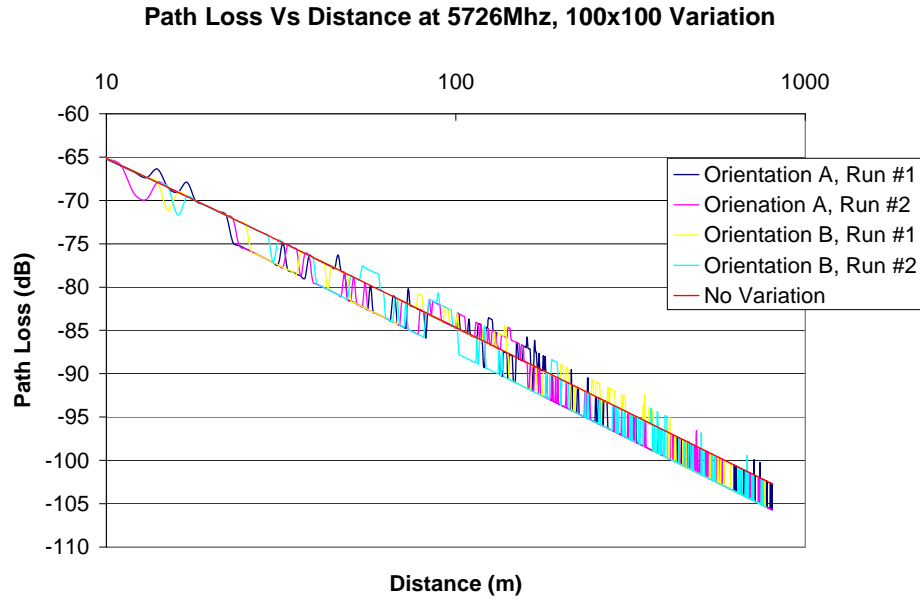


**Figure 25:** *100x100 Variation at 5726MHz.*


**2402 MHz:**

**Path Loss Vis Distance at 2402Mhz, 5x5 Variation**
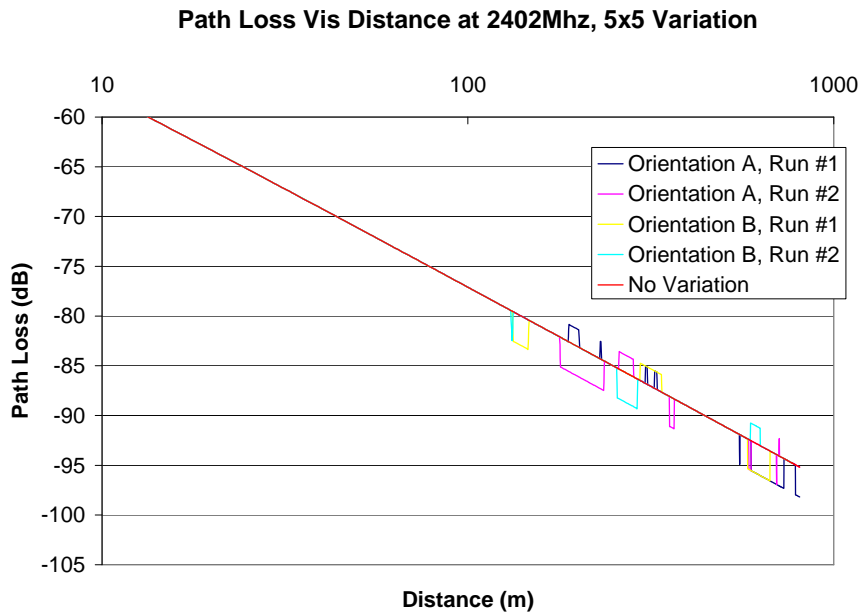


**Figure 26: 5x5 variation at 2402MHz.**

**Path Loss Vs Distance at 2402Mhz, 10x10 Variation**
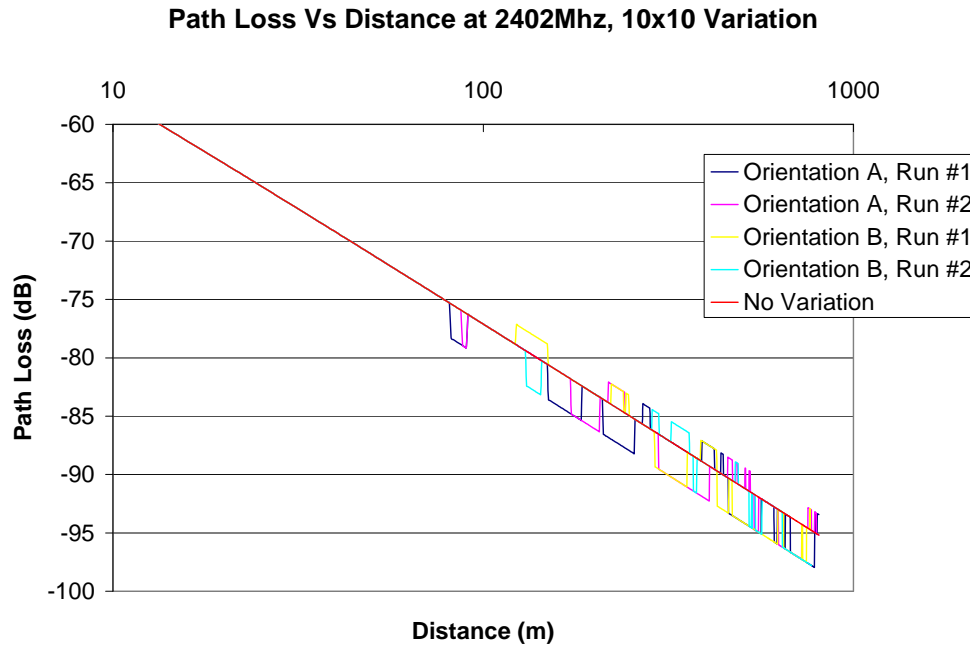


**Figure 27: 10x10 Variation at 2402MHz**

**Path Loss Vs Distance at 2402Mhz, 50x50 Variation**
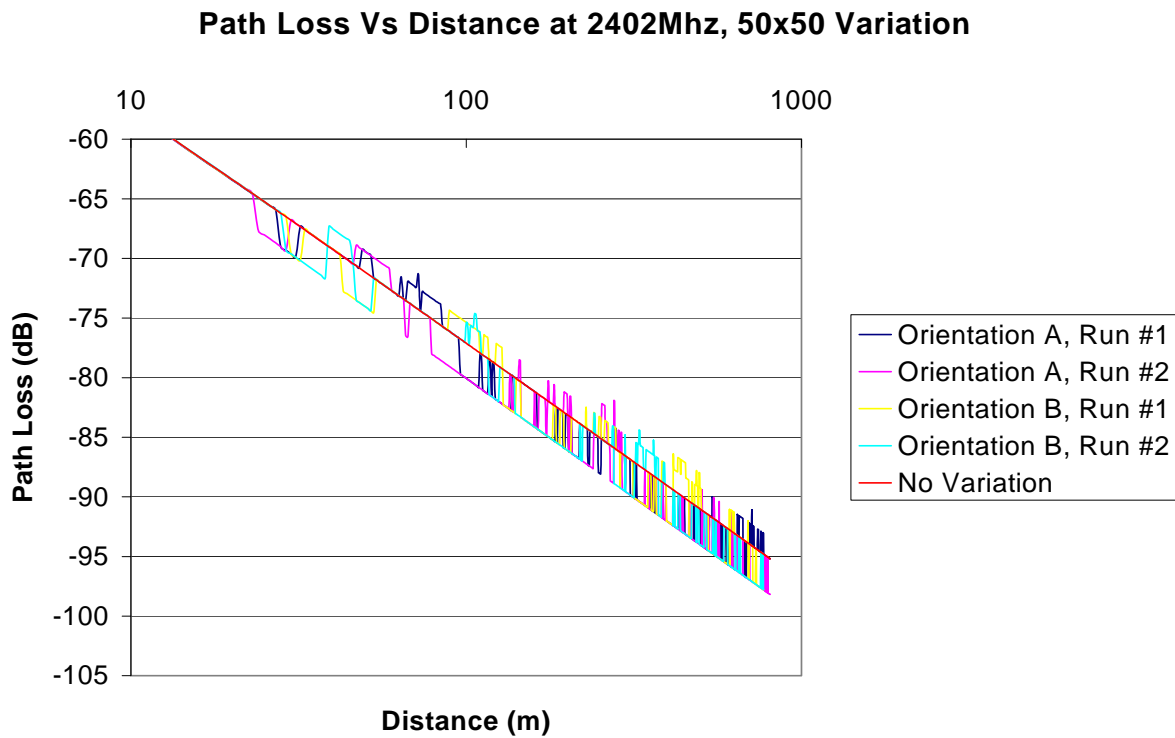


**Figure 28: 50x50 variation at 2402MHz.**

**Path Loss Vs Distance at 2402Mhz, 100 x 100 Variation**
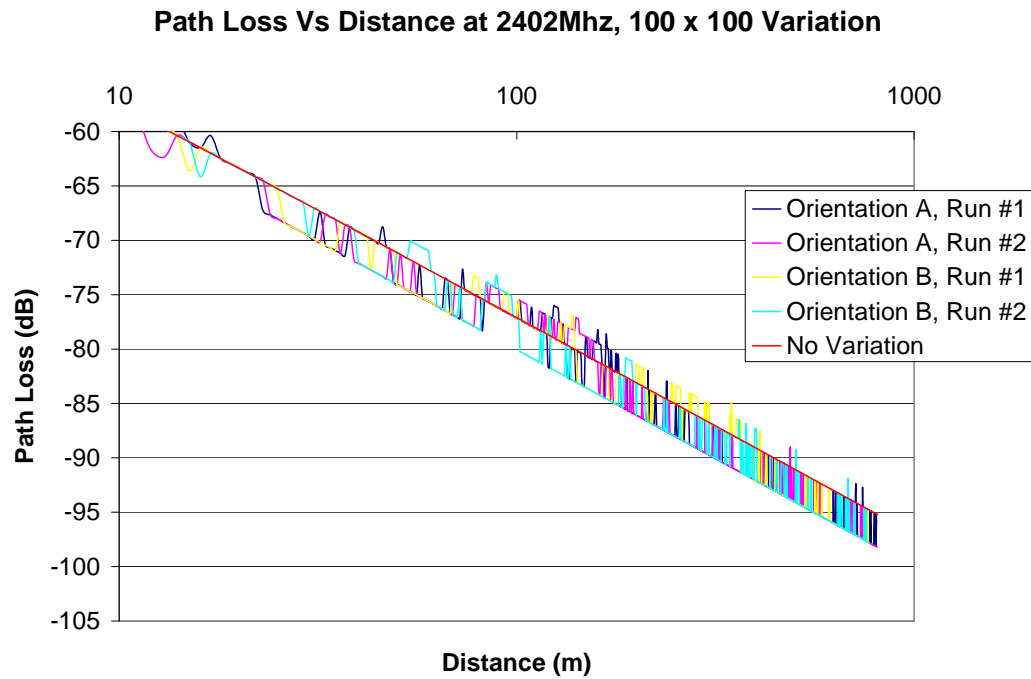


**Figure 29: 100x100 Variation at 2402MHz**

## 904MHz:

**Path Loss Vs Distance at 904Mhz, 5x5 Variation**



**Figure 30: 5x5 at 904MHz.**

**Path Loss Vs Distance at 2402Mhz, 100 x 100 Variation**
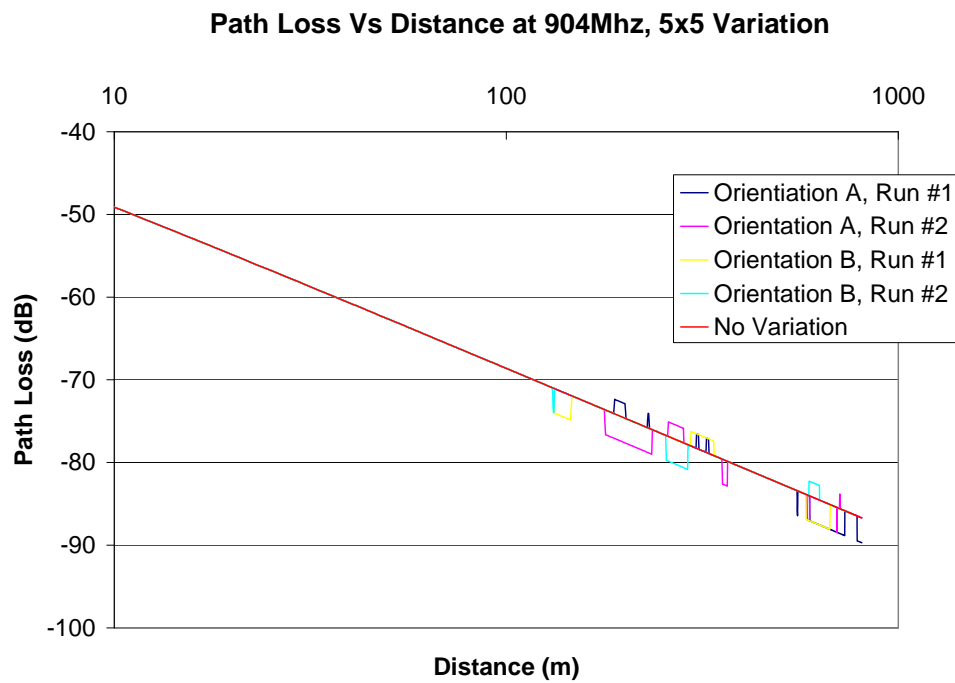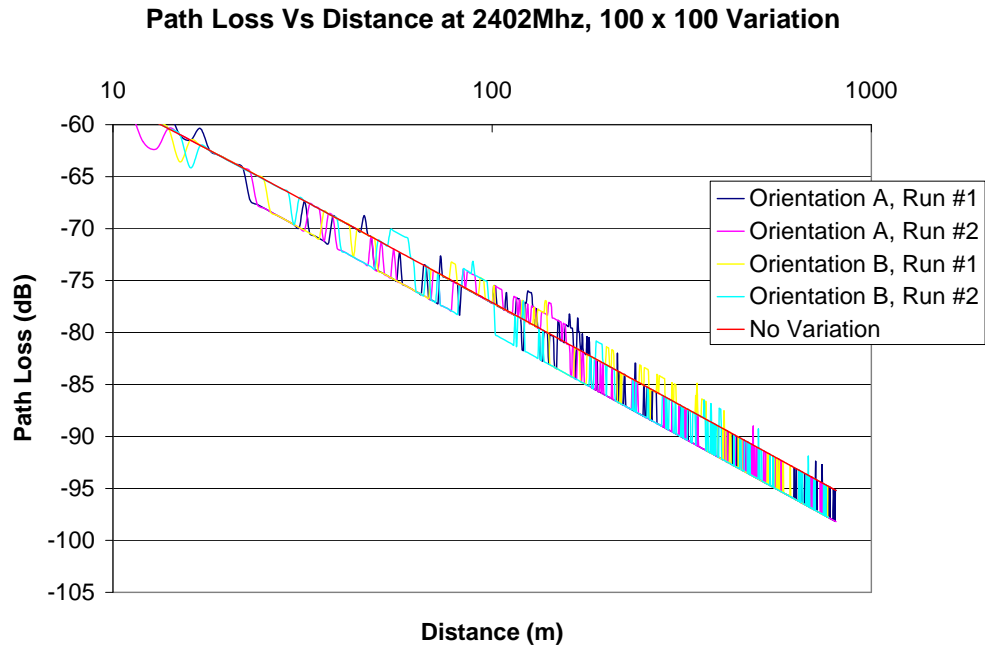


**Figure 31: 10x10 Variation at 904MHz**

**Path Loss Vs Distance at 904Mhz, 50x50 Variation**
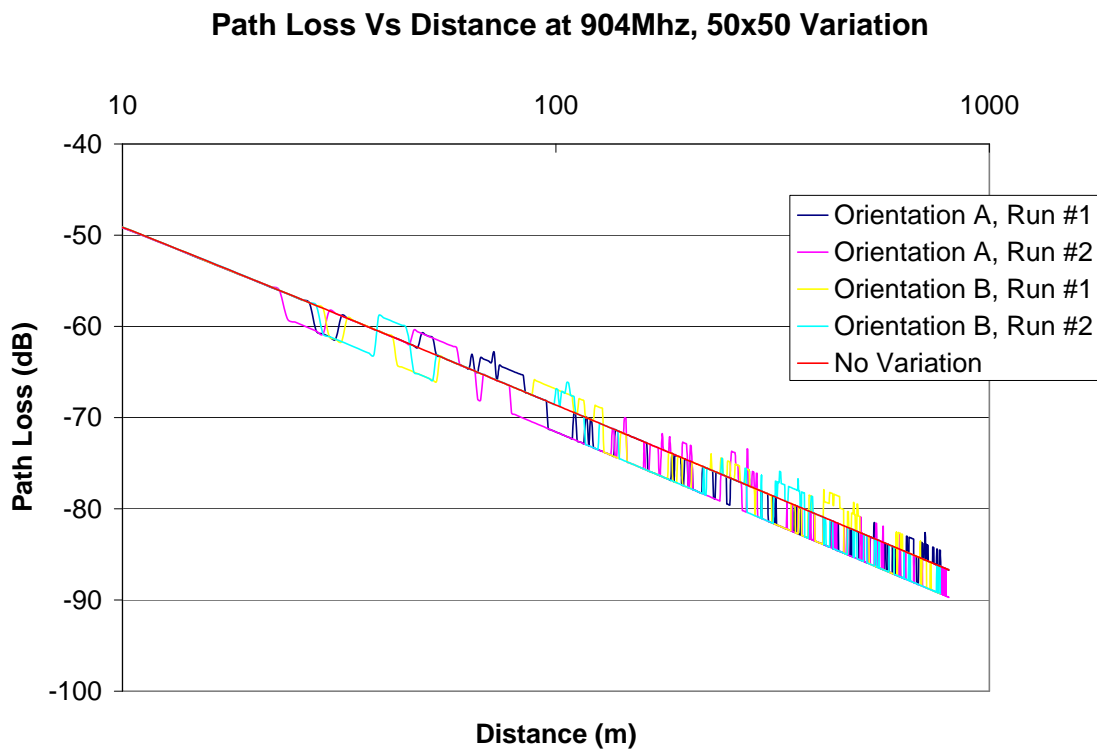


**Figure 32: 50x50 variation at 904MHz.**

**Path Loss Vs Distance at 904Mhz, 100x100 Variation**
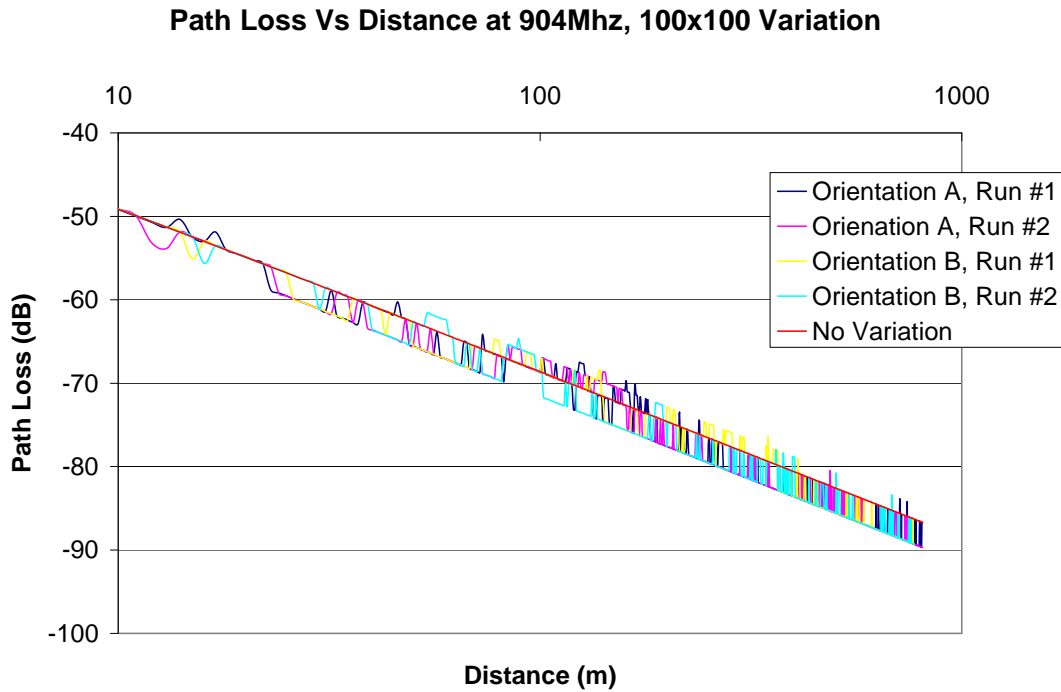


**Figure 33:  100x100 Variation at 904MHz**

Numerical modeling of the influence of surface roughness within a scale of 5cm demonstrates levels within ±3dB of variation. In addition these preliminary findings seem to indicate that the surface roughness does not play a substantial role in decreasing the overall path loss though a limit of the strength of the ground bounce ray in the two-ray analogy. Thus the decrease in path loss described in the results in this report at short ranges seen in the vegetation and urban environments is the result of elevated scatterers and not a result of increased surface roughness, since in the surfaces modeled increased surface roughness is seen to have both a positive and a negative impact on path loss.

# PROPAGATION STUDIES: INITIAL MEASUREMENTS

To assess the variety of environment seen by a network of PicoWINS tags, and for tag-to-munition RF link, measurements over a flat grassy field, over a flat asphalt surface, and in a cluttered indoor environment were initially collected to with a single radio system. In all these initial measurements the same 2.4GHz system was utilized which provided average spread spectrum received signal strength over 10 frequency hops and over 1000 frequency hops in the 2.4GHz to 2.4875GHz ISM band. Comparison of the asymptotic half-space solution over the grassy field, and $r^{-\alpha}$ fall off with $\alpha$ from 2 to 4, is demonstrated, prior to the broader empirical study provided in the next section. The substantial influence of antenna height off the ground and importance of cancellation of the incident and reflected term fields along grazing are shown.

The measurement system used consisted of two hand-held units of the type shown in figure 34. In this system the antenna and radio are attached as a separate module to enable emulation of arbitrary tag placement. Frequency hopped spread spectrum radios were used with 20ms hop duration and 750kHz bandwidth allotted to each hop in a pseudo random sequence spaced throughout the 2.4GHz to 2.485GHz ISM band. The receivers had a –93dBm sensitivity, the channel capacity was set at 460kbps and the transmit power was selectable as either 10mW or 100mW. Shown in figures 34 and 35 is the configuration with a patch antenna used for the majority of measurements, however measurements with a dipole antenna attached to the radio were also conducted.



**Figure 34: Measurement system used to obtain received signal strength. Unit shown operates as either a transmitter or a receiver, with the real time interface visible on the PDA. The antenna and radio are attached separately with a five-foot cable.**

Measurements of Tag to Tag and Tag to Munition propagation were performed by operating multiple 2.4 GHz transceivers at distributed locations with a 2.4 GHz transceiver operating as a Tag and being worn by an individual at boot level. In this case, the Tag, attached at boot level at a point 10 cm above the surface. Corresponding transceivers were distributed at the surface and at an elevation.
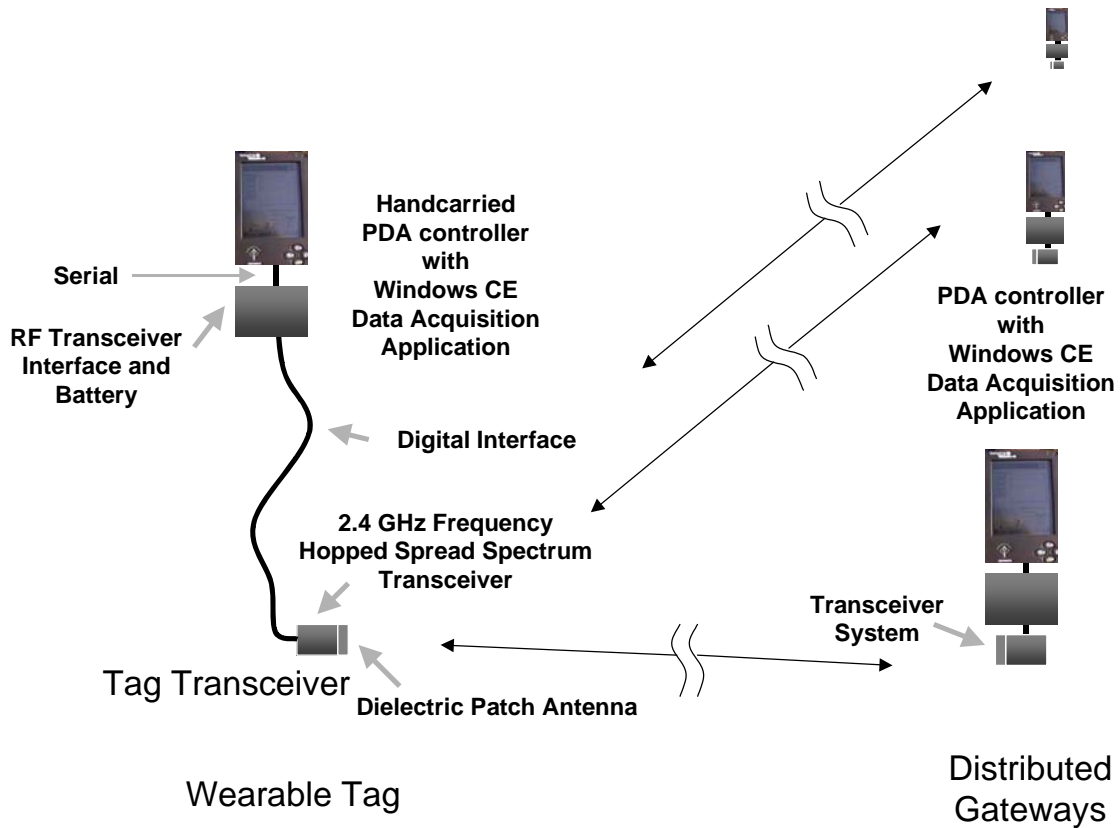
**Figure 35: The PicoWINS Tag Field Test System. The Tag PDA controller is packaged with a RF transceiver interface and a battery pack. This is, in turn, in communication with multiple transceivers over a digital link. The Gateway is a second compact package placed directly on the surface. This system is now operating in a networked fashion that permits many simultaneous measurements to occur.**

The first measurement environment considered was a flat grassy covered soccer field. Measurements were taken in two directions from a central transmission point with both the patch antenna and the dipole antenna. The resulting data is shown in figures 36 and 37. In each case the radio and antenna were set on the ground resulting in an antenna height of 1cm for the dipole (the base of the dipole) and 1cm for the patch (1cm from the ground to the center or patch feed). In figure 36 three measurement scenarios are shown. Measurements with a transmit power of 10mW in two directions away from the transmitter, and measurements with 100mW transmit power. The two directions are considered to demonstrate the homogeneous nature of this uncluttered environment. Each data point in figure 36 and 37 represents an average over the signal strength recorded in one thousand frequency hops. Also shown in these figures is a simple power law fit of the form $P=aR^{-\alpha}$ and the resulting predictions from numerically solving the Sommerfeld integral for a low permittivity soil case ($\varepsilon=3$, $\sigma=0.1$) and a high permittivity case ($\varepsilon=20$, $\sigma=0.5$). In each case the Sommerfeld integral solution is equivalent to the geometric optics solution considering only the incident and ground reflected fields.
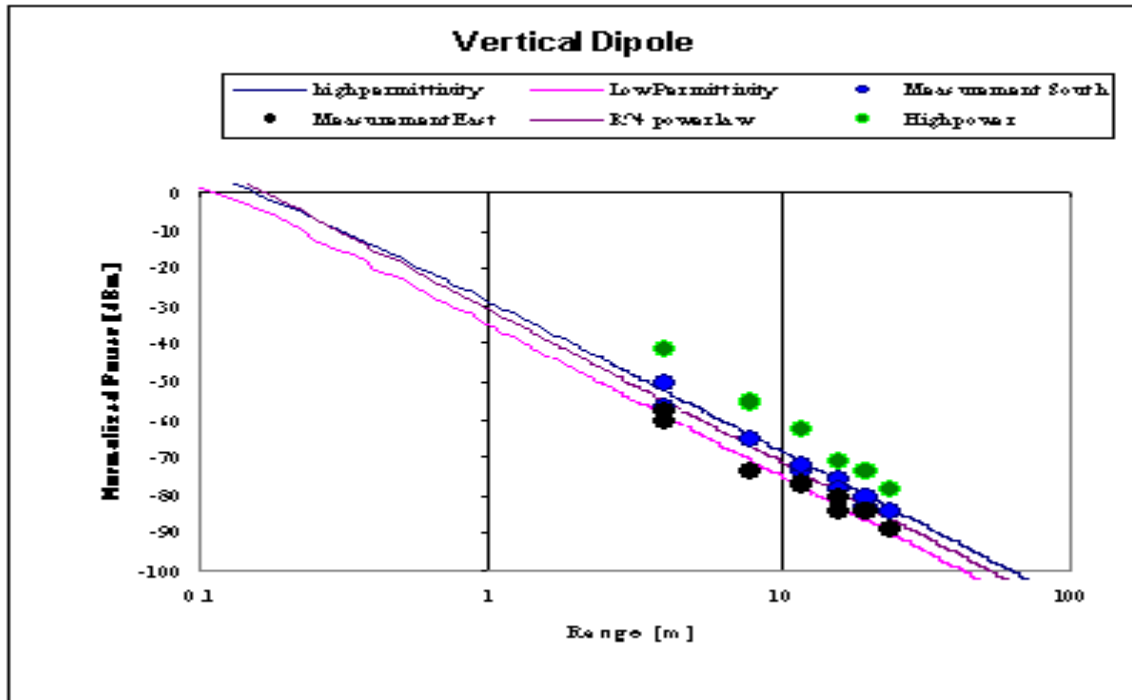
**Figure 36:Measured signal strength with monopole antennas at a base height of 1cm above a flat field.**
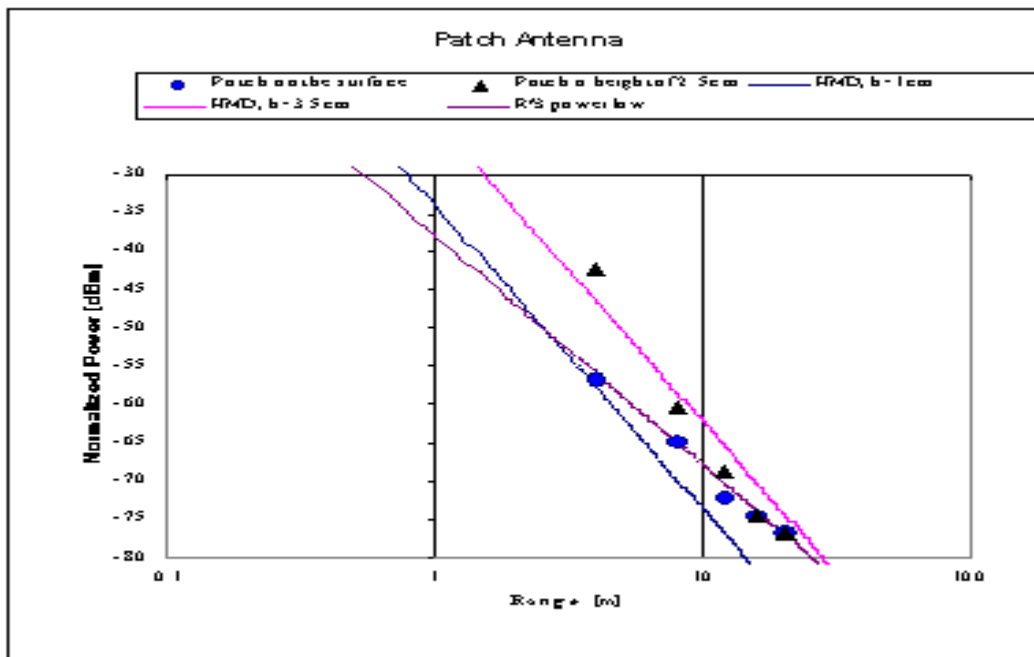


**Figure 37: Measured signal strength with patch antennas at patch center height of 1cm above a flat field.**

Additional measurements were taken in more cluttered environments. First measurements were taken in the outdoor environment shown in figure 38. Multiple trials were considered with the transmitting antenna placed approximately 1cm above the ground and the receiving antenna located at a persons boot height or waist height as they walked along a trail that snaked past the transmit point. The location of the receive antenna at both boot and waist height are shown in figure 39. In these measurements a path (faintly visible in figure 38) snakes past the transmit location. At the nearest point the path is 16 feet from the transmitter. During the path length measured on the path changes elevation by approximately 30 feet. The measured results (ten frequency hops per point shown in figure 40) demonstrate the substantial fading observed as well as the limited range of approximately 25m seen along the path. In addition a consistent 15dB increase is seen in moving from foot level to waist level for the receiver.



**Figure 38: View from the transmitting location of an outdoor cluttered environment.**

**Figure 39: Receiving antenna location at boot level and waist level in a cluttered outdoor environment.**
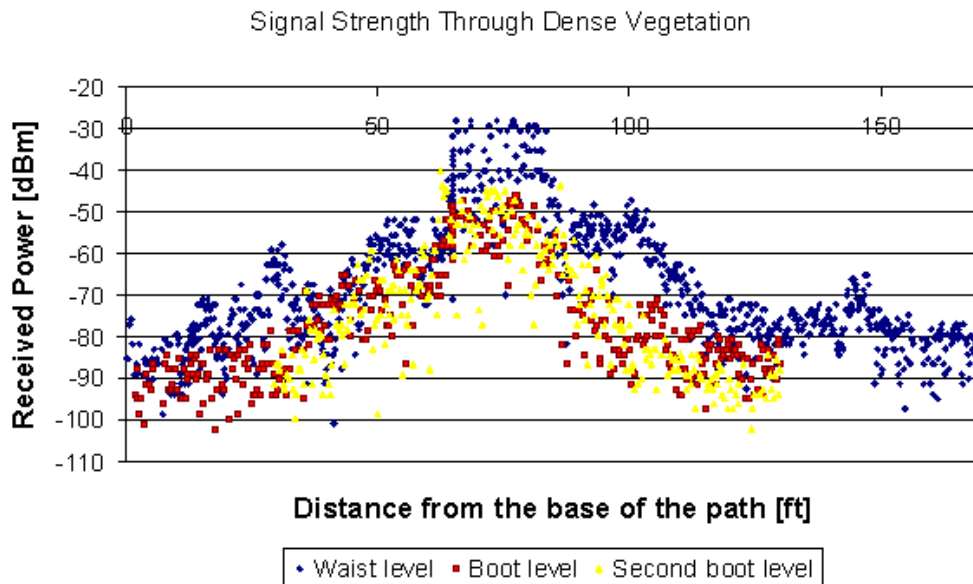


**Figure 40: Received signal strength as a function of distance from the nearest point on the path to a transmitting antenna.**

Additional measurements were taken in an indoor cluttered environment to demonstrate the fading levels seen. Shown in figures 41 and 42 are pictures of the office environment used, showing the office considered from each corner. The office was an approximately 4000 square foot facility located on the third story of a three-story complex. The measured data is then shown in figure 43 along with an average over the last 10 points or 2 seconds. Measurements were taken with the transmitting antenna located on the floor in the approximate center of the office

and the receive antenna attached to a person at boot level as they walked slowly circled from one side of the office to the other reaching a maximum distance of approximately 20m from the transmitter.



**Figure 41: View of office environment used for indoor propagation testing from one end of the central office space.**



**Figure 42: View from the opposite corner of indoor environment considered for testing.**
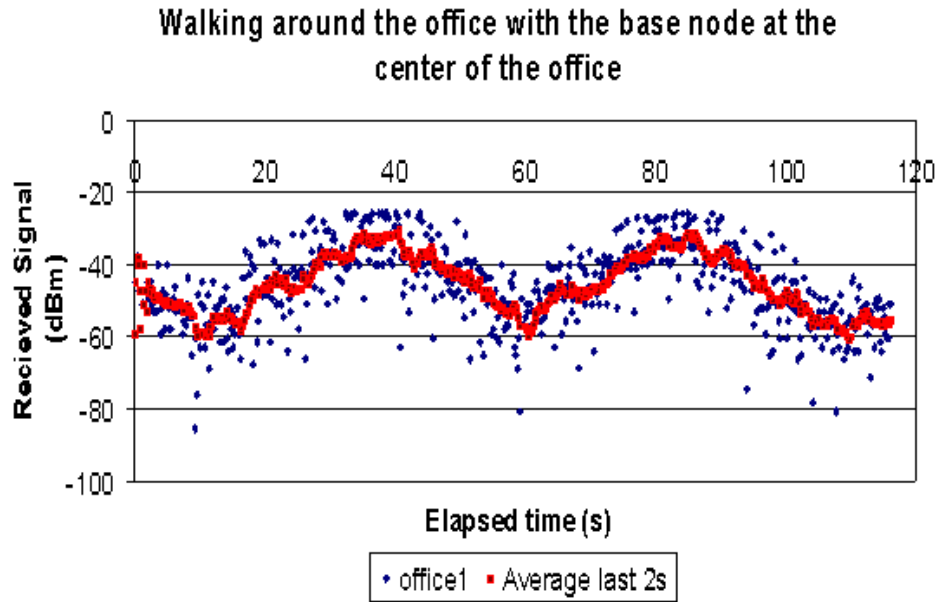
**Figure 43: Measured indoor signal strength for a stationary transmitter at the center of the office and a figure eight loop made around both sides of the office.**

The measurement environments considered demonstrated substantial clutter for the frequency hopped 2.4GHz ISM band radios. Worst-case range with both transmitter and receiver on the ground was approximately 25m with 100mW of transmit power. In addition substantial variation in the power law fit of the propagation fall off was seen although never worse than $\alpha=4$. In addition in the preliminary environments considered even with non-line-of-sight the propagation fall off approached $\alpha=4$ as a worst case as multi-path scattering in conjunction with frequency fading provided a similar range fall off as the cancellation of the incident and ground reflected geometrical optics terms of the Sommerfeld (uncluttered) lossy half-space solution. To further investigate the propagation as a function of range, a number of additional uncluttered environments were considered at angles away from grazing.

### DEVELOPMENT OF PICOWINS TAGS: PICOWINS TAG RF PROPAGATION MEASUREMENTS FOR THE TAG TO MUNITION GUIDANCE LINK

The propagation of signals from Tag to Munition are critical for design of a homing munition system. In order to investigate the propagation characteristics between a PicoWINS tactical Tag and an incoming munition a number of measurements have been conducted between 2.4GHz FHSS wireless RF modems in which one modem was attached to personnel (as for a Tag) and another was elevated above the surface to establish an angle of propagation.

Now, of course, in free space the propagation loss between two radios should vary as $1/R^2$. In the presence of strong reflections off the ground (cancellation at grazing) and of multi-path (the line of sight signal does not dominate) this propagation falls off according to a power law decay rate approaching $1/R^4$. However, at angles increasing away from grazing (for which cancellation of the incident and reflected components of a propagating wave is not necessarily the case) particularly when a line of sight path exists, $1/R^2$ range dependent path loss is expected. This is the case expected for a munition homing on a tag either attached to a target or the ground.

An experimental apparatus was implemented to provide a means to measure propagation at constant angle between Tag and Munition RF Modem. This was accomplished by raising an RF modem to a height (using a cable apparatus) that varied with the range between Node and Munition. This provided a system having variable range, but, a fixed angle of propagation. Results for this measurement are shown in figure 44.



$$P[mW] = 0.003r^{-2.8474}$$
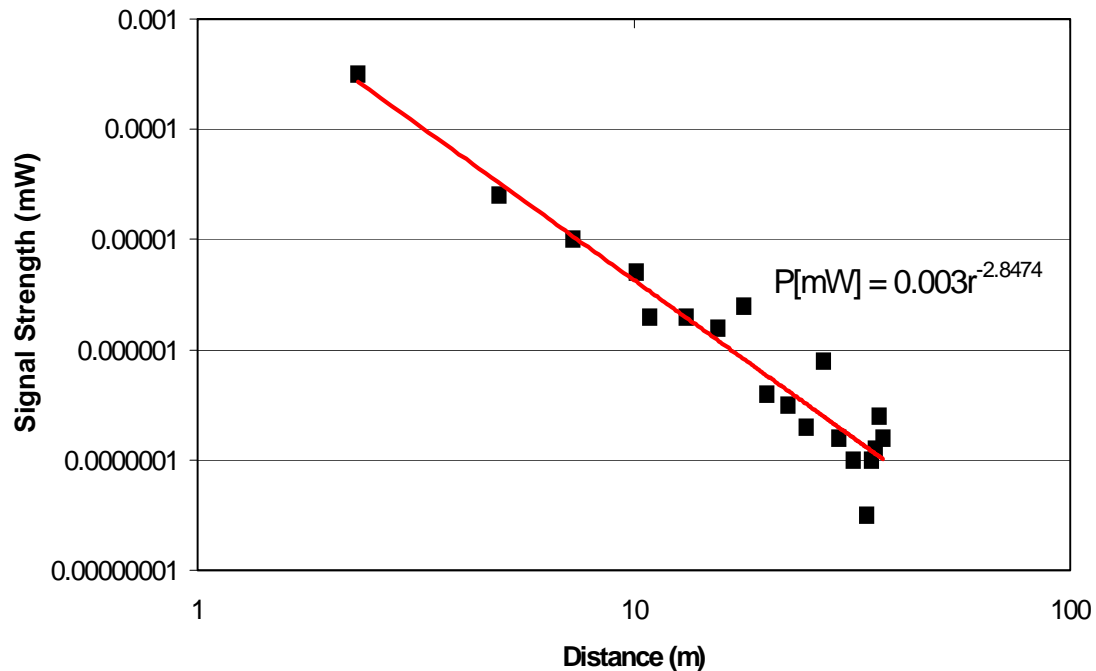
**Figure 44.  Measured signal propagation for the Tactical Tag to Munition link.  Angle of propagation relative to the earth's surface is 79 degrees.**

### PROPAGATION AT ANGLES AWAY FROM GRAZING

In order to investigate the propagation characteristics between a PicoWINS tactical tag and an incoming munition a number of measurements have been conducted between 2.4GHZ FHSS wireless radios in which one radio was elevated off the ground. Theoretically in free space the

propagation loss between two radios should vary as $1/R^2$. In the presence of strong reflections off the ground (cancellation at grazing) and of multi-path (when the line of sight signal does not dominate) this propagation falls off up to variation approaching $1/R^4$. However, at angles increasing away from grazing (for which cancellation of the incident and reflected components of a propagating wave is not necessarily the case) particularly when a line of sight path exists $1/R^2$ fall off is expected. This is the case for a munition homing in on a tag either attached to a target or on the ground.

Measurements in three environments have been first conducted to investigate the propagation fall off between antennas at angles above grazing. The first environment was a sandy beach with one radio placed atop a wooden pier. Measurements were conducted with the second radio at various distances from the pier along the beach. Shown in figure 45 is the variation with distance of the received signal strength when the first radio was both on top of the pier, and on the beach next to the pier (grazing angles). Also shown in the figure is a power law fit to the measured points. It is interesting to note that the power law fit to the measured data when the first node is on top of the pier falls off more quickly than the case at grazing. This can be understood since the pier height is constant, while the distance between radios is constantly increasing, thus as the distance increases the line of sight angle between the two radios approaches grazing and cancellation between incident and reflected signal components increase. As the angle approaches grazing the fall off approaches the beach-to-beach measurements.

A second set of measurements was conducted in a grassy park with a radio placed on top of an eight-foot high wall. In this environment there were a number of widely spaced trees in the park however, in all cases measured, a direct line of sight existed between the two radios. Measured values and the power law fit for a radio on top of the wall and on the ground next to the wall versus distance to a second radio on the ground are shown in figure 46. Similar variation as on the beach is seen in this case. Again as the line of sight angle increased the values for the elevated case approached those for the grass-to-grass measurements. In order to verify the supposition that the increased rate of fall off versus distance seen in figures 45 and 46 for elevated antennas can be explained in terms of the changing incidence angle (and as a result does not counter the expectation of $R^2$ propagation at angels away from grazing) measurements were also taken at a constant angle between the two transceivers.

49
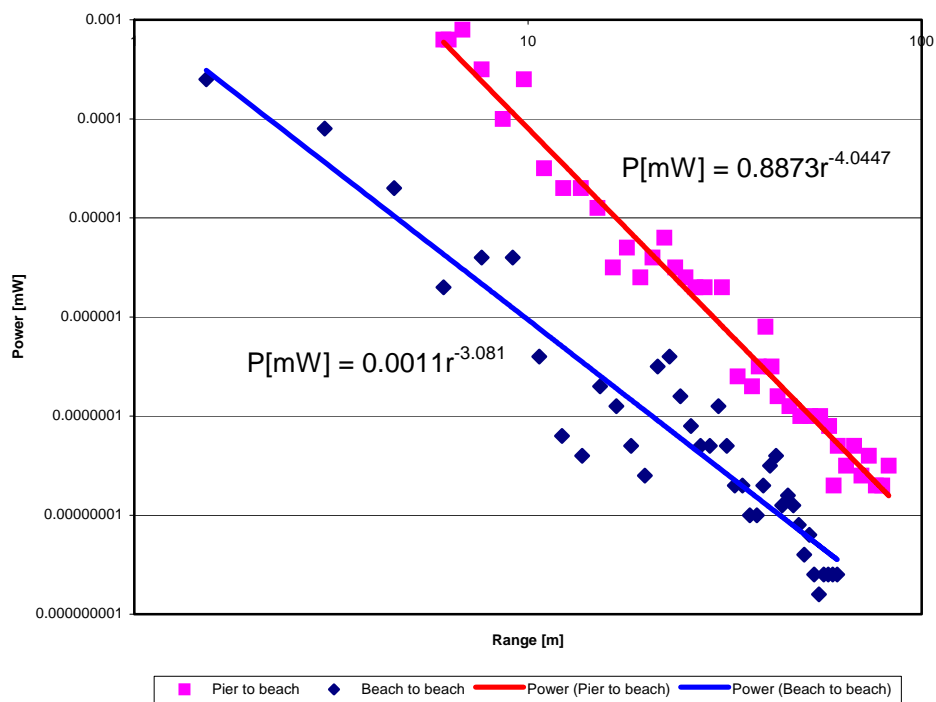
**Figure 45: Measurements on a sandy open beach.**

**Propagation in a grassy park**
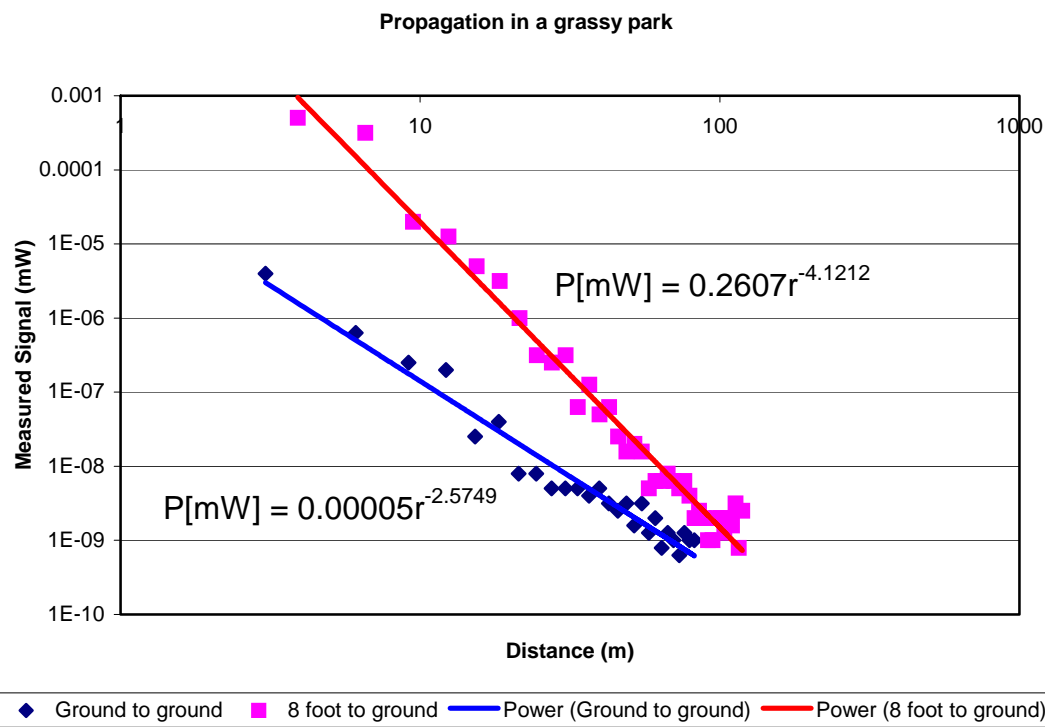


**Figure 46: Measurements from the top and base of a wall into a field with a sparse distribution of trees.**

The third measurement set was taken on a grassy baseball field. One radios antenna was placed on the ground while the second antenna was tied to a cord attached to the top of a metal light pole. This second antenna was then pulled up the pole as the first antenna was moved further away. In this manner a constant line of sight angle was achieved between the two antennas. Measurement results are shown in figure 47. As expected the severe fall off seen in the previous two figures (of constant non-zero height rather than constant angle) is not seen. Instead similar power law fall of was seen in both the elevated and non-elevated cases. The similarities may be understood in terms of incomplete cancellation between the reflected and incident field components even at grazing due to the inconsistency of the reflection coefficient with angle because of the uneven nature of the grass and presence of multi-path signals. The interaction of the incident and ground reflected fields is analyzed more thoroughly in the next section for this environment. When combined with the prior two figures these measurements demonstrate the increased range at non-grazing angles between two radios such as seen by an incoming munition. In none of the cases was pure $1/R^2$ variation with range seen, however in each case the environment was cluttered and particularly for the measurements on grass, when a line of sight existed between antennas it was approached as compared with the $R^{-4}$ response. In figure 47 the increase in exponent for the power law fit at a constant angle (11.3 degrees above grazing) as compared with grazing is counter intuitive, however more data is needed to make a definitive comparison of the grazing and non-grazing (constant incidence angle) cases. The validity of modeling the fields in this uncluttered field with incident and reflected ray terms is explored more thoroughly in the next section.

**Angle Dependent Propagation Loss**



$$P[mW] = 0.003r^{-2.8474}$$

$$P[mW] = 0.00002r^{-2.5735}$$

Legend: ■ Angle of 78.7 degrees   ◆ Grazing angle   —— Fit (78.7 degrees)   —— Fit (Grazing angle)
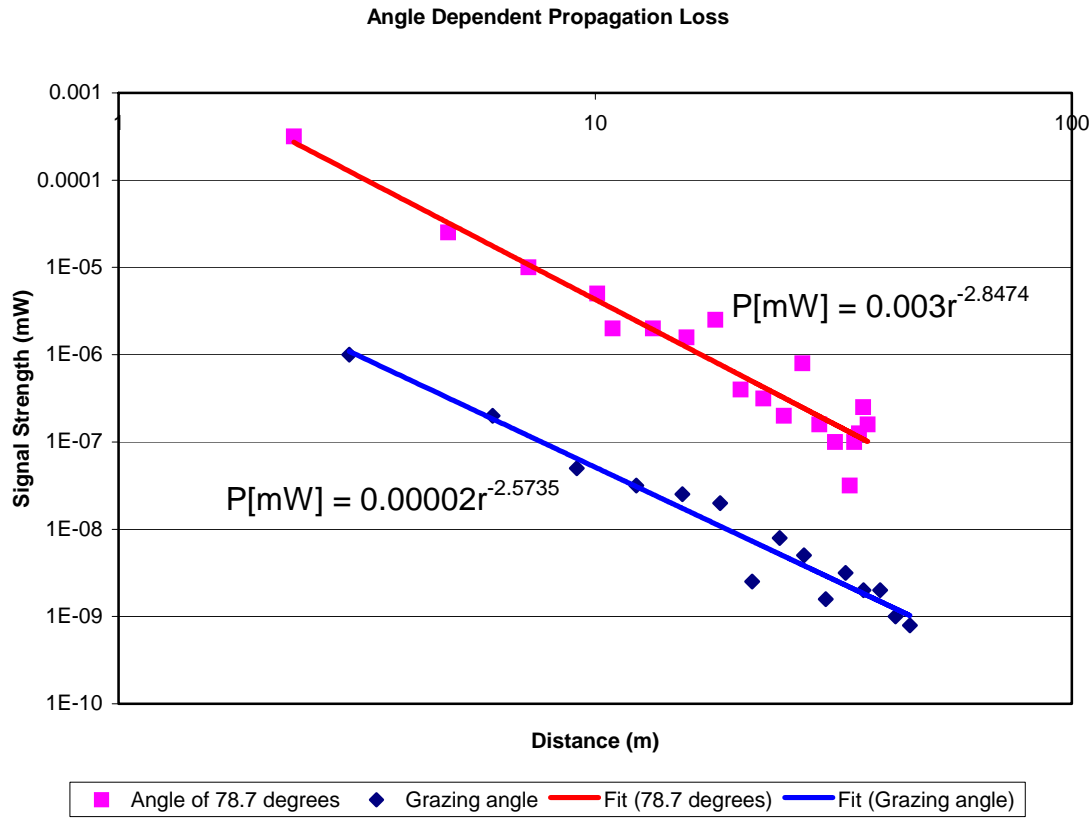
**Figure 47: Propagation at grazing and a constant angel of 78.7 degrees over a flat baseball field.**

In addition to measurements on a grassy field and over sand, a number of measurements were taken in a predominantly open parking lot environment moving out from the base of a multi-level parking garage. Figure 48 displays results for propagation tests in an environment with a dense (asphalt) ground surface. Transceivers were distributed at heights of surface, 3.9m, 5.5m, and 8.1 m. The surface-to-surface propagation link demonstrated the expected (Range)$^{-4}$ path loss power law. However, at elevated heights, and at range greater than 10m, the (Range)$^{-2}$ power law is seen. At this range, propagation behavior appears to join the free-space dependence. (It should be notes that for these range characteristics, propagation angle relative to the surface varies with range). For the case of 8.1 m, this angle varies from 53 to 24 degrees as range varies from 10m to 20m. For all heights, (and exploring a range of angles) the (Range)$^{-2}$ dependence is observed. Further analysis and measurements in additional environments are being planned.
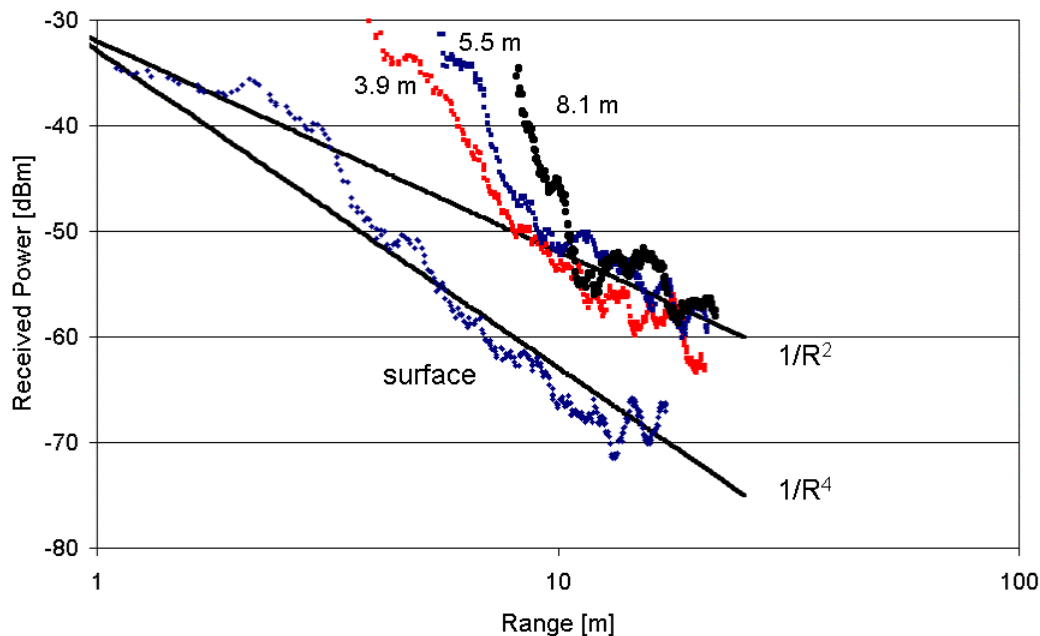
**Figure 48: Received power vs. Range for the link between a compact 2.4 GHz communicator (worn by personnel at boot level at a height of 10cm above the surface) and an communicator at the surface (as indicated) and a communicator located at an overhead location at various heights (as indicated). Angle of transmission relative to the surface varies with Range. This measurement was performed over an asphalt surface environment.**

**PICOWINS TAG RF PROPAGATION MEASUREMENTS FOR THE TAG TO MUNITION GUIDANCE LINK: SAND SURFACE CONDITIONS.**

Measurements of Tag-to-Munition propagation were performed by operating multiple 2.4 GHz transceivers at distributed locations with a 2.4 GHz transceiver operating as a Tag and being worn by an individual at boot level. In this case, the Tag, attached at boot level at a point 10 cm above the surface. Corresponding transceivers were distributed at the surface and at an elevation.

In the previous Monthly Report, Tag-to-Tag communication signal propagation was measured for standard soil and dense foliage conditions. Also, Tag-to-Munition links were measured over a dense asphalt surface.

In this period, Tag-to-Tag communication signal propagation was measured for the contrasting environment of sand surfaces and without vegetation.

53
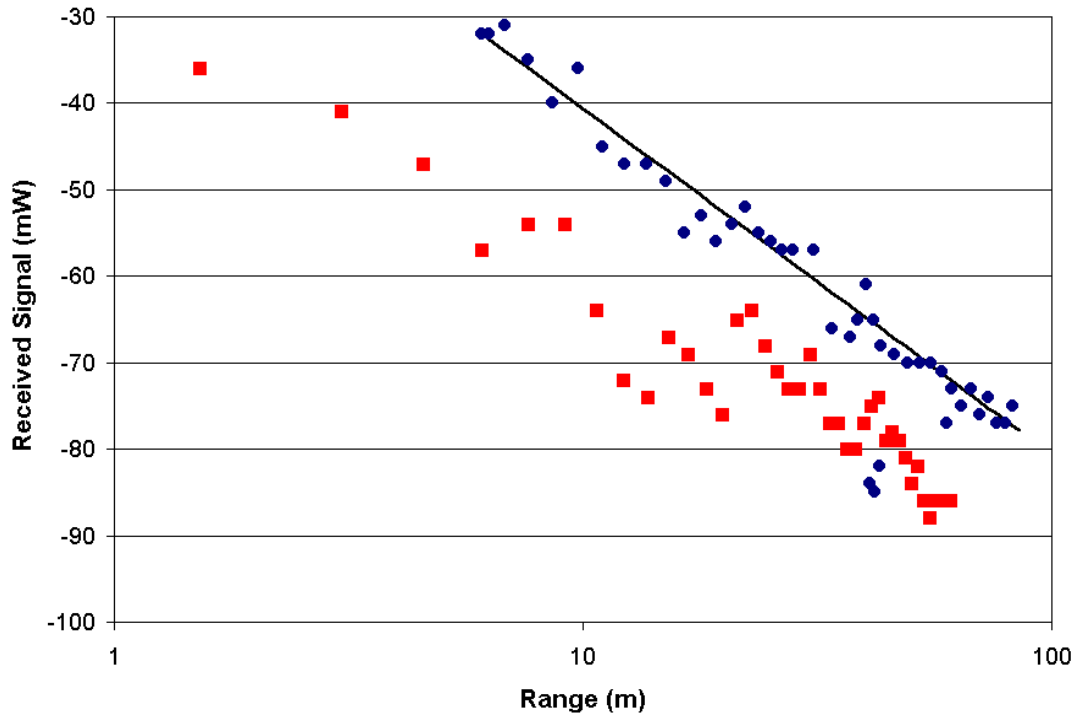
**Figure 49. Received power vs. Range for the link between a compact 2.4 GHz communicator (worn by personnel at boot level at a height of 10 cm above the surface) and an communicator at the surface (square symbols) and a communicator located at an overhead location at a height of 6m (circular symbols). Angle of transmission relative to the surface varies with Range. This measurement was performed in a sand surface environment. The solid line indicates the typical $(1/Range)^4$ power law path loss.**

## PROPAGATION STUDIES: MULTI-PATH CHARACTERIZATION

In an uncluttered environment, local signal propagation (at distances of less than 100m) is dominated by the line of sight direct wave, and primary reflections off the ground. Signal propagation over a clear field has been experimentally characterized in order to demonstrate the importance of the reflected wave, and to demonstrate that the power fall off of $R^{-2.5}$ previously observed for grazing incidence in the environment considered is a result of the primary reflection off the ground. The environment chosen is a baseball field that has been utilized for a variety of previous 2.4GHz measurements and provides a predominantly uncluttered path.

In order to demonstrate the influence of the wave reflected off the ground as compared to other multi-path components signal propagation as a function of transmitter height has been documented. The measurement set up was conducted on a baseball field surrounded on all sides by a small rise. The transmitting unit was hoisted a variable distance up a metallic light post to provide a repeatable elevation. While a large amount of scattering is expected off the pole, it is very near to the transmitter hence while modifying the polarization of the transmitted signal, the resulting multi-path interference should be small as the scattering is predominantly within the antenna near field. For all measurements the receiving node was located a distance of 20m from

the light pole to which the transmitting node was affixed.  The measurement environment consisted of flat, dry earth with a sparse covering of grass.

Shown in figure 50 is the power received as a function of the transmitters height above the ground. This figure is plotted for a receiver height of 0 inches, that is the edge of the radiating patch antenna was resting on the ground. Also shown in this figure is the power as a function of transmitter height from a geometric optics analysis considering only interference between the reflected and incident waves for each polarization. The patch antennas used transmit and receive predominantly signals polarized perpendicular to the plane of incidence. Shown in the figure are both the parallel and perpendicular predictions predicted from coherent interference between the direct incident wave and the signal reflected off the ground.  In determining the reflection coefficient off the flat ground the ground was assumed to have a relative permittivity of 15 and loss tangent of 0.001 at 2.4GHz. The predicted curve was based on 100mW radiated power and does not include any normalization for antenna efficiency or the presence of the metal pole to which the antenna was attached, only the spherical wave propagation loss factor ($R^{-2}$) for each component. Shown in figures 51 and 52 are similar comparisons of measured and geometric optics predicted fields for receiver heights of 12 inches and 25 inches. A similar quantitative correspondence between the measured and simulated results is seen in each case. Particularly the presence of the nulls in figures 53 and 54 demonstrate the validity of assuming that ground reflected wave dominates multi-path scattering. The difference in null location may be attributed to both errors in modeling the soils permittivity at 2.4GHz, unevenness of the ground (both of which will affect the phase of the ground reflection coefficient.
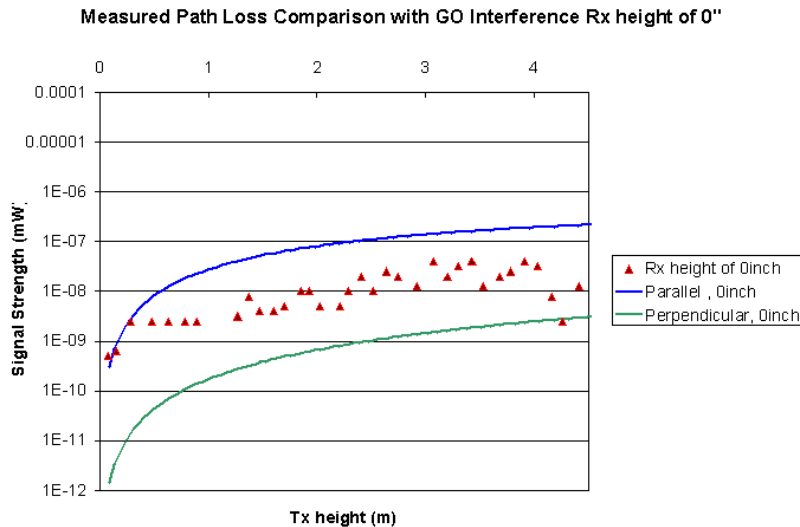


**Figure 50: Measured signal strength for a receiver height of 0m and simulated response for flat ground with $\varepsilon_r$=15, $\sigma$=0.001 and Rx height of 0 inches, a distance of 20m (65.6 feet), and a frequency of 2.4GHz. In the simulated response the parallel and perpendicular components are differentiated while the measured data's polarization is dependent on the patch antenna, which receives predominantly, perpendicular (horizontal) polarized waves.**

**Measured Path Loss Comparison with GO Interference, Rx height of 1 foot**
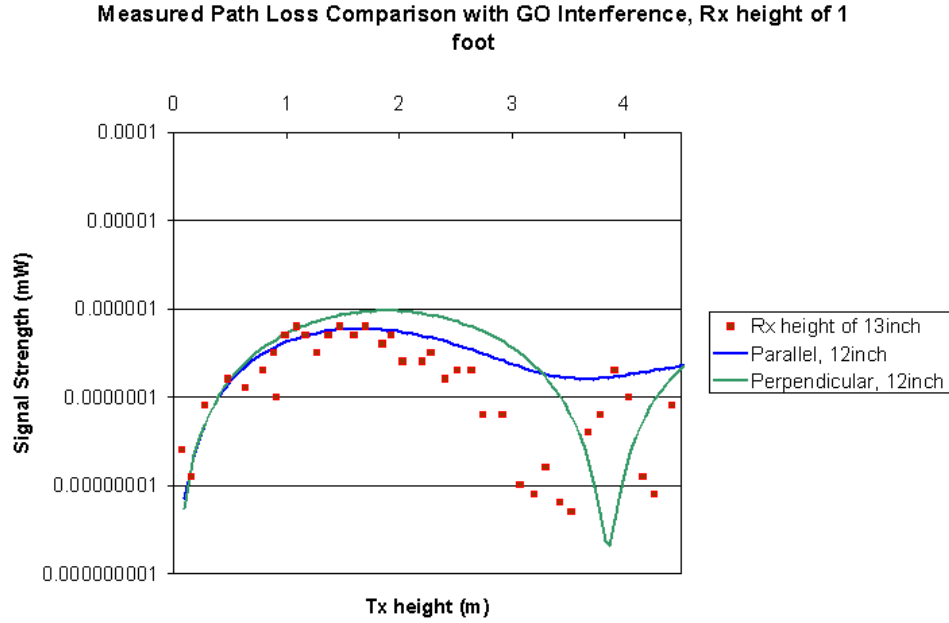
**Figure 51: Measured signal strength for a receiver height of 12 inches and simulated response for flat ground with $\varepsilon_r=15$, $\sigma=0.001$ and receive height of 12 inches, a distance of 20m (65.6 feet), and a frequency of 2.4GHz. In the simulated response the parallel and perpendicular components are differentiated while the measured data's polarization is dependent on the patch antenna, which receives predominantly perpendicular (horizontal) polarized waves.**



**Measured Path Loss Comparison with GO Interference, Rx height of 25 inches**
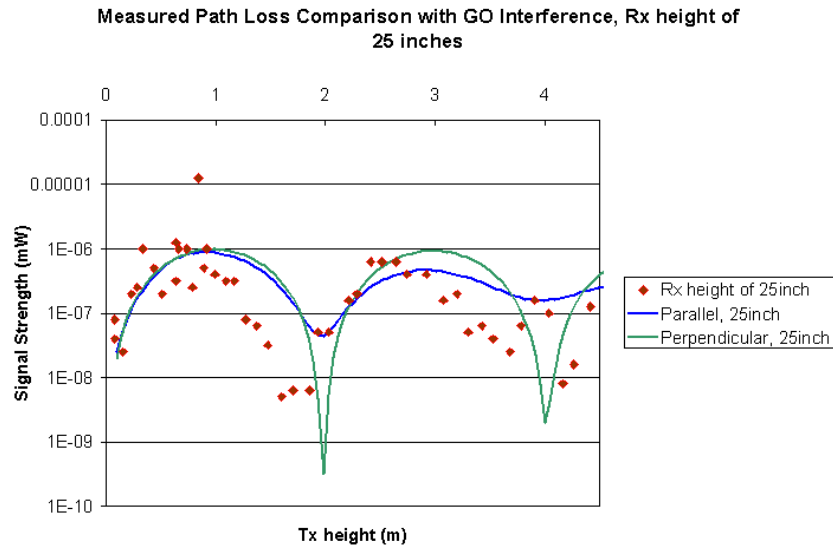
**Figure 52: Measured signal strength for a receiver height of 25 inches and simulated response for flat ground with $\varepsilon_r=15$, $\sigma=0.001$ and Rx height of 25 inches, a distance of 20m (65.6 feet), and a frequency of 2.4GHz. In the simulated response the parallel and perpendicular components are differentiated while the measured data's polarization is dependent on the patch antenna, which receives predominantly perpendicular (horizontal) polarized waves.**

56

In the same uncluttered baseball field the fading seen with the FHSS system was also measured. This is shown in figure 53. In these measurements both the transmitter and receiver are on the ground. Two measurements are shown in figure 53 versus time, a distance of 10m and a distance of 20m both at grazing incidence. Even in this relatively uncluttered environment substantial fading is observed. The variation is about +10dB and –20dB of the average signal received.
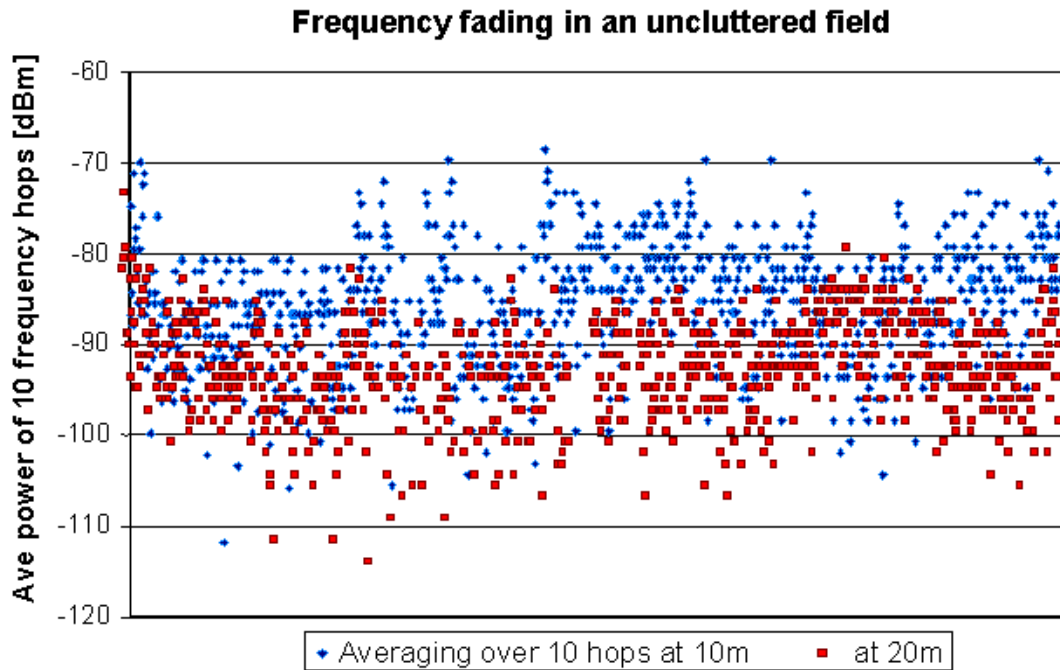


**Figure 53: Measuring the fading environment in the grassy baseball field of the previous measurements. Each data point is averaged over 10 hops, with transmitter and receiver on the ground.**

This experimental study demonstrates the dominance of the ground reflected wave on propagation at distances of less than 100m from the antenna. It demonstrates the order of validity of using only a geometrical optics description of propagation when considering the earth a flat lossy ground in modeling a relatively clear environment such as a the baseball field used. However substantial questions remain particularly as to what causes the substantial fading seen even in uncluttered environments and how much variation is observed in the power law attenuation off grazing. Ideally in an uncluttered environment at grazing incidence the reflection coefficient for each polarization will approach –1 for any frequency so that the cancellation of the dominant incident and reflected fields becomes frequency independent, resulting in a fourth power law attenuation. However in all environments considered substantial fading was observed as the frequency was changed slightly, which should result in a negligible change in reflection

coefficient. This indicates strong frequency dependence in every measurement environment, some of which may be attributed to the antenna itself, however measurements within a variety of antennas demonstrate consistency in the large fading seen even in uncluttered environments.

# BROAD PROPAGATION STUDY INVESTIGATION

## DATA COLLECTION SYSTEM

Within the follow up phase of the PicoWINS program a more intensive data collection system was utilized. This propagation measurement system used to collect the data presented in this section is shown in figure 54. Shown on each tripod (made of PVC and nylon screws) are the 900MHz, 2.4GHz, and 5.7GHz antennas at an elevation of 9cm (measured from the antenna feed point) oriented horizontally. The tripod cross bar provides mounting holes for both the vertical and horizontal (parallel to the crossbar) orientations. These mounting locations are at set points at each end of the crossbar (2ft from the center tubing) and a few inches from the center bar on either side. The 5.7Ghz antenna mounts near the PVC center cross bar. While the cabling attached to each antenna will depolarize and scatter the signal from the antennas this effect is minimized as much as possible with consistent cable placement away from the antennas for each measurement. The tripod antenna system provides a stable platform for the antennas with adjustable heights from 9cm to 180cm using the center column shown. In addition it is easily broken down for transportation. The stabilizing cross is removable (piece by piece) to provide options for varying degrees of stability on rougher surfaces. In addition to provide stability at heights below 9cm (the height of the PVC base joint), Styrofoam mounts have been constructed to place the antennas consistently at a height of 5cm for the bulk of measurements presented in this paper.
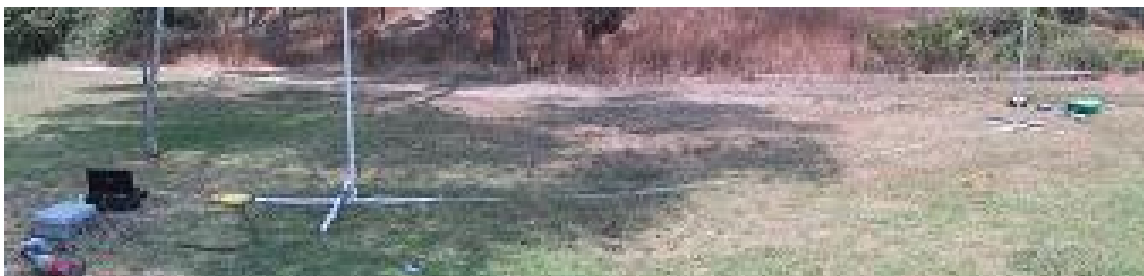


**Figure 54: Picture of the measurement system in the field.**

Within figure 54 the 900MHz, 2.4GHz, and 5.7GHz transmitters are shown on the far right. These operate on battery power, and with a spare set of batteries support a full day of operation. The gray case on the left is the tri-band receiver. Next to this are a laptop computer used to log the data measured and a portable power supply to support full day operation of the receiver. The system as shown is portable with two people. Data logging and antenna adjustment only requires a single person to fully characterize an environment.

The antennas themselves are low directivity dipole coated with a plastic radome. These antennas are commercially available ISM half-wave antennas from Mobile Mark Communications. A summary of the antenna specifications provided by the manufacturer is shown in table 1. All antennas are 50Ω nominal impedance with 10W maximum power, and designed to work without a ground plane. The antennas are connected to each transmitter and receiver over a twelve-foot span of LMR cabling.

**Table 1: Summary of manufacturer's specifications for the ISM band antennas.**

| Frequency Range | Directivity | Length | 10dB Horizontal Beamwidth | Connector |
|---|---|---|---|---|
| 870-960MHz @ 2:1 SWR | 2.5dBi | 18.3cm | 25° to 140° | SMA male |
| 2.4-2.485GHz @ 2:1 SWR | 2.5dBi | 12.2cm | 20° to 155° | SMA male, right angle |
| 5.72-5.83GHz @ 2:1 SWR | 2.2dBi | 5.7cm | 80° to 1710° | SMA male |

The transmitter and receiver components are supplied calibrated to their operation band, with RSSI accuracy within one dBm. To verify the operation of the antenna's selected the input impedance into each antenna and cable was measured, demonstrating the matching connection between the cables and the antennas as well as the antennas resonant operation in the desired band. $S_{11}$ measurements for all six antenna and cable assemblies are shown in figures 55, 56, and 57. Shown in each figure is a comparison of the two antennas used (transmit and receive). These measurements were not taken in an antenna range and some variability in the antennas near field results in the fluctuations. Additionally a standing wave pattern due to a slight mismatch between the antennas and cable is evident in the 2.4GHz and 5.8GHz bands, although in both cases the reflection coefficient across the band is less than –10dB representing a good match with less than 1dB variation across the signal band.
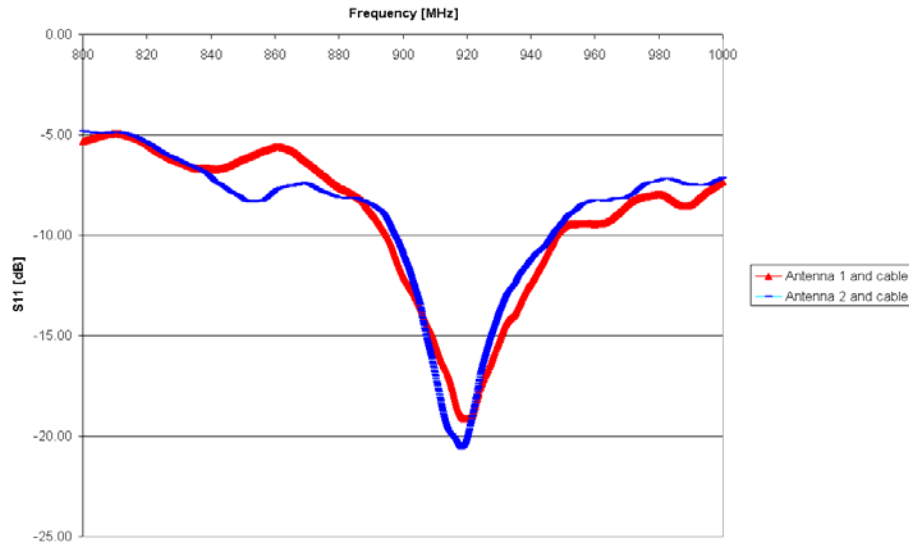


**Figure 55: Reflection Coefficient looking into each of the 900MHz antenna and cable assemblies.**
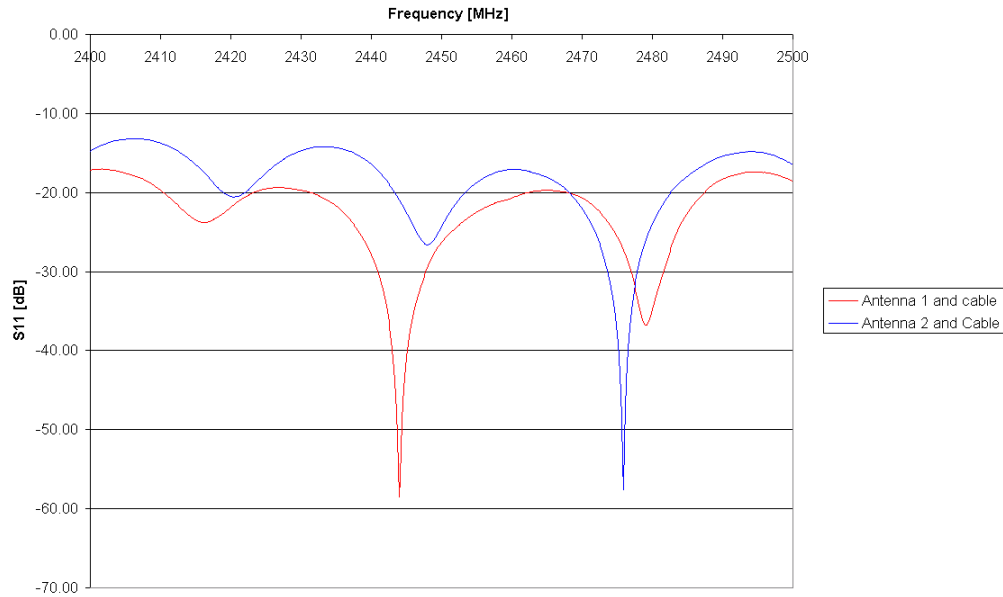
**Figure 56: Reflection Coefficient looking into each of the 2.4GHz antenna and cable assemblies.**
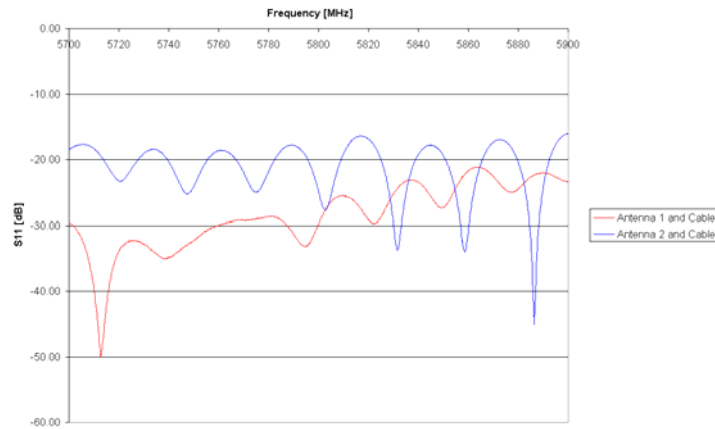


**Figure 57: Reflection Coefficient looking into each of the 5.8GHz antenna and cable assemblies.**

To quantify the loss through the antenna cables a measurement of the transmission coefficient through twelve feet of the LMR-195 cable and the N-type and SMA connectors used is shown in figure 58 from 500MHz to 6GHz. Within the 900-930MHz band each 12 feet of LMR-195 cable (and connectors) provides 1.5± 0.05dB of loss, within the 2.4-2.4835GHz band each 12 feet of cable and connectors provides -2.75 ± 0.15dB of loss, and within the 5.725-

61

5.875GHz band -4.5 ± 0.25dB of loss. The cable loss particularly in the highest band adds up (9dB in both cables) however to reduce the influence of the system in the antennas pattern and provide antenna height flexibility 12-foot cable lengths are used initially with the same cable type for all three bands. During the course of the measurements a few cable were damaged and replaced with alternate cables. Specifically replacements were made to one of the two cables used within the 900MHz band and provided less than 4dB of loss across the 900-928MHz band through both cables (twenty four feet and connectors). Additionally the two 5.7GHz cables were replaced with LMR 240 cabling. The LMR 240 cabling and connectors provides a loss of 7 ± 1dB through both cables. The replacements were made prior to the measurements described below made in rough vegetation, in the urban environments, in the rolling hills areas, in the Fort Leonard Wood test site, the near vehicle measurements, the different transmitter and receiver height measurements, and the park 2 vegetation environment.
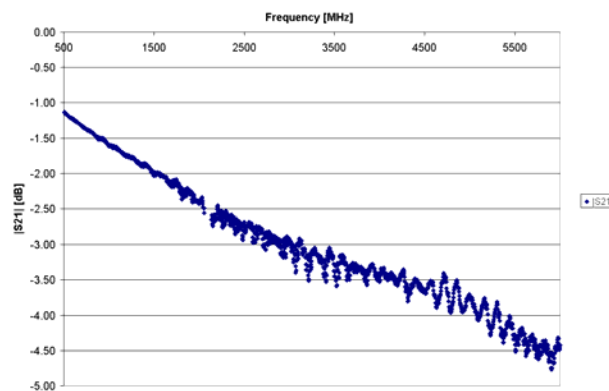


**Figure 58: Transmission coefficient through twelve feet of LMR-195 cable and antenna connectors used to connect to all the antennas.**

The measurement system is set up with an autonomous transmitter and receiver pair. Thus at each location and height the transmitter sends out a CW signal for three seconds, during which time the receiver is cycling through a table of receive frequencies and recording the received signal strength. Then as the CW transmitter sweeps it's transmit frequency (over the same table for which the receiver is recording values) the received signal strength at a location is captured over the table of frequencies.  The lack of synchronization between the transmitter and receiver allows the use of smaller, cheaper, portable equipment, at the price of accuracy for a limited number of RSSI points, and lack of phase measurements. The equipment provides an RSSI accuracy within 1dB, however the occasional received signal strength measurement that is captured only during part of the time when the transmitter is transmitting, gives occasional erroneously low RSSI. In general these points are infrequent (at least 30 measurements at the receiver per transmit window) and as the receivers set is filtered out to provide RSSI for only the strongest source in each frequency sweep, these artifacts tend to have little effect on the data collected.

In this paper, measurements of the received signal strength versus antenna distances, heights, and signal frequencies are shown for nineteen locations. These locations are grouped into six similar types. Three measurements made in the first type of environment, predominantly open, flat areas include: a turf farm in Palm Desert California, a grassy park in Los Angeles California, and an open beach in Santa Monica California. Panoramic views of these areas with the measurement equipment deployed are shown in figures 59, 60, and 61. These three areas constitute the open field environments, which will be used for a base line comparison to quantify the influence of scattering in the other environments.



**Figure 59: Turf farm open field environment.**



**Figure 60: Grassy park open field environment.**



**Figure 61: Beach open field environment.**

The second type of environments considered with limited scattering included three parking lot environments. The locations used for measurement are shown in panoramic views in figures 62, 63, and 64. They include the roof of a midsize parking garage, an empty parking lot near the beach, and the roof of a large parking garage. These three environments all had similar ground conditions (smooth asphalt or concrete) with limited scatterers as seen in the pictures (railings, lights, and parked cars). These three areas provide comparison with the open field environments described above with different ground conditions, and the addition of limited scattering.



**Figure 62: Mid size parking garage roof.**

**Figure 63: Beach parking lot.**



**Figure 64: Large parking garage roof.**

In addition three flat areas with various density and type of vegetation were also measured. These three vegetation environments are shown in figures 65, 66 and 67. These three environments include: a grassy park with various trees, a brush covered field, and a second grassy park with denser trees.



**Figure 65: First vegetation scattering environment.**



**Figure 66: Second vegetation scattering environment.**



**Figure 67: Third vegetation scattering environment.**

In addition to the nine environments described above, data has been collected in ten more environments. These are shown in panoramic views in figures 68 to 76. These nine environments are grouped into three types, rolling hills, rough and vegetation covered, and outdoor urban areas. The rolling hill environments shown in figures 68 to 70 provide a comparison for the previous flat open areas. These areas provide some surface roughness as well as a sloped surface. The second group, shown in figures 74 and 76 consists of hiking trails providing areas to set up the equipment in rough, vegetation-covered terrain. These areas are much rougher than the first

group in addition to providing a LOS path through vegetation in most cases. The last types of measurements were made in three outdoor urban locations. These are presented in figures 71 to 73 and provide a comparison with the rural and natural areas considered in the first five areas. The nineteenth environment shown in figure 77 is a test site at Fort Leonard Wood Missouri. Measurements were taken in this site in support of the DARPA Self-Healing Minefield program. This site is a slowly sloping brush covered field, with an eroded ditch through the center and along one side of the field. Measurements were taken along the east-west center of the field. Due to problems with the 900MHz transmitter, consistent measurements were only taken out to 100ft in that band and out to past 100m in the other two frequency bands.



**Figure 68: First rolling hills environment.**



**Figure 69: Second rolling hills environment.**



**Figure 70: Third rolling hills environment.**



**Figure 71: First urban environment, Kelton avenue.**



**Figure 72: Second Urban environment, UCLA bruin walk.**



**Figure 73: Third urban environment, UCLA court of Sciences.**

**Figure 74: First rough vegetation environment, Topanga trail.**



**Figure 75: Second rough vegetation environment, fist Will Rogers trail.**



**Figure 76: Third rough vegetation environment, second Will Rogers trail.**



**Figure 77: Fort Leonard Wood test field.**

In addition to the baseline frequencies, heights, and distances for which data was collected in nineteen environments, two additional scenarios were considered. The first of these was conducted on the beach environment at different receiver and transmitter heights. These measurements provide empirical validation of the two-ray model and specifically focus on a jamming scenario in which a local jammer may be elevated a meter or two with respect to a short-range autonomous network. The second scenario considered looked at fading in and around a vehicle environment as seen in figure 78. For this scenario a few locations within and on top of a car were measured at the small parking garage roof earlier measured. The fading resulting from a complex scatterer such as an automobile was measured.



**Figure 78: Antenna vehicle interaction measurements, in the environment of figure 62.**

66

In addition to the photographic record of figures 59 to 78, and GPS position of each measurement environment, a soil moisture probe has also been used in each environment in which the soil is soft enough to characterize the ground. This is done with Delta-T Devices Theta probe type ML2x. This probe sets up a 100MHz standing wave along the 4 prongs. Based on the soil in which the prongs are inserted reference voltages are provided through the attached cable that correspond to the size of the standing wave, i.e. to the magnitude of the dielectric constant of the soil as described in [9]. This dielectric constant magnitude at 100MHz can be accurately correlated to the soil moisture content, one of the dominant contributions to the soil's permittivity and conductivity [10,13].

In [9] the dielectric constant of wet soils at frequencies below 1GHz is generally accepted to be of the form:

$$\varepsilon = \varepsilon' + j(\varepsilon'' + \frac{\sigma_{dc}}{2\pi f \varepsilon_0}) \qquad (3)$$

This equation is a first order approximation to the frequency dependence of soil appropriate within a local frequency range, however it only provides a broad model of the frequency dependence of a material. To provide a more accurate representation both ε' and ε'' in the above equation would be frequency dependent such as in the casual Debye series expansions of [10] or [11]. The soil moisture probe provides a voltage readout that is proportional to the impedance with which the soil and prongs load the coaxial transmission within the probe. The length of the prongs is optimized to maximize the standing wave voltage seen at the prong/probe junction, with this standing wave voltage providing a measure of the magnitude of the dielectric constant. The soil probe is then used to determine the volumetric moisture content of the soil as this can be directly related to the magnitude of the dielectric constant in equation (3). In order to use the probe in varying soil conditions Delta-T devices provides a calibration procedure to define the slope and offset of a linear relation between the soil's moisture volume fraction and the magnitude of the dielectric constant based on the soils type. As moisture is added to the soil, the salinity of that water determines the conductivity, and hence relative imaginary proportion of equation (3). This is based on the assumption that ʺ is small compared to the other two components of eq. (3), which is generally accurate below 1GHz[9]. The calibration allows the relation between the soil moisture content and the measured voltage to be accurately, empirically, set, even without knowing the ratio of the real and imaginary part of the dielectric constant. This is demonstrated in the accuracy comparison with other moisture measurement types shown in[9] and as a function of water salinity placed at the ends of the probe shown in[12]. This results from the design of the probe to minimize the effect of any quality of the soil other than its moisture content, on the voltage variation (designed length of the probe, calibration procedure, and voltage measurement method).

The soil moisture probe provides an accurate assessment of the moisture in the soil (an important factor in ensuring propagation measurement repeatability) however without an accurate representation of the real and imaginary components of the dielectric constant. As a result based on the soil moisture constant and catalogued measurements in [13] qualitative values were selected within each frequency band. These are the values used in the following section within the ray optics model of propagation over a flat surface (based on equation 2). The permittivity assumed for each environment is shown in table 2. In this table representative values for concrete are also

given from [14], these representative values were used for comparison in all of the parking lot environments.

**Table 2: Soil properties used for each environment based on soil moisture content. For relative permittivity and conductivities the arguments of $\varepsilon_r()$ or $\sigma()$ correspond to the frequency in GHz, and $\theta_g$ is the gravimetric soil moisture content.**

| Environment | $\varepsilon_r(0.9)$ | $\sigma(0.9)$ | $\varepsilon_r(2.4)$ | $\sigma(2.4)$ | $\varepsilon_r(5.8)$ | $\sigma(5.8)$ | $\theta_g$ | Figure |
|---|---|---|---|---|---|---|---|---|
| Turf Farm | 3.8 | 0.0004S/m | 3.8 | 0.01 S/m | NA | NA | 0% | 59 |
| Grassy Open Park | 8 | 0.03 S/m | 7 | 0.05 S/m | 6 | 0.2 S/m | 10% | 60 |
| Open Beach | 2.8 | 0.003 S/m | 2.8 | 0.01 S/m | 2.8 | 0.02 S/m | 1% | 61 |
| Concrete and Asphalt Surfaces | 5.3 | 0.05 S/m | 5.3 | 0.05 S/m | 5.3 | 0.05 S/m | NA | 62-64, 71-73, 78 |
| Sepulveda Park | 20 | 0.1 S/m | 19 | 0.3 S/m | 18 | 0.9 S/m | 35% | 65 |
| Bushes | 2.8 | 0.008 S/m | 2.7 | 0.025 S/m | 2.65 | 0.06 S/m | 5% | 66 |
| Whittier Park | 10 | 0.05 S/m | 9.5 | 0.2 S/m | 9.4 | 0.25 S/m | 22% | 67 |
| Schbarum Park | 3.3 | 0.01 S/m | 3.1 | 0.040 S/m | 3 | 0.079 S/m | 23% | 68 |
| Hahn Park | 4.5 | 0.01 S/m | 4.3 | 0.040 S/m | 4.2 | 0.1 S/m | 12% | 70 |
| Test Field | 3.4 | 0.01 S/m | 3.2 | 0.03 S/m | 3.1 | 0.08 S/m | 6.6% | 77 |
| Organic surface to hard to probe | 3.3 | 0.01 S/m | 3.1 | 0.040 S/m | 3 | 0.079 S/m | NA | 69, 74-76 |

**RESULTS**

The measurement system described above was deployed in the environments shown in figures 59 to 78. Results are presented in this section for the received signal strength values within the first 27MHz of each of the three ISM bands, at varying distances, heights, and polarizations. First the results are presented in terms of the fading seen within each of these environments, followed by an assessment of propagation as a function of distance, and propagation as a function of height.

FREQUENCY DEPENDENT FADING

As the frequency of the CW transmitter is swept across each ISM band the amount of multi-path present is represented in the level of fading seen in the received signal strength. At each different frequency the electrical distance to each scatterer varies and thus the coherent contribution of the multi-path components changes at the receiver. Thus the fading seen in sweeping the frequency provides an indication of the amount of scattering that exists within each environment. Particularly in scenarios where the delay spread is small enough to limit multi-path produced inter symbol interference this RSSI interpretation of fading provides a metric of the impact of scattering within each environment, and the impact on a propagation budget, or benefit that can be made up through spatial or antenna diversity schemes. Thus to focus on the scenario of ground based, autonomous, battery operated systems, fading across a 27MHz swath of each of the three frequency bands at antenna heights of 5cm and propagation distances of 15.24m (50ft) are presented below.

The frequency fading clearly correlates with the amount of scattering in the predominantly static environments considered (fixed location of the transmitter and receiver antennas with limited motion of the dominant scatterers). Shown in figures 79 to 135 is the fading in the first 27MHz of the three ISM bands for vertically oriented antennas (vertical-to-vertical or VV polarization), for horizontally oriented antennas (horizontal-to-horizontal or HH polarization), and for a horizontal transmit and vertical receive antenna (horizontal-to-vertical or HV polarization) at a height of 5cm and a distance of either 45 or 50 feet. In these figures the turf environment corresponds to the turf farm of figure 20, the open field park environment to the park of figure 60, the beach environment to the open beach of figure 61, the large roof to the parking garage roof of figure 62, the roof environment to the parking garage roof of figure 63, the parking lot environment to figure 64, the park 1 environment to figure 65, the bushes environment to figure 66, the park 2 environment to figure 67, the Schbarum rolling hills environment to figure 68, the Topanga rolling hills environment to figure 69, the Hahn rolling hills environment to figure 70, the Kelton urban environment to figure 71, the Bruin urban environment to figure 72, the Court urban environment to figure 73, the Topanga rough vegetation environment to figure 74, the Will Rogers rough vegetation environment to figure 75, the 2nd Will Rogers rough vegetation environment to figure 76, the Fort Leonard Wood test field to figure 77, and the near vehicle measurements to figure 78. From figures 79 to 135 the level of fading seen in each environment correlates well with the general amount of scatterers seen within 50m or so.

The nineteen environments considered range from predominantly flat and smooth to vehicle impassable, however most were relatively smooth. The largest amount of clutter due to in ground roughness, vegetation, and nearby structures is seen in the urban and the rough vegetation environments. The open field environments provide a flat surface with limited scattering (the beach has some roughness on the order of 5cm in height), while the rolling hills environments provide limited scatterers with gently sloping surfaces. The parking lot environments compare this with a smooth surface and limited man made scatterers, while the vegetation environments provide predominantly flat areas with natural scatterers. These environments were chosen to compare the general influence of the ground surface roughness, of vegetation scatterers, or man made scatterers, of ground type, and of the impact of combinations of these effects. Significant fading is seen particularly as the amount of scatterers in the environments increased, with less apparent influence of surface roughness on the multipath present as seen in the figures below.
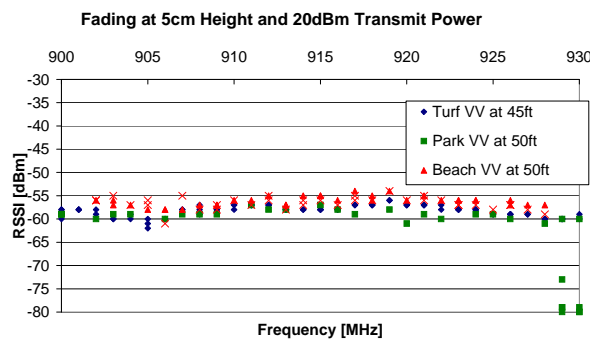


**Figure 79: Fading for VV in open fields.**
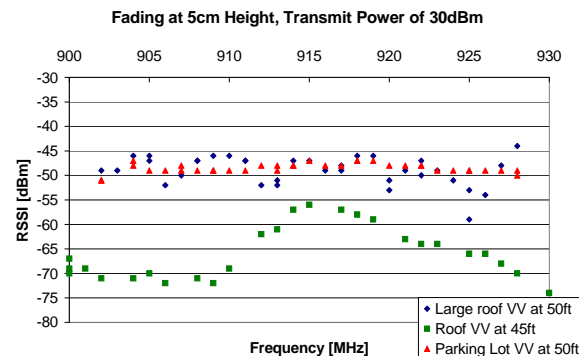


**Figure 80: VV fading in parking lots.**
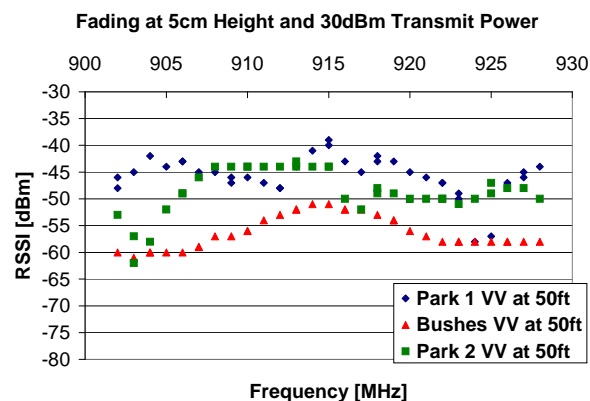


**Figure 81 VV fading in vegetation.**
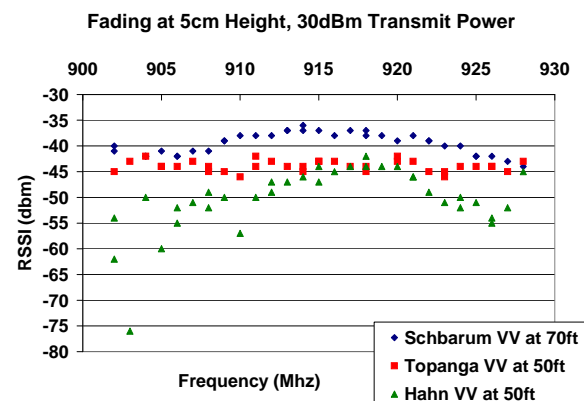


**Figure 82: VV fading in rolling hills.**

**Fading at 5cm Height, 30dBm Transmit Power**
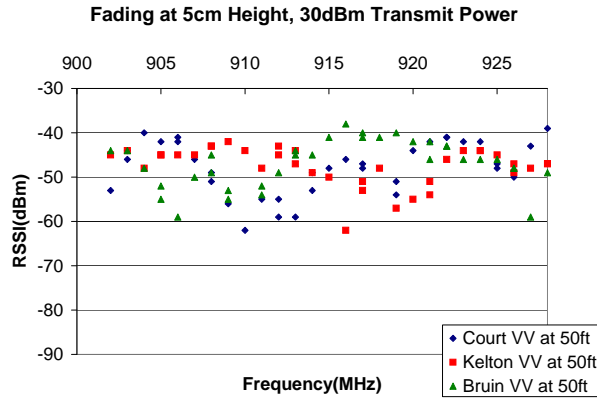
**Figure 83: Fading in urban areas.**

**Fading at 5cm Height, 30dBm Transmit Power**
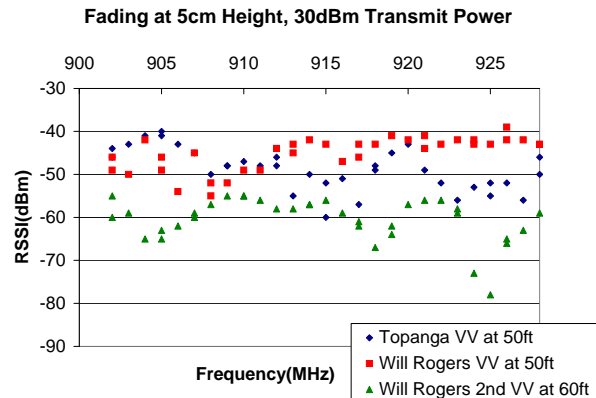
**Figure 84: Fading in rough vegetation.**

**Fading at 5cm height, 20dBm Transmit Power**
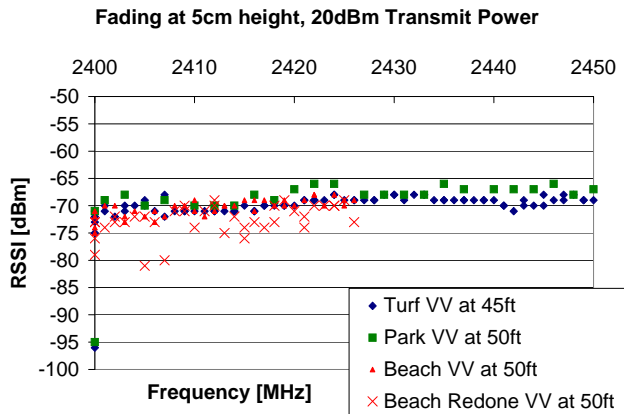
**Figure 85: VV fading in open fields.**

**Fading at Height of 5cm, Transmit Power of 20dBm**
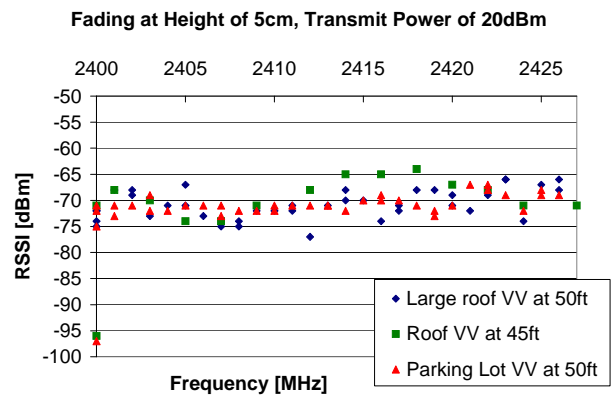
**Figure 86: VV fading in parking lots.**

**Fading at 5cm Heights and 20dBm Transmit Power**
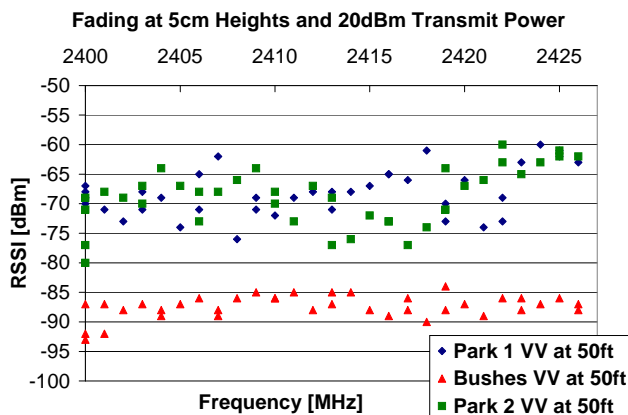
**Figure 87: VV fading in vegetation.**

**Fading at 5cm Height, 20dBm Transmit Power**
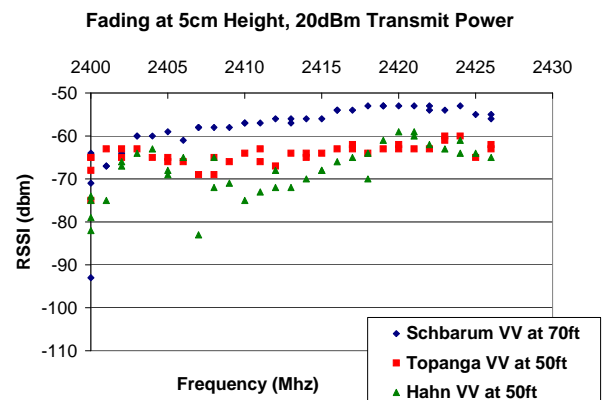
**Figure 88: VV fading in rolling hills.**

**Fading at 5cm Height, 20dBm Transmit Power**
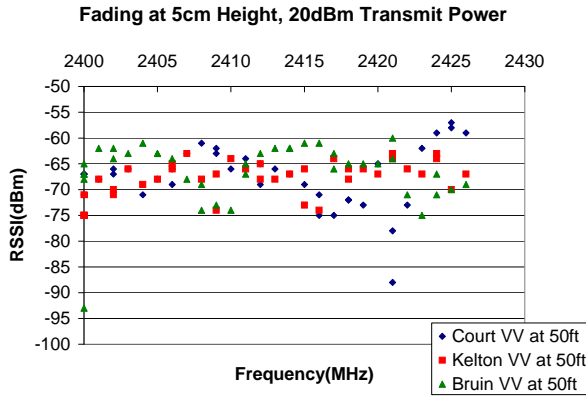


Figure 89: Fading in urban areas.

**Fading at 5cm Height, 20dBm Transmit Power**
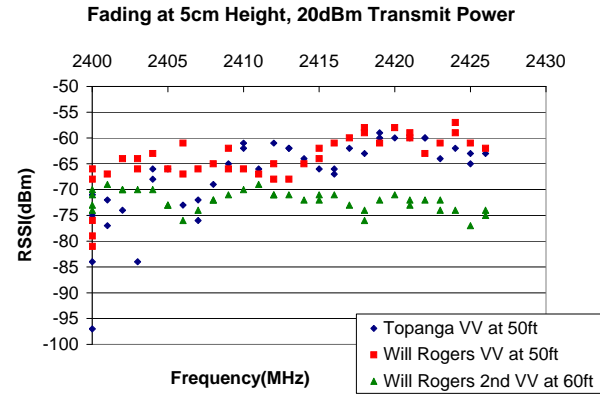


Figure 90: Fading in rough vegetation.

**Fading at 5cm Height, 27dBm Transmit Power**
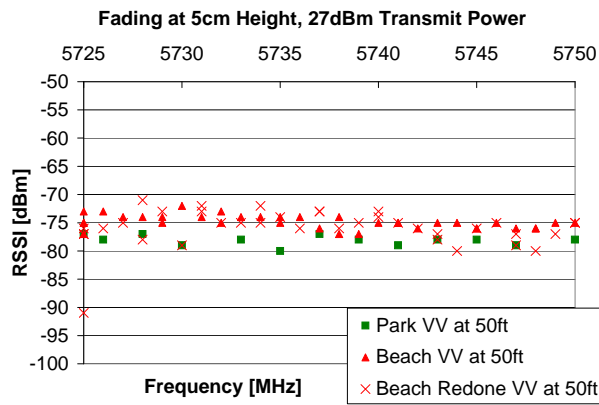


Figure 91: VV fading in open fields.

**Fading at 5cm Height, Transmit Power of 27dBm**
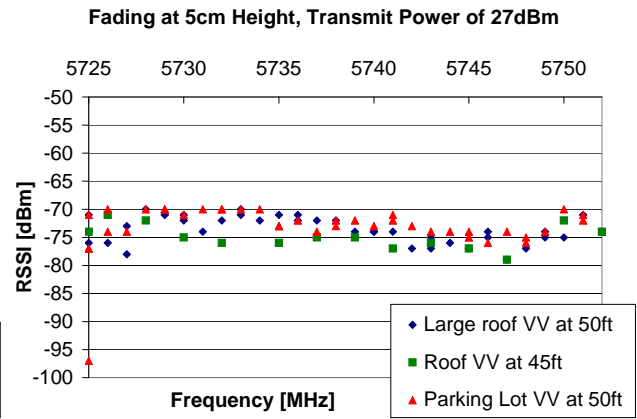


Figure 92: VV fading in parking lots.

**Fading at 5cm Heights, 27dBm Transmit Power**
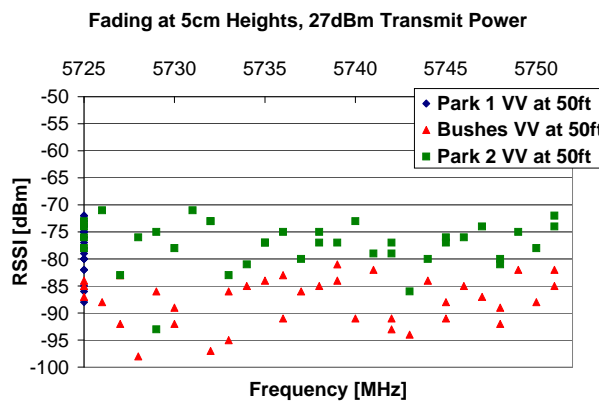


Figure 93: Fading in vegetation, VV.

**Fading at 5cm Height, 27dBm Transmit Power**
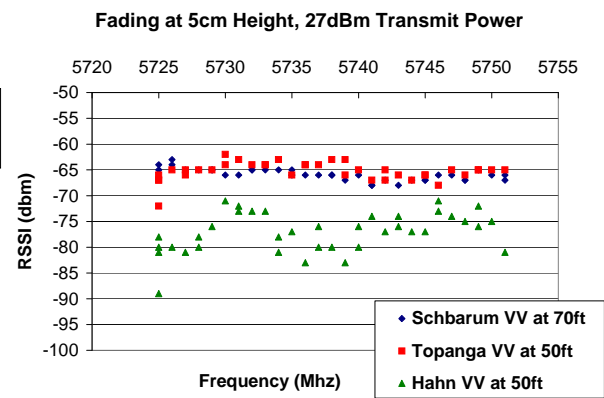


Figure 94: Fading in rolling hills, VV.

**Fading at 5cm Height, 27dBm Transmit Power**
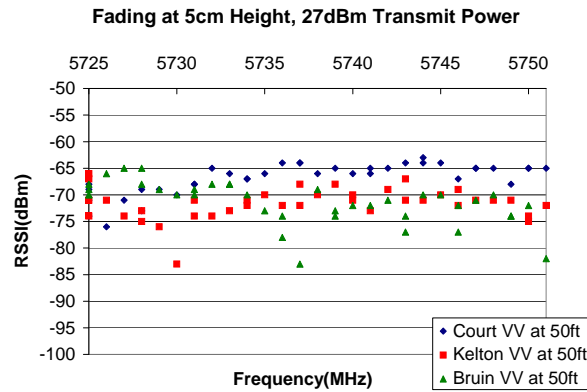


**Figure 95: Fading in urban areas, VV.**

**Fading at 5cm Height, 27dBm Transmit Power**
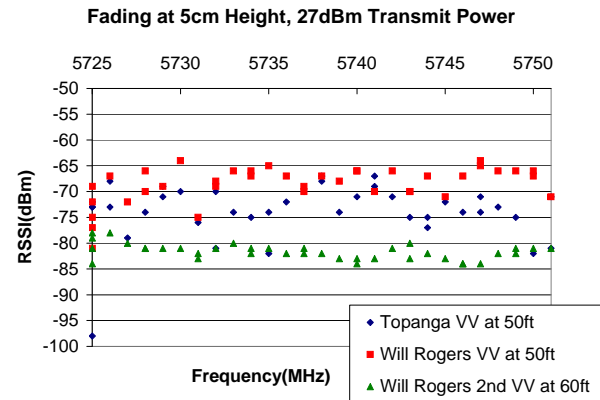


**Figure 96: Fading in rough vegetation, VV.**

**Fading at 5cm Height, 20dBm Transmit Power**
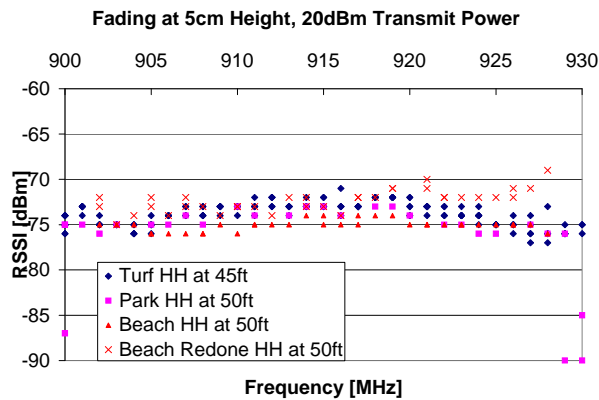


**Figure 97: HH fading in open fields.**

**Fading at 5cm Height, Transmit Power of 30dBm**
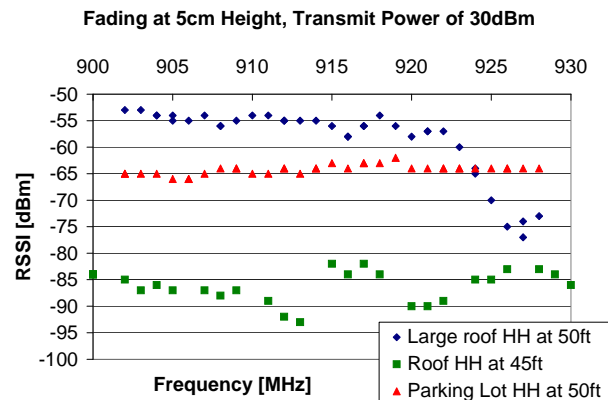


**Figure 98: HH fading in the parking lots.**

**Fading at 5cm Height, 30dBm Transmit Power**
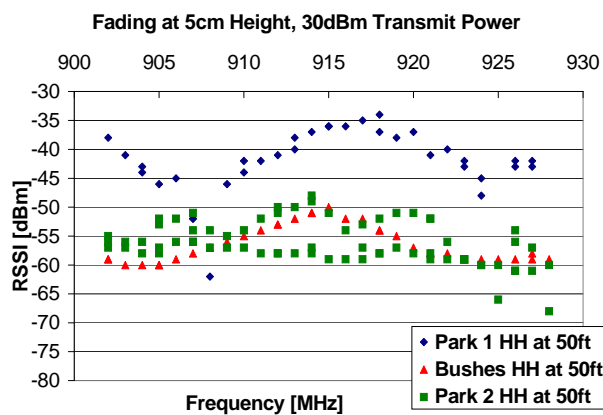


**Figure 99: HH fading in vegetation.**

**Fading at 5cm height, 30dBm Transmit Power**
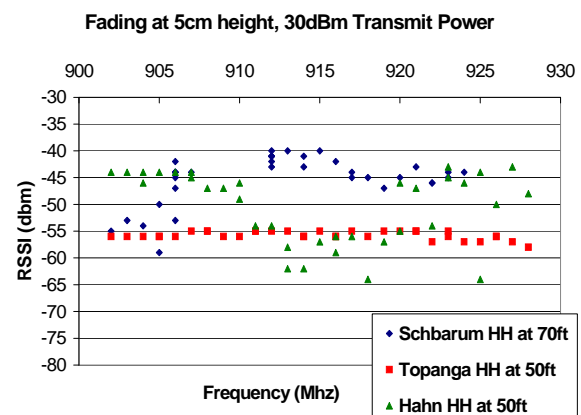


**Figure 100: HH fading in rolling hills.**

73
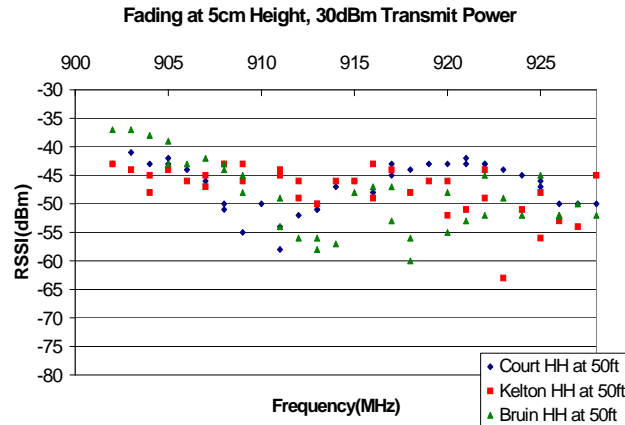
**Figure 101:** *HH fading in urban areas.*
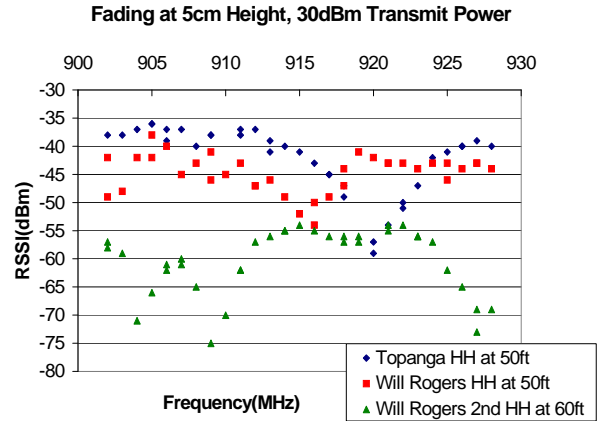


**Figure 102:** *HH fading in rough vegetation.*
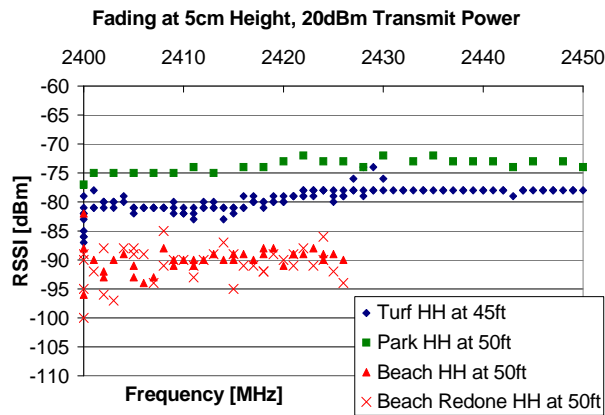


**Figure 103: HH fading in the open fields.**
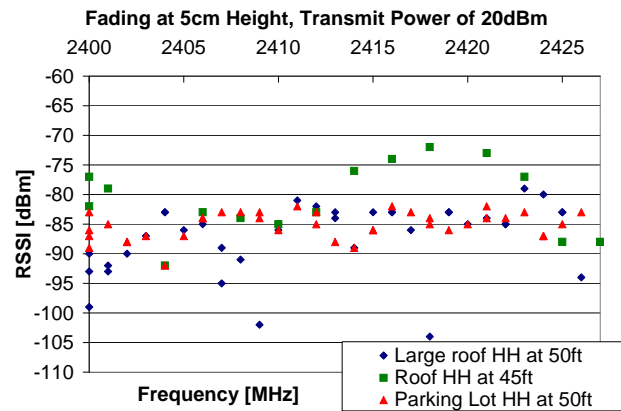


**Figure 104: HH fading in the parking lots.**
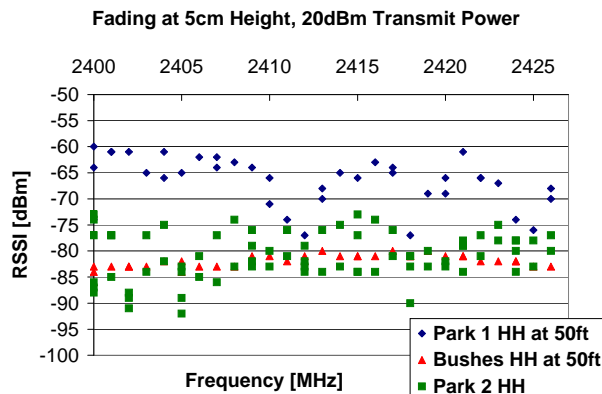


**Figure 105: HH fading in vegetation.**
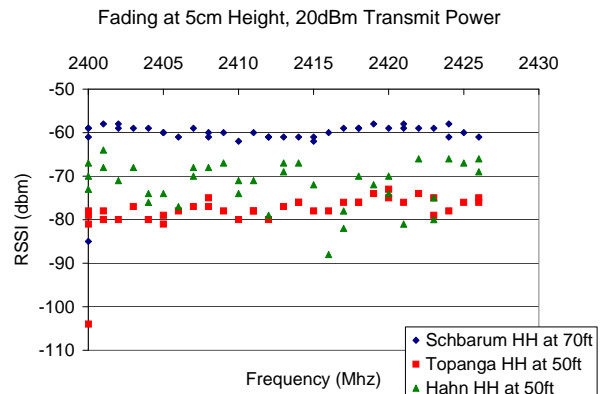


**Figure 106: HH fading in rolling hills.**
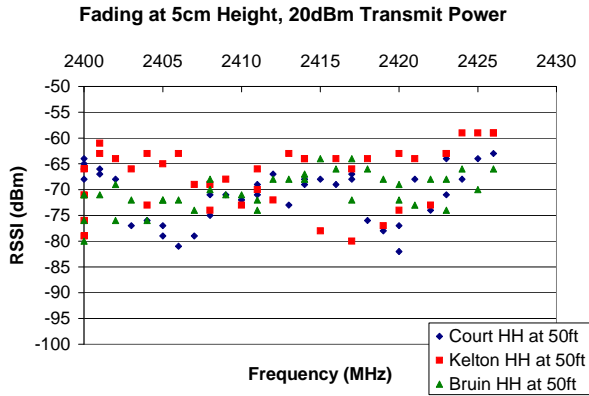
**Figure 107:** *HH fading in urban areas.*
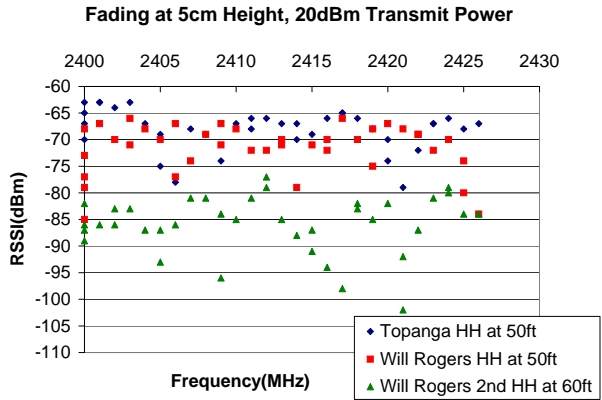


**Figure 108:** *HH fading in rough vegetation.*
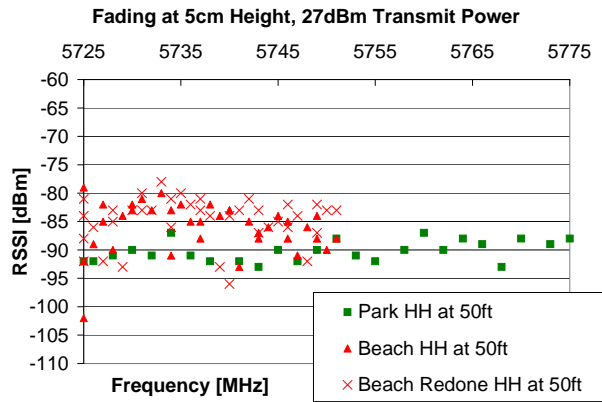


**Figure 109: HH fading in open fields.**
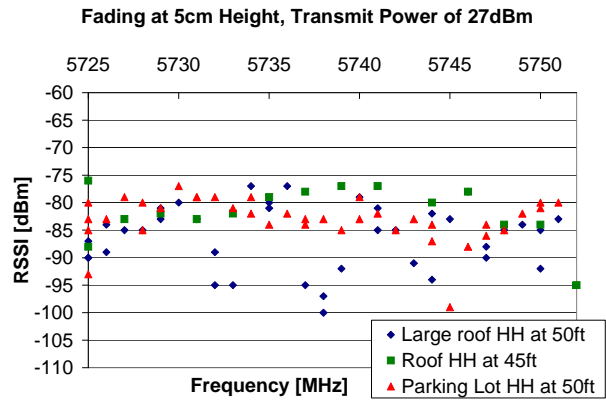


**Figure 110: HH fading in parking lots.**
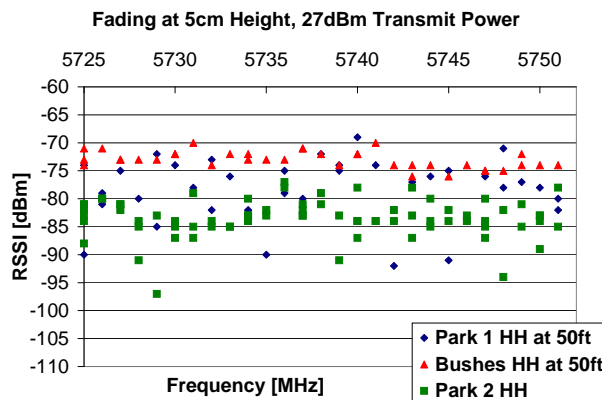


**Figure 111: HH fading in vegetation.**
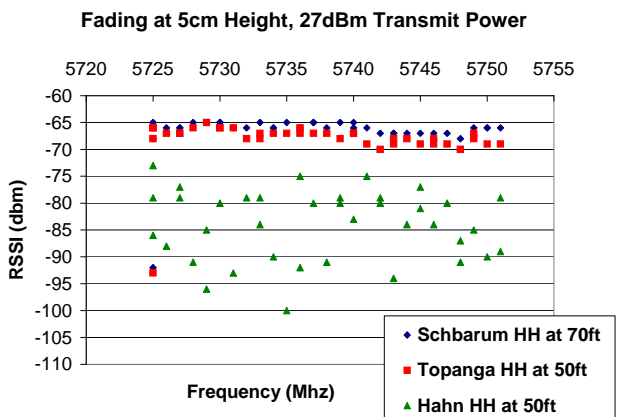


**Figure 112: HH fading in rolling hills.**

**Fading at 5cm Height, 27dBm Transmit Power**
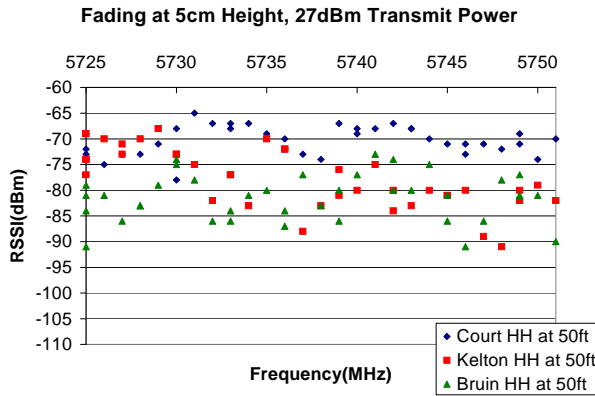


**Figure 113:** *HH fading in urban areas*

**Fading at 5cm Height, 27dBm Transmit Power**
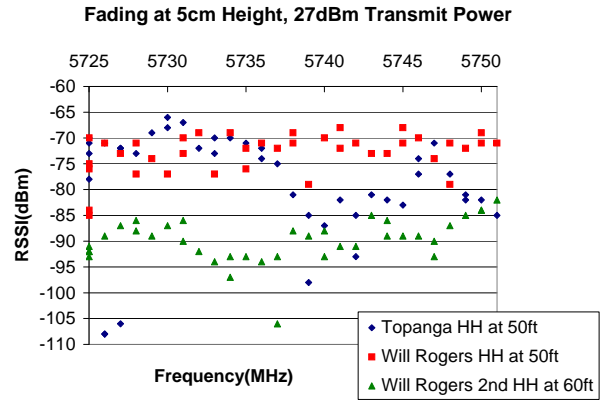


**Figure 114:** *HH fading in rough vegetation.*

**Fading at 5cm Height, 20dBm Transmit Power**
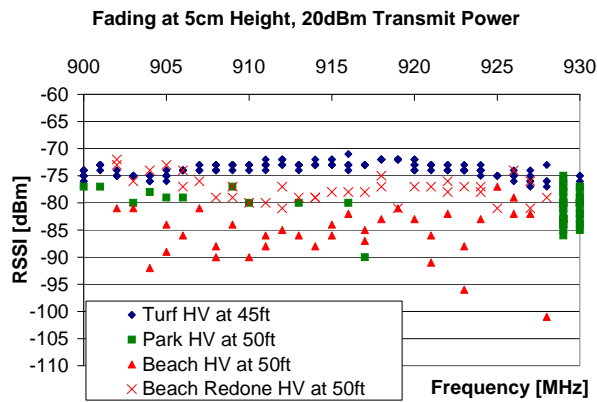


**Figure 115: HV fading in the open fields.**

**Fading at 5cm Height, Transmit Power of 30dBm**
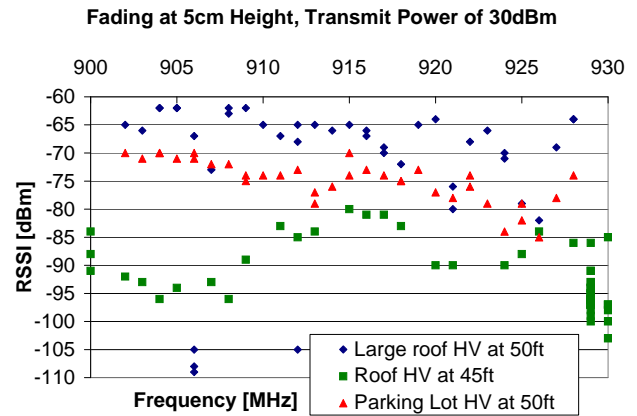


**Figure 116: HV fading in the parking lots.**

**Fading at 5cm Height, 30dBm Transmit Power**
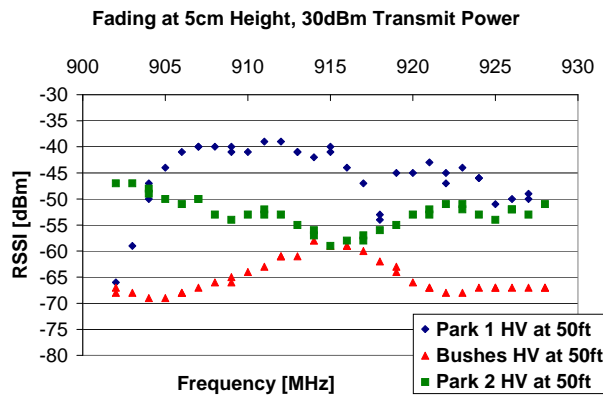


**Figure 117: HV fading in vegetation.**

**Fading at 5cm Height, 30dBm Transmit Power**
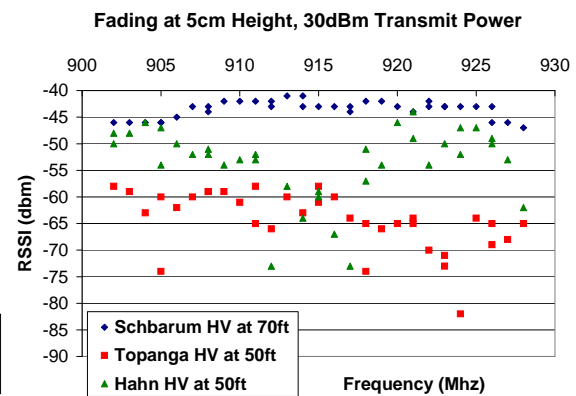


**Figure 118: HV fading in rolling hills.**

**Fading at 5cm Height, 30dBm Transmit Power**
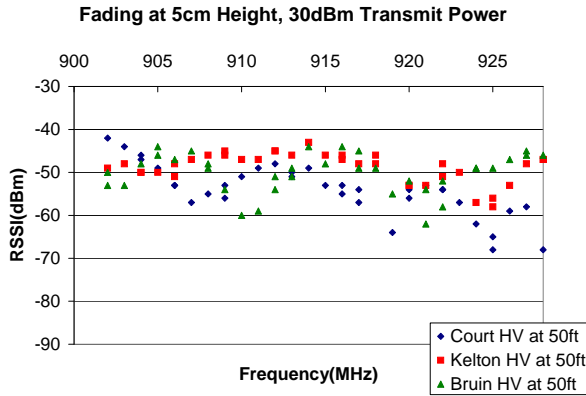


Figure 119: *HV fading in urban environments.*

**Fading at 5cm Height, 30dBm Transmit Power**
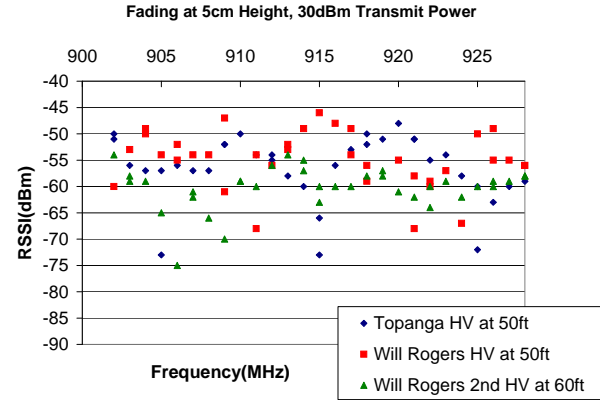


Figure 120: *HV fading in rough vegetation*.

**Fading HV at 5cm Height, 20dBm Transmit Power**
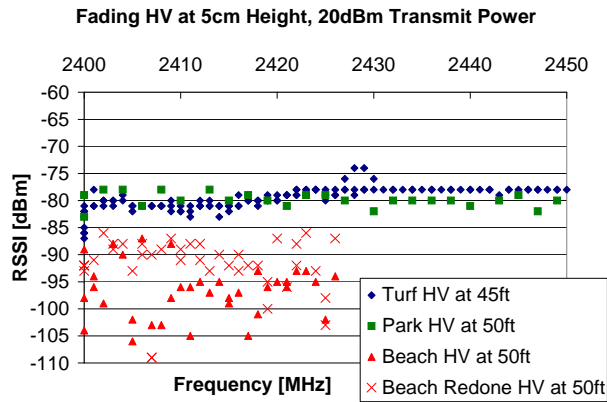


Figure 121: HV fading in open fields.

**Fading at 5cm Height, Transmit Power of 20dBm**
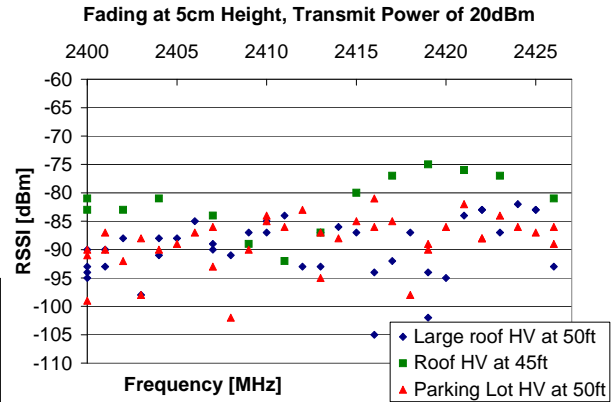


Figure 122: HV fading in parking lots.

**Fading at 5cm Height, 20dBm Transmit Power**
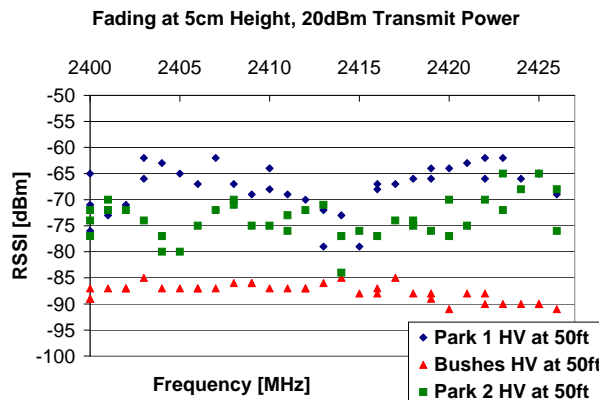


Figure 123: HV fading in vegetation.

**Fading at 5cm Height, 20dBm Transmit Power**
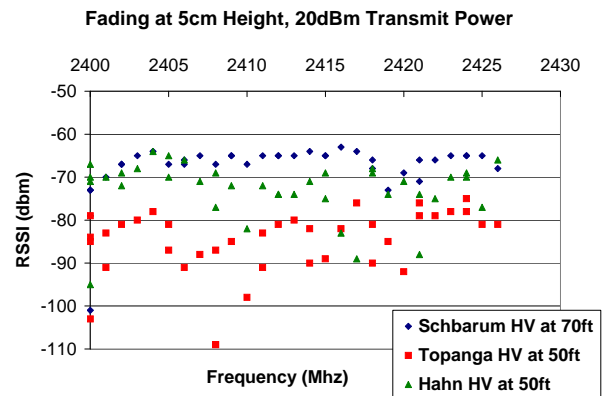


Figure 124: HV fading in rolling hills.

**Fading at 5cm Height, 20dBm Transmit Power**

Court HV at 50ft
Kelton HV at 50ft
Bruin HV at 50ft
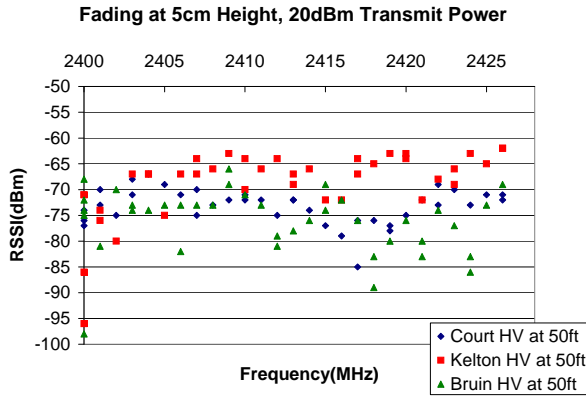
**Figure 125:** *HV fading in urban environments*

**Fading at 5cm Height, 20dBm Transmit Power**

Topanga HV at 50ft
Will Rogers HV at 50ft
Will Rogers 2nd HV at 60ft
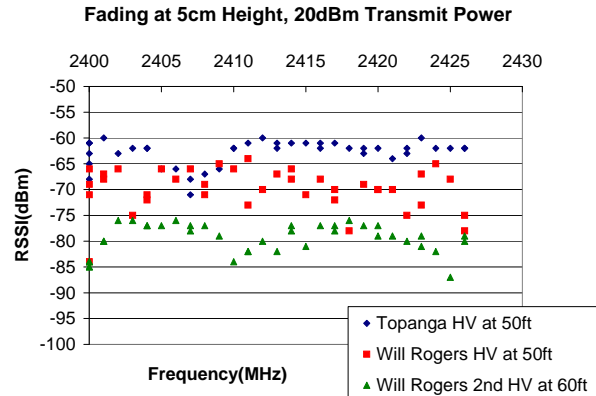
**Figure 126:** *HV fading in rough vegetation.*

**Fading at 5cm Height, 27dBm Transmit Power**

Park HV at 50ft
Beach HV at 50ft
Beach Redone HV at 50ft
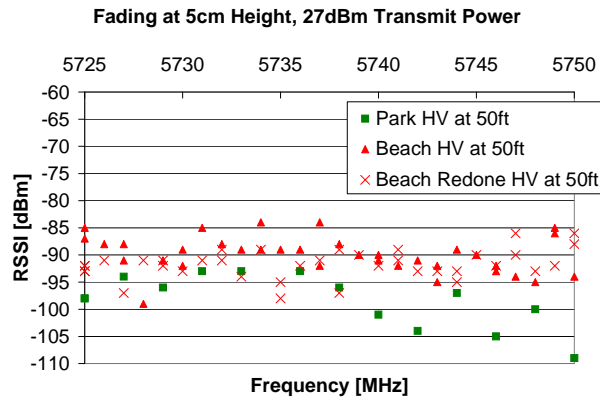
**Figure 127: HV fading in open fields.**

**Fading at 5cm Height, Transmit Power of 27dBm**

Large roof HV at 50ft
Roof HV at 45ft
Parking Lot HV at 50ft
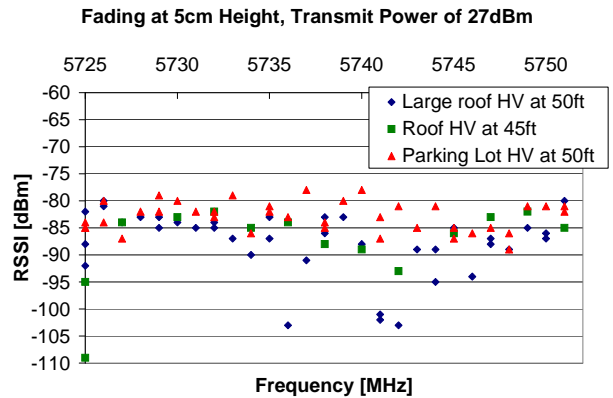
**Figure 128: HV fading in parking lots.**

**Fading at 5cm Height, 27dBm Transmit Power**

Park 1 HV at 50ft
Bushes HV at 50ft
Park 2 HV
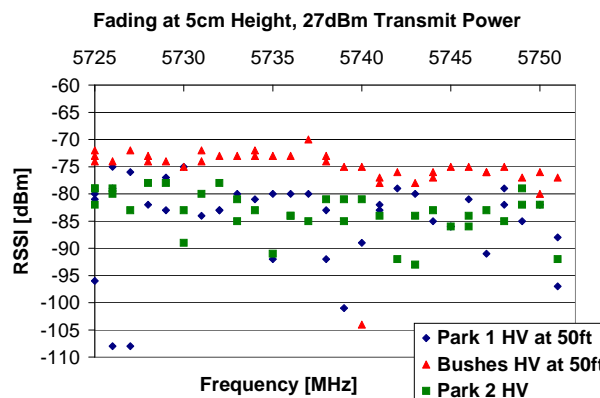
**Figure 129: HV fading in vegetation.**

**Fading at 5cm Height, 27dBm Transmit Power**

Schbarum HV at 70ft
Topanga HV at 50ft
Hahn HV at 50ft
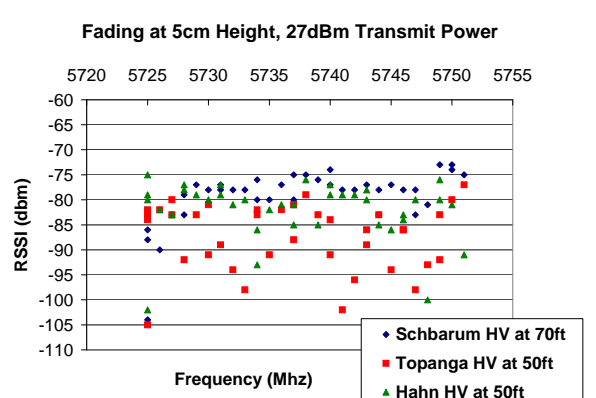
**Figure 130: HV Fading in rolling hills.**

**Fading at 5cm Height, 27dBm Transmit Power**
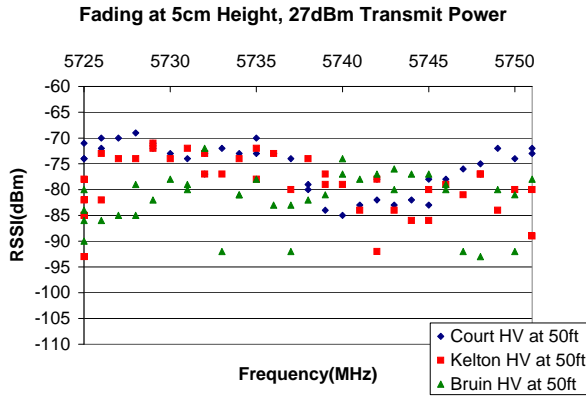


Figure 131: *HV fading in urban environments*

**Fading at 5cm Height, 27dBm Transmit Power**
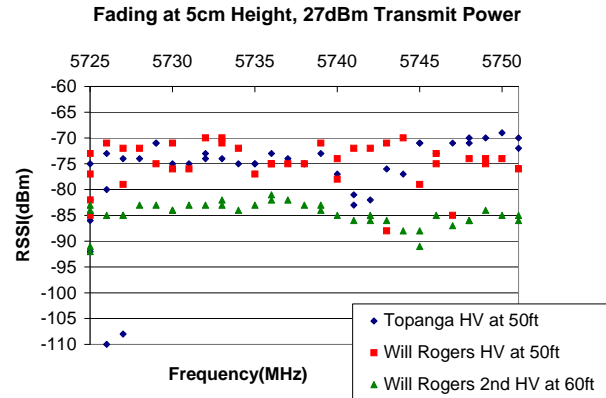


Figure 132: *HV fading in rough vegetation*

**Fading at antenna heights of 5cm, 30dBm Transmit Power**
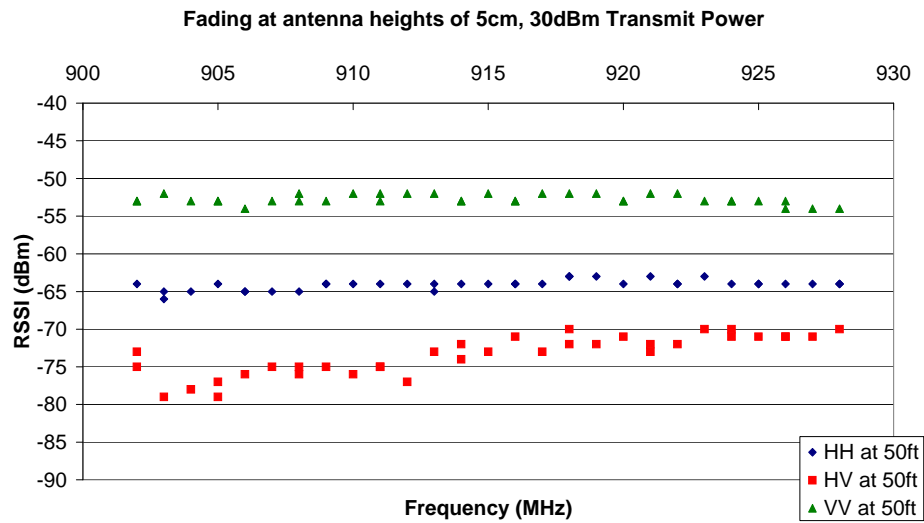


Figure 133: Fading in the 900MHz ISM band at the Fort Leonard Wood Test field.
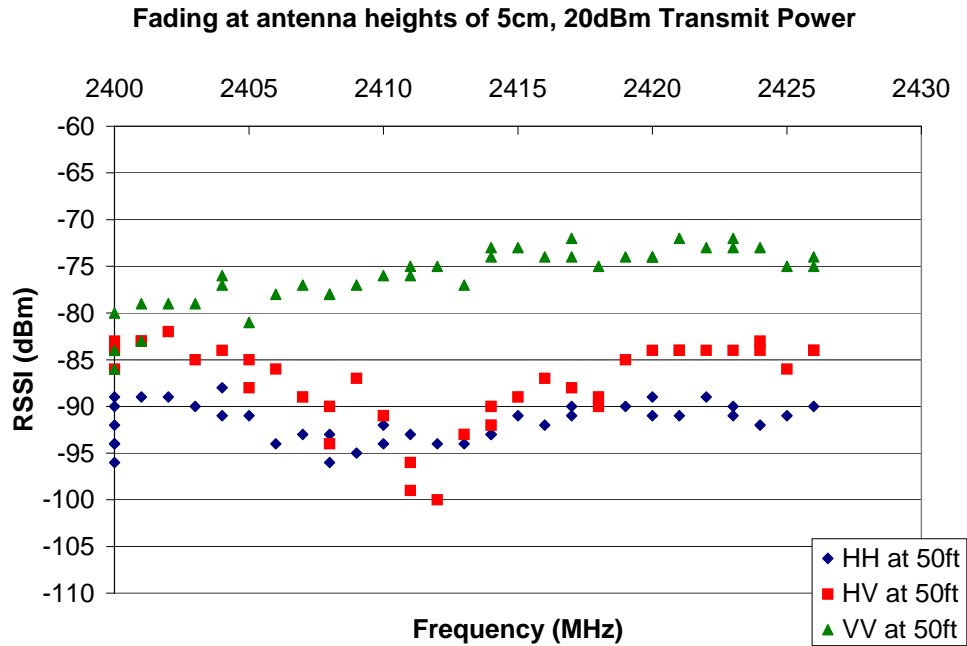
**Figure 134: Fading in the 2400MHz ISM band at the Fort Leonard Wood Test field.**
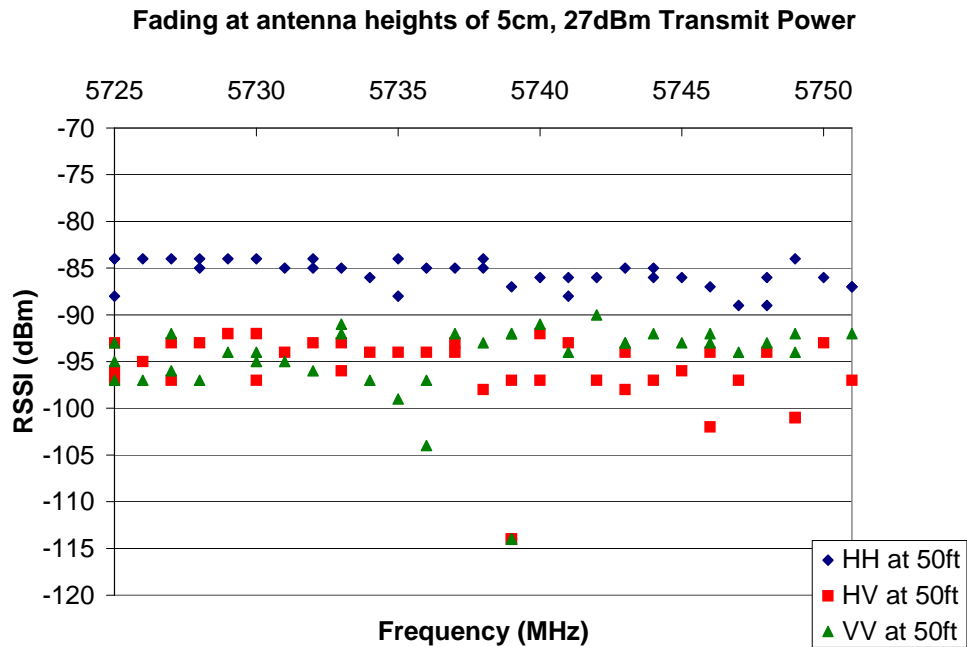


**Figure 135: Fading in the 5725MHz ISM band at the Fort Leonard Wood Test field.**

Figures 79 through 135 provide the fading in all nineteen environments at all three polarizations and three frequency bands at antenna heights of 5cm and distances of approximately 15m. In addition plots of the propagation power loss with distance at antenna heights of 5cm for all three polarization are shown in figures 136-192. In these figures plotted with the data is the prediction of a two-ray model over a flat lossy ground with permittivity and permeability correlated to the environment measured in as provided in table 2. As is seen in the figures similarities are seen in the propagation fall off between all three-polarization combinations shown.

**VV Power Fall off at 5cm Height, 20dBm Transmit Power**
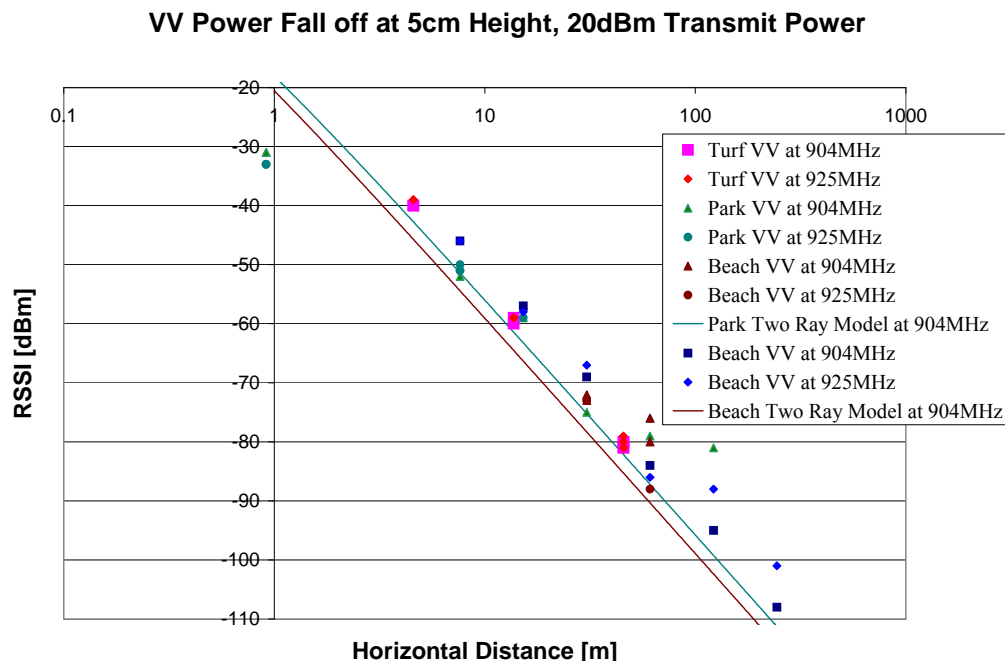


**Figure 136: Propagation fall-off in the open field environments, VV.**

**HH Power Fall off at 5cm Height, 20dBm Transmit Power**

Legend:
- Turf HH 904MHz
- Turf HH 925MHz
- Park HH 904MHz
- Park HH at 925MHz
- Beach HH at 904MHz
- Beach HH at 925MHz
- Park Two Ray Model 904MHz
- Beach Redone HH at 904MHz
- Beach Redone HH at 925MHz
- Beach Two Ray Model at 904MHz

*y-axis: RSSI [dBm], x-axis: Horizontal Distance [m]*
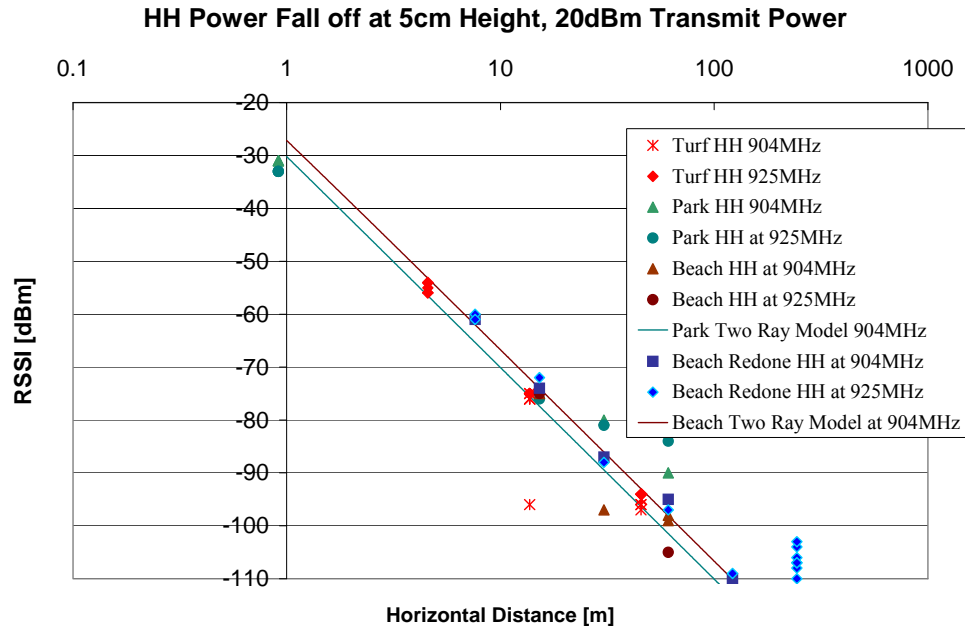
**Figure 137: Propagation fall-off in the open field environments, HH.**

**HV Power Fall off at 5cm Height, 20dBm Transmit Power**

Legend:
- Turf HV at 904MHz
- Turf HV at 925MHz
- Park HV at 904MHz
- Park HV at 925MHz
- Beach HV at 904MHz
- Beach HV at 925MHz
- Beach Redone HV at 904MHz
- Beach Redone HV at 925MHz

*y-axis: RSSI [dBm], x-axis: Horizontal Distance [m]*
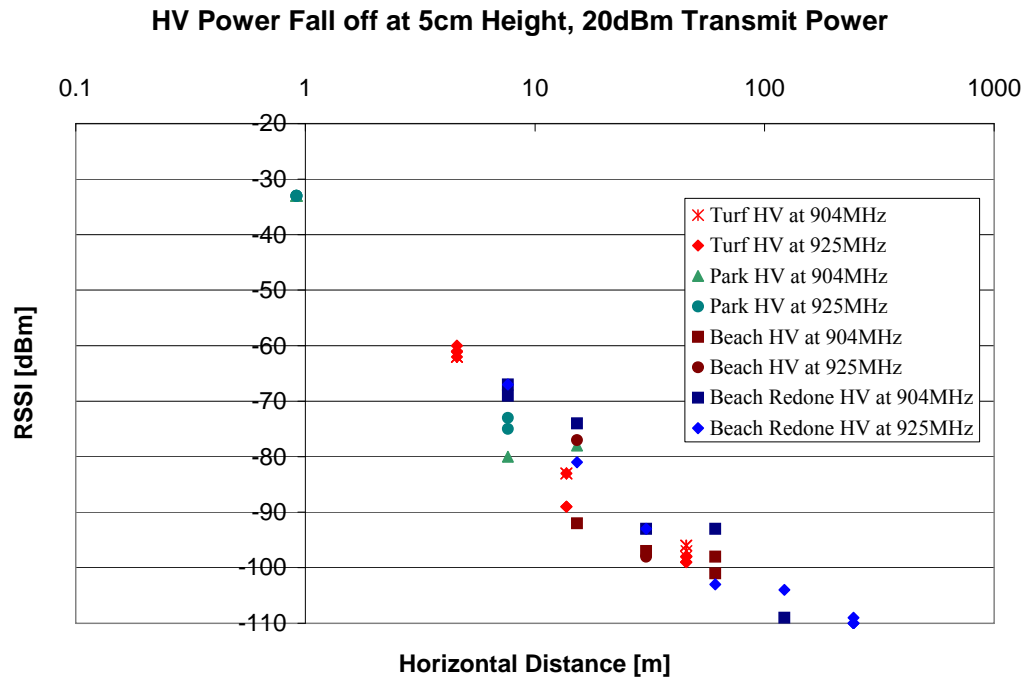
**Figure 138: Propagation fall-off in the open field environments, HV.**

**VV Propagation at 5cm height and 30dBm Transmit Power**
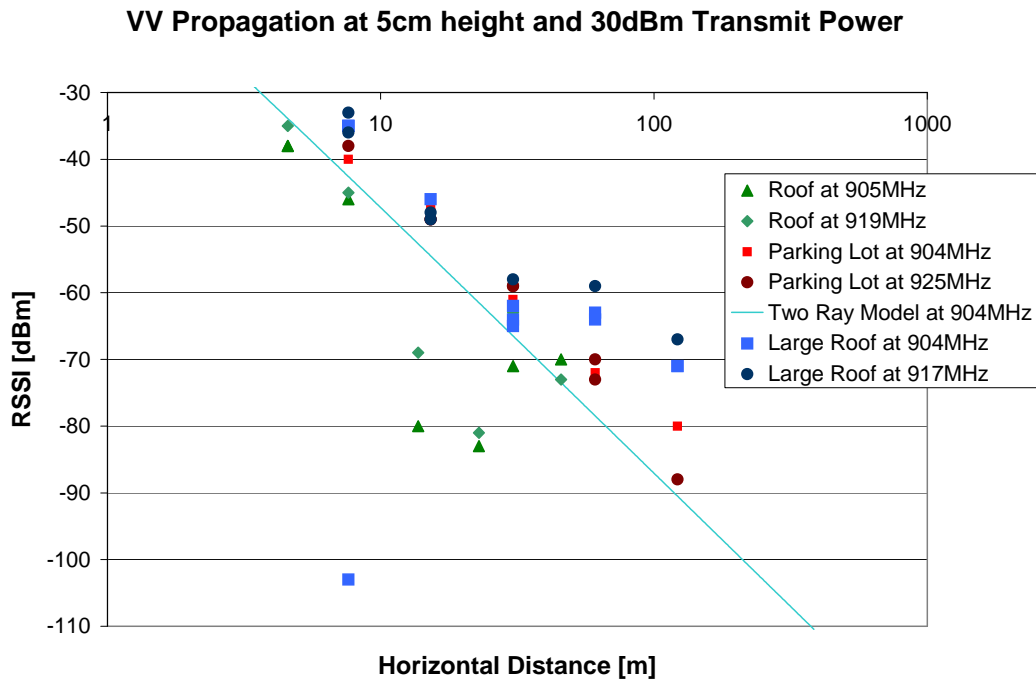


**Figure 139: Propagation fall-off in the parking lot environments, VV.**

**HH Propagation at 5cm Heights,  30dBm Transmit Power**
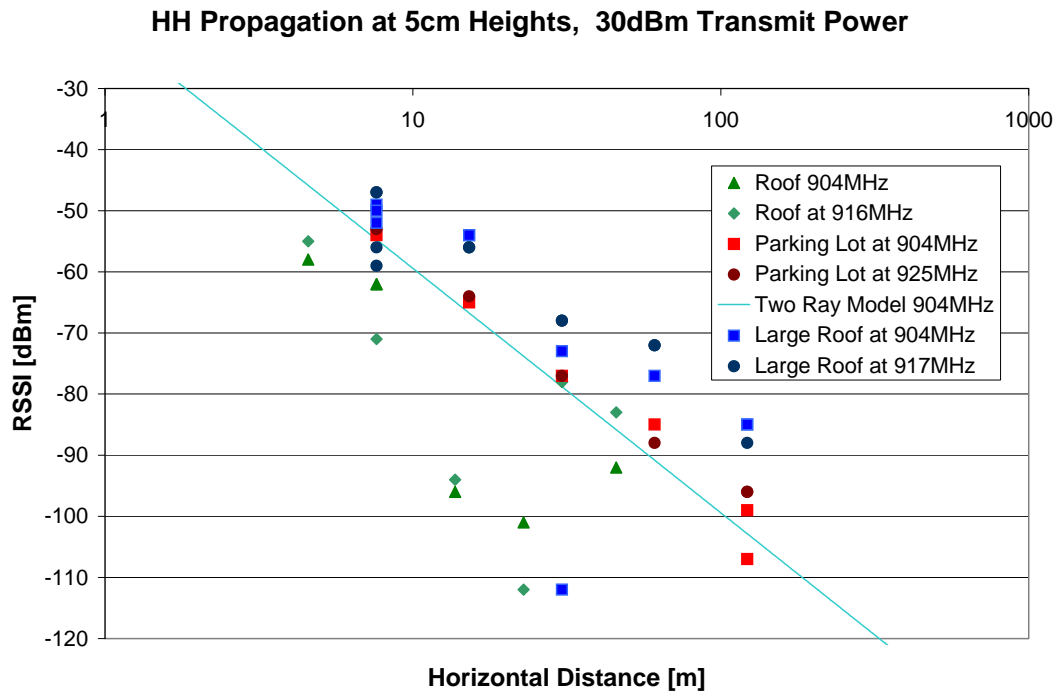


**Figure 140: Propagation fall-off in the parking lot environments, HH.**

83
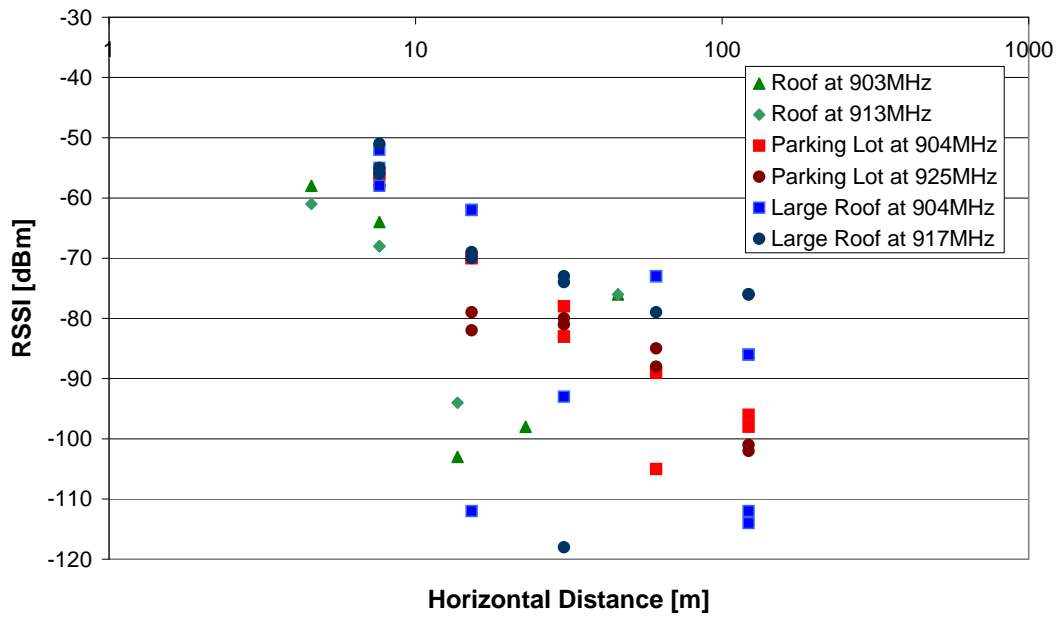
**Figure 141: Propagation fall-off in the parking lot environments, HV.**
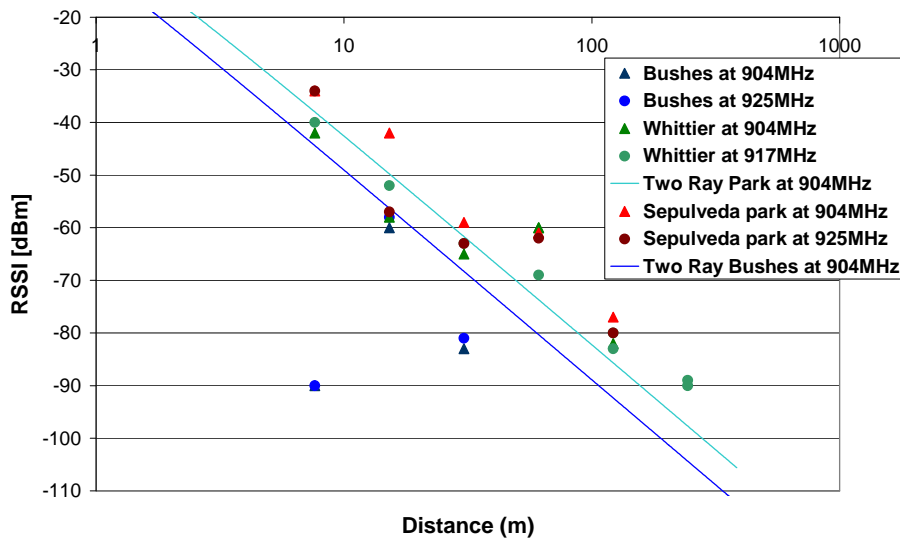


**Figure 142: Propagation fall-off in the areas with vegetation, VV.**

84

## HH Propagation at 5cm 30dBm Transmit Power
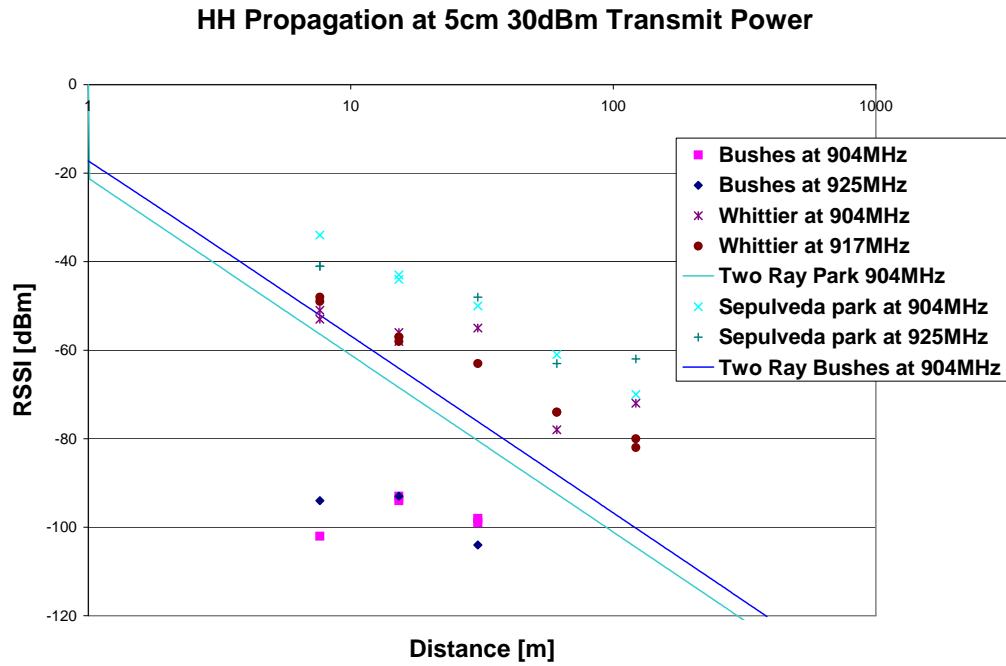


**Figure 143: Propagation fall-off in the areas with vegetation, HH.**

## HV at 5cm
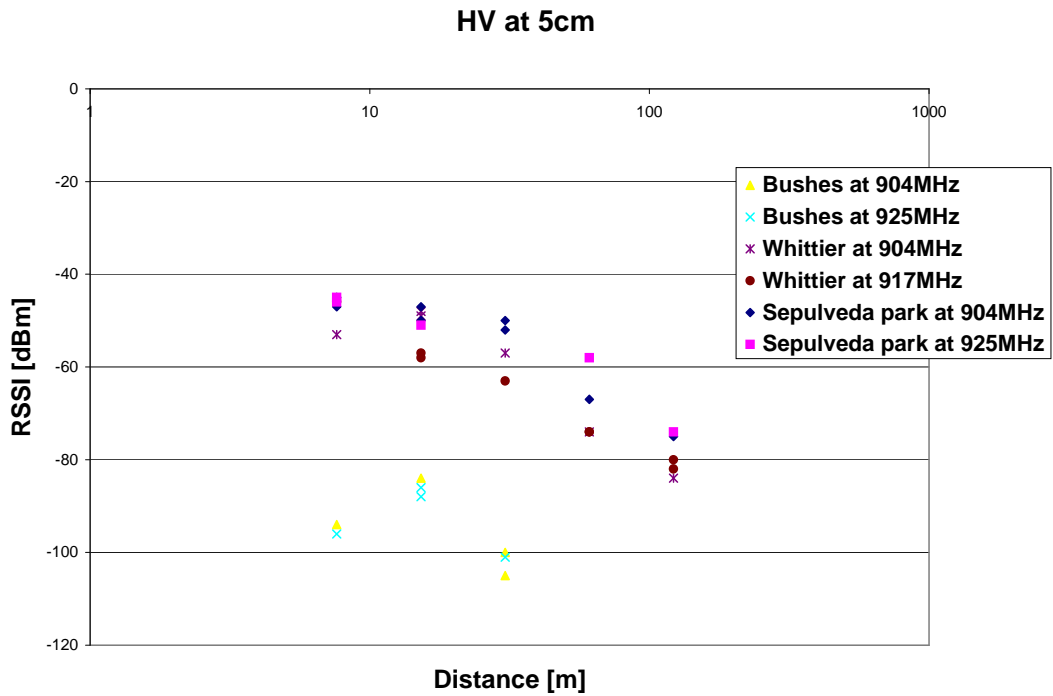


**Figure 144: Propagation fall-off in the areas with vegetation, HV.**
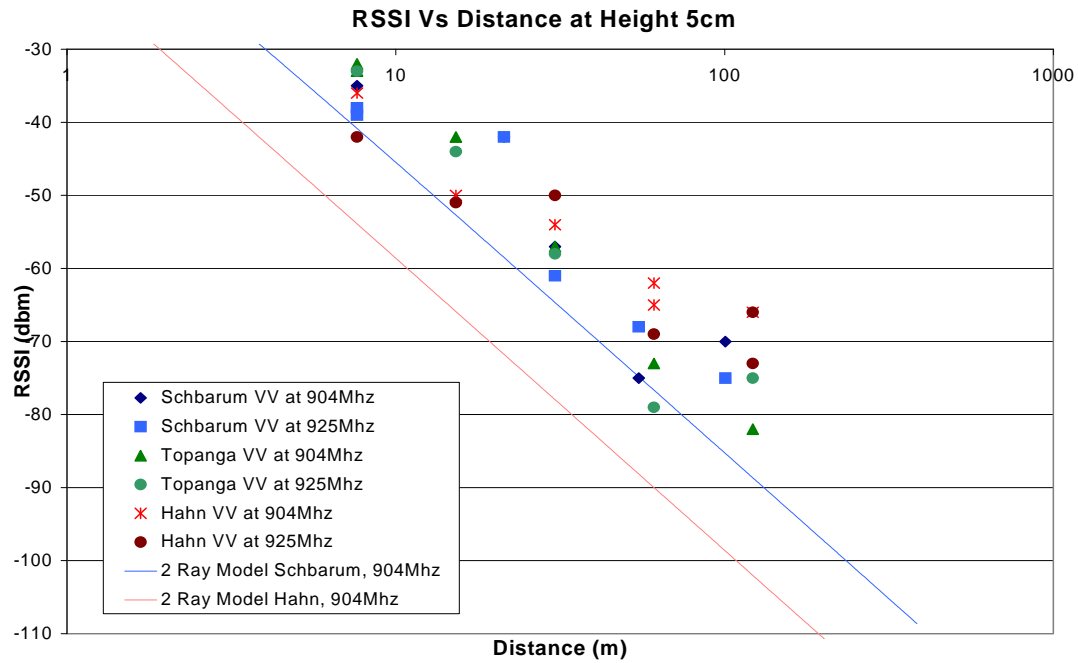
**Figure 145: Propagation fall-off in the areas with rolling hills, VV.**
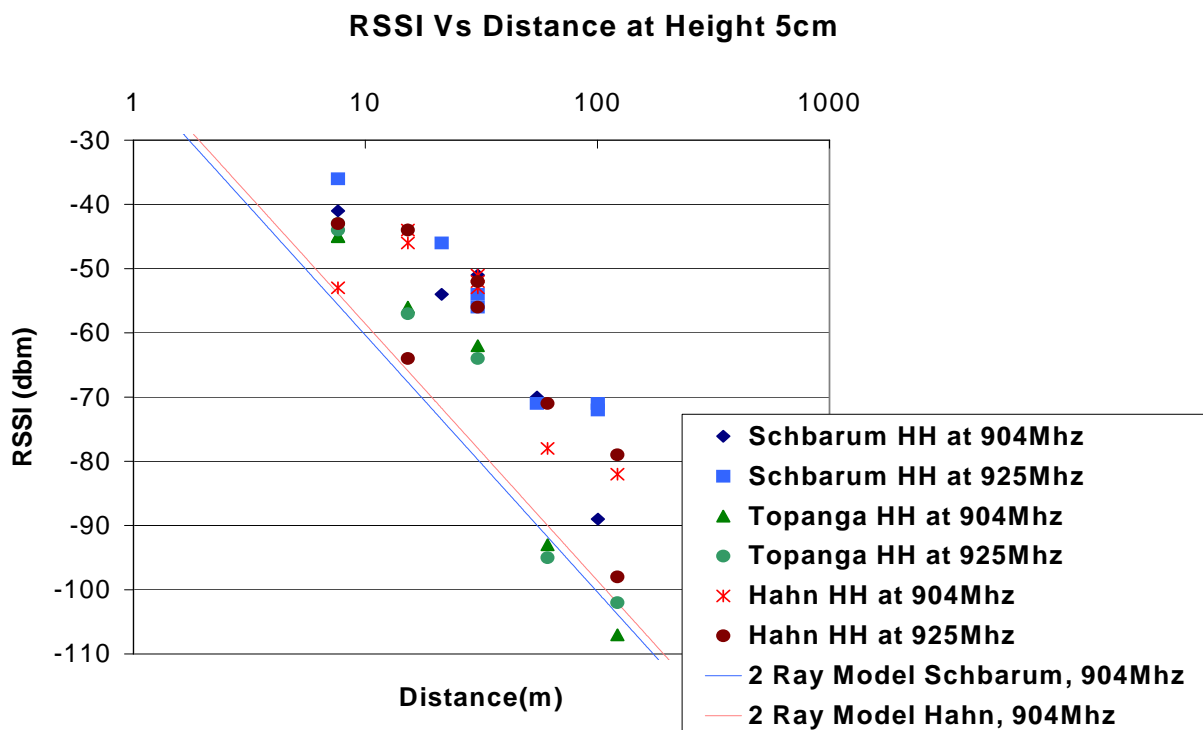


**Figure 146: Propagation fall-off in the areas with rolling hills, HH**

**RSSI Vs Distance at Height 5cm**
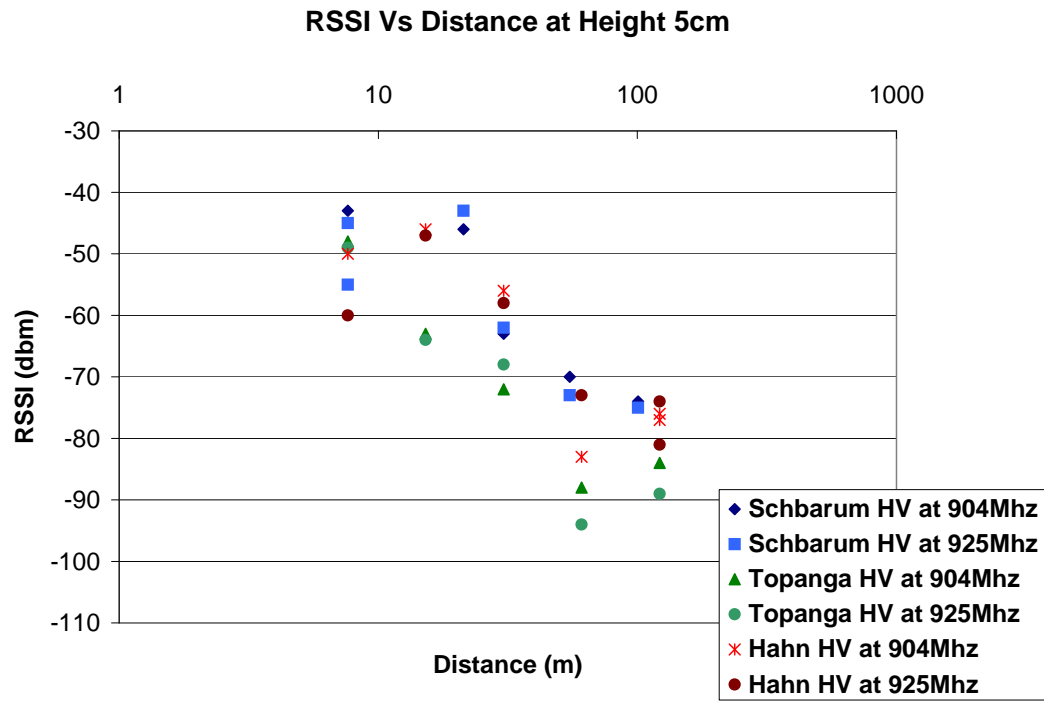


Figure 147: Propagation fall-off in the areas with rolling hills, HH.

**Path Loss over Distance, VV, 5cm Antenna Height**
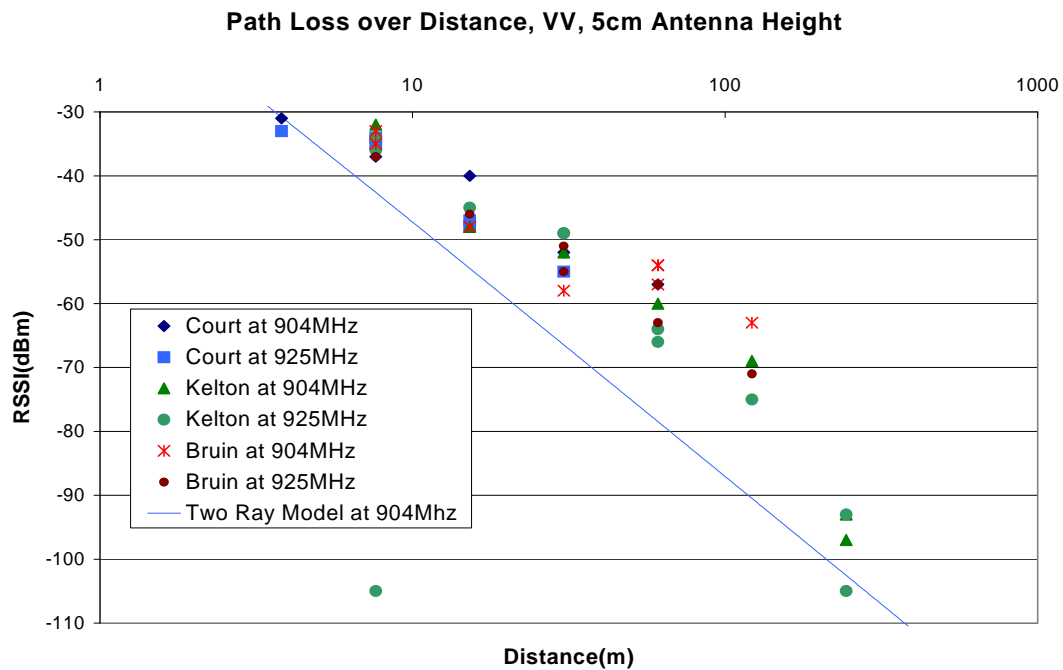


Figure 148: Propagation fall-off in urban areas, VV.

**Path Loss over Distance, HH, 5cm Antenna Heights**
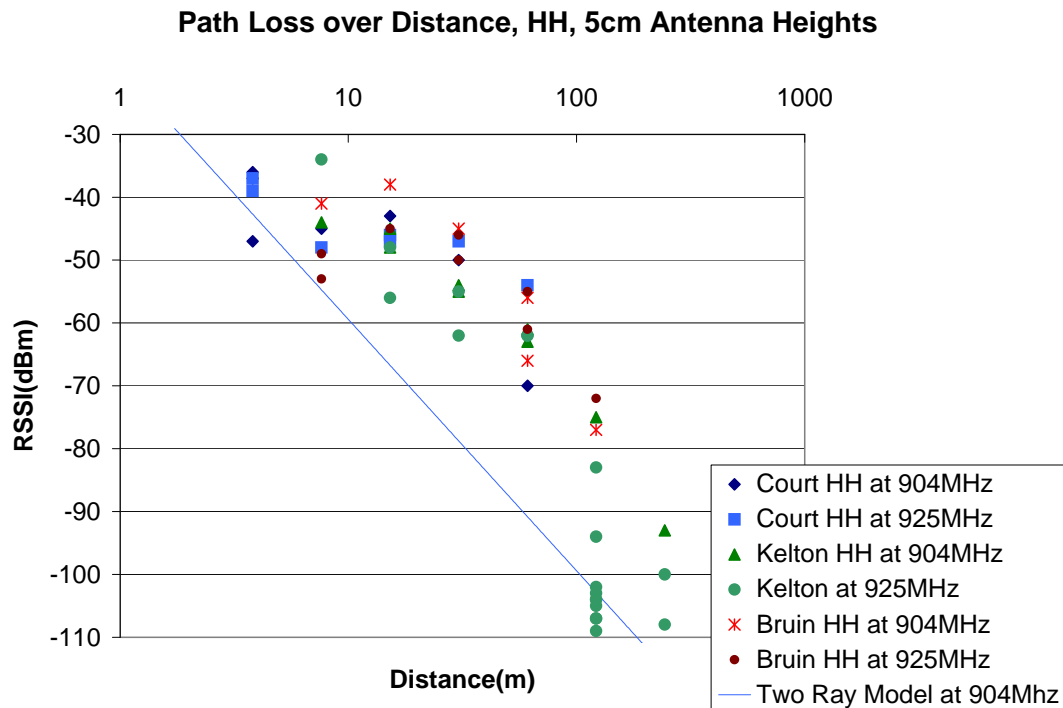


Figure 149: Propagation fall-off in urban areas, HH

**Path Loss over Distance, HV, 5cm Antenna Heights**
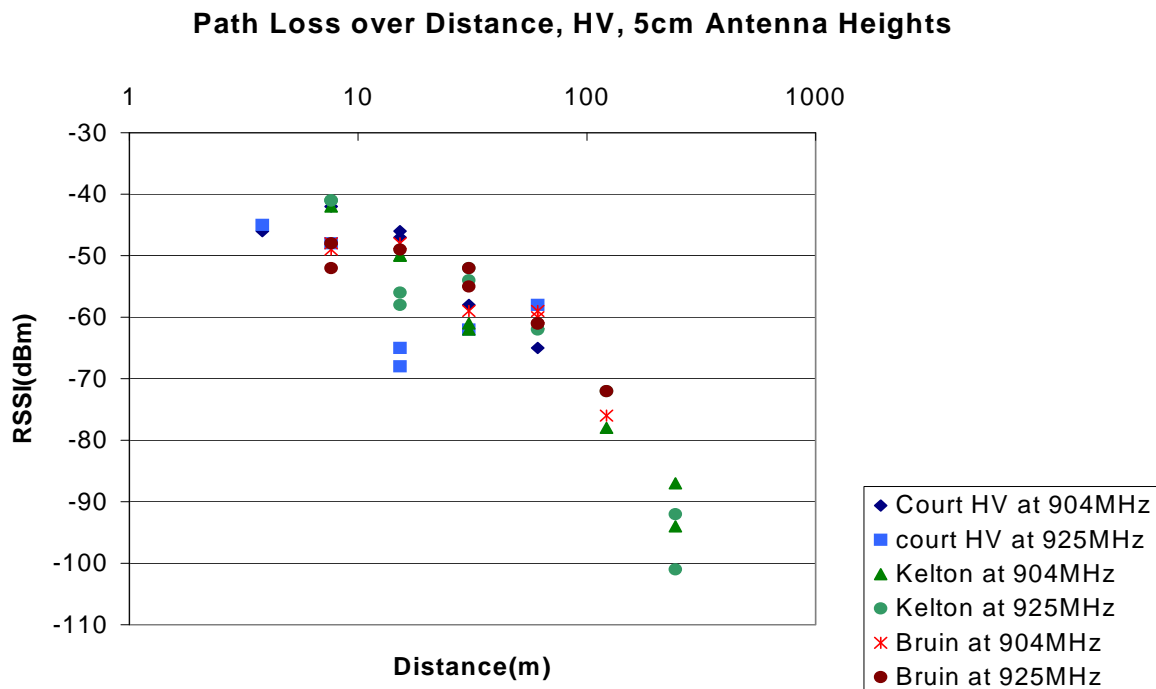


Figure 150: Propagation fall-off in urban areas, HV.

**Path loss over distance at 5cm Antenna Heights VV**
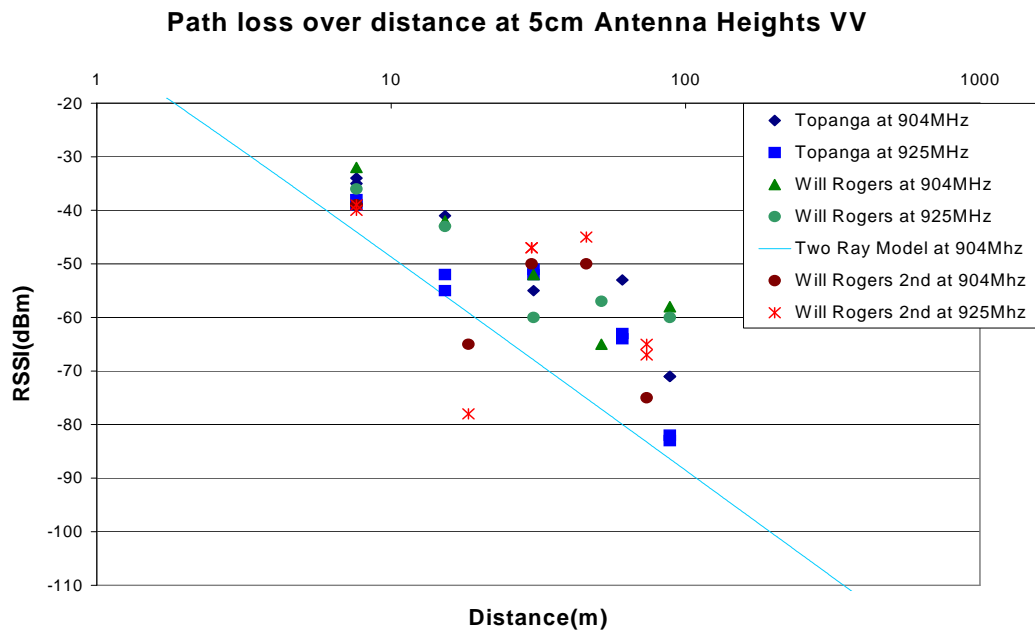


Figure 151: Propagation fall-off in areas with rough vegetation, VV.

**Path loss over distance at 5cm Antenna Height HH**
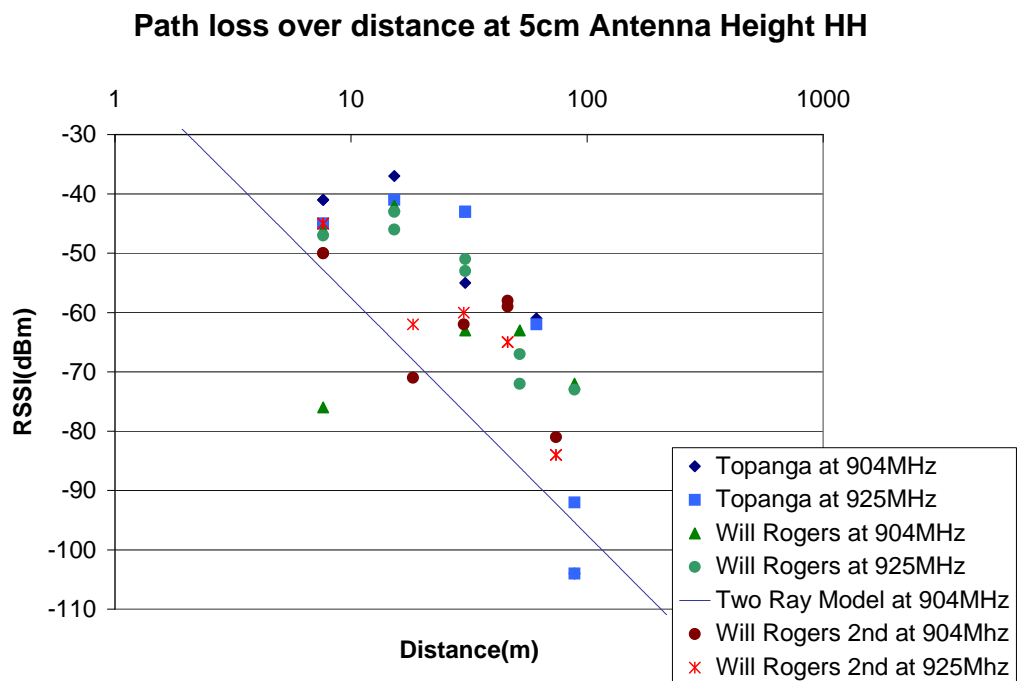


Figure 152: Propagation fall-off in areas with rough vegetation, HH.

## Path loss over distance at 5cm Antenna Heights HV
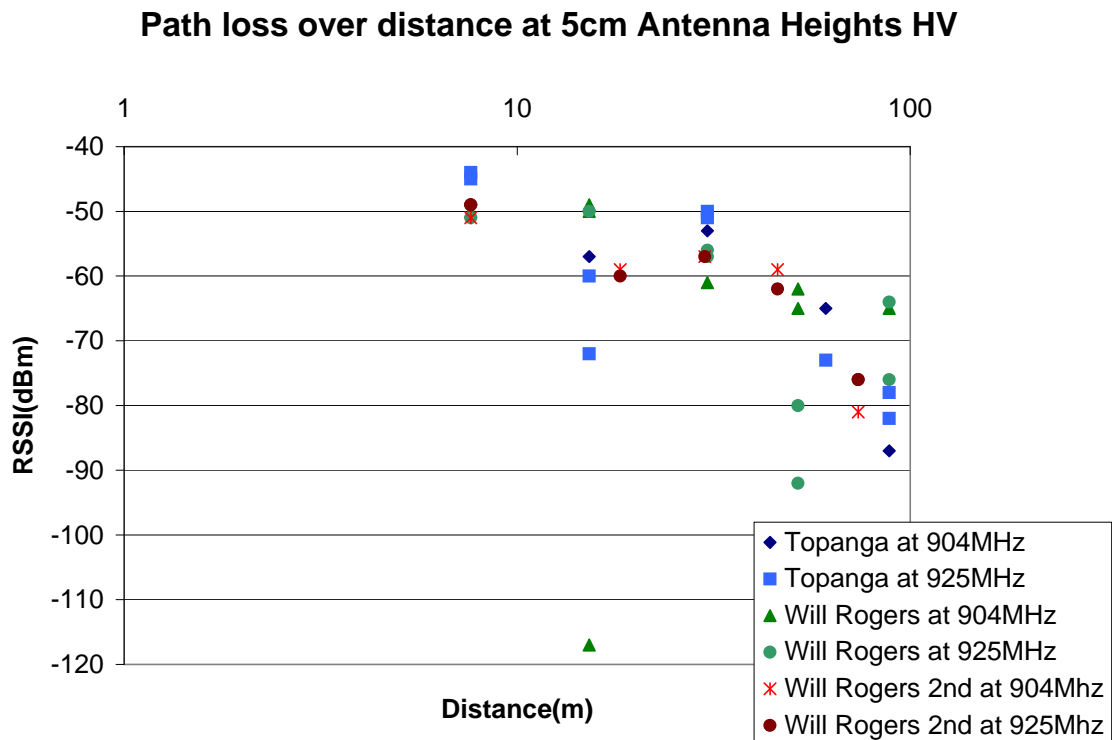


**Figure 153: Propagation fall-off in areas with rough vegetation, HV.**

## VV Power Fall off at 5cm Height, 20dBm Transmit Power
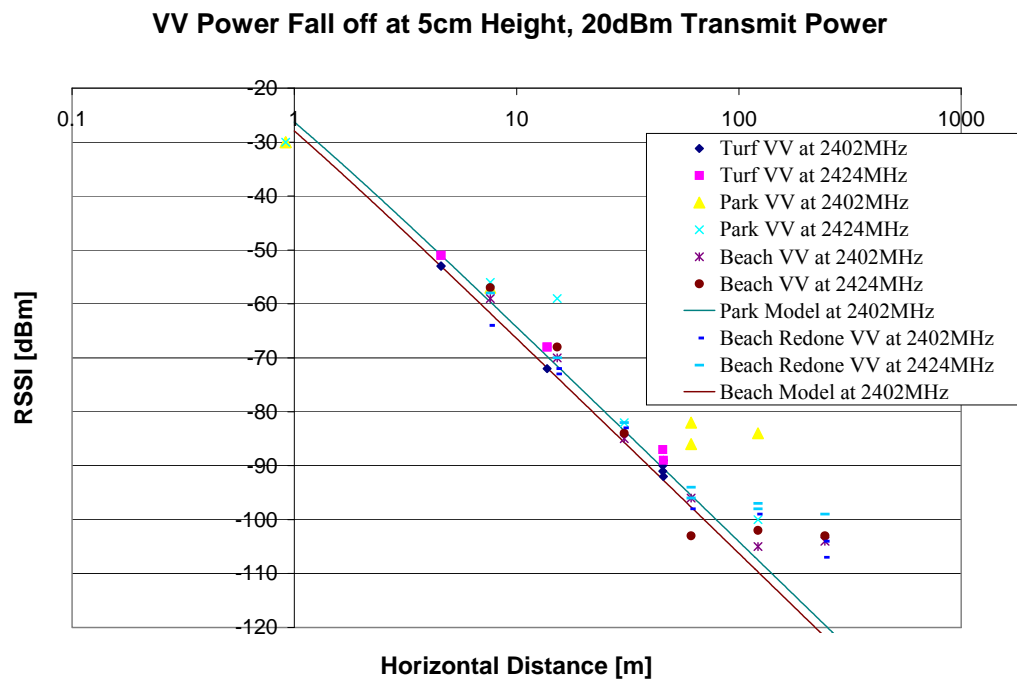


**Figure 154: Propagation fall-off in open environments, VV.**

## HH Power Fall off at 5cm Height, 20dBm Transmit Power
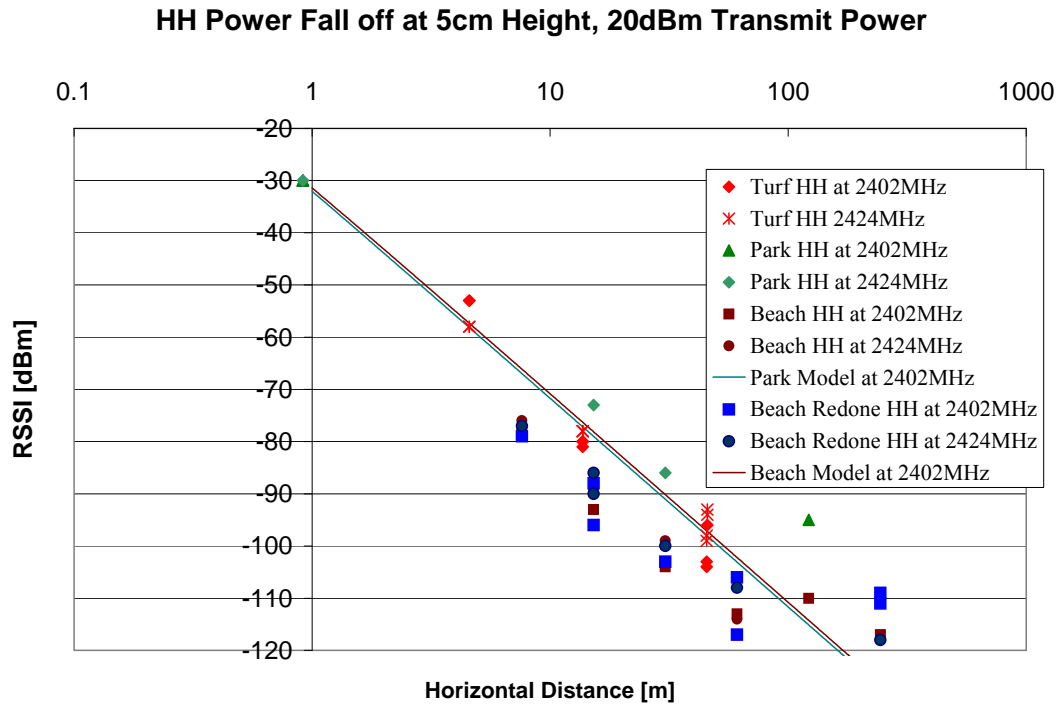


**Figure 155: Propagation fall-off in open environments, HH.**

## HV Power Fall off at 5cm, 20dBm Transmit Power
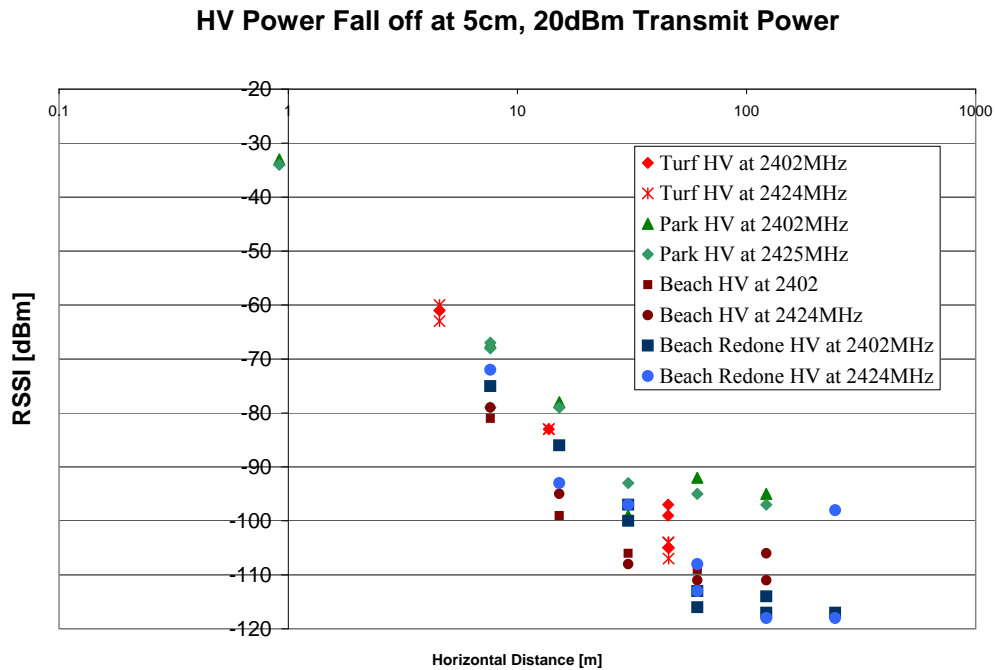


**Figure 156: Propagation fall-off in open environments, HV.**

**VV Propagation at 5cm Height and 20dBm Transmit Power**
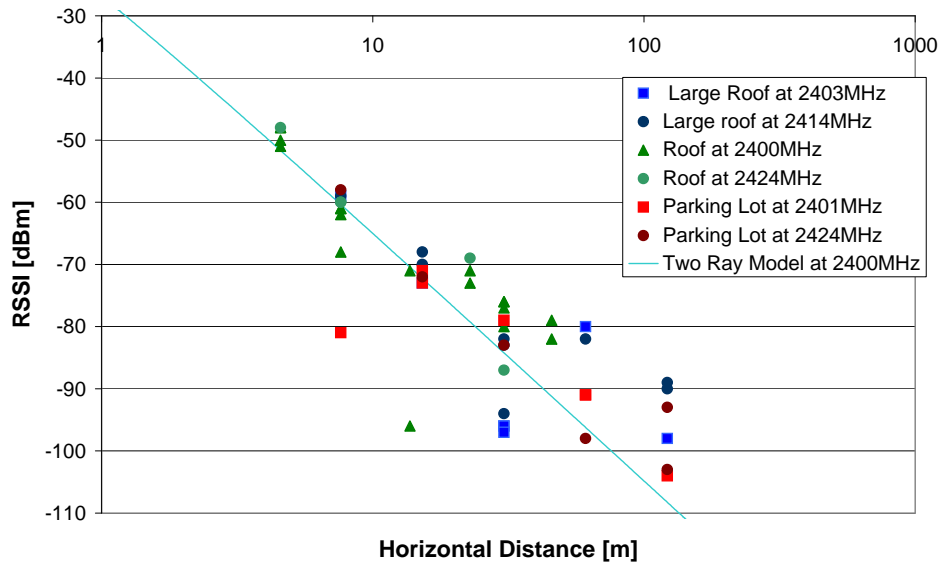


**Figure 157: Propagation fall-off in the parking lots measured, VV.**

**HH  Propagation at 5cm Height, 20dBm Transmit Power**
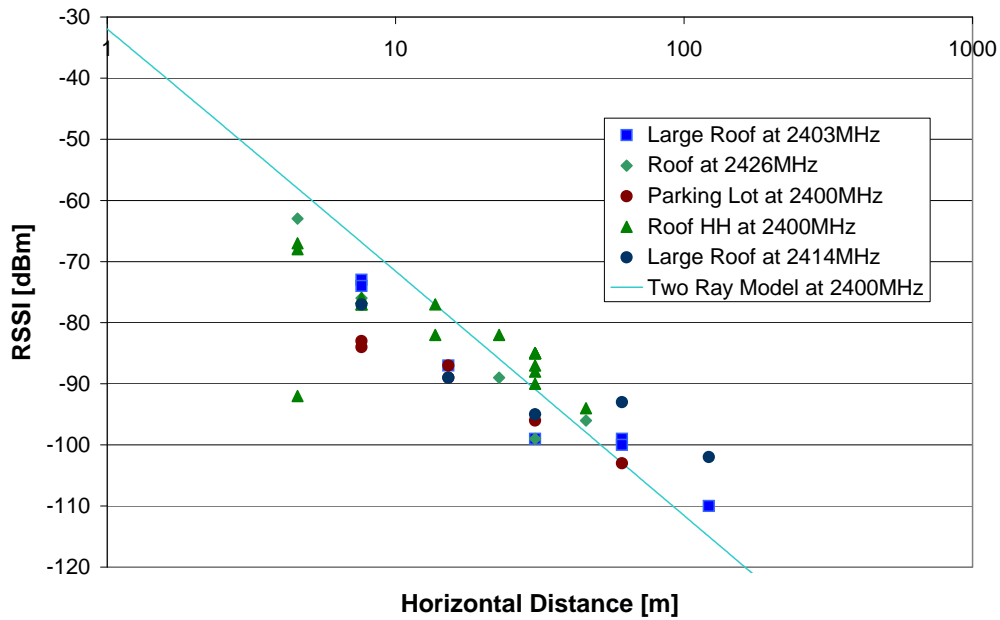


**Figure 158:  Propagation fall-off in the parking lots measured, HH.**

**HV Propagation at 5cm Height and 20dBm Transmit Power**
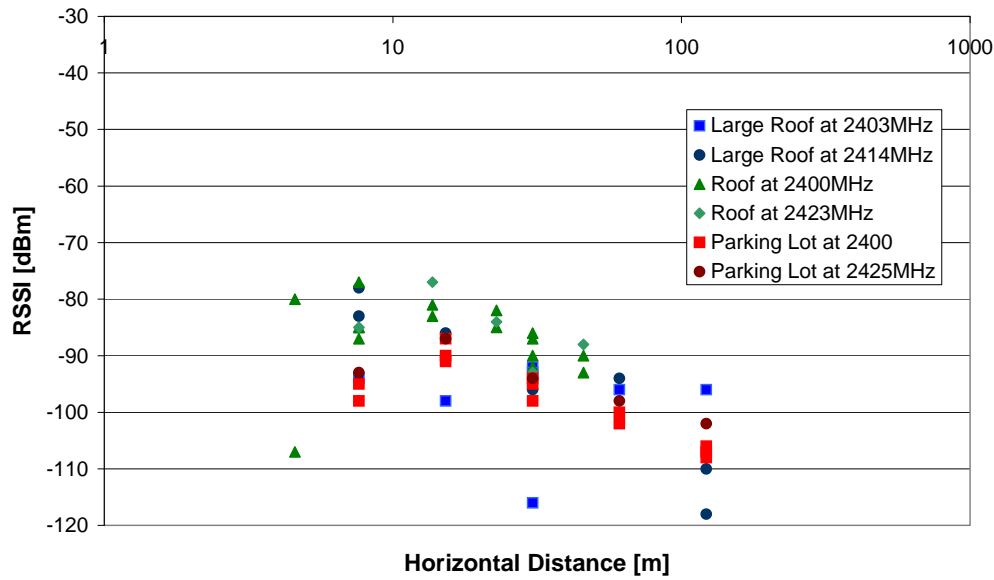


**Figure 159: Propagation fall-off in the parking lots measured, HV.**

**VV at 5cm and 20dBm Transmit Power**
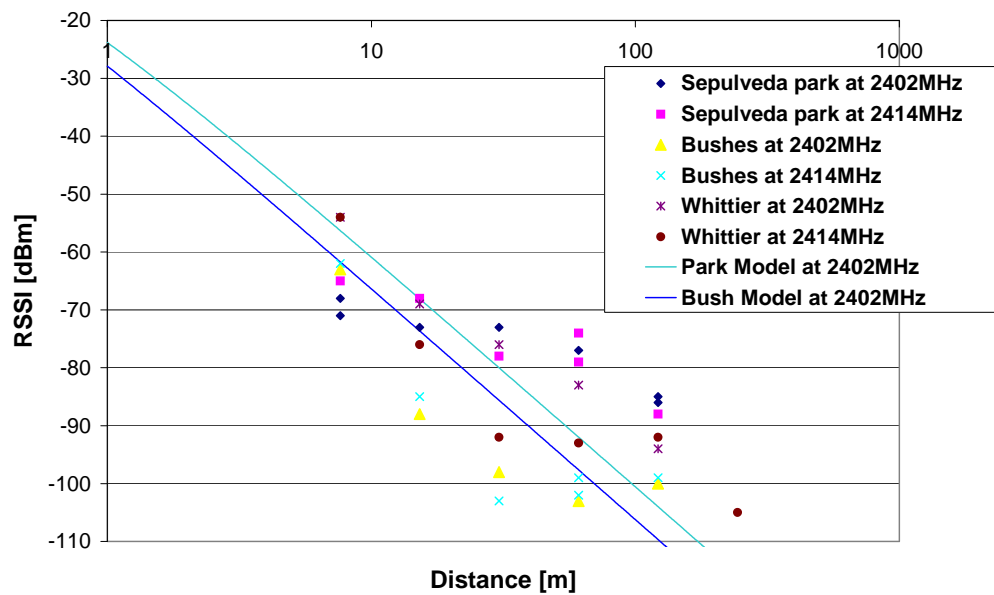


**Figure 160: Propagation fall-off in vegetation, VV.**

93

**HH at 5cm**
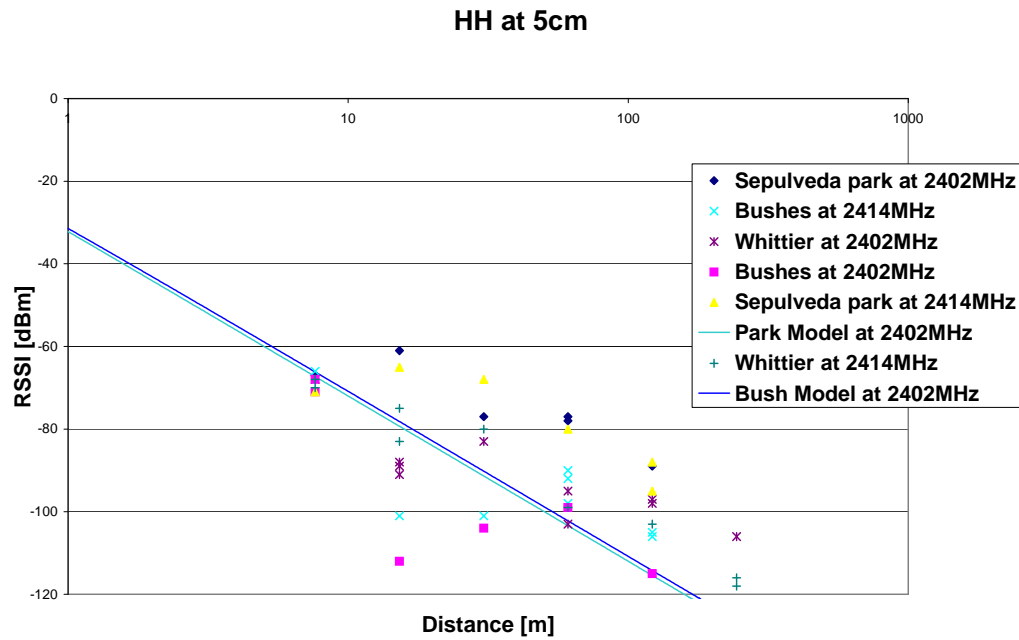


**Figure 161: Propagation fall-off in vegetation, HH.**

**2.4GHz HV at 5cm**
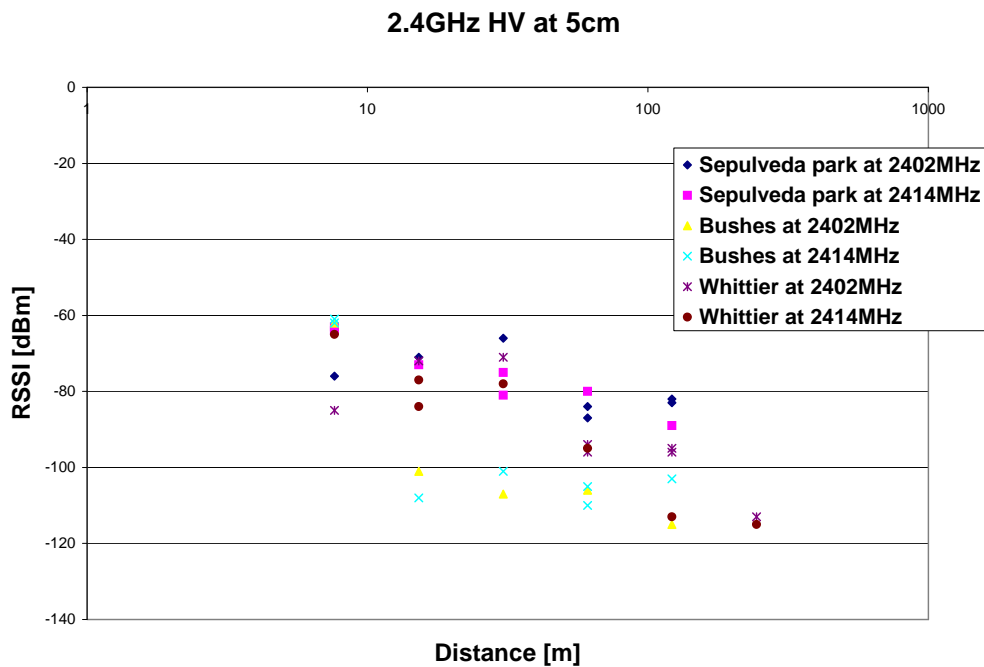


**Figure 162: Propagation fall-off in vegetation, HV.**

**RSSI Vs Distance at Height 5cm**
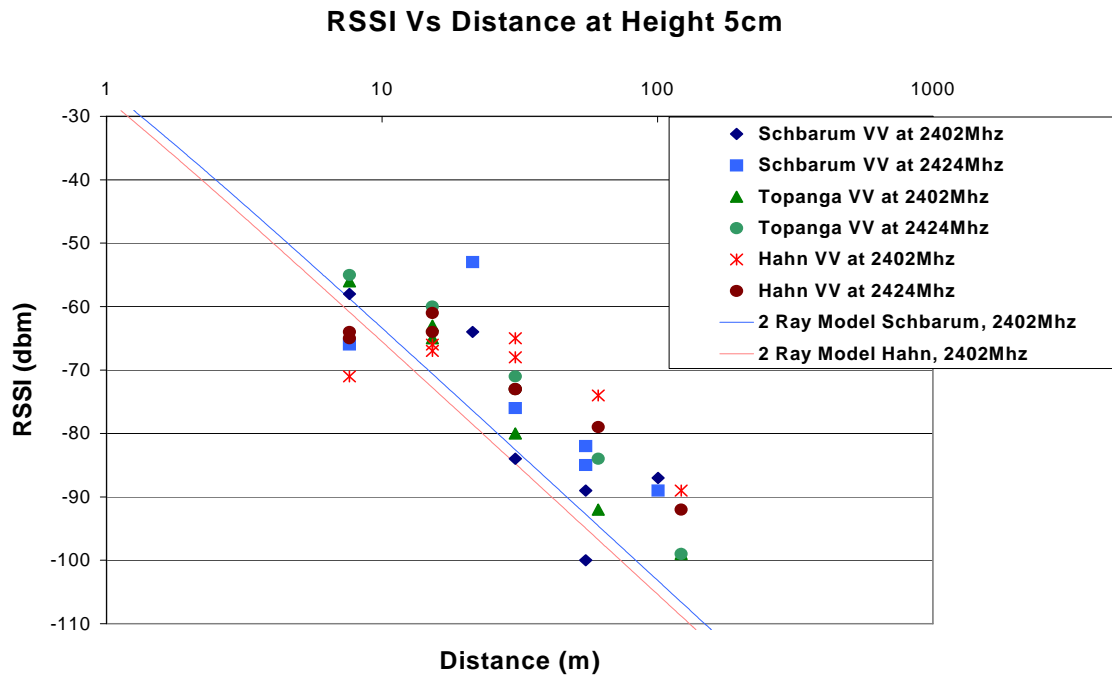


**Figure 163: Propagation fall-off in areas with rolling hills, VV.**

**RSSI Vs Distance at Height 5cm**
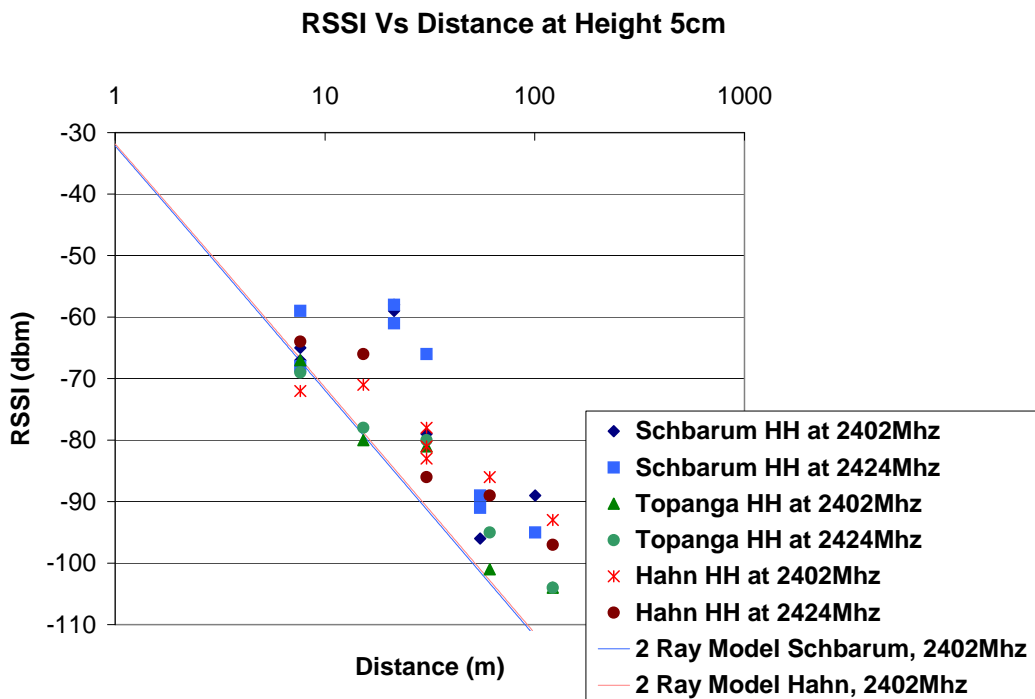


**Figure 164: Propagation fall-off in areas with rolling hills, HH.**

**RSSI Vs Distance at Height 5cm**
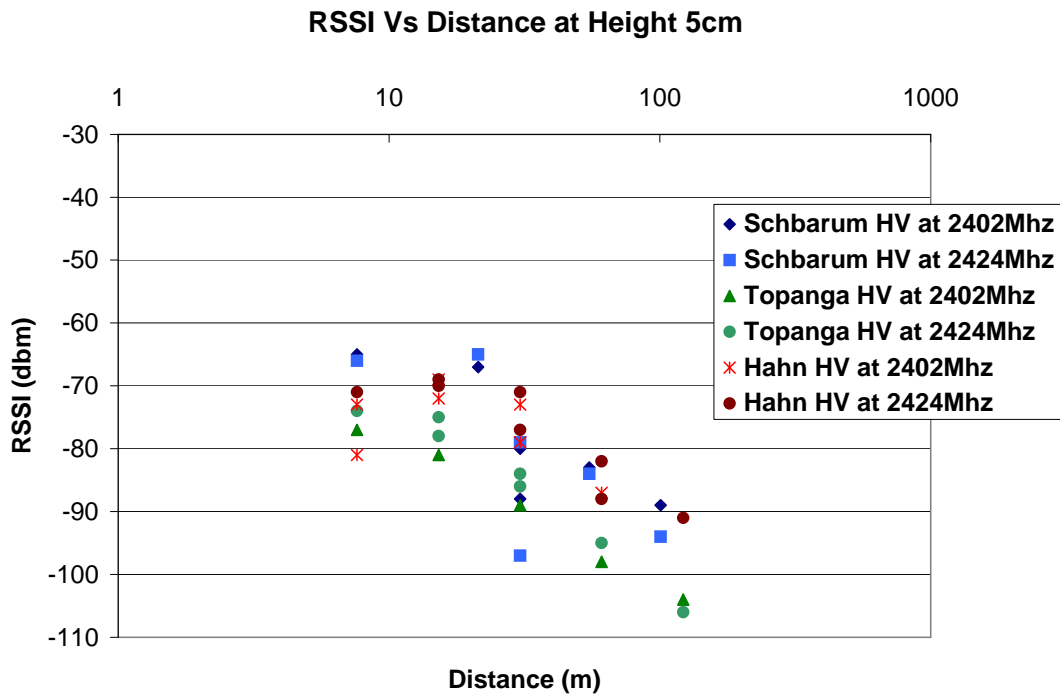


**Figure 165: Propagation fall-off in areas with rolling hills, HV.**

**Path Loss over Distance, VV, 5cm Antenna Heights**
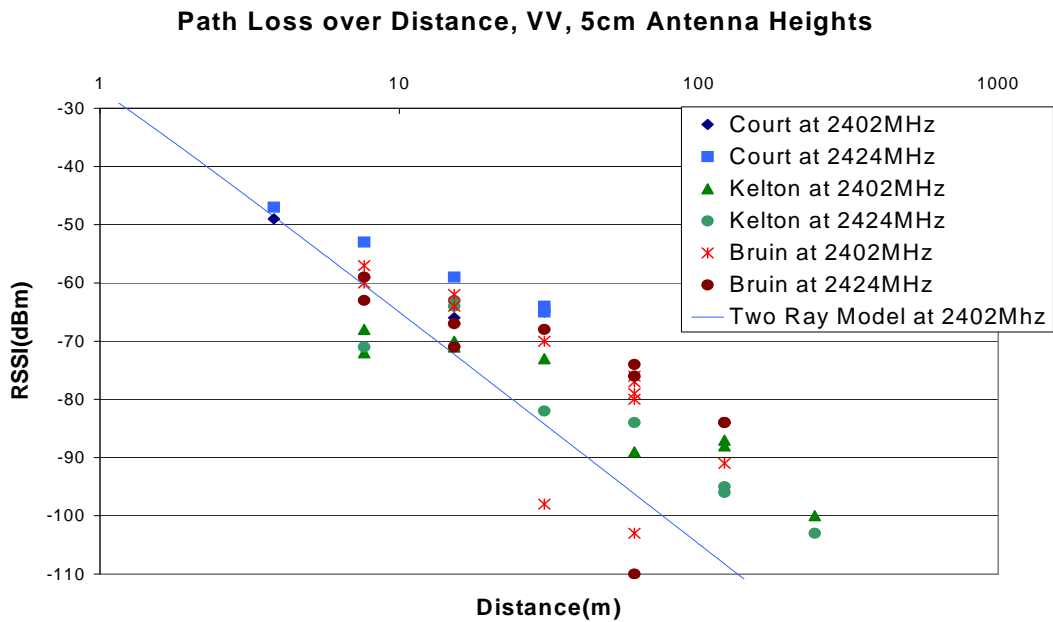


**Figure 166: Propagation fall-off in urban areas, VV.**

96

**Path Loss over Distance, HH, 5cm Antenna Heights**
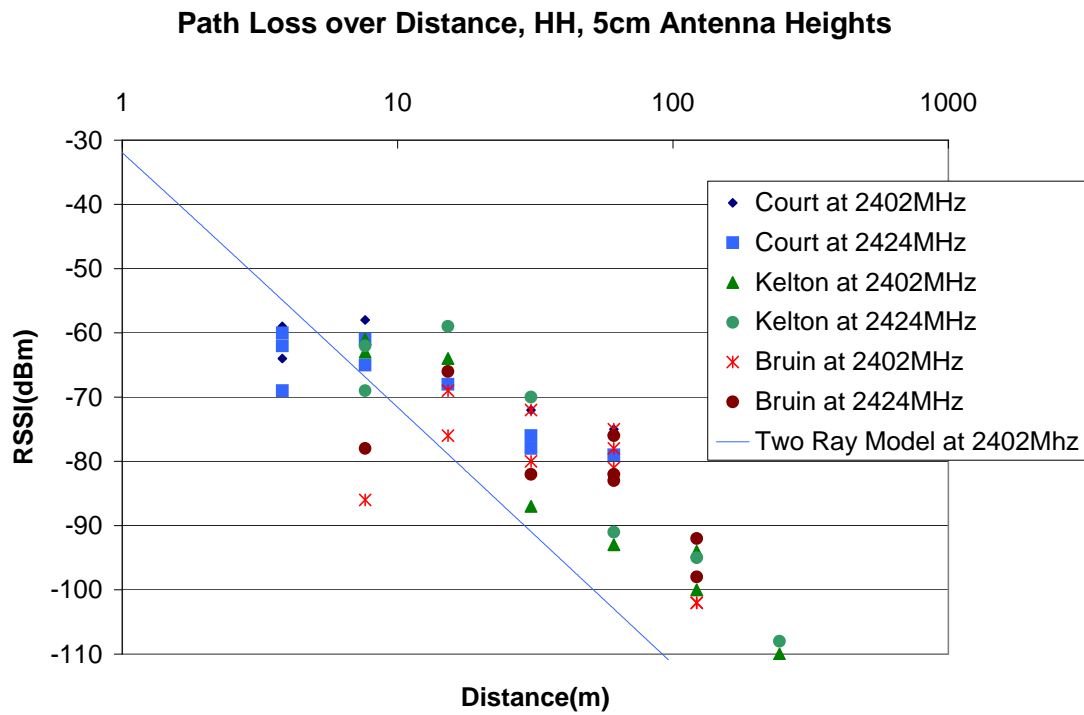


**Figure 167: Propagation fall-off in urban areas, HH.**

**Path Loss over Distance, HV, 5cm Antenna Heights**
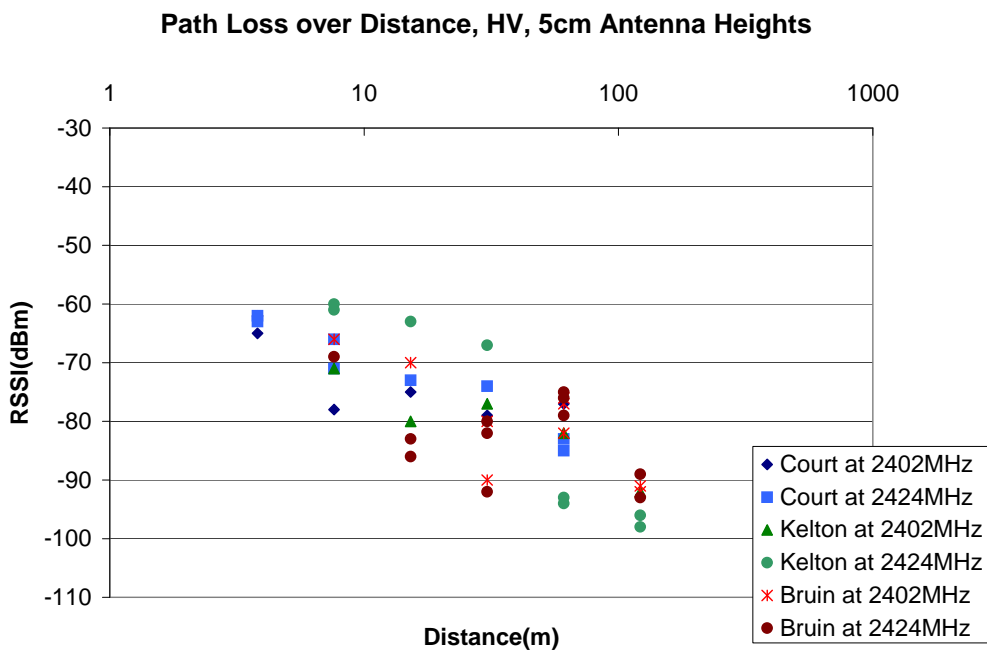


**Figure 168: Propagation fall-off in urban areas, HV.**

**Path loss over distance at 5cm Antenna Heights VV**
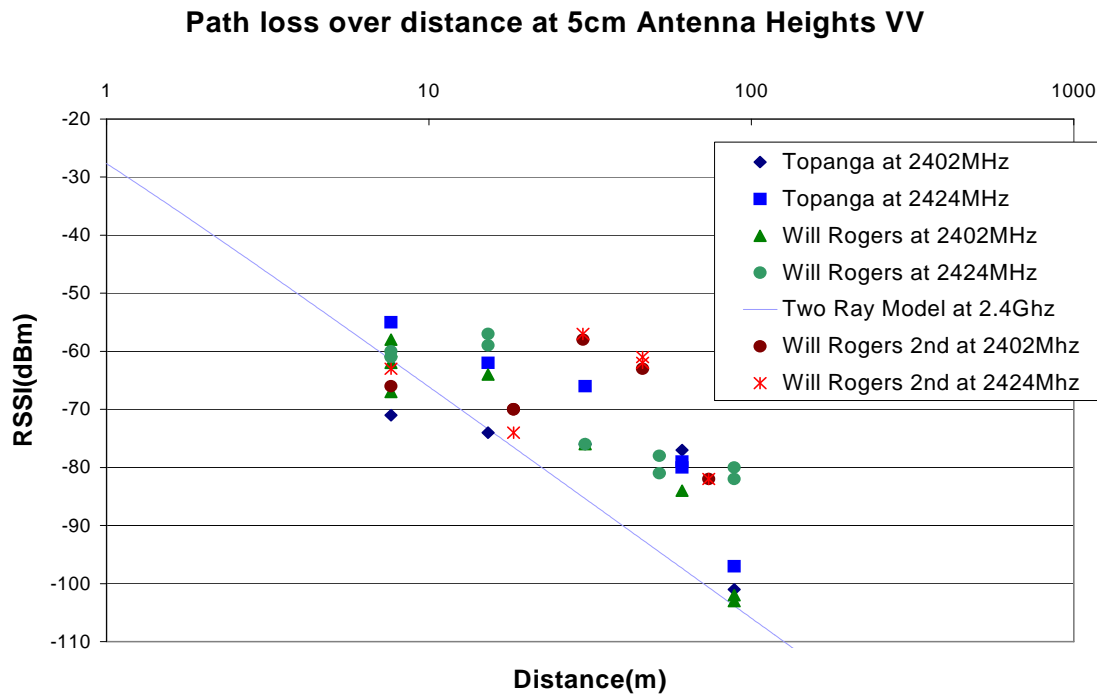


**Figure 169: Propagation fall-off in areas with rough vegetation, VV.**

**Path loss over distance at 5cm Antenna Heights HH**
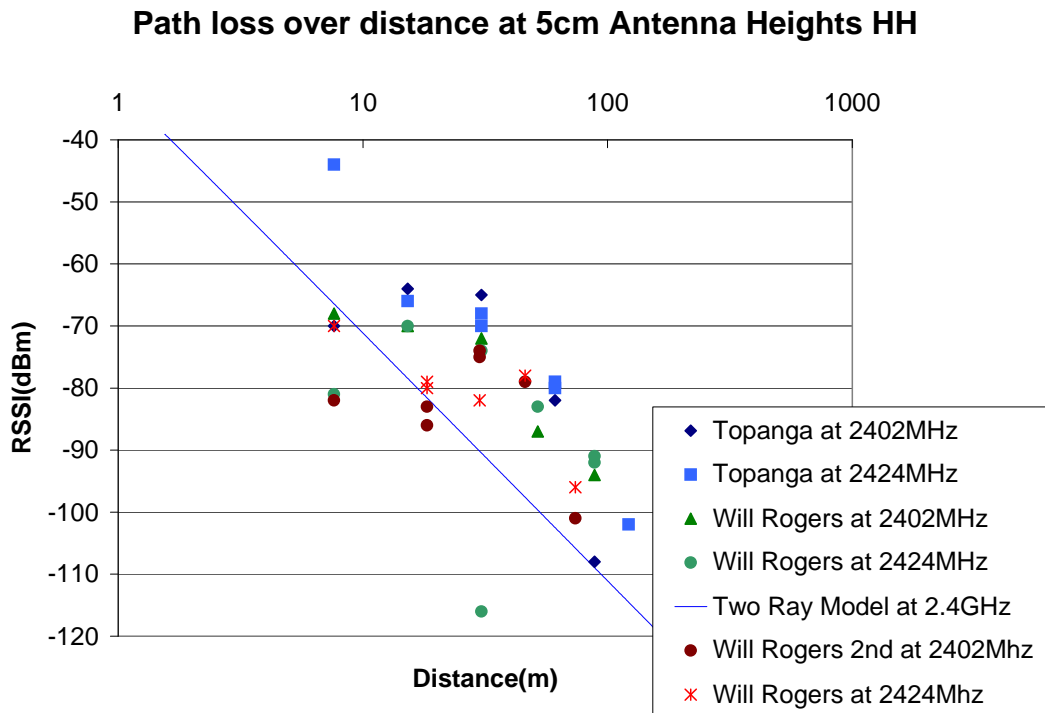


**Figure 170: Propagation fall-off in areas with rough vegetation, HH.**

98

## Path loss over distance at 5cm Antenna Height HV



**Figure 171: Propagation fall-off in areas with rough vegetation, HV.**

## VV Power Fall off at 5cm Height, 27dBm Transmit Power
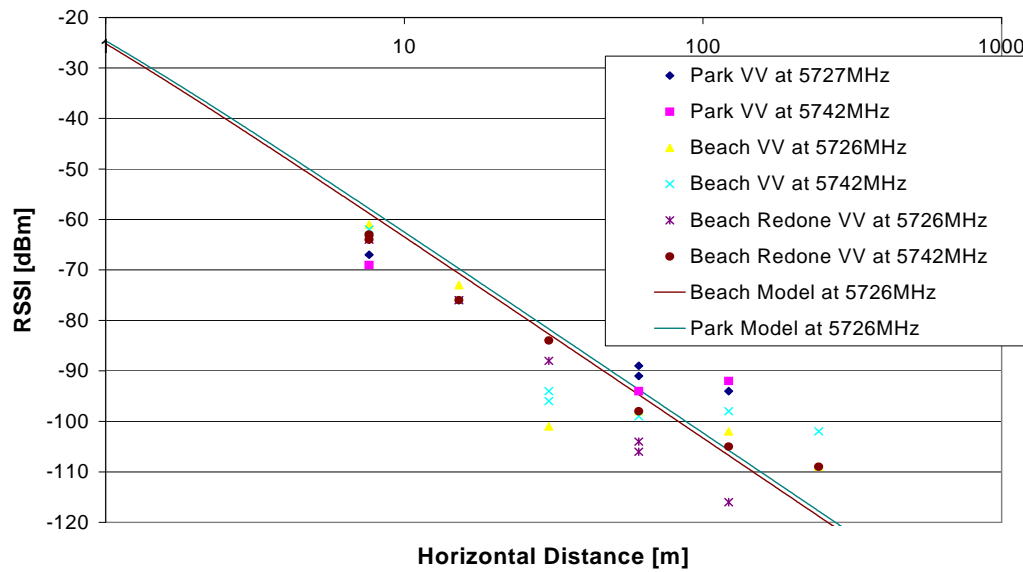


**Figure 172: Propagation fall-off in open environments, VV.**

## HH Power Fall off at 5cm Height, 27dBm Transmit Power
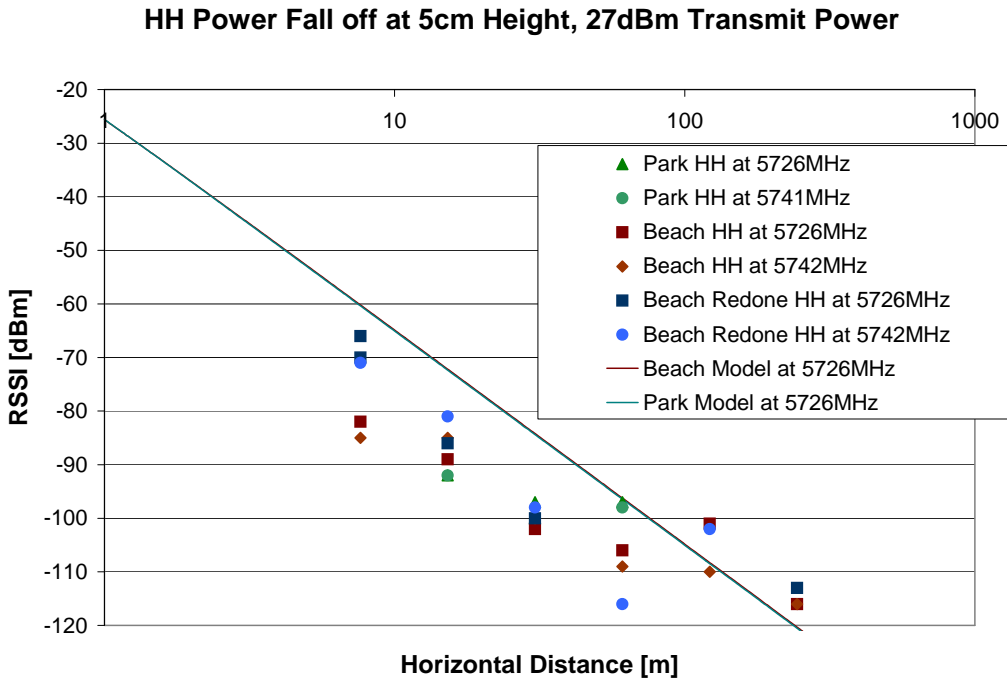


**Figure 173: Propagation fall-off in open environments, HH.**

## HV Power Fall off at 5cm Height, 27dBm Transmit Power
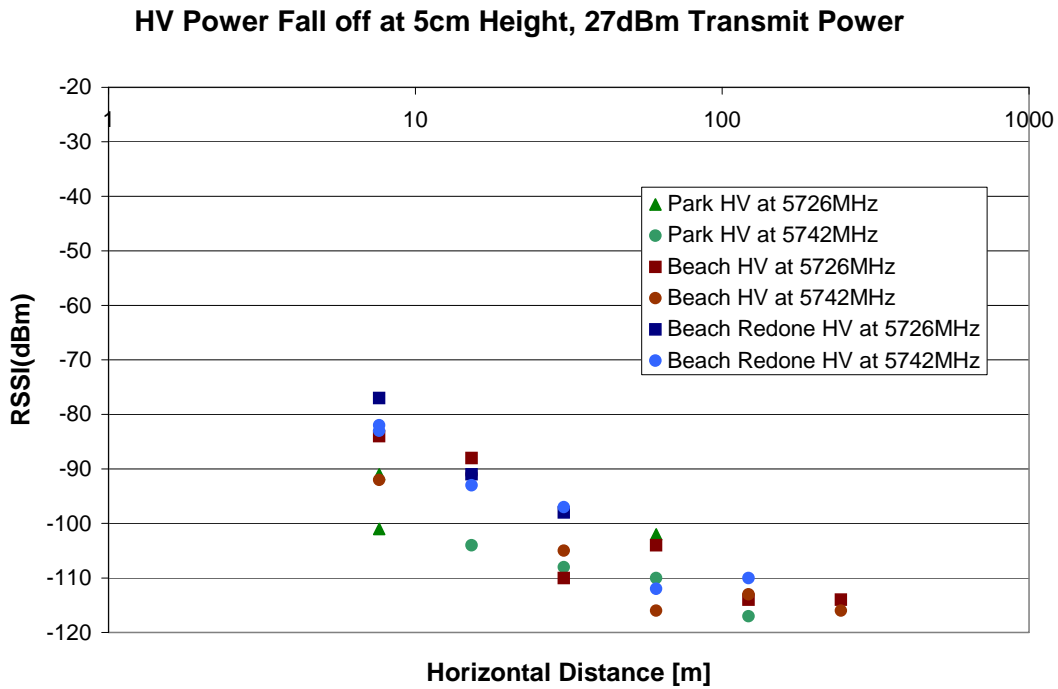


**Figure 174: Propagation fall-off in open environments, HV.**

## VV Propagation at 5cm Height and 27dBm Transmit Power
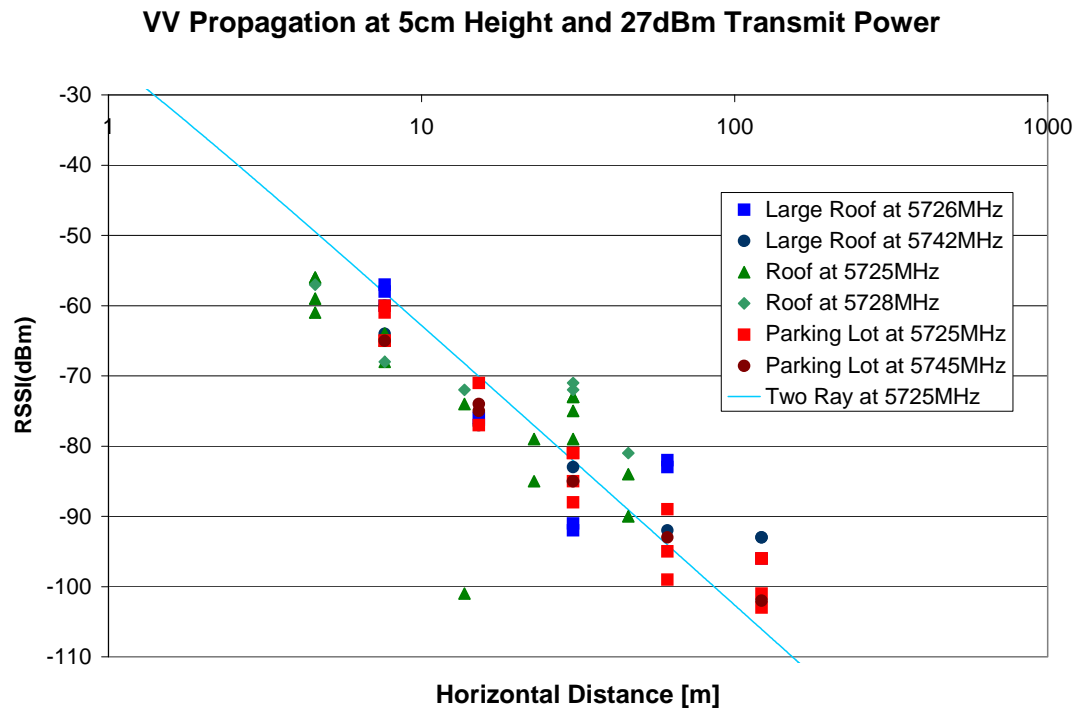


**Figure 175: Propagation fall-off in parking lots measured, VV.**

## HH Propagation at 5cm Height and 27dBm Transmit Power
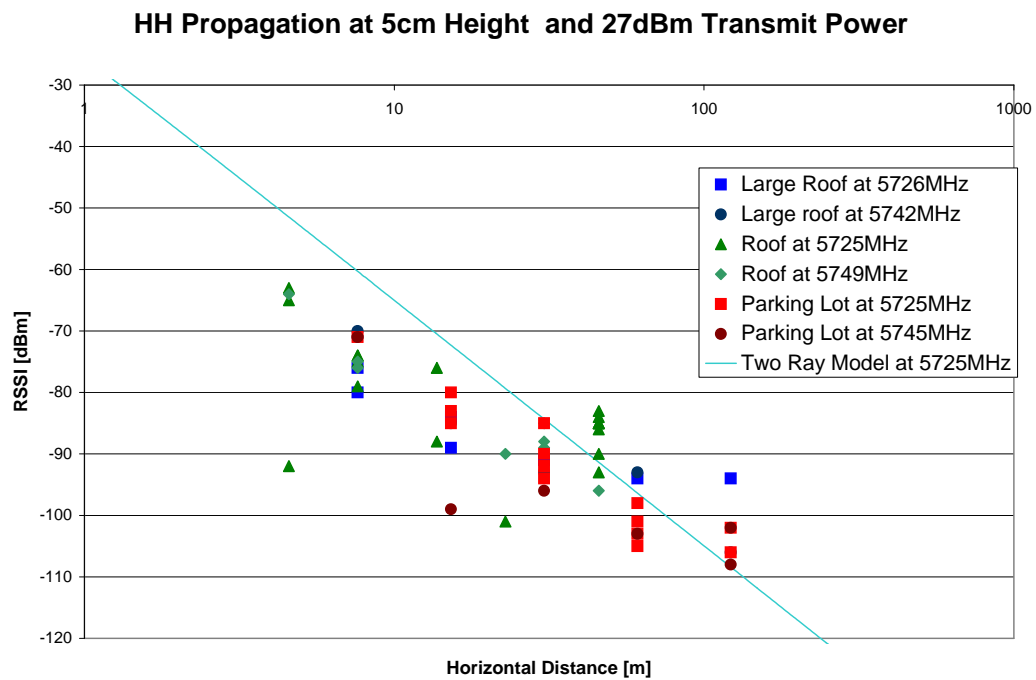


**Figure 176: Propagation fall-off in parking lots measured, HH.**

101

**HV Propagation at 5cm Height and 27dBm Transmit Power**
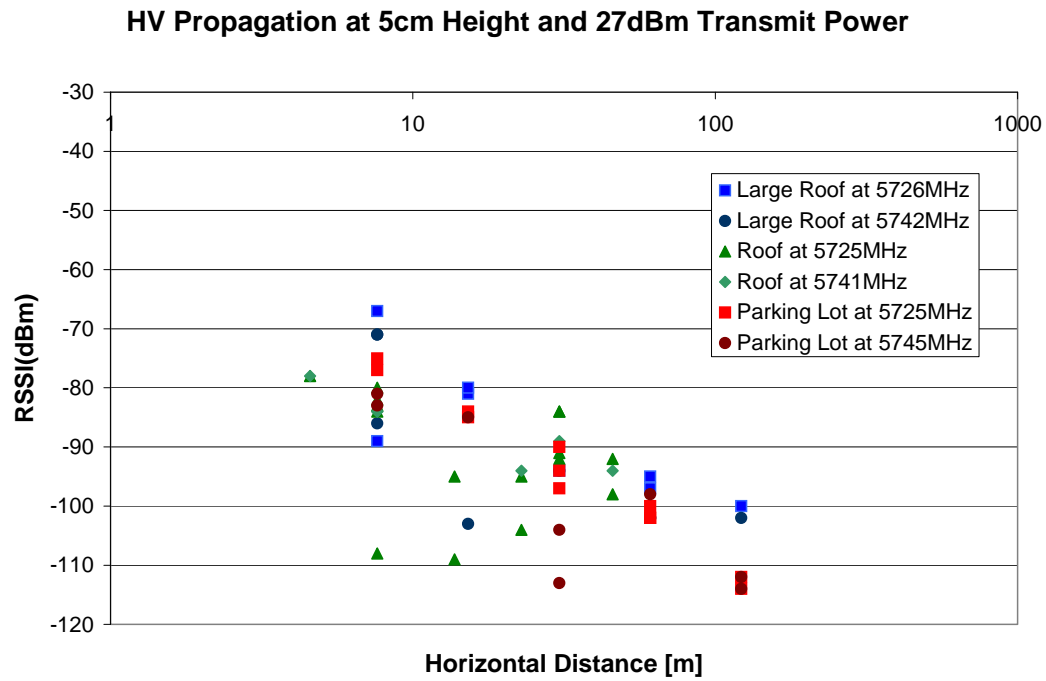


**Figure 177: Propagation fall-off in parking lots measured, HV.**

**VV at 5cm and 27dBm Transmit Power**
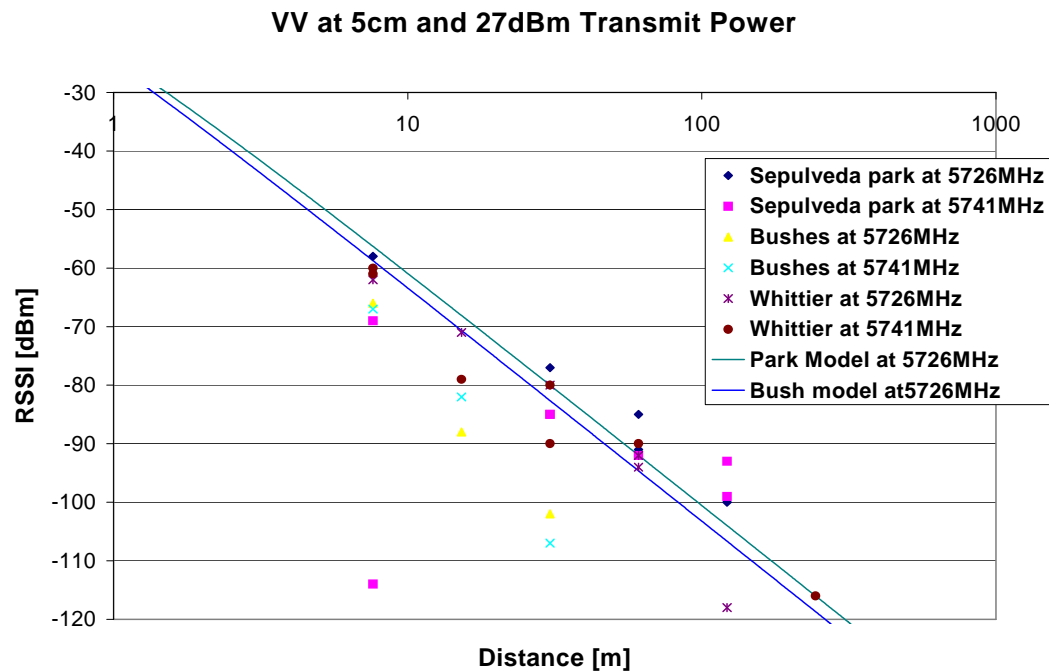


**Figure 178: Propagation fall-off in areas with vegetation, VV.**

## 5.7GHz HH at 5cm 27dBm Transmit Power
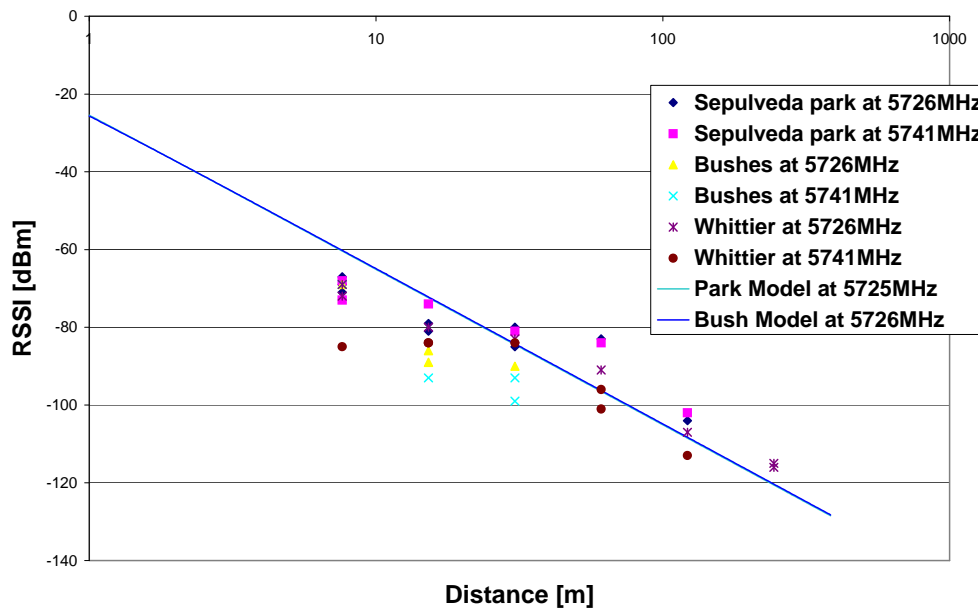


**Figure 179: Propagation fall-off in areas with vegetation, HH.**

## HV Polarization for 5cm Heights
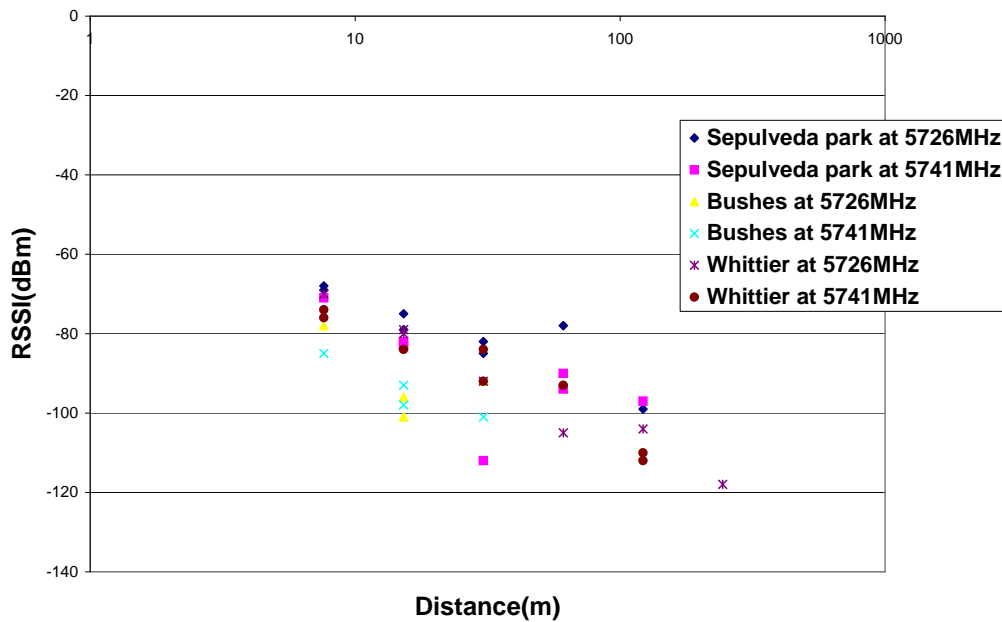


**Figure 180: Propagation fall-off in areas with vegetation, HV.**

**RSSI Vs Distance at Height 5cm**
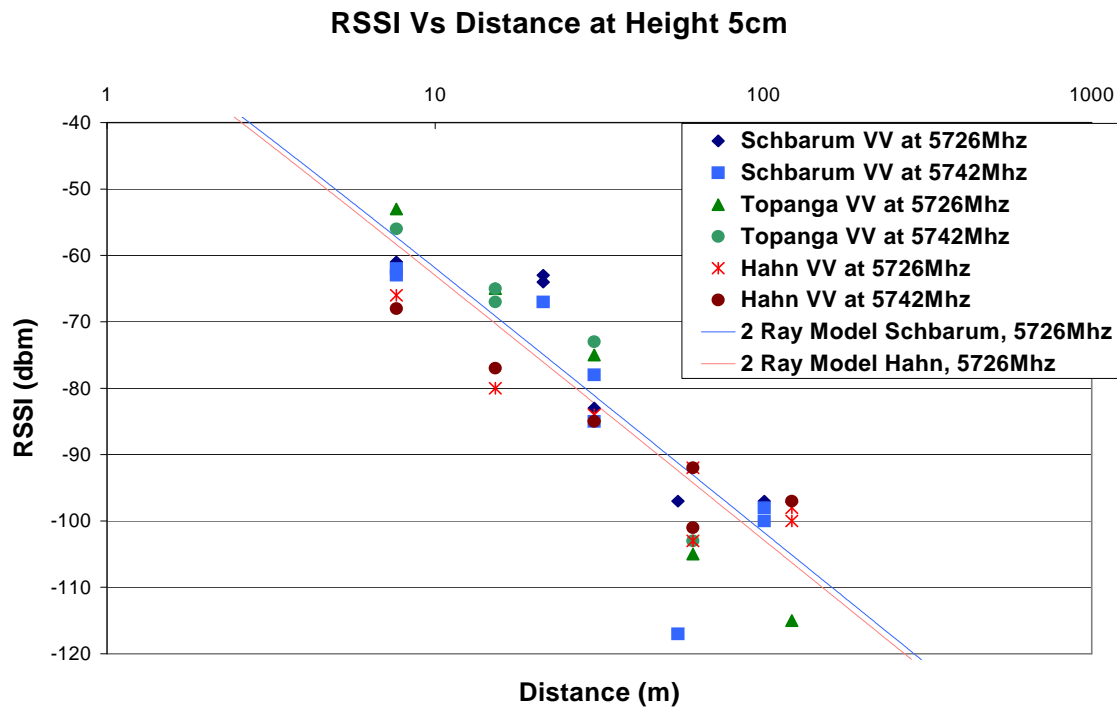


**Figure 181: Propagation fall-off in areas with rolling hills, VV.**

**RSSI Vs Distsance at Height 5cm**
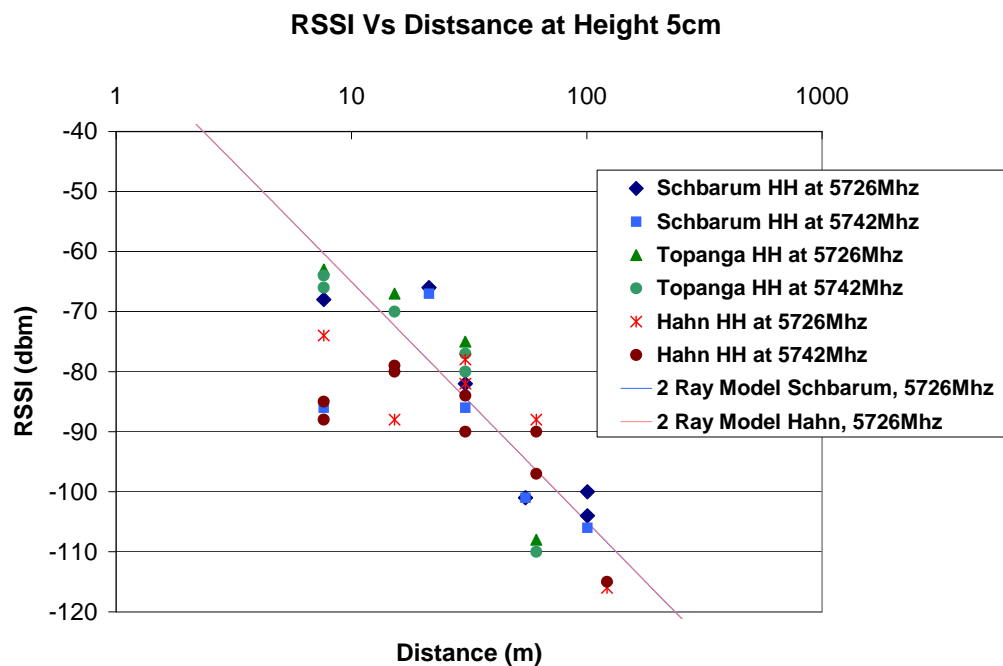


**Figure 182: Propagation fall-off in areas with rolling hills, HH.**

**RSSI Vs Distasnce at Height 5cm**
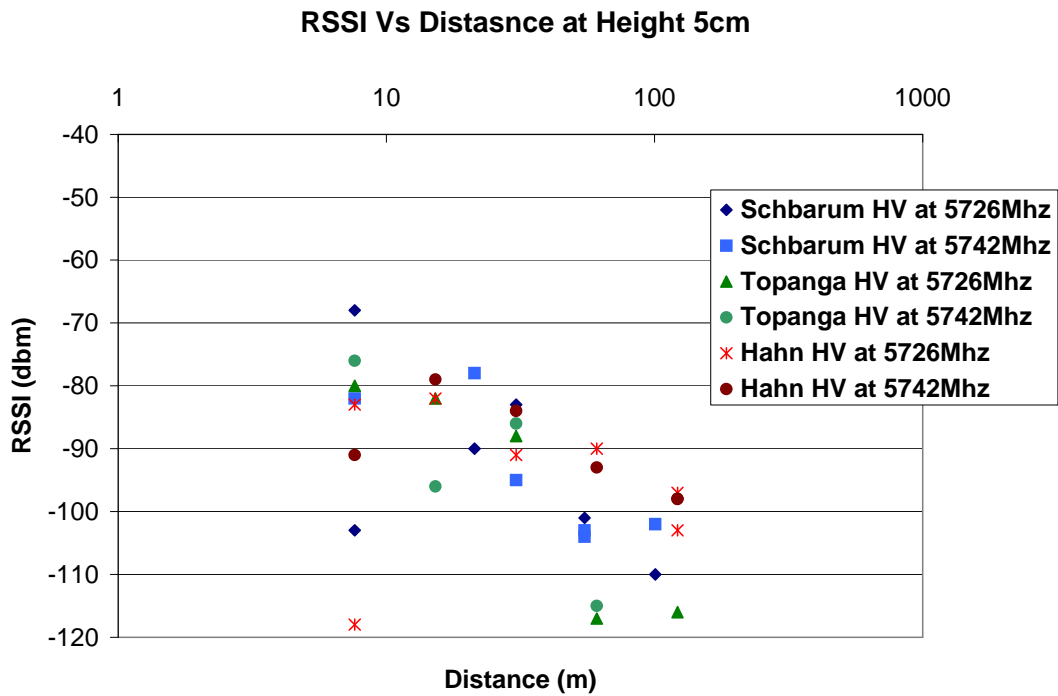


**Figure 183: Propagation fall-off in areas with rolling hills, HV.**

**Path Loss over Distance VV 5cmh**
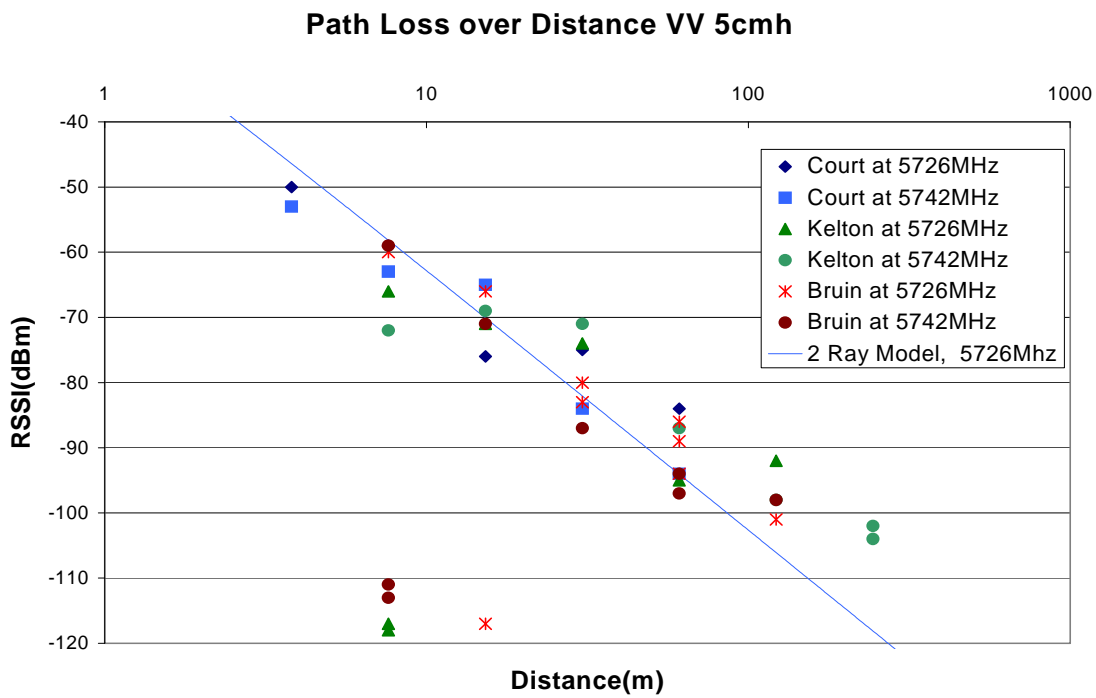


**Figure 184: Propagation fall-off in urban areas, VV.**

**Path Loss over Distance, HH, 5cm Antenna Heights**
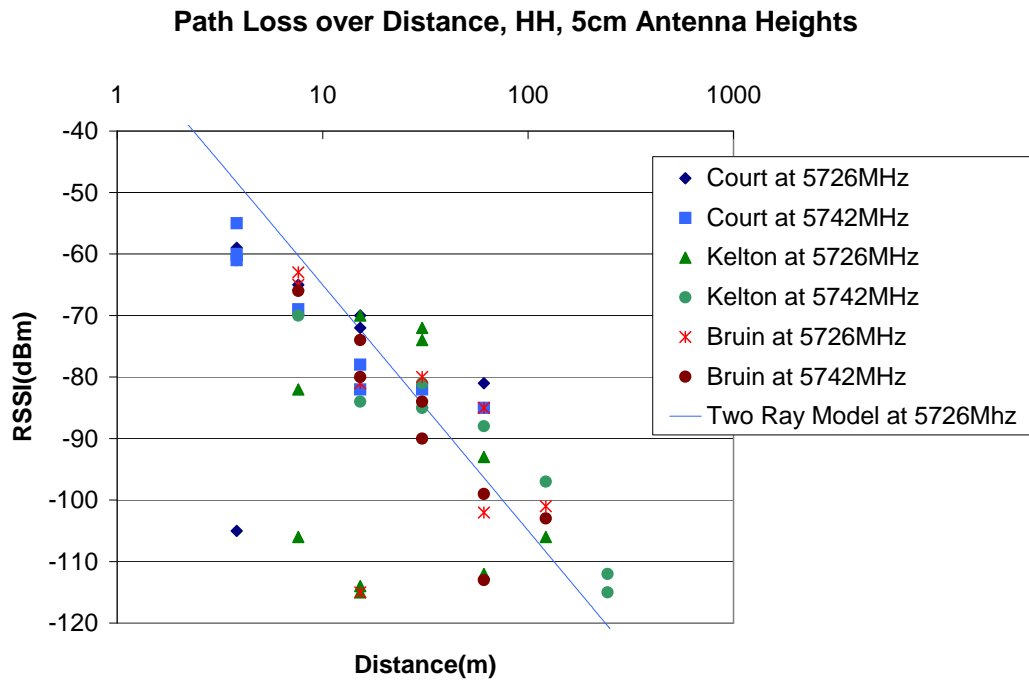


**Figure 185: Propagation fall-off in urban areas, HH.**

**Path Loss over Distance, HV, 5cm Antenna Heights**
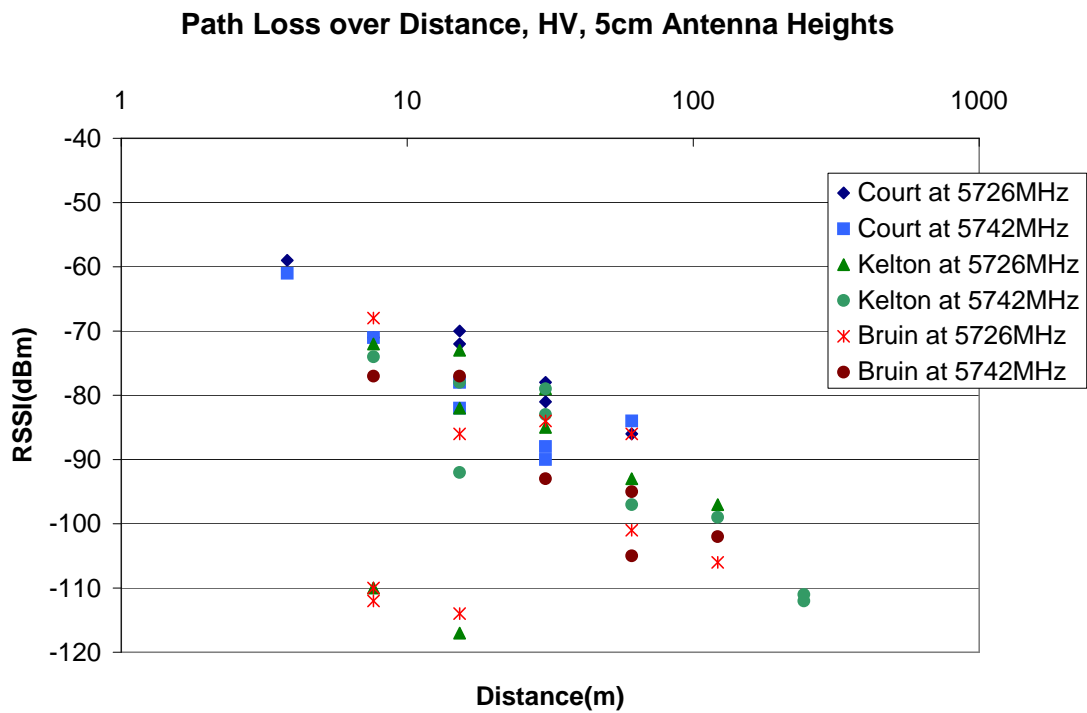


**Figure 186: Propagation fall-off in urban areas, HV.**

**Path loss over distance at 5cm Antenna Heights VV**
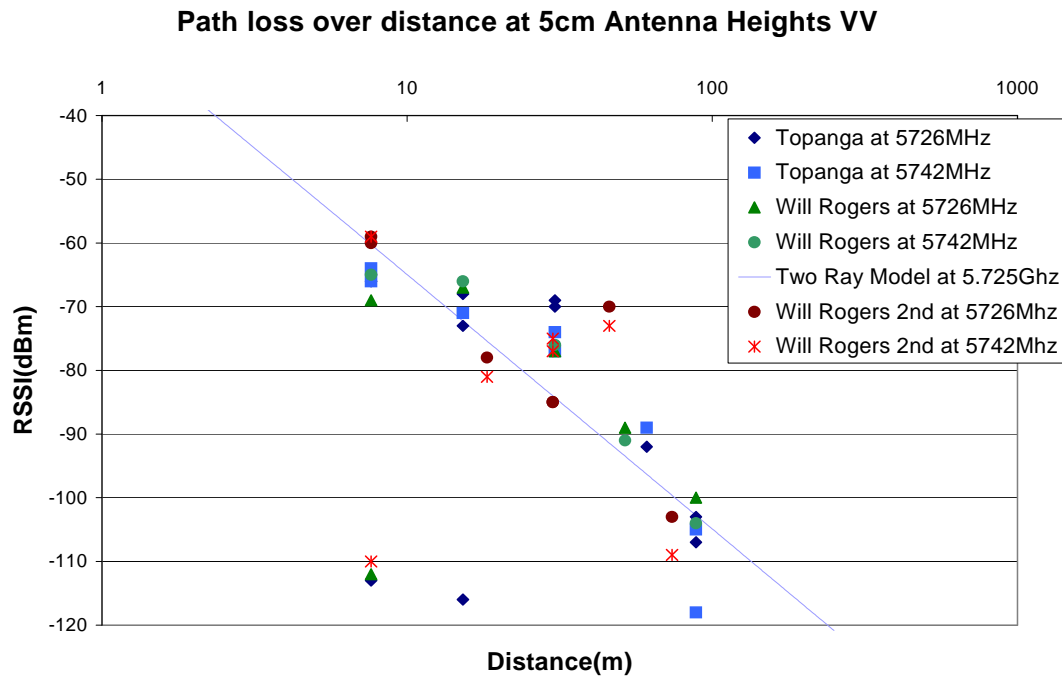


**Figure 187: Propagation fall-off in areas with rough vegetation, VV.**

**Path loss over distance at 5cm Antenna Heights, HH**
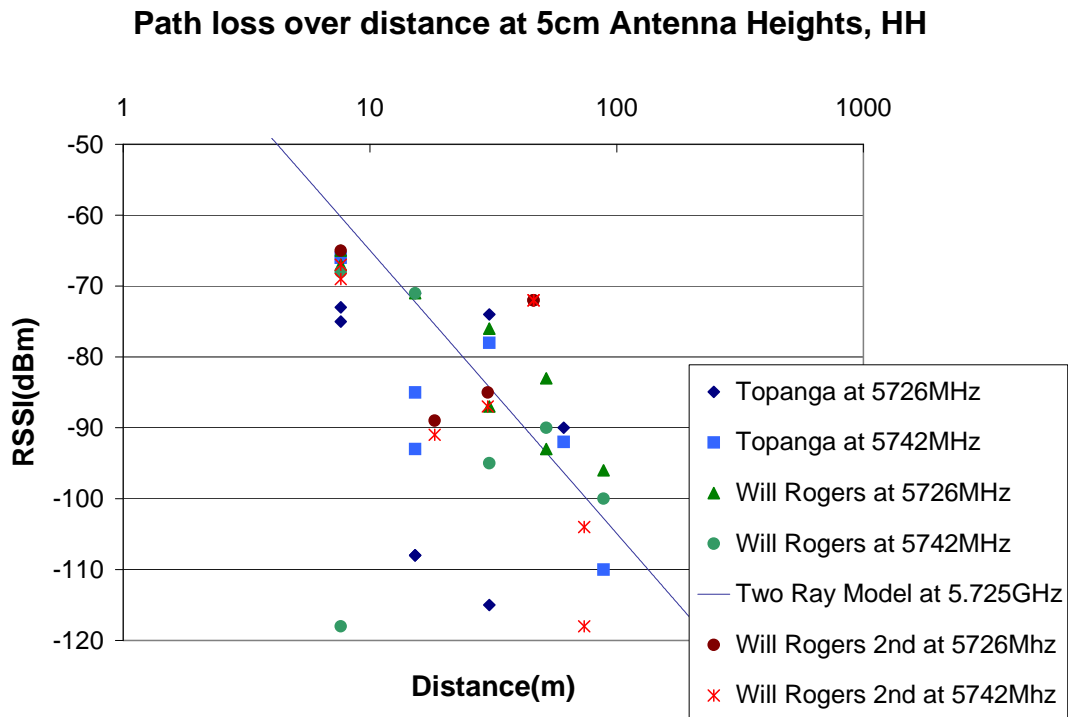


**Figure 188: Propagation fall-off in areas with rough vegetation, HH.**

107

# Path loss over distance at 5cm Antenna Heights HV
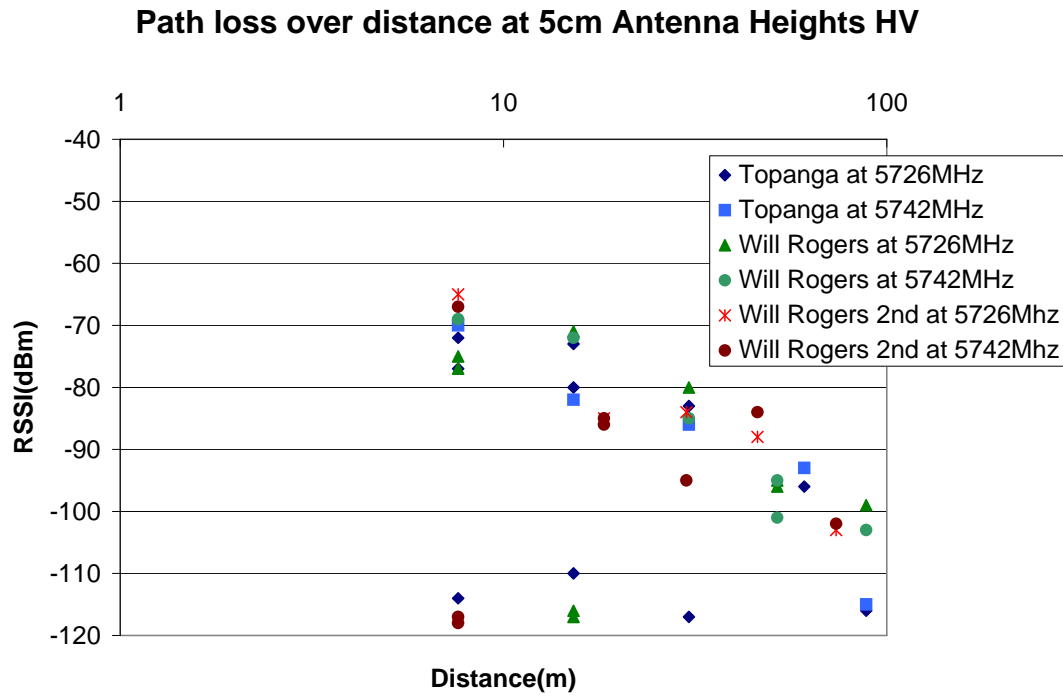


**Figure 189: Propagation fall-off in areas with rough vegetation, HV.**

# Path Loss at 5cm Antenna Heights and VV Polarization
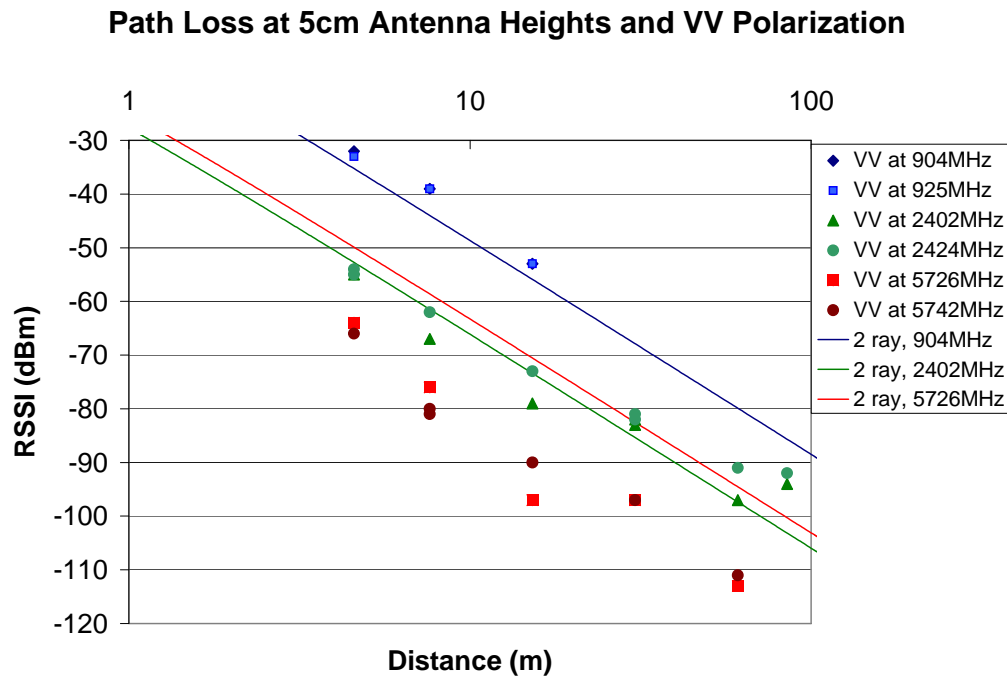


**Figure 190: Propagation fall-off in the Fort Leonard Wood test field, VV.**

**Path Loss at 5cm Antenna Heights and HH Polarization**
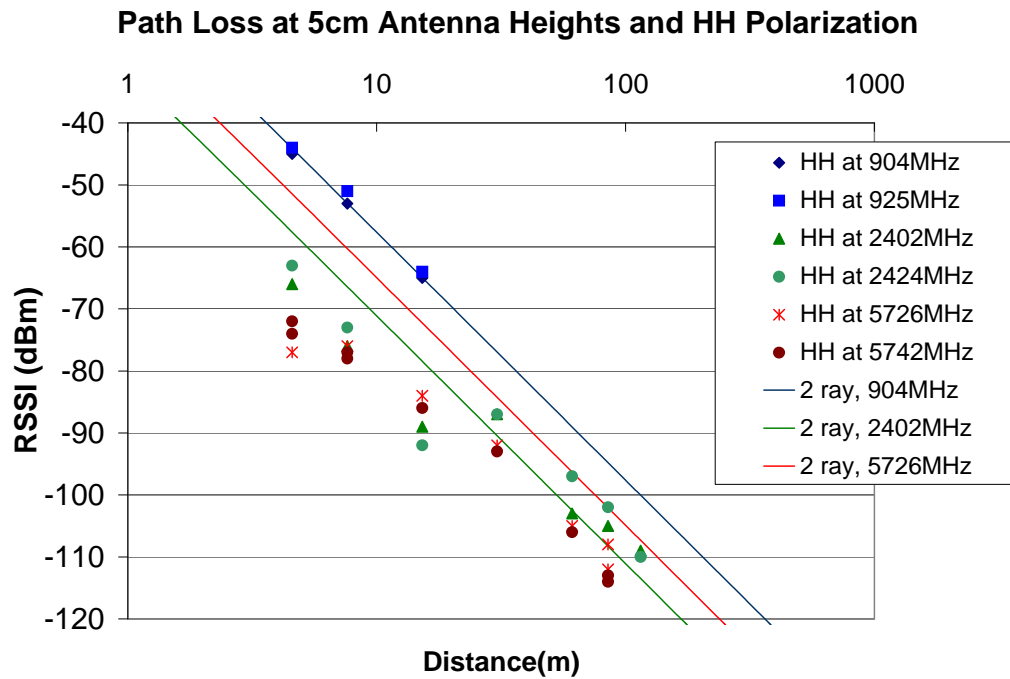


**Figure 191: Propagation fall-off in the Fort Leonard Wood test field, HH.**

**Path Loss at 5cm Antenna Heights and HV Polarization**
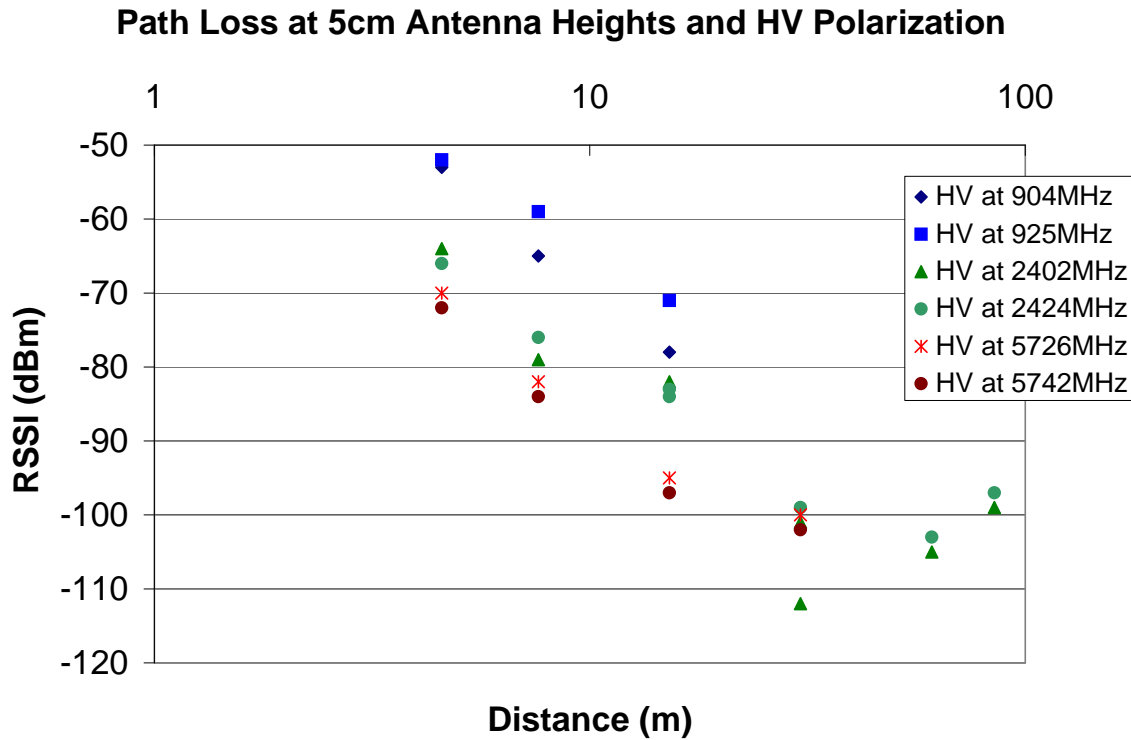


**Figure 192: Propagation fall-off in the Fort Leonard Wood test field, HV.**

 Plots of the propagation power loss with height at a distance of approximately 15m and all three polarizations considered are shown in figures 193 to 247.  As with the path loss as a function of distance figures above, for the VV and HH cases the two-ray model predictions are also shown for comparison. Since in a flat-earth, two-ray model there is no mechanism for cross polarization (i.e. assuming each rays reflections can be approximated with a single plane wave) there is no similar comparison for the HV measured data.

**VV Signal vs. Antenna Height at 20dBm Transmit Power**
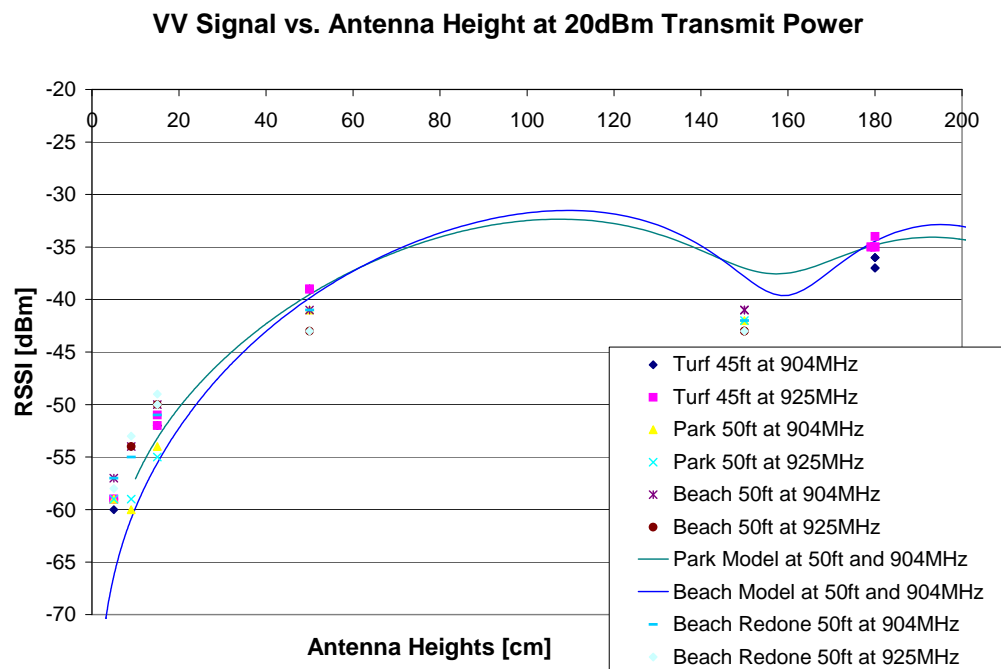


**Figure 193: Propagation loss as a function of height for the open areas, VV.**
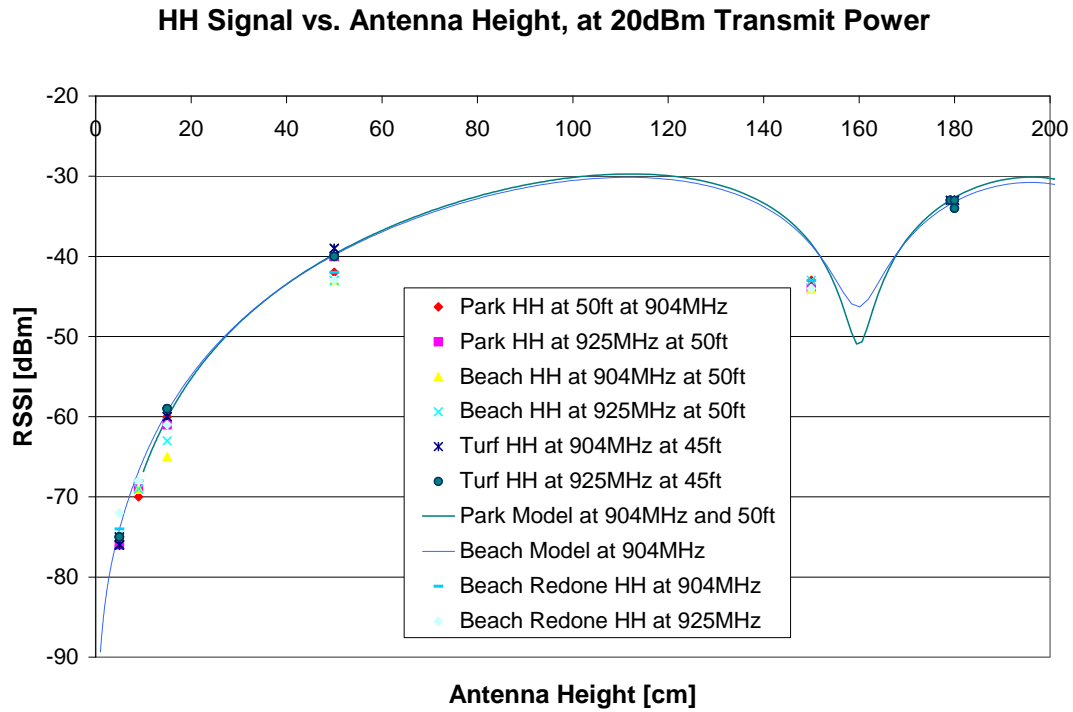
**Figure 194: Propagation loss as a function of height for the open areas, HH.**
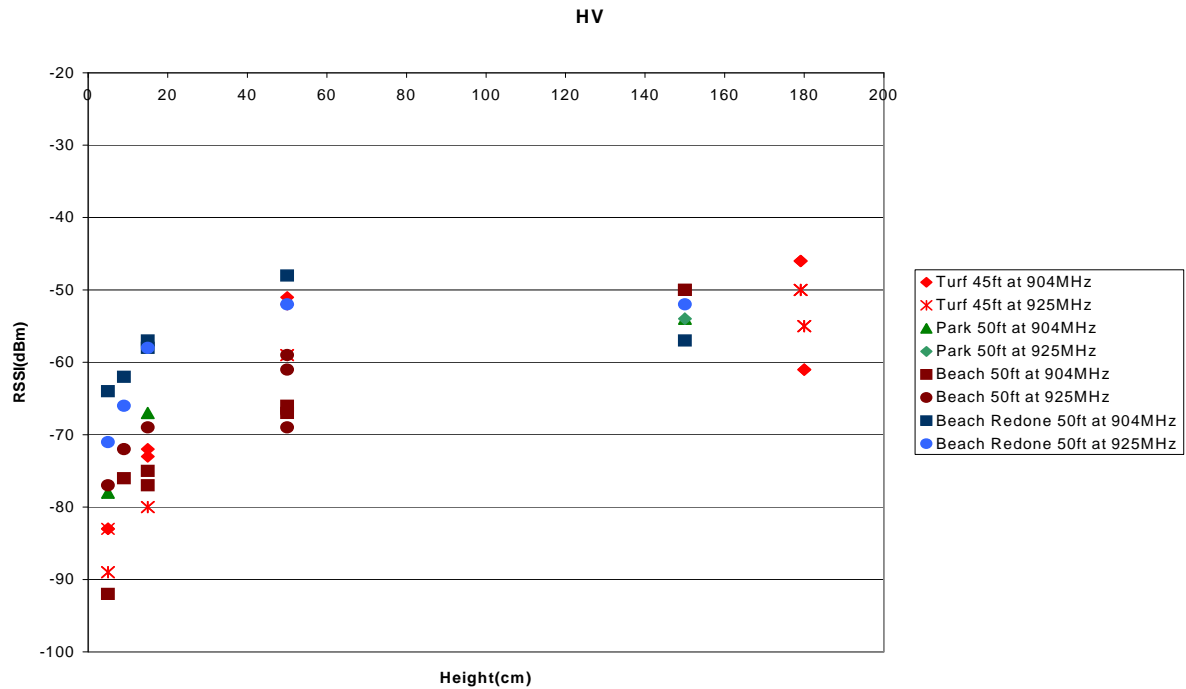


**Figure 195: Propagation loss as a function of height for the open areas, HV.**

**VV Signal vs. Height at 50ft and 30dBm Transmit Power**
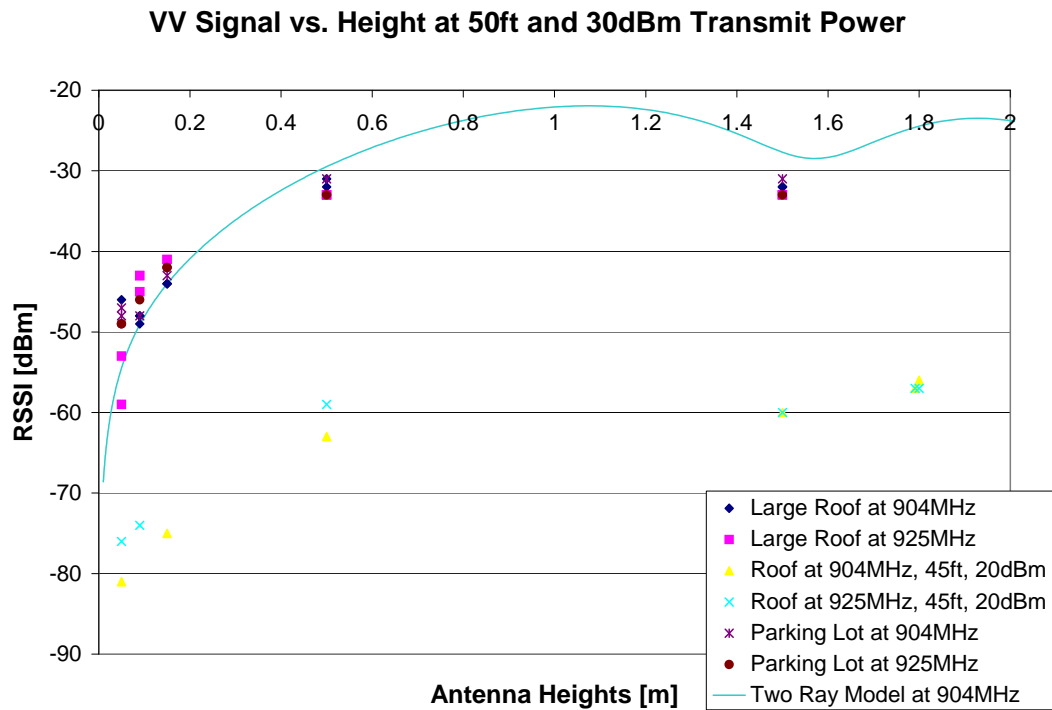


**Figure 196: Propagation loss as a function of height for the parking lots, VV.**

**HH Signal vs. Height at 50ft, 30dBm Tranmsit Power**
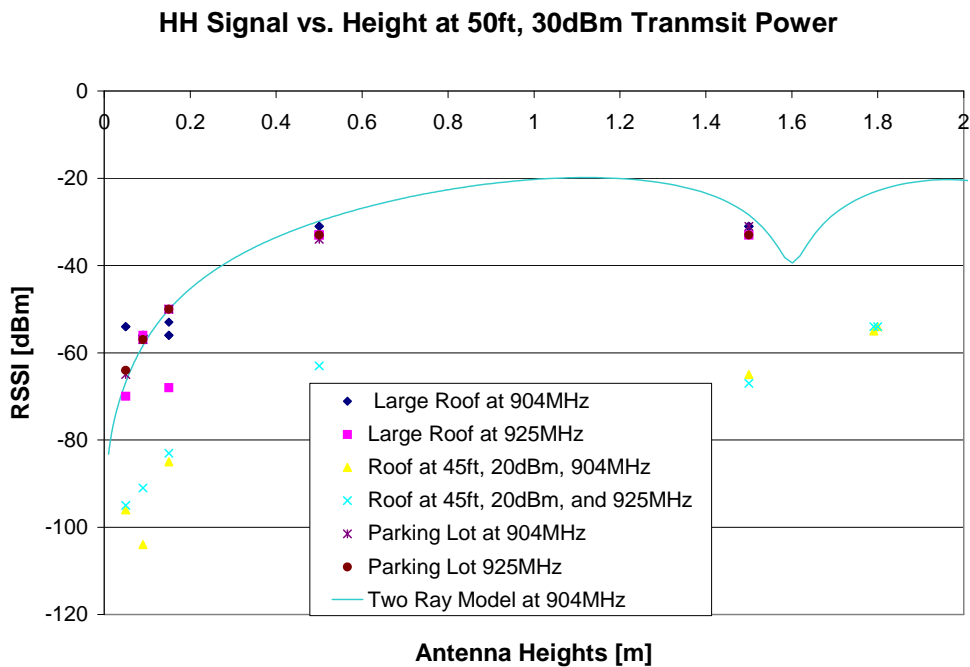


**Figure 197: Propagation loss as a function of height for the parking lots, HH.**

**HV Signal vs. Height at 50ft and 30dBm Transmit Power**
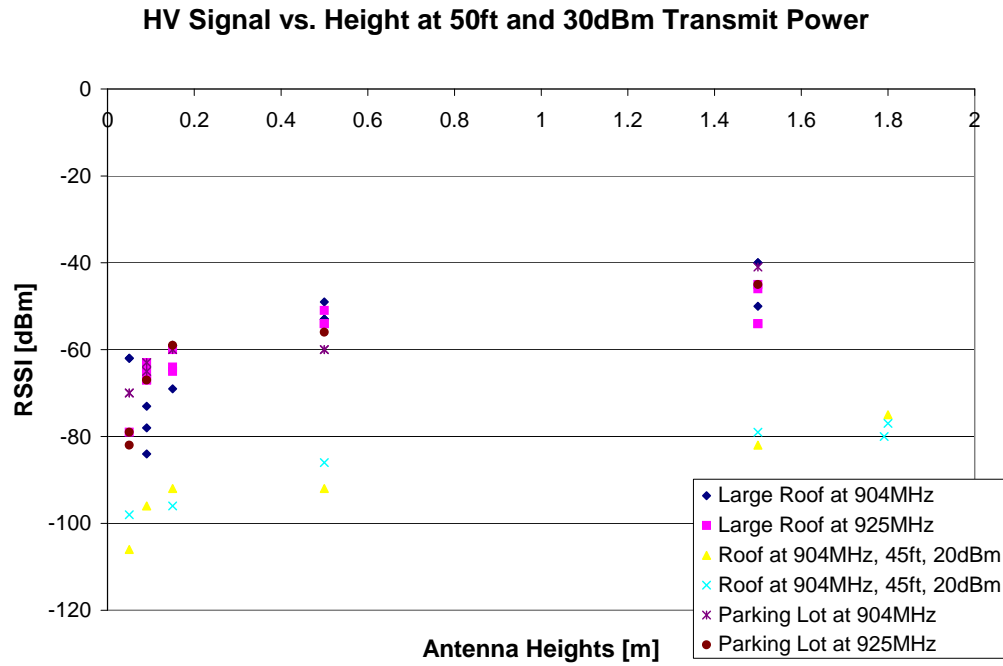


**Figure 198: Propagation loss as a function of height for the parking lots, HV.**

**VV at 50ft and 30dBm Transmit Power**
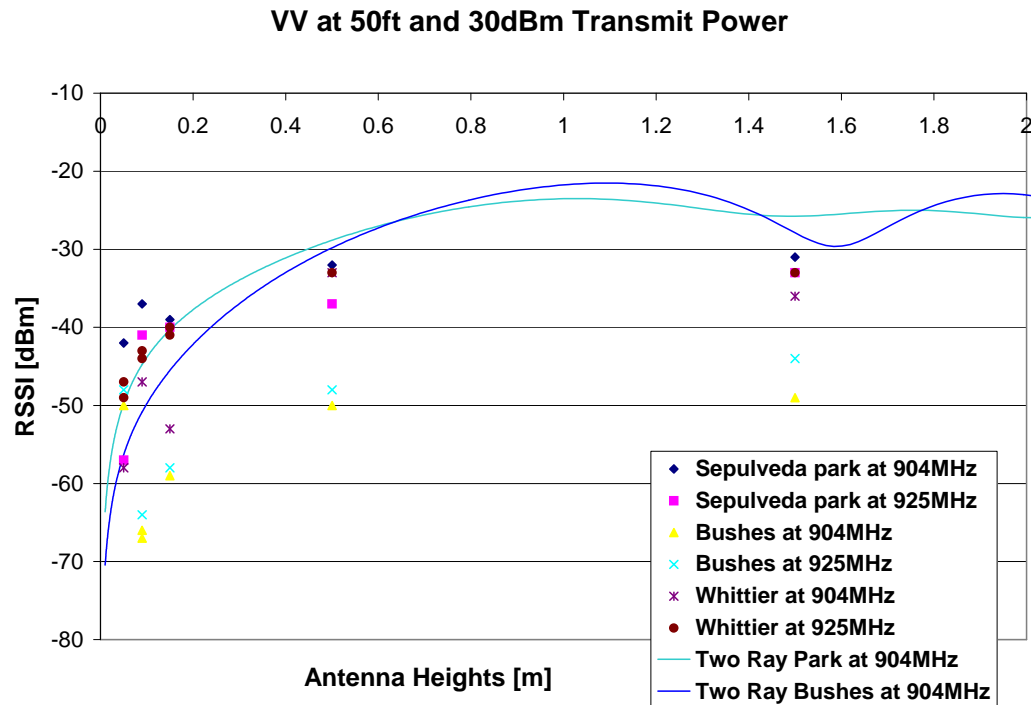


**Figure 199: Propagation as a function of height for the areas with vegetation, VV.**

113

## HH at 50ft, 30dBm Transmit Power
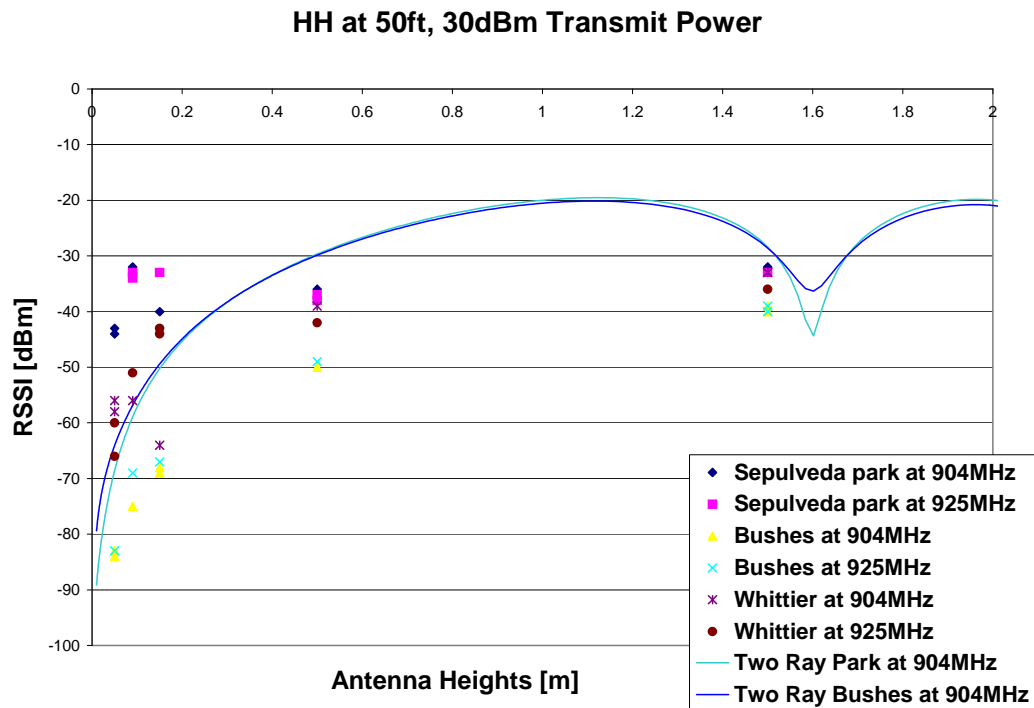


**Figure 200: Propagation as a function of height for the areas with vegetation, HH.**

## HV at 50ft and 30dBm Transmit Power
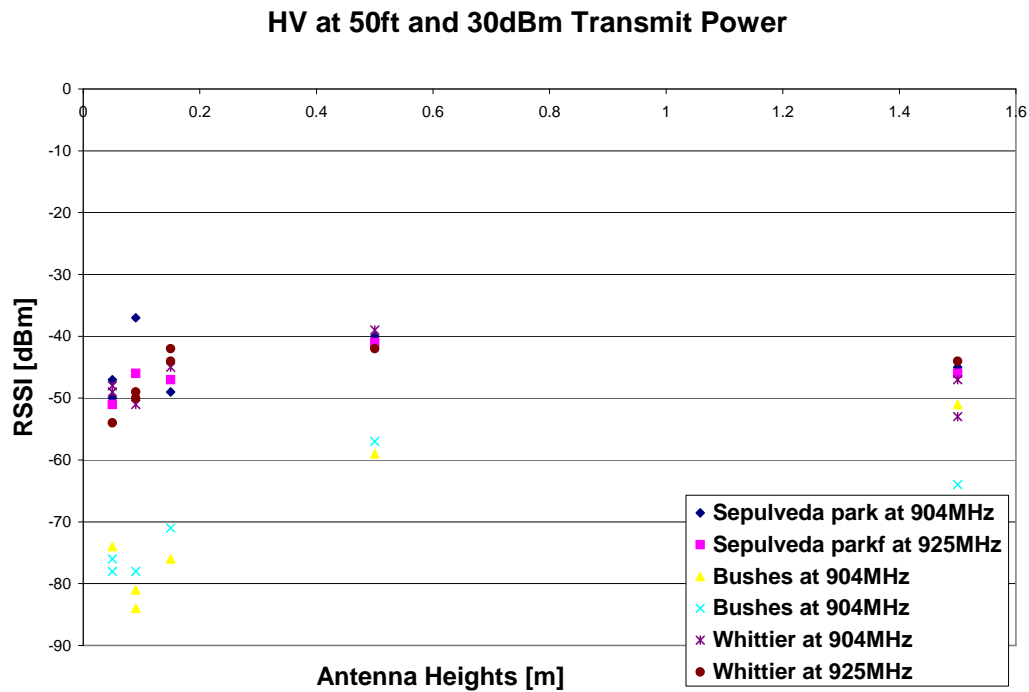


**Figure 201: Propagation as a function of height for the areas with vegetation, HV.**

**RSSI Vs Height**
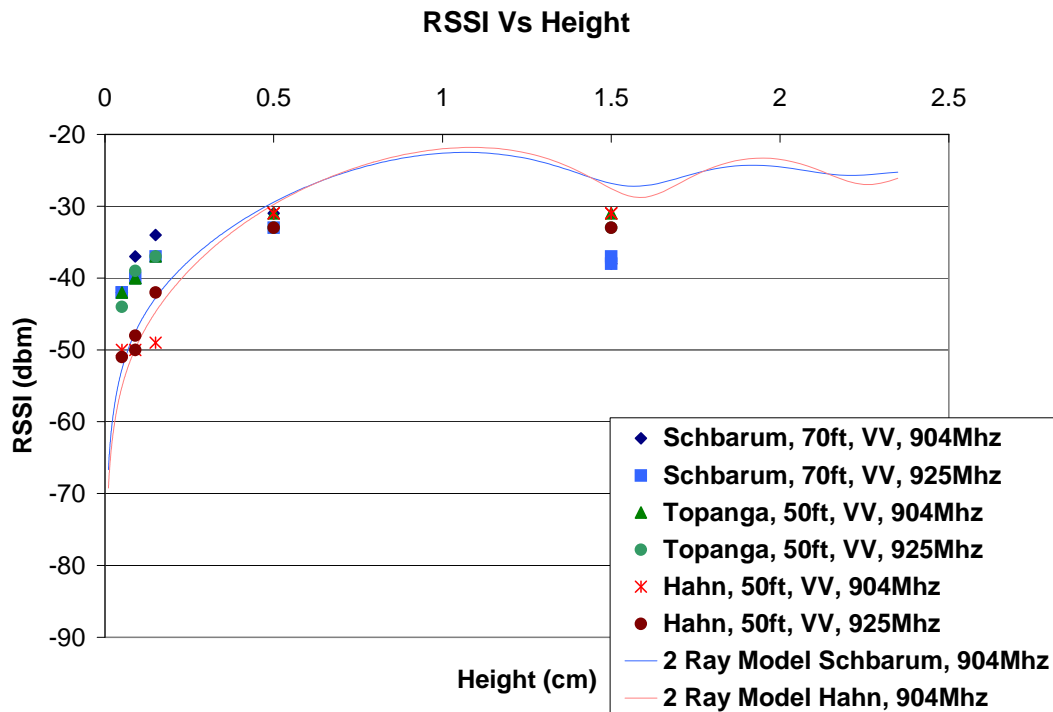


**Figure 202: Propagation as a function of height for rolling hills, VV.**

**RSSI Vs Height**
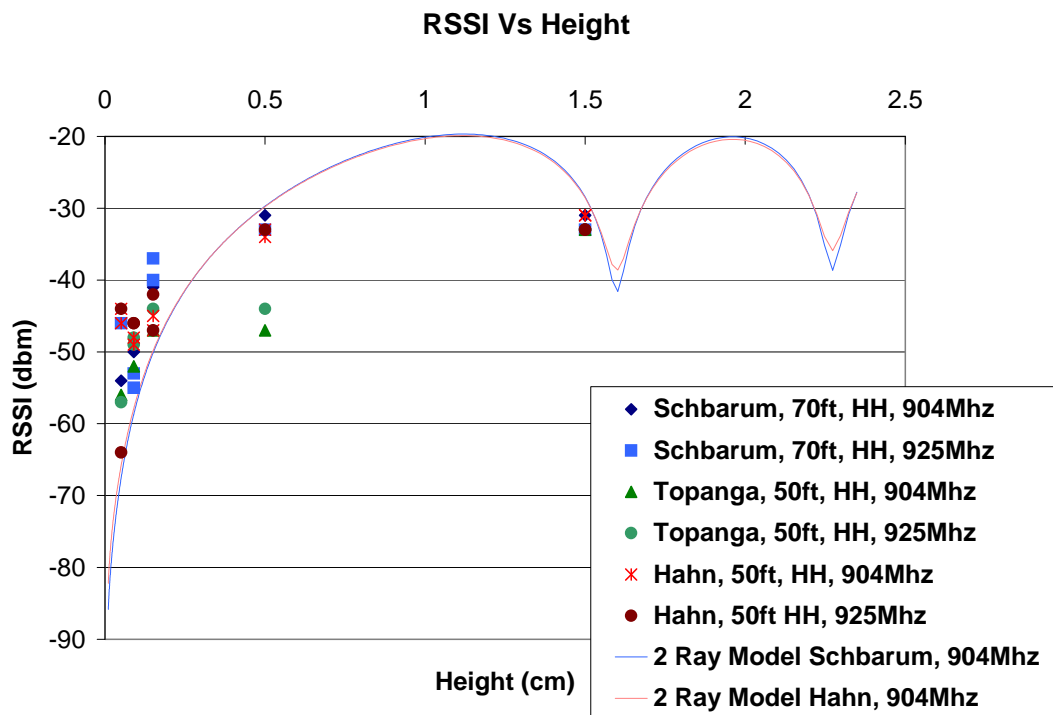


**Figure 203: Propagation as a function of height for rolling hills, HH.**

**RSSI Vs Height**
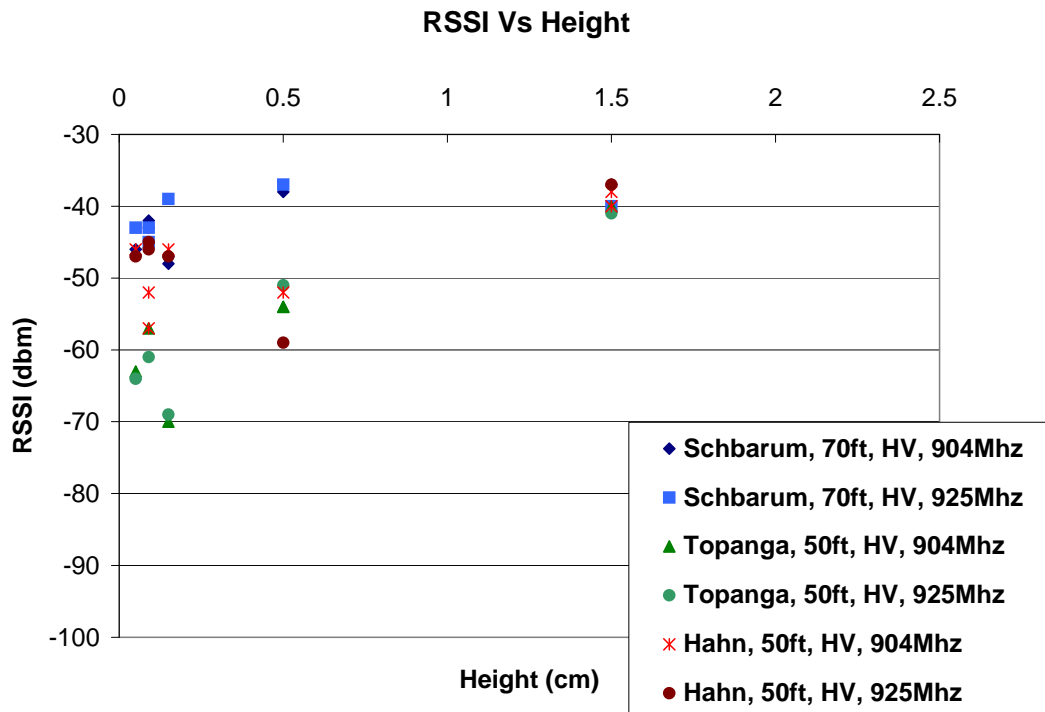


**Figure 204: Propagation as a function of height for rolling hills, HV.**

**Signal vs. Antenna Height VV 50ft**
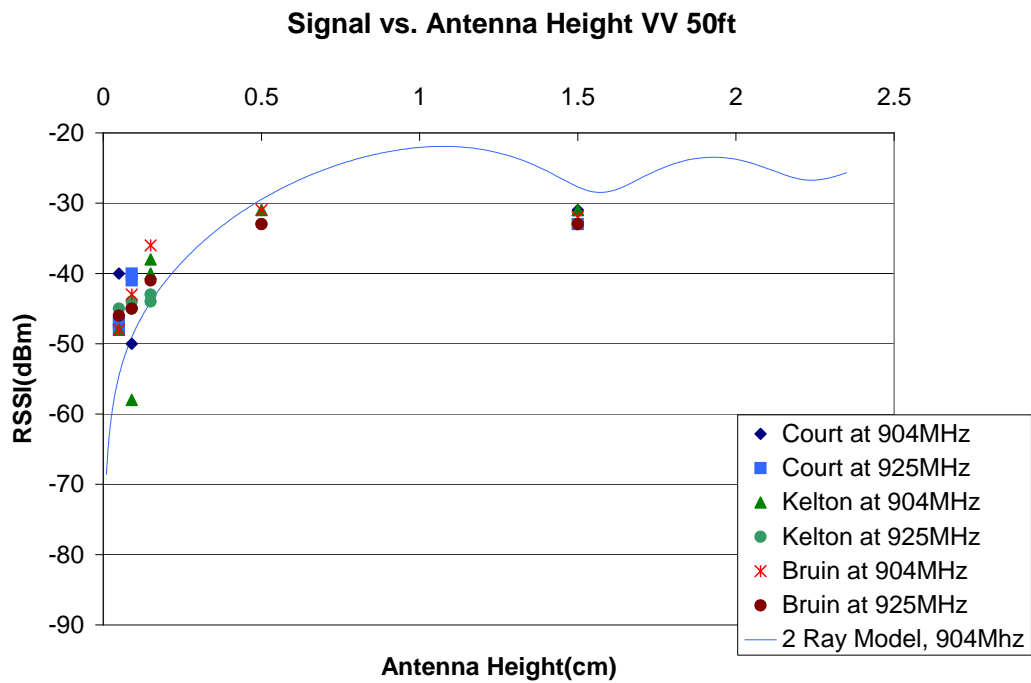


**Figure 205: Propagation as a function of height for urban areas, VV.**

116

**Signal vs. Antenna Height, HH, 50ft**
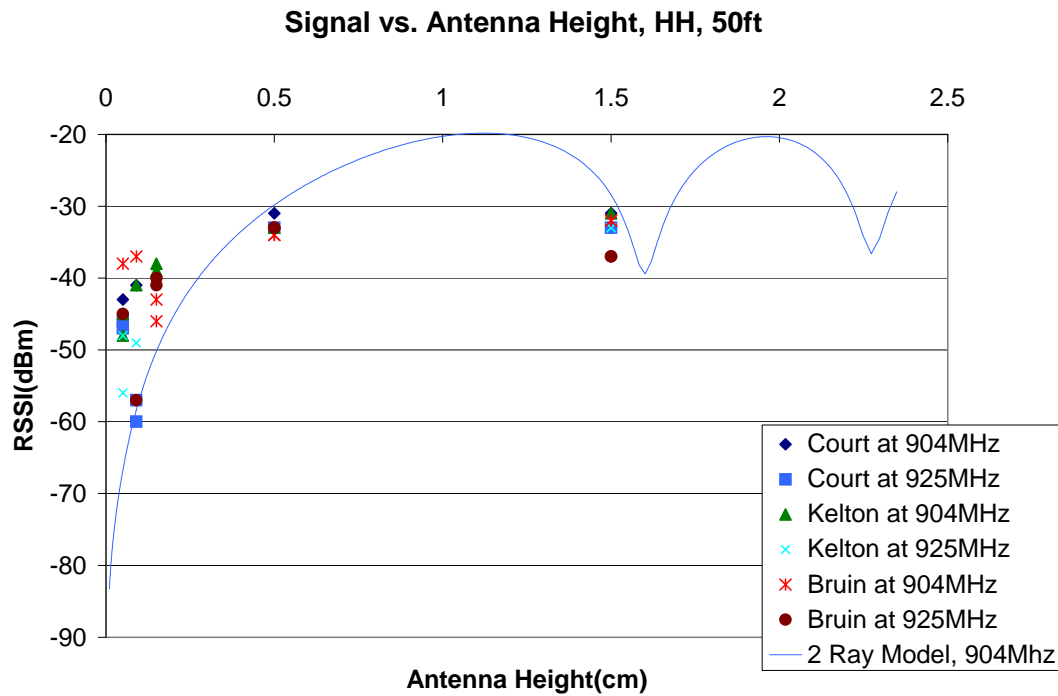


**Figure 206: Propagation as a function of height for urban areas, HH.**

**Signal vs. Antenna Height HV 50ft**
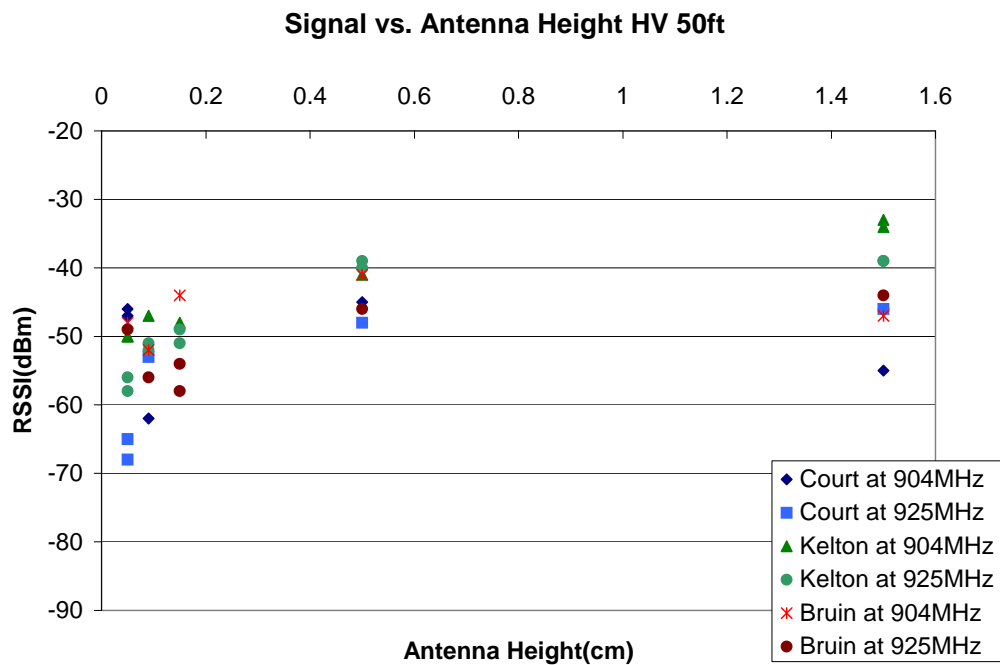


**Figure 207: Propagation as a function of height for urban areas, HV.**
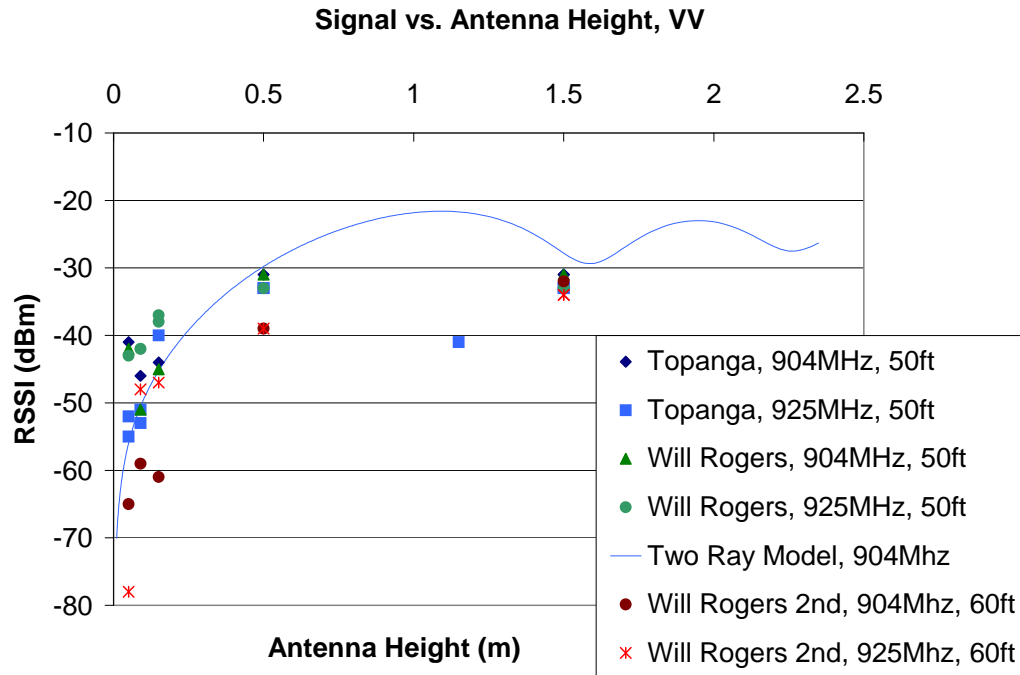
**Figure 208: Propagation as a function of height for rough vegetation, VV.**
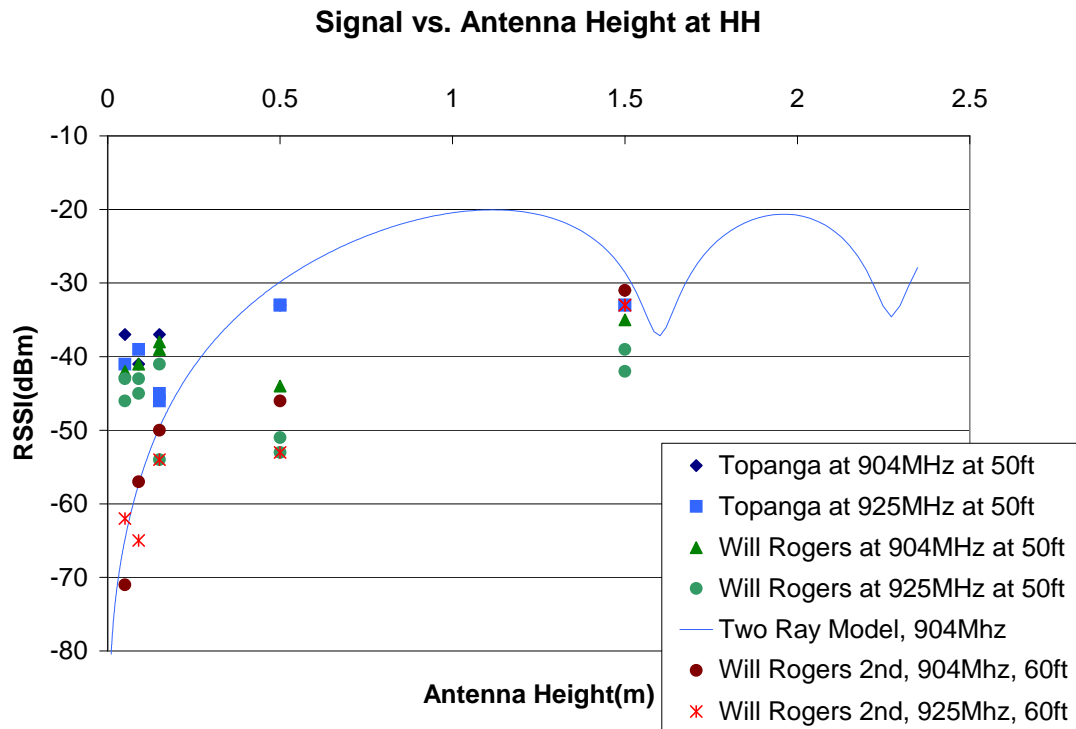


**Figure 209: Propagation as a function of height for rough vegetation, HH.**

118

**Signal vs. Antenna Height at HV**
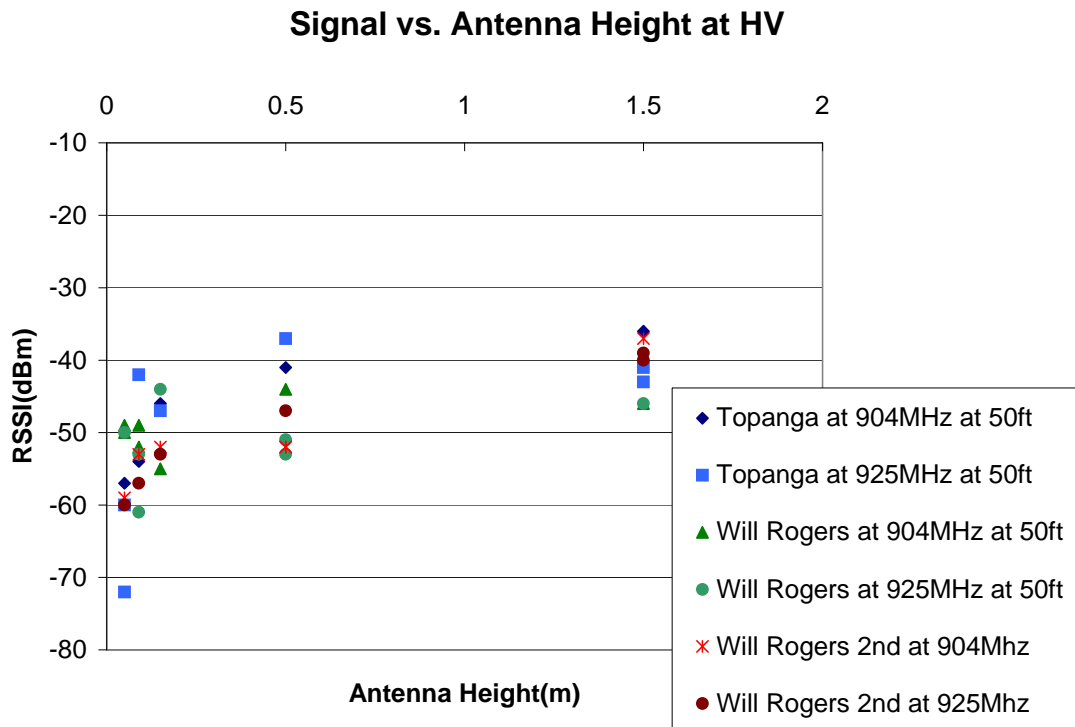


**Figure 210: Propagation as a function of height for rough vegetation, HV.**

**VV Signal vs Antenna Height at 20dBm Transmit Power**
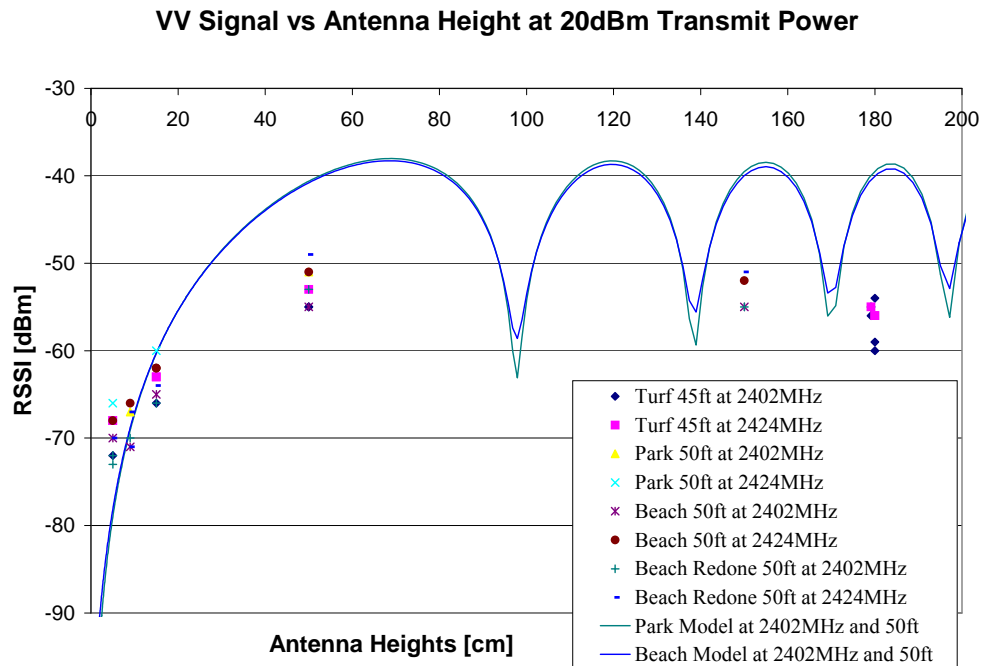


**Figure 211: Propagation as a function of height for the open areas, VV.**

**HH Signal vs. Antenna Heights for 20dBm Transmit Power**
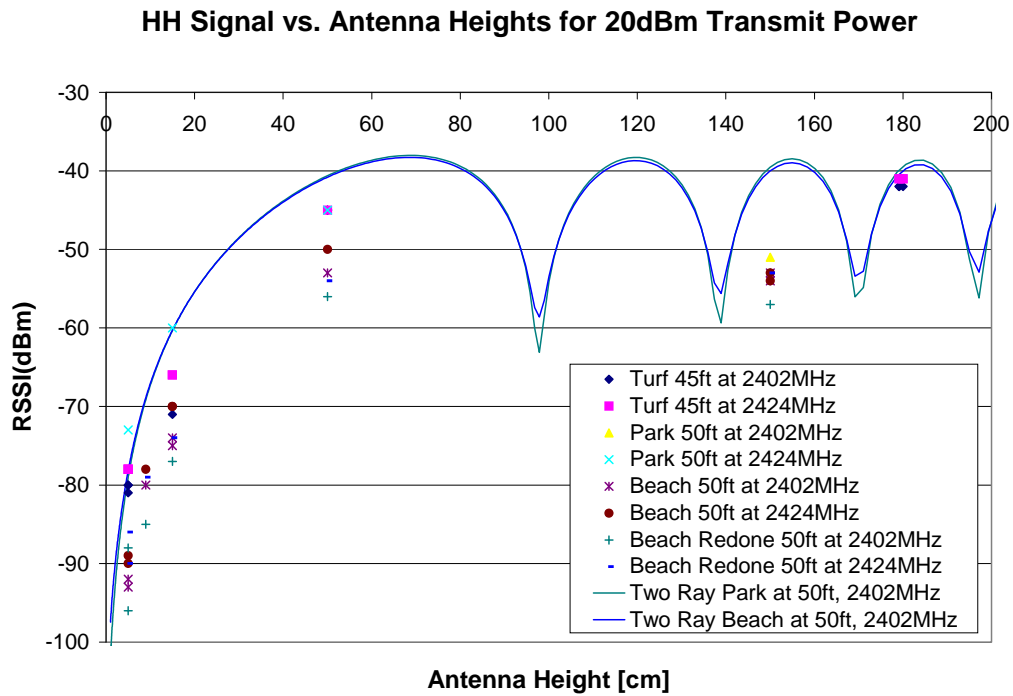


**Figure 212: Propagation as a function of height for the open areas, HH.**

**HV**
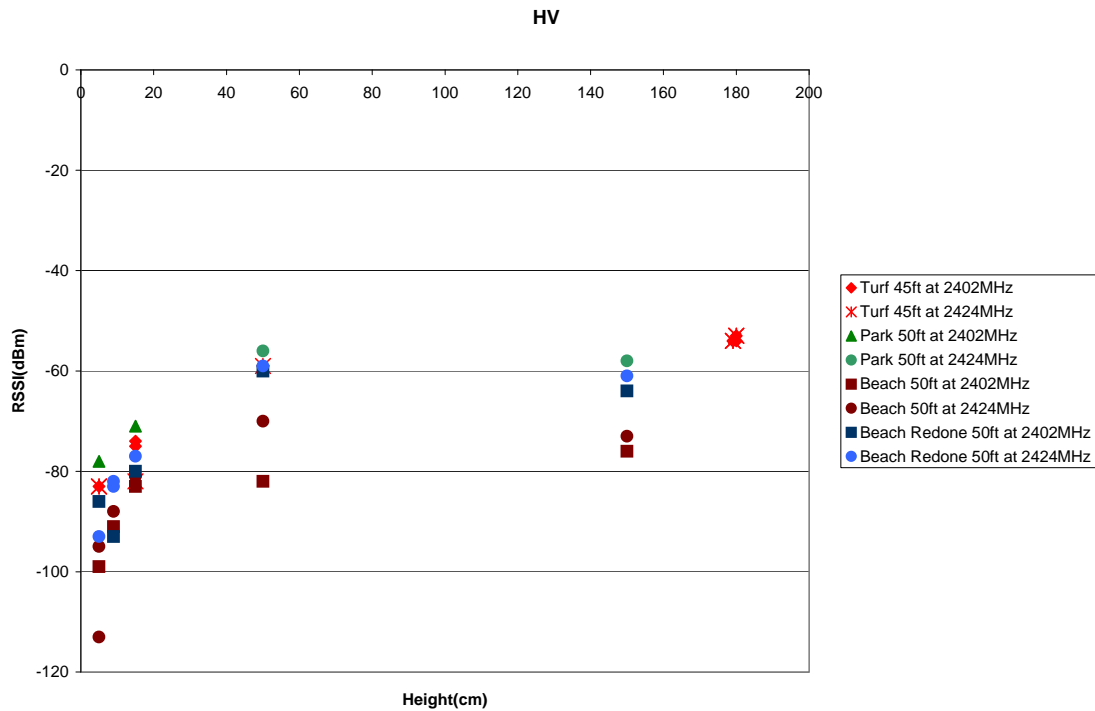


**Figure 213: Propagation as a function of height for the open areas, HV.**

**VV Signal vs. Height at 50ft, 20dBm Transmit Power**
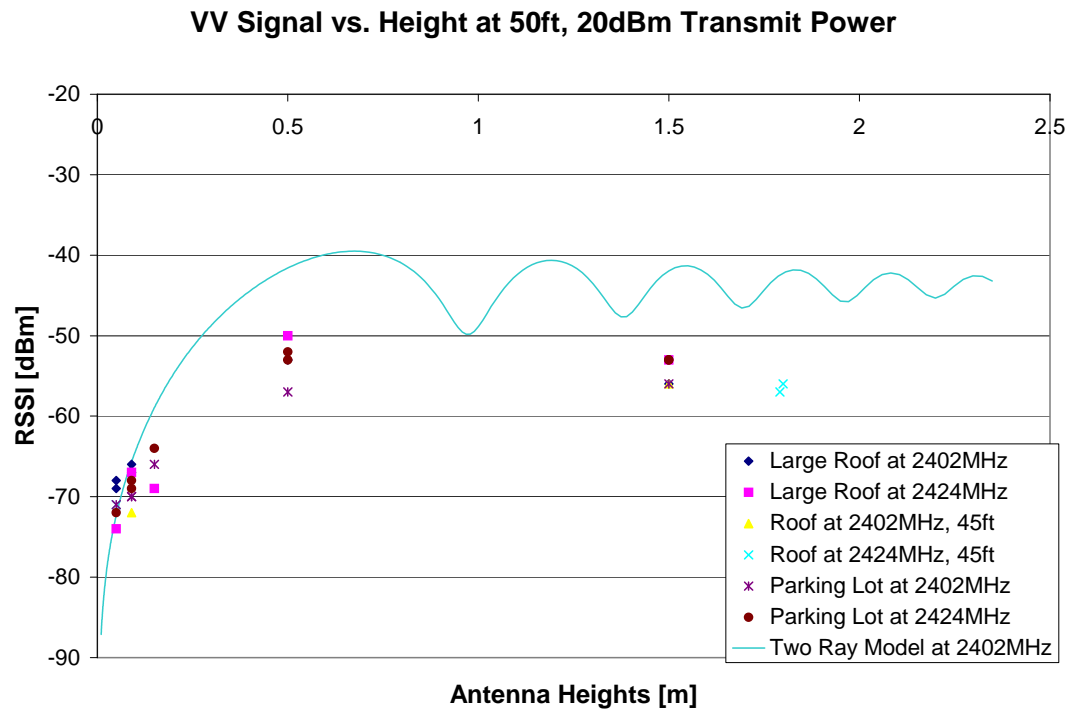


**Figure 214: Propagation loss as a function of height for the parking lots, VV.**

**HH Signal vs. Height at 50ft, 20dBm Transmit Power**
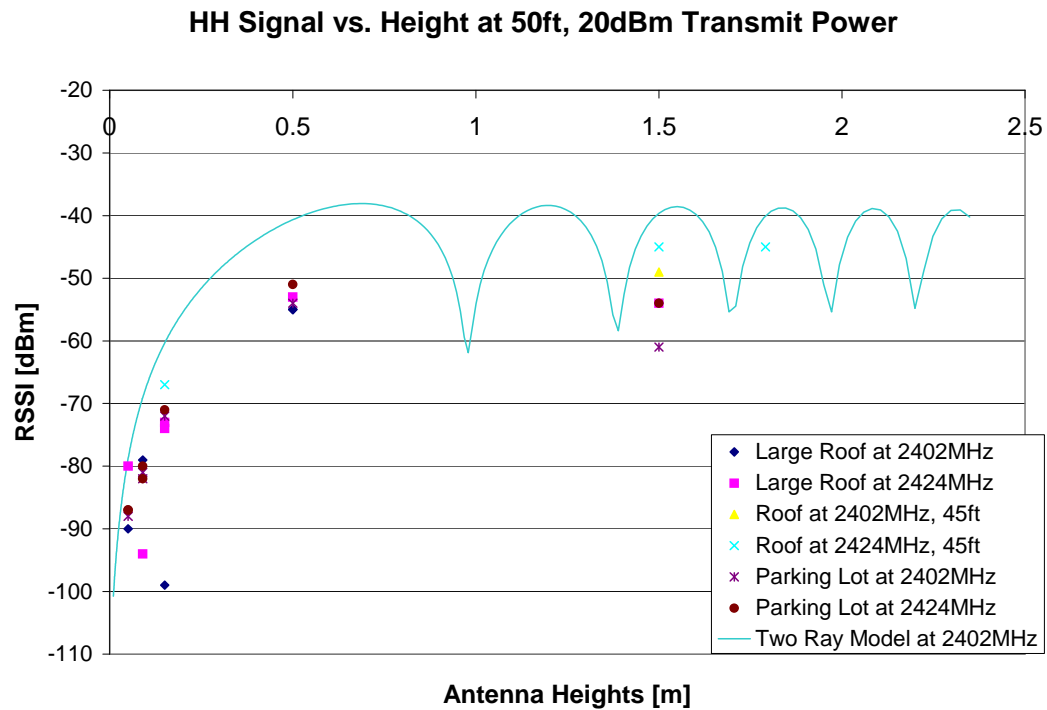


**Figure 215: Propagation loss as a function of height for the parking lots, HH.**
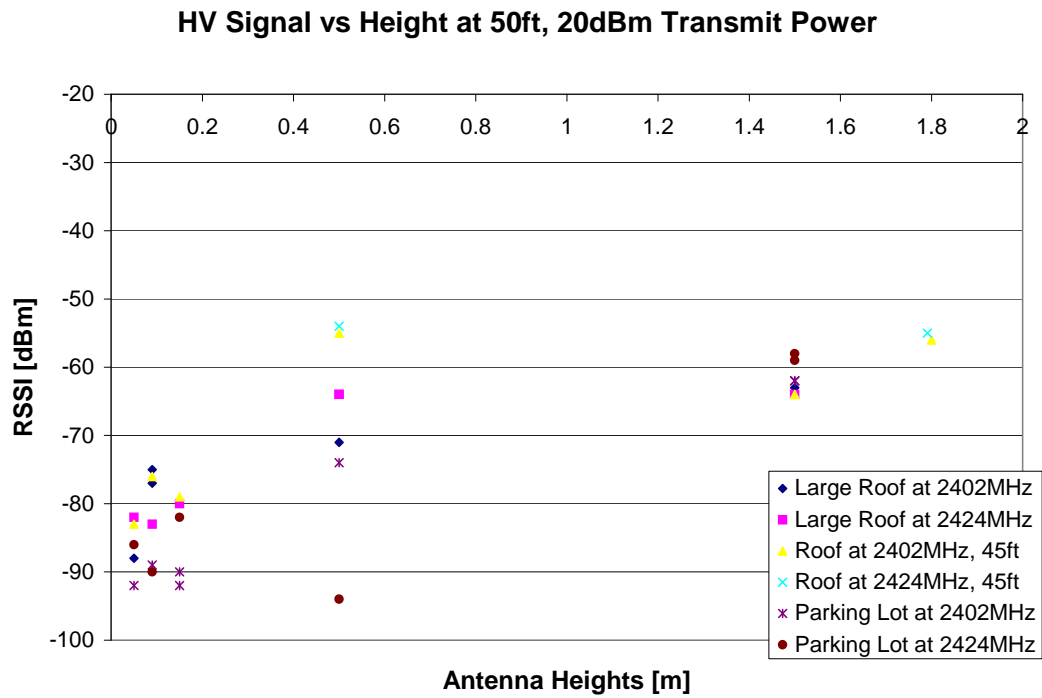
**Figure 216: Propagation loss as a function of height for the parking lots, HV.**
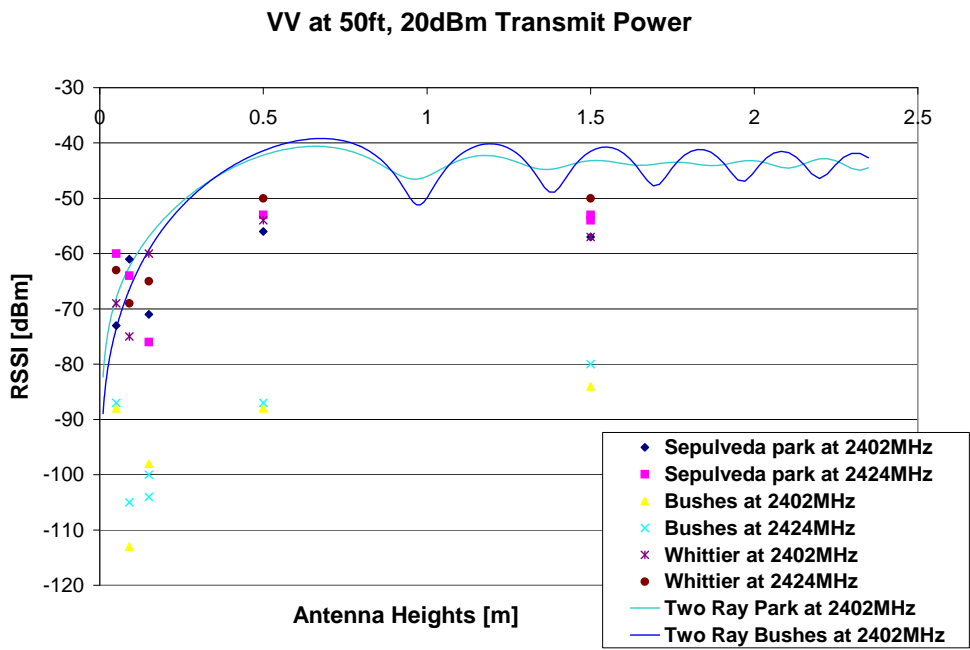


**Figure 217: Propagation as a function of height for the areas with vegetation, VV.**

**HH at 50ft, 20dBm Transmit Power**
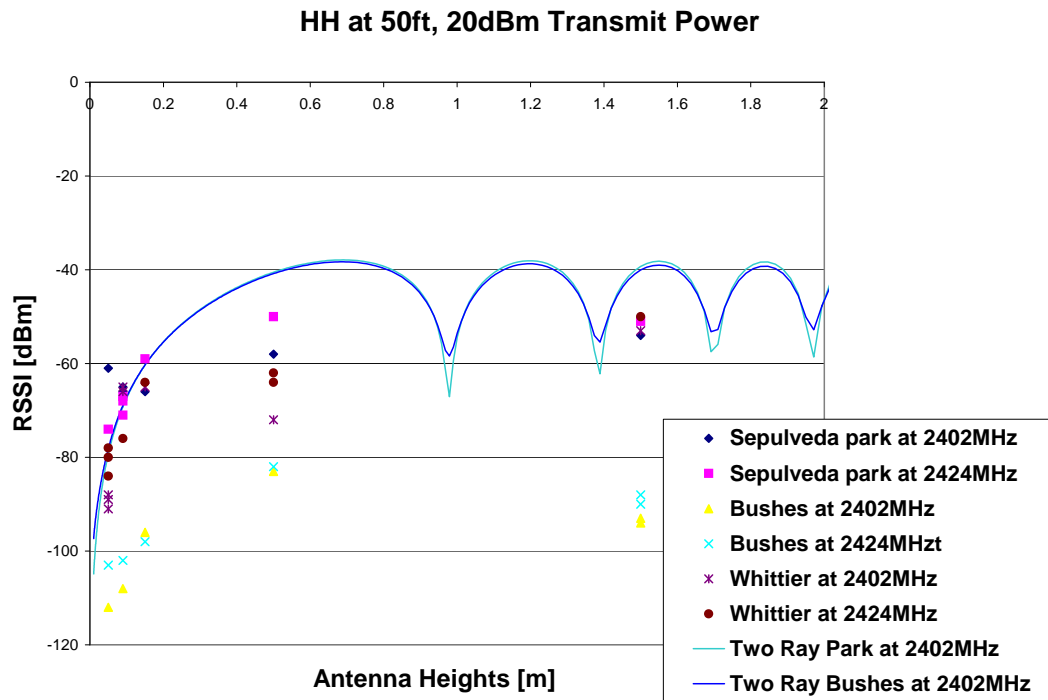
Figure 218: Propagation as a function of height for the areas with vegetation, HH.



**HV at 50ft, 20dBm Transmit Power**
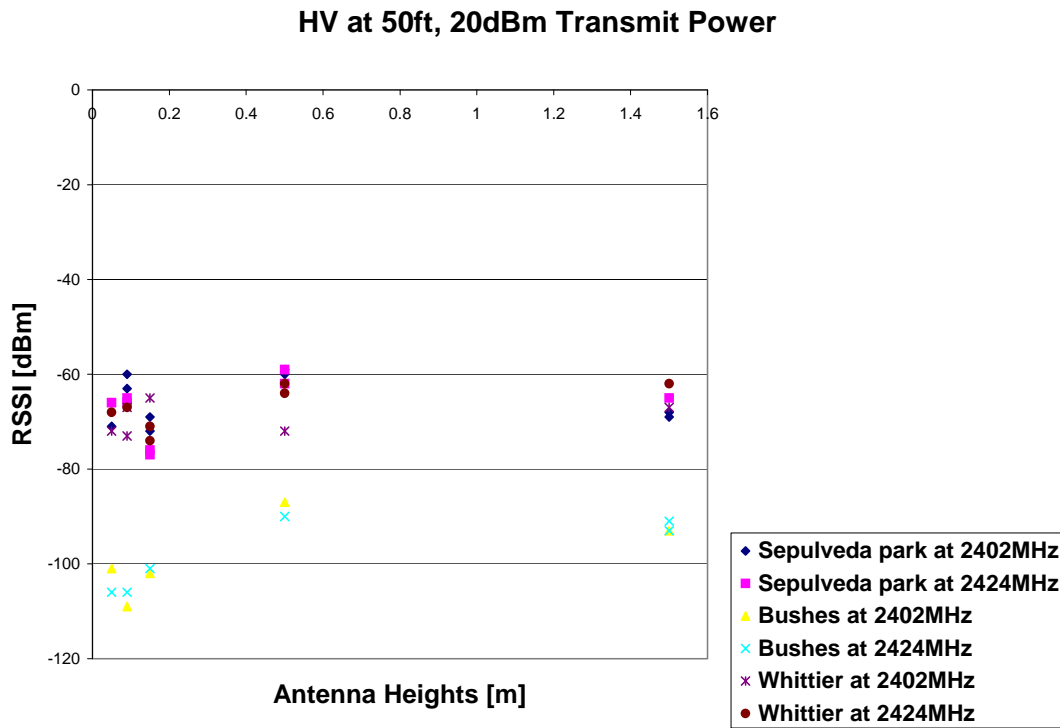
Figure 219: Propagation as a function of height for the areas with vegetation, HV.

**RSSI Vs Height**
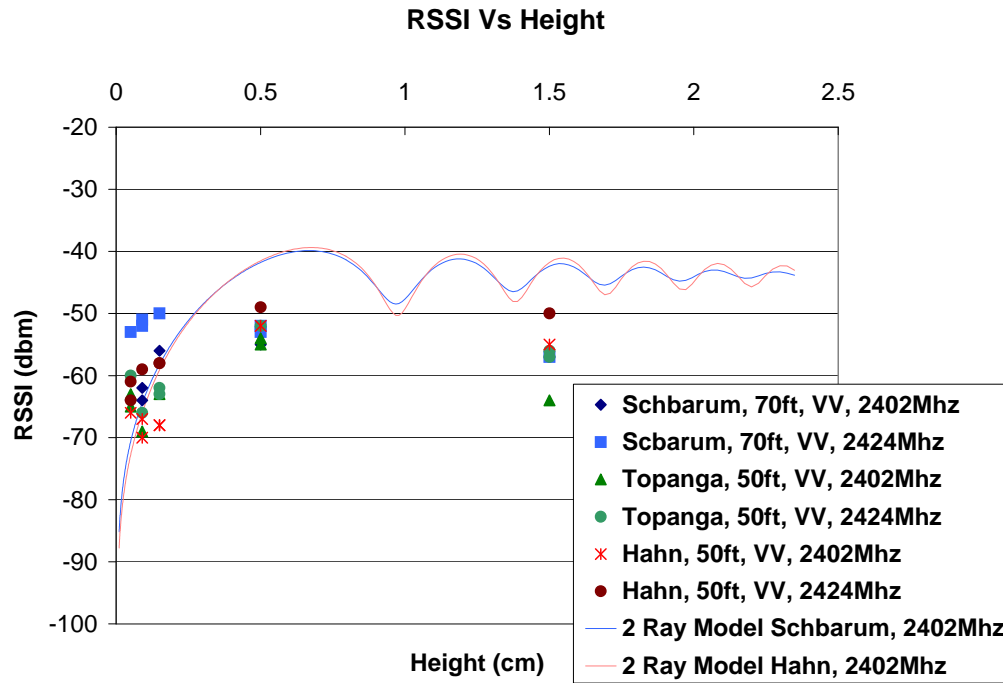


**Figure 220: Propagation as a function of height for rolling hills, VV.**

**RSSI Vs Height**
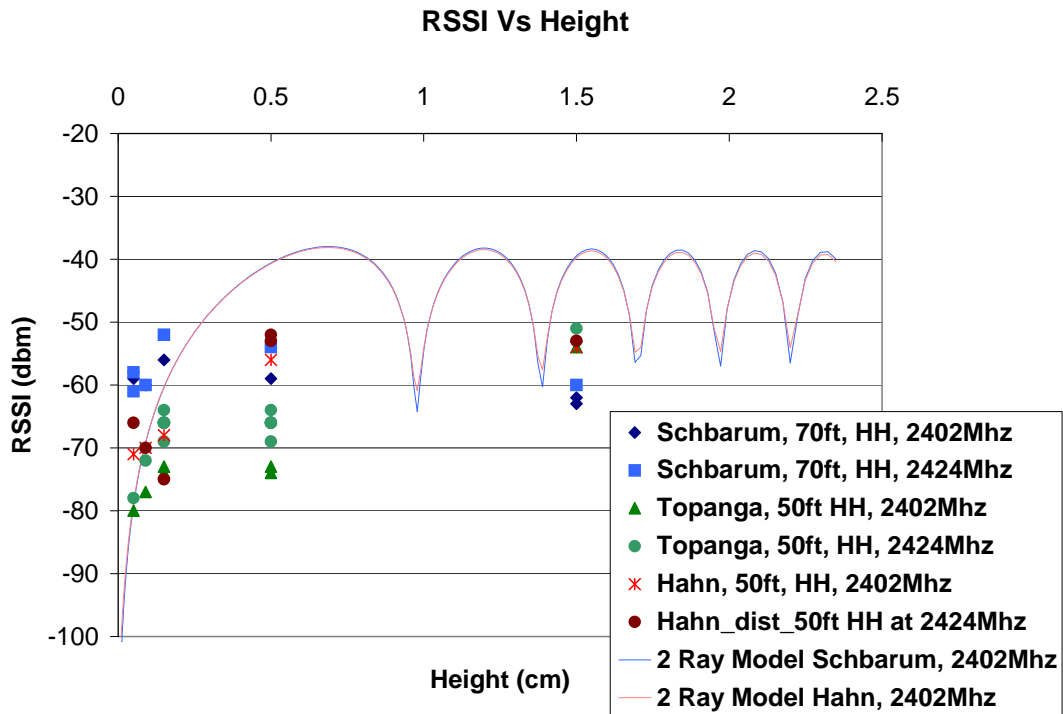


**Figure 221: Propagation as a function of height for rolling hills, HH.**

**RSSI Vs Height**
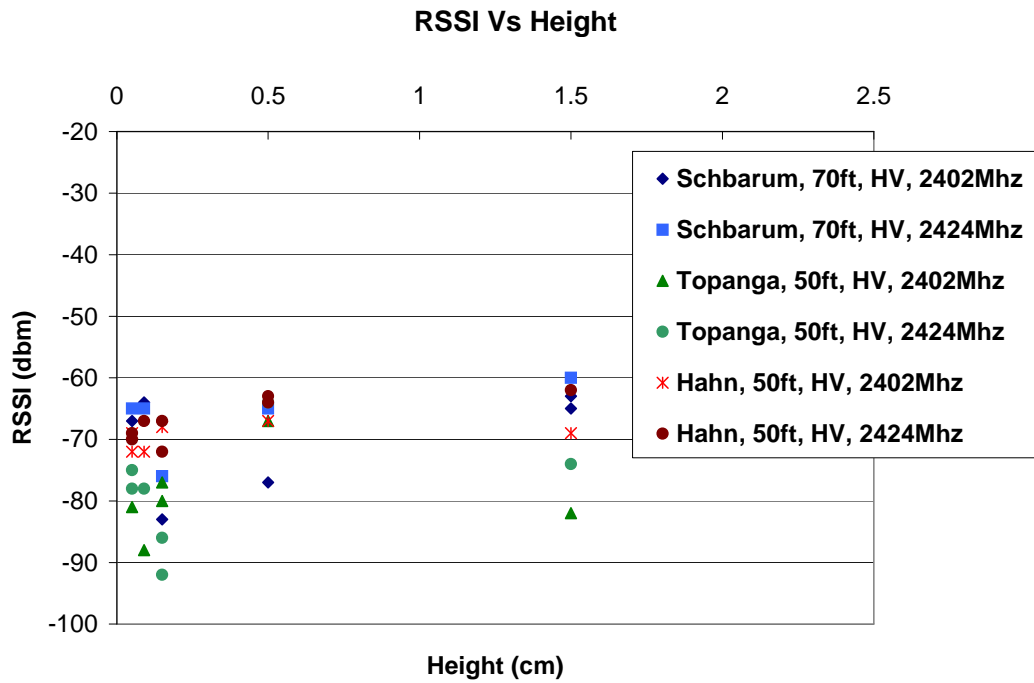


**Figure 222: Propagation as a function of height for rolling hills, HV.**

**Signal vs. Antenna Height VV 50ft**
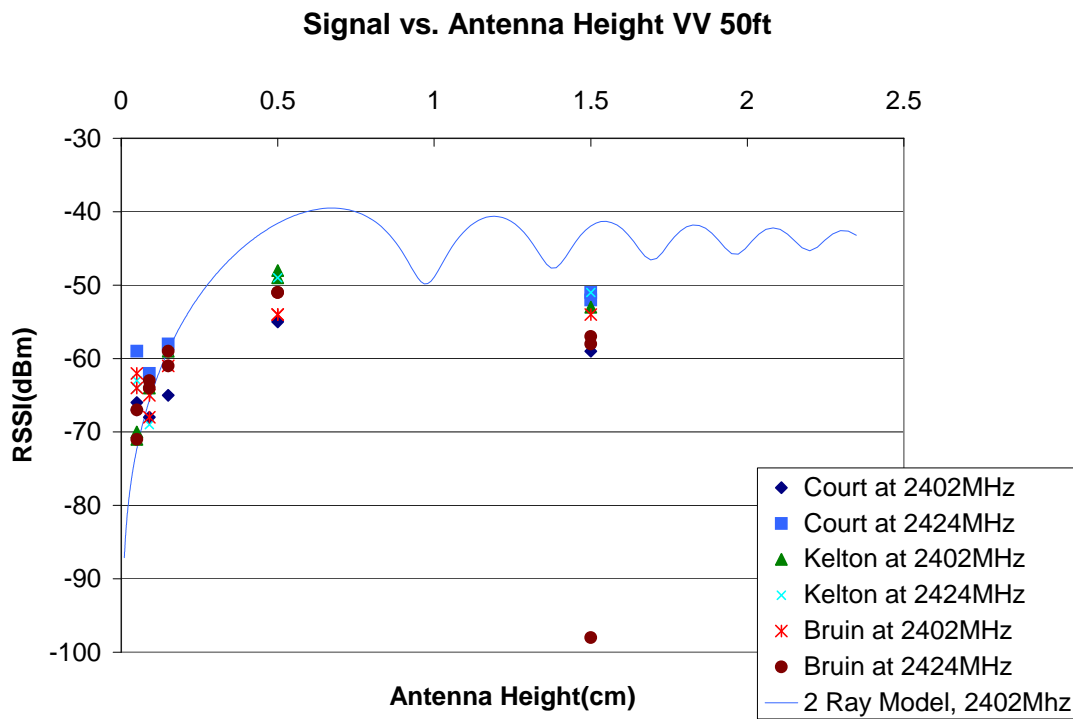


**Figure 223: Propagation as a function of height for urban areas, VV.**

125

## Signal vs. Antenna Height HH 50ft
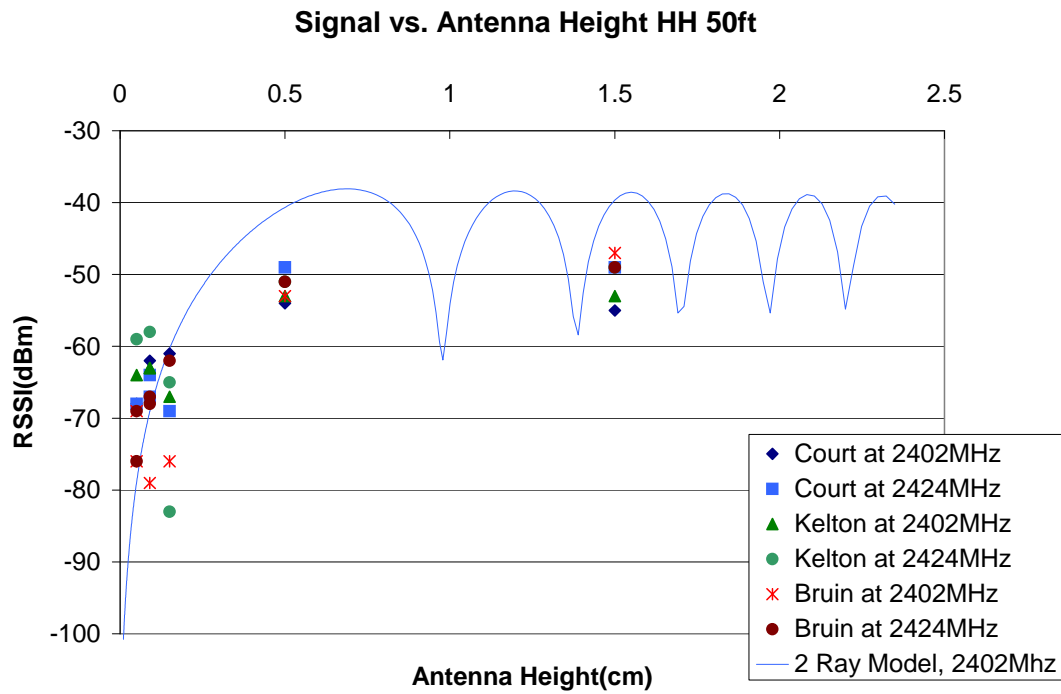


**Figure 224: Propagation as a function of height for urban areas, HH.**

## Signal vs. Antenna Height HV 50ft
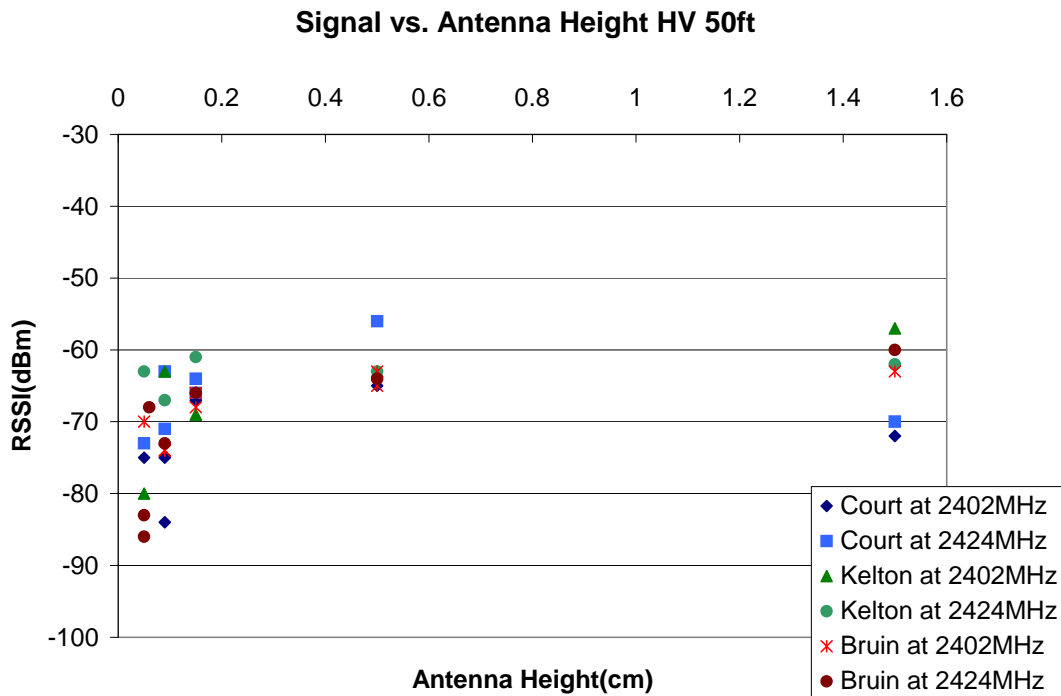


**Figure 225: Propagation as a function of height for urban areas, HV.**

126
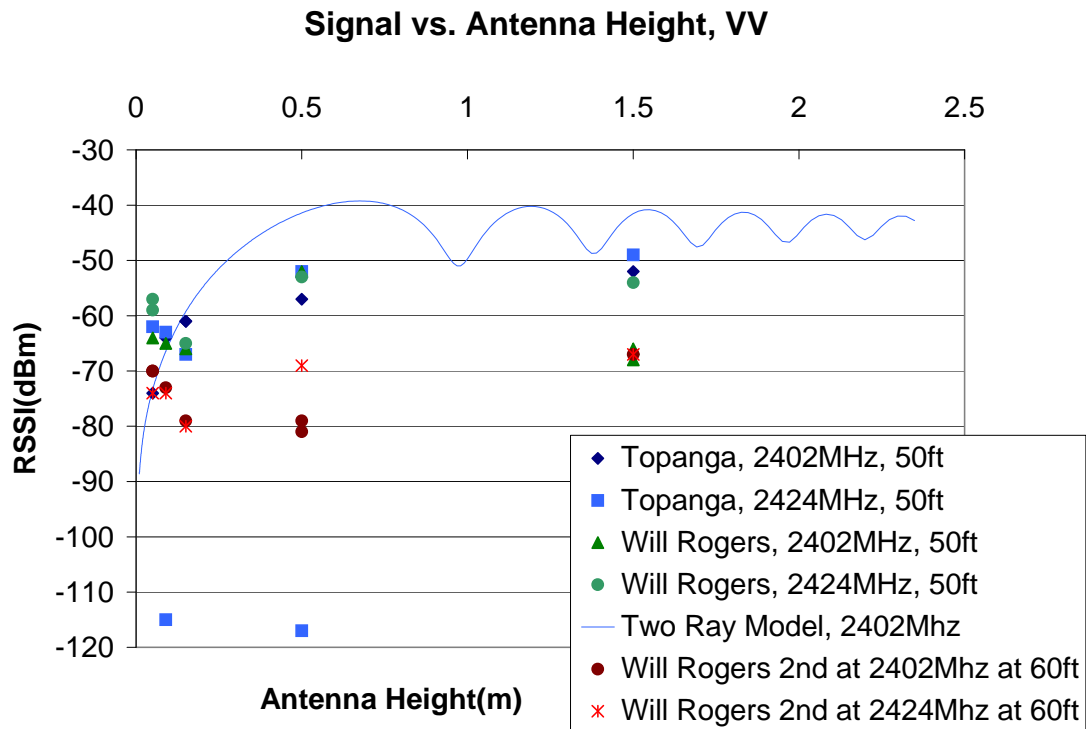
**Figure 226: Propagation as a function of height for rough vegetation, VV.**
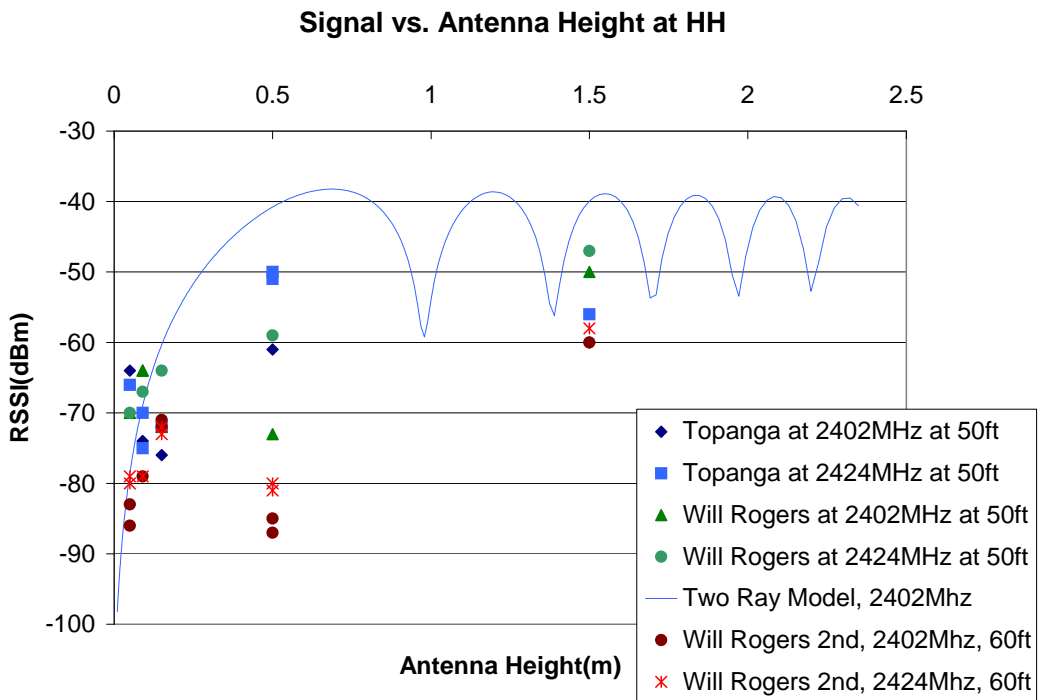


**Figure 227: Propagation as a function of height for rough vegetation, HH.**

**Signal vs. Antenna Height at HV**
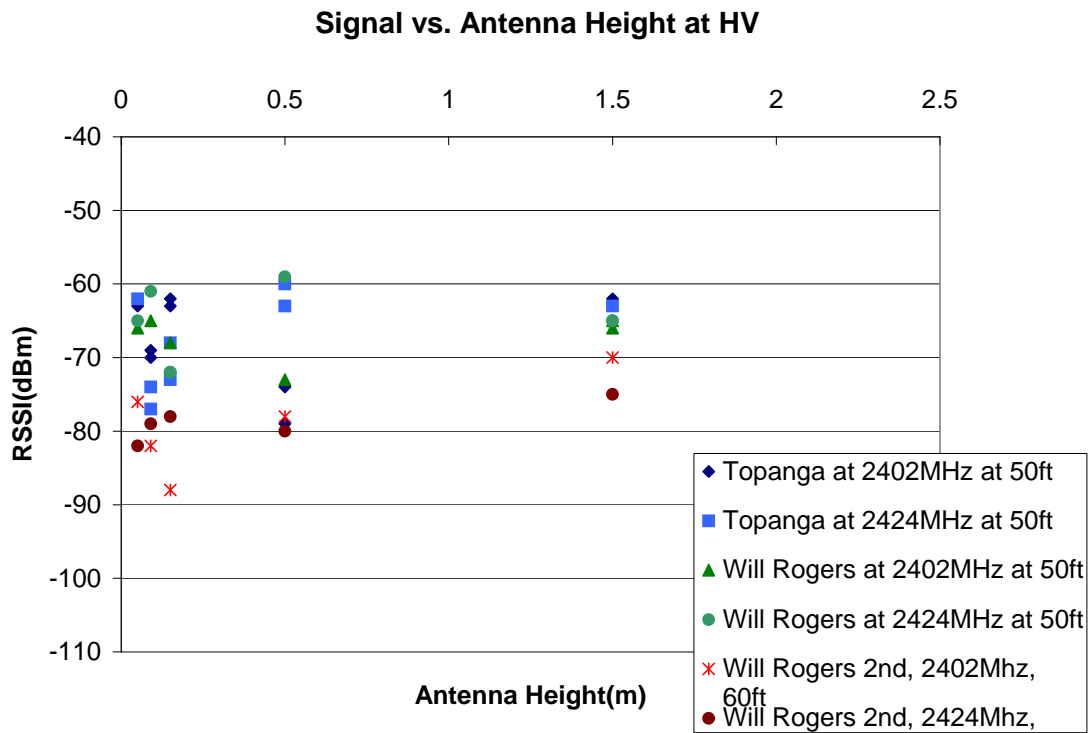


**Figure 228: Propagation as a function of height for rough vegetation, HV.**

**VV Signal vs. Antenna Height for 27dBm Transmit Power**
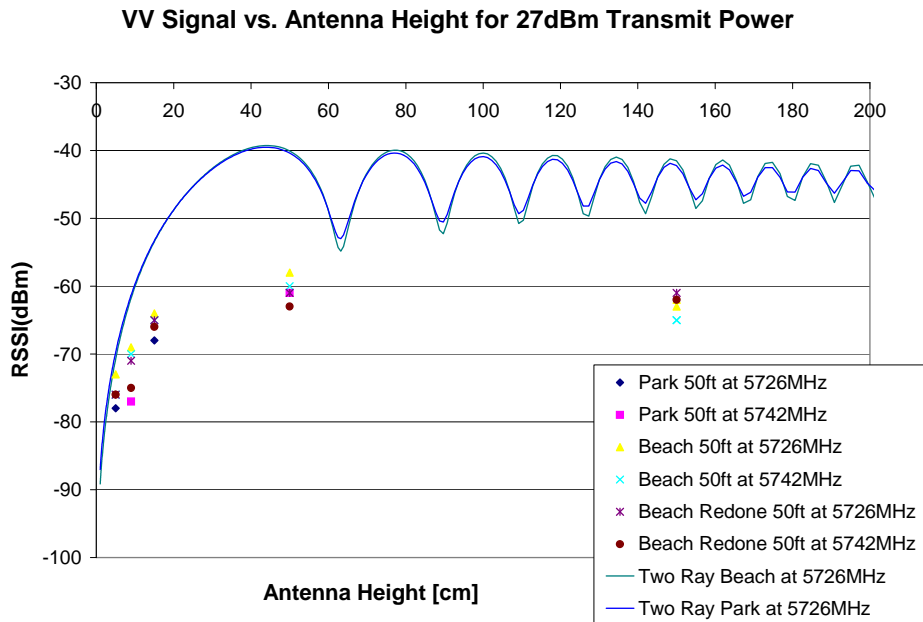


**Figure 229: Propagation as a function of height for the open areas, VV.**

128

**HH Signal vs. Antenna Height, 27dBm Transmit Power**
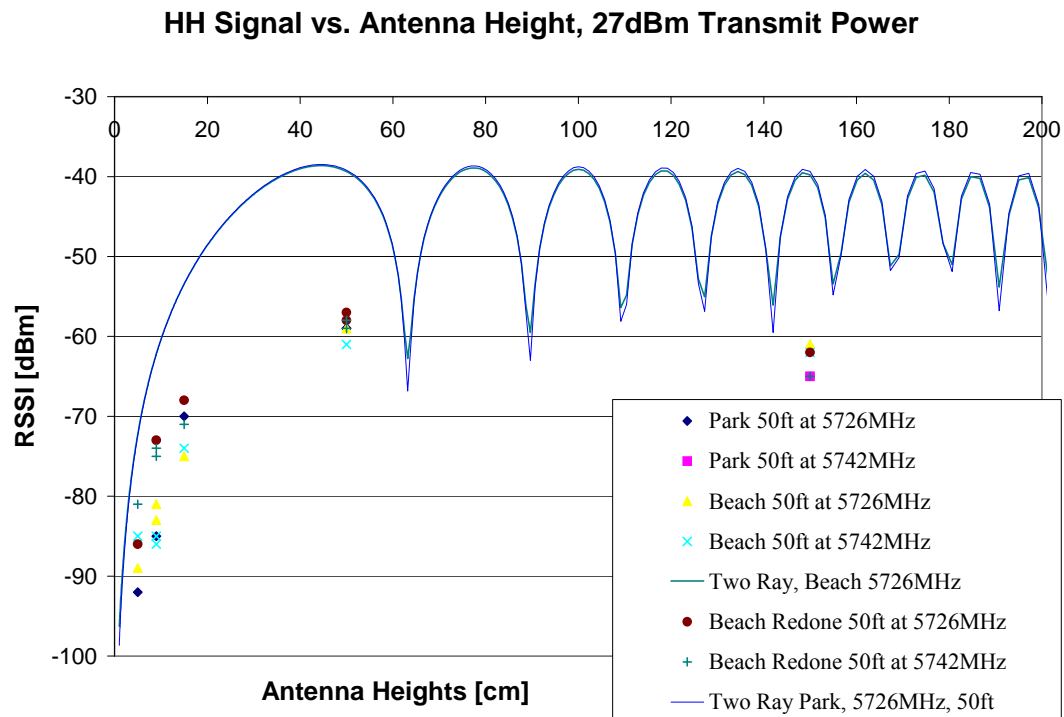


**Figure 230: Propagation as a function of height for the open areas, HH.**

**HV Signall vs. Antenna Height, 27dBm Transmit Power**
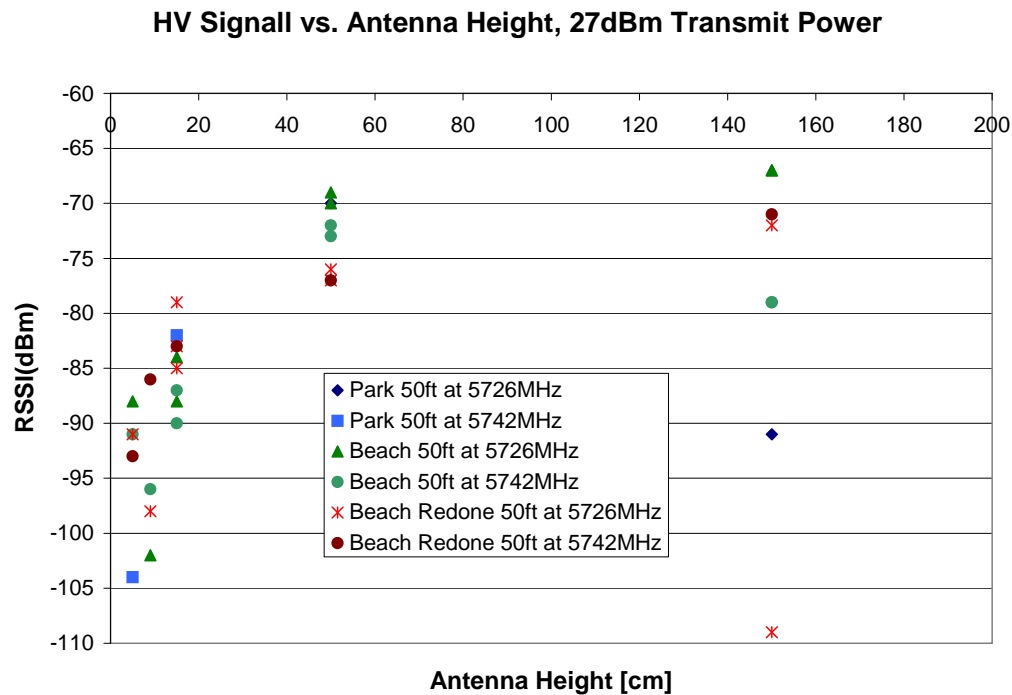


**Figure 231: Propagation as a function of height for the open areas, HV.**

**VV Signal vs. Height at 50ft with 27dBm Transmit Power**
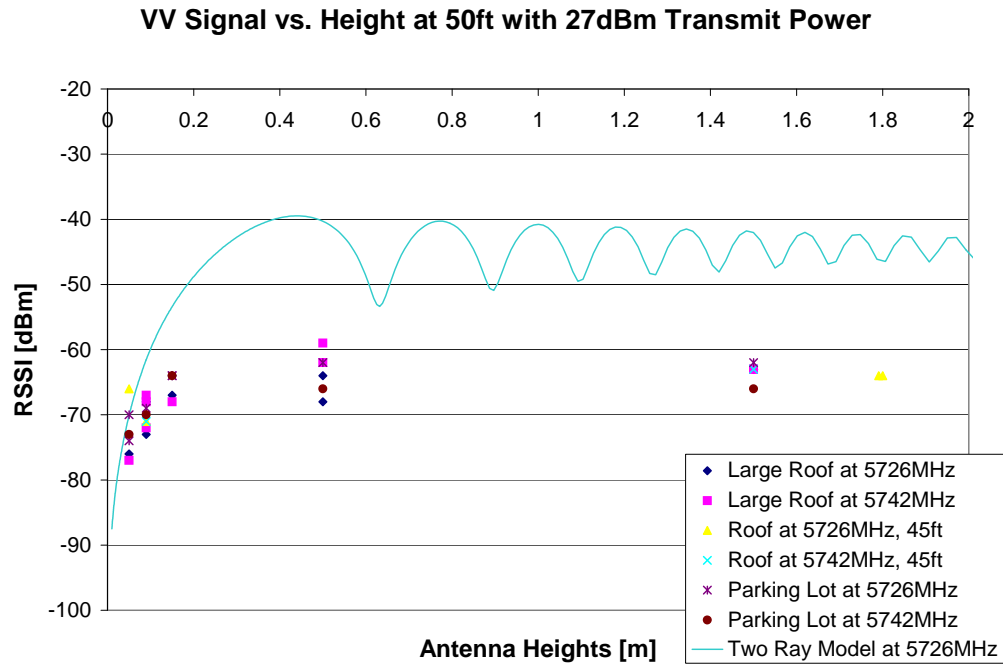
**Figure 232: Propagation loss as a function of height for the parking lots, VV.**



**HH Signal vs. Height at 50ft, 27dBm Transmit Power**
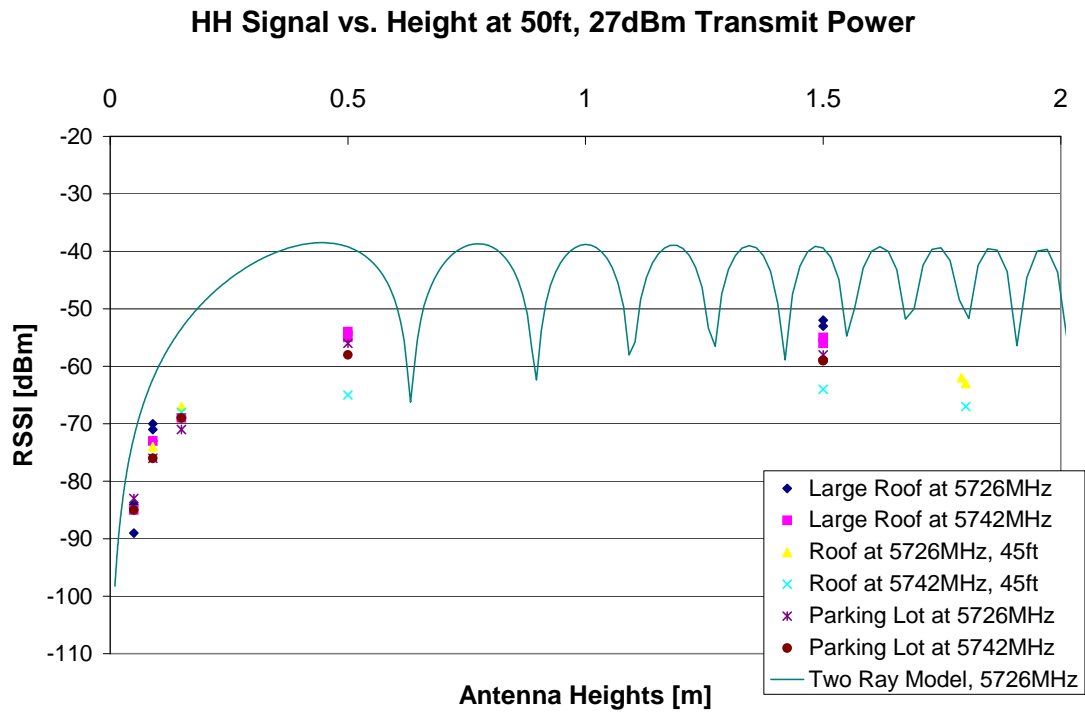
**Figure 233: Propagation loss as a function of height for the parking lots, HH.**

**HV Signal vs. Height at 50ft and 27dBm Transmit Power**

Legend:
- Large Roof at 5726MHz
- Large Roof at 5742MHz
- Roof at 5726MHz, 45ft
- Roof at 5742MHz, 45ft
- Parking Lot at 5726MHz
- Parking Lot at 5742MHz
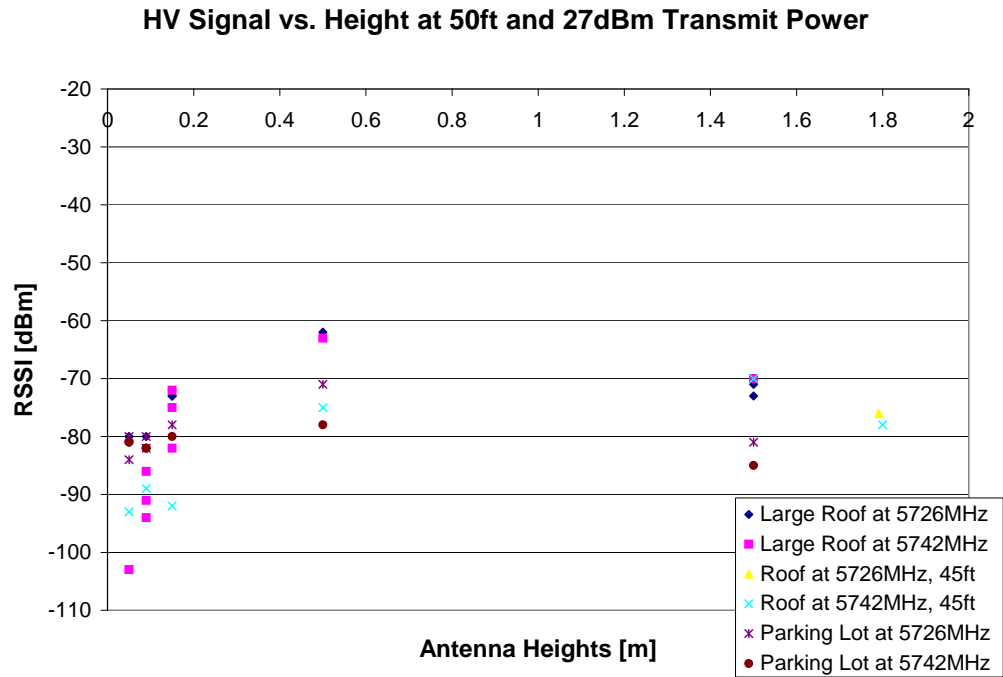
**Figure 234: Propagation loss as a function of height for the parking lots, HV.**



**VV at 50ft with 27dBm Transmit Power**

Legend:
- Sepulveda park at 5726MHz
- Sepulveda parkf at 5742MHz
- Bushes at 5726MHz
- Bushes at 5742MHz
- whittier at 5726MHz
- Whittier at 5742MHz
- Two Ray Park at 5726MHz
- Two Ray Bushes at 5726MHz
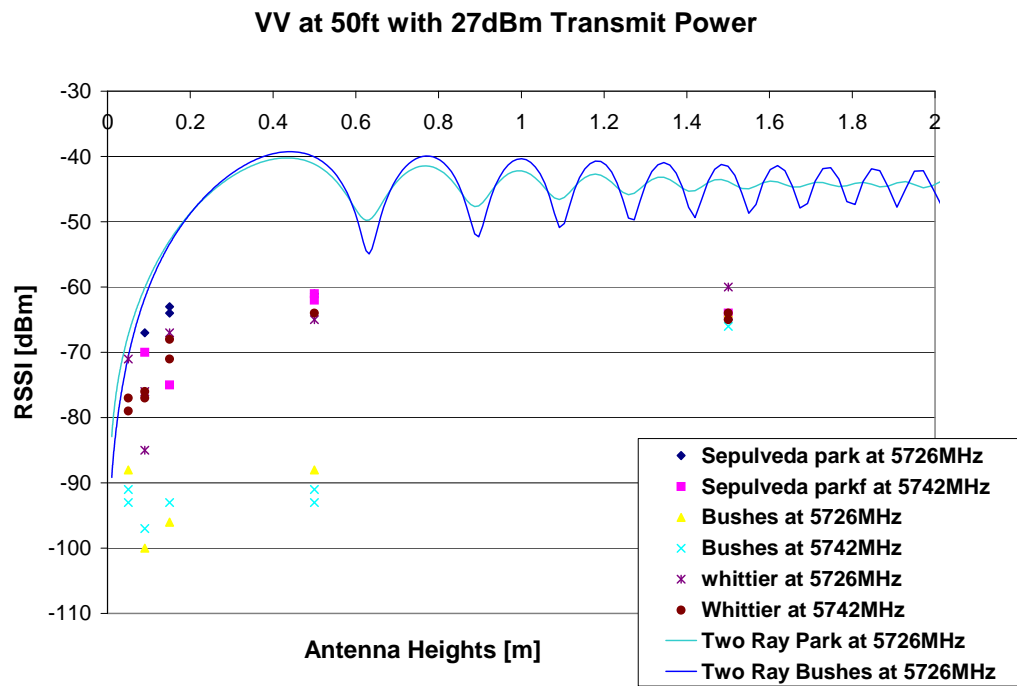
**Figure 235: Propagation as a function of height for the areas with vegetation, VV.**

131

**HH at 50ft, 27dBm Transmit Power**



**Figure 236: Propagation as a function of height for the areas with vegetation, HH.**

**HV at 50ft and 27dBm Transmit Power**



**Figure 237: Propagation as a function of height for the areas with vegetation, HV.**

**Figure 238: Propagation as a function of height for the areas with rolling hills, VV.**
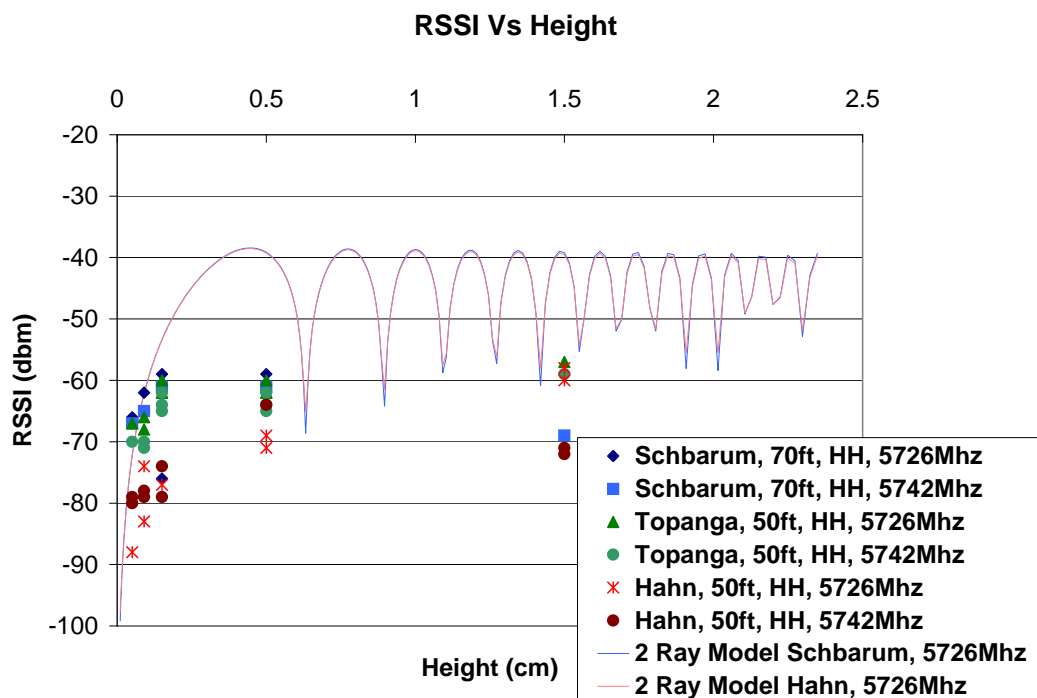


**Figure 239: Propagation as a function of height for the areas with rolling hills, HH.**

133

**RSSI Vs Height**
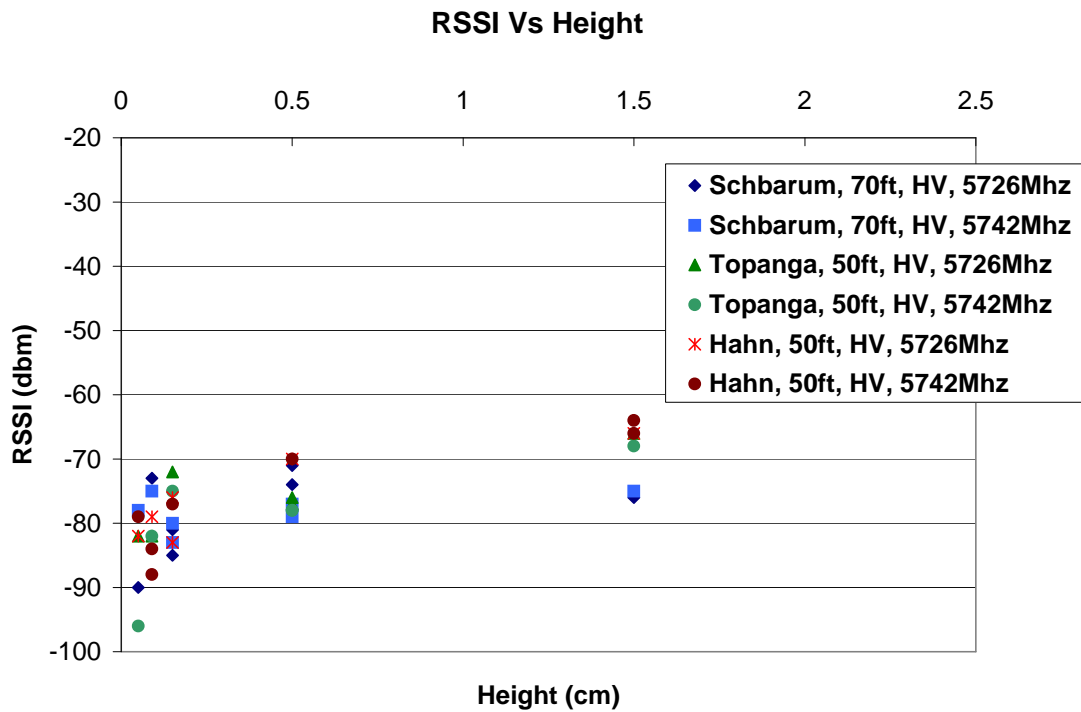


**Figure 240: Propagation as a function of height for the areas with rolling hills, HV.**

**Signal vs. Antenna Height vv 50ft**
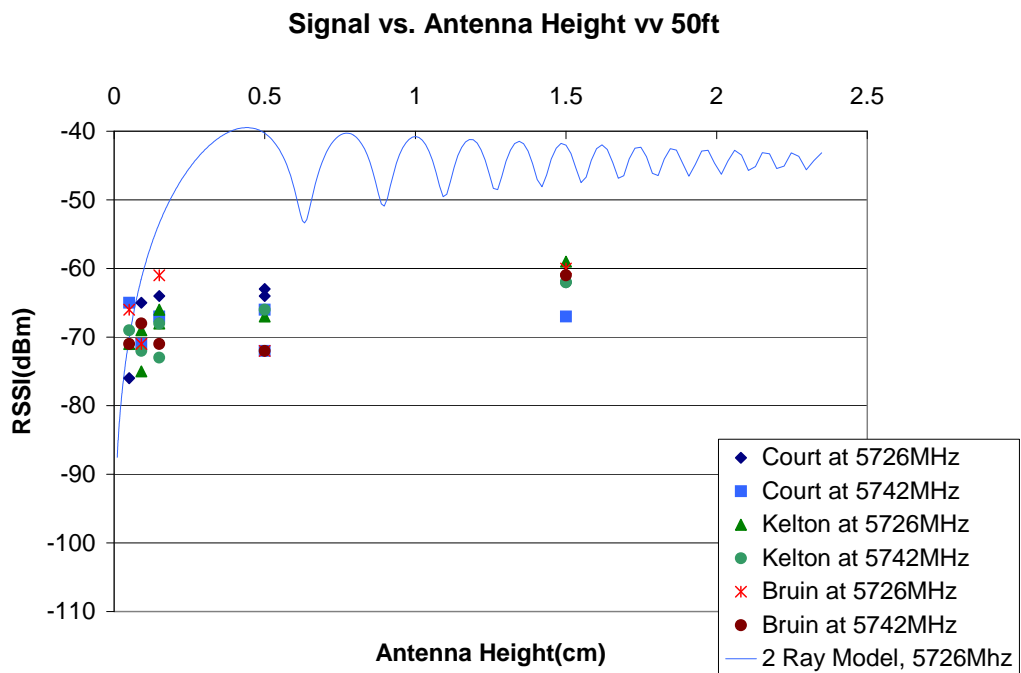


**Figure 241: Propagation as a function of height for the urban areas, VV.**

**Signal vs. Antenna Height HH 50ft**
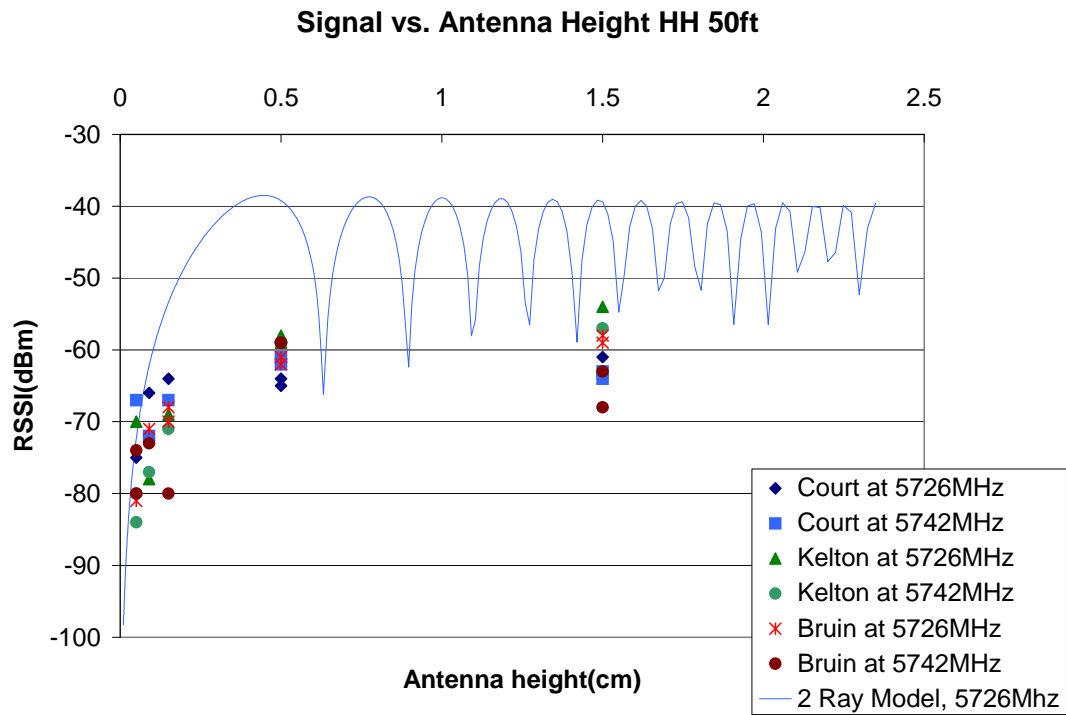


**Figure 242: Propagation as a function of height for the urban areas, HH.**

**Signal vs. Antenna Height HV 50ft**
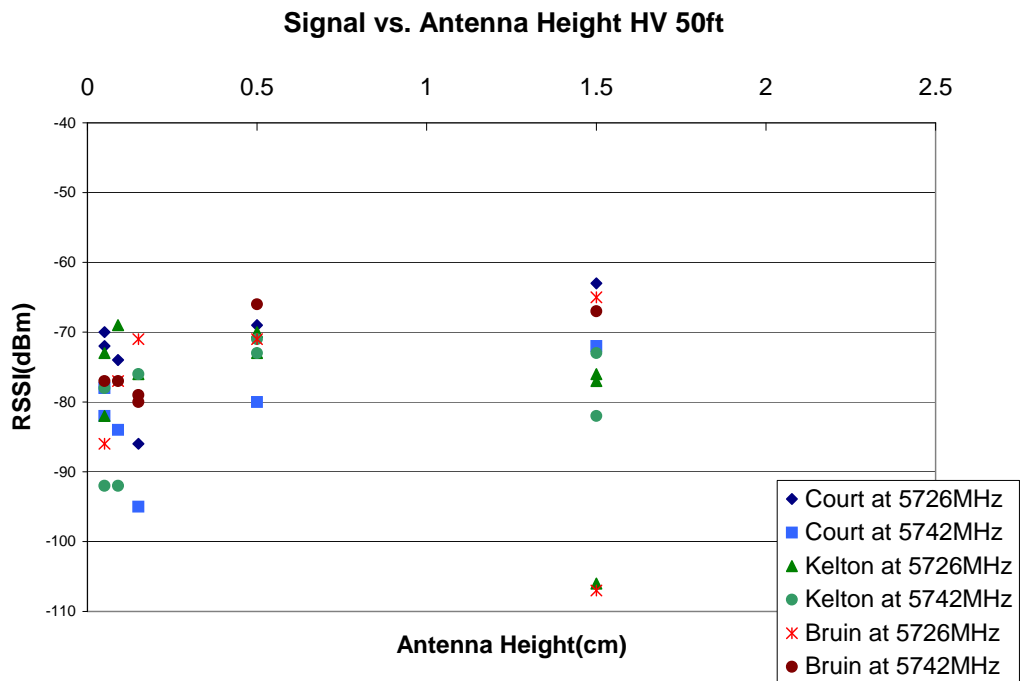


**Figure 243: Propagation as a function of height for the urban areas, HV.**

135

**Signal vs. Antenna Height at VV**
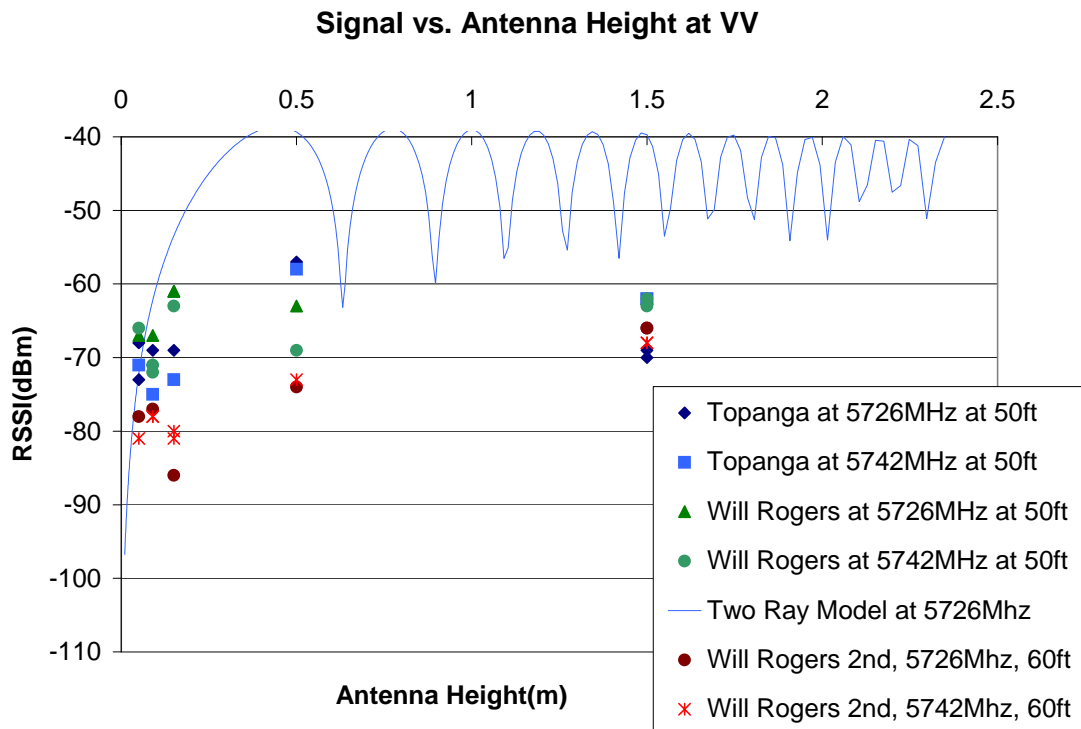


**Figure 244: Propagation as a function of height for the areas with rough vegetation, VV.**

**Signal vs. Antenna Height at HH**
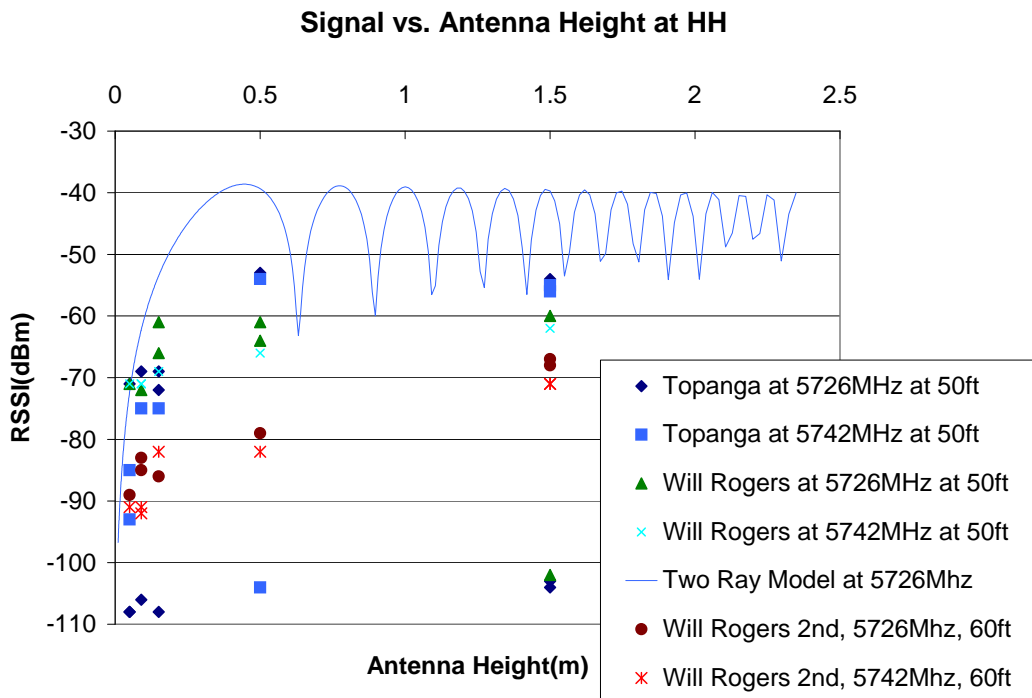


**Figure 245: Propagation as a function of height for the areas with rough vegetation, HH.**

136

**Signal vs. Antenna Height at HV**
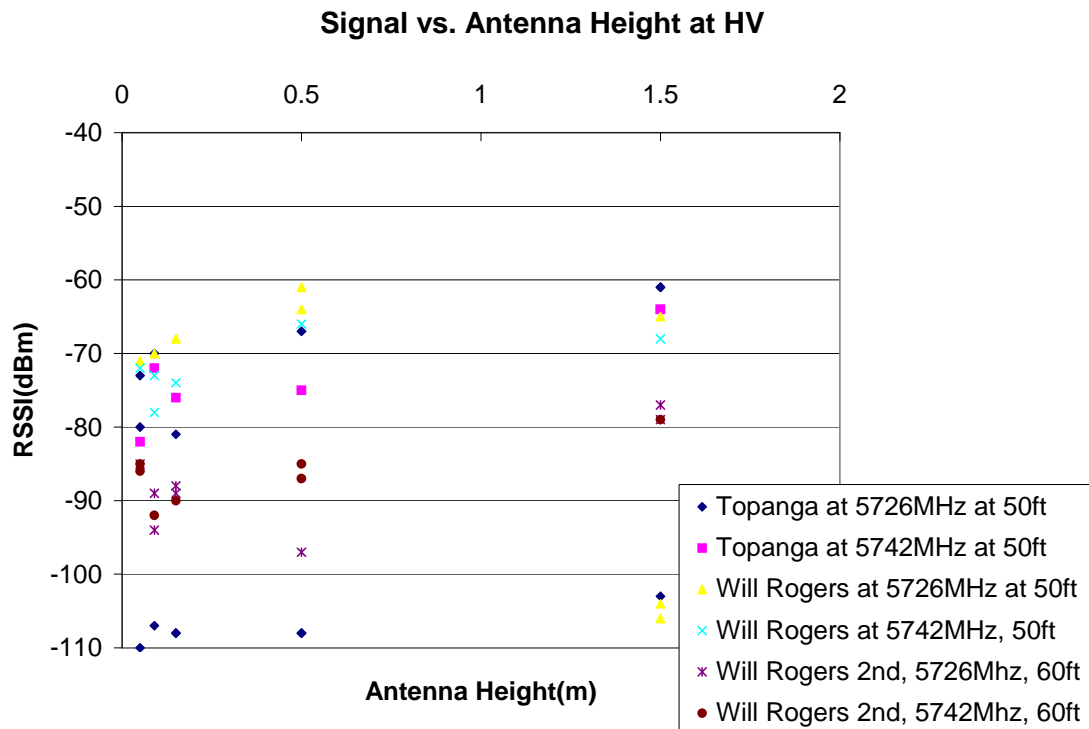


Figure 246: Propagation as a function of height for the areas with rough vegetation, HV.

**Path Loss at 50ft and VV Polarization**
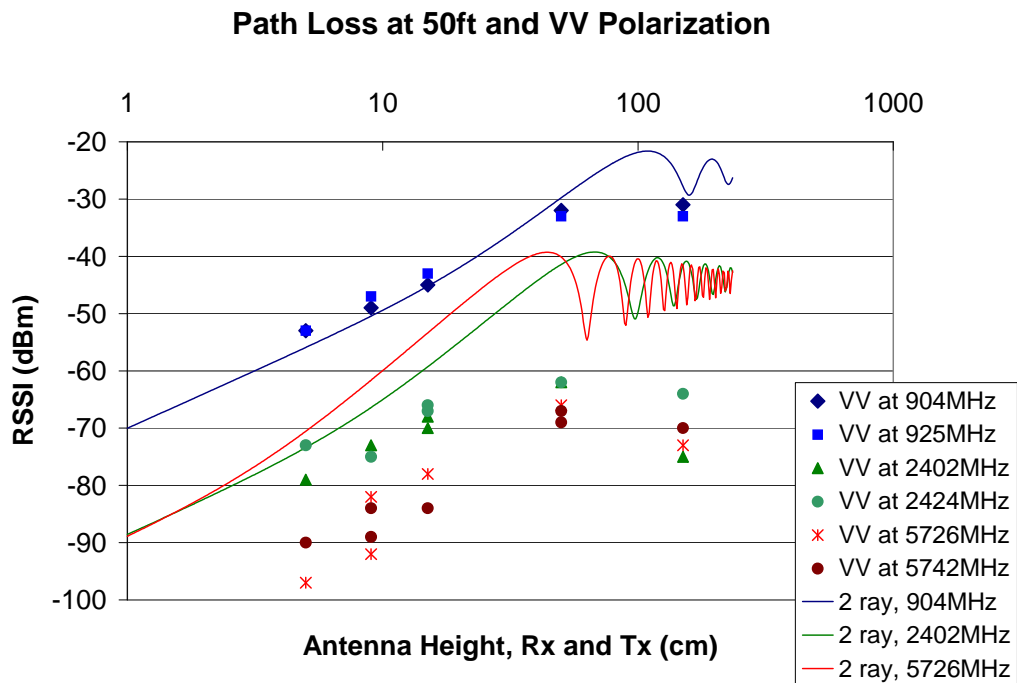


Figure 247: Propagation as a function of height for the Fort Leonard Wood test site.

PATH LOSS AS A FUNCTION OF DISTANCE FOR DIFFERENT TRANSMITTER AND RECEIVER HEIGHTS

In addition to the measurements for the same transmit antenna and receive antenna heights conducted on the beach, a number of additional measurements were taken at differing transmitter and receiver heights. The intent of these measurements was to provide an empirical data set for considering non-peer-to-peer connections with ground based autonomous systems, such as the deployment of a portable jamming system. Results are shown below in figures 248-250 for the path loss with a transmit height of 1.5m and a receiver height of 5cm within each of the three ISM bands.
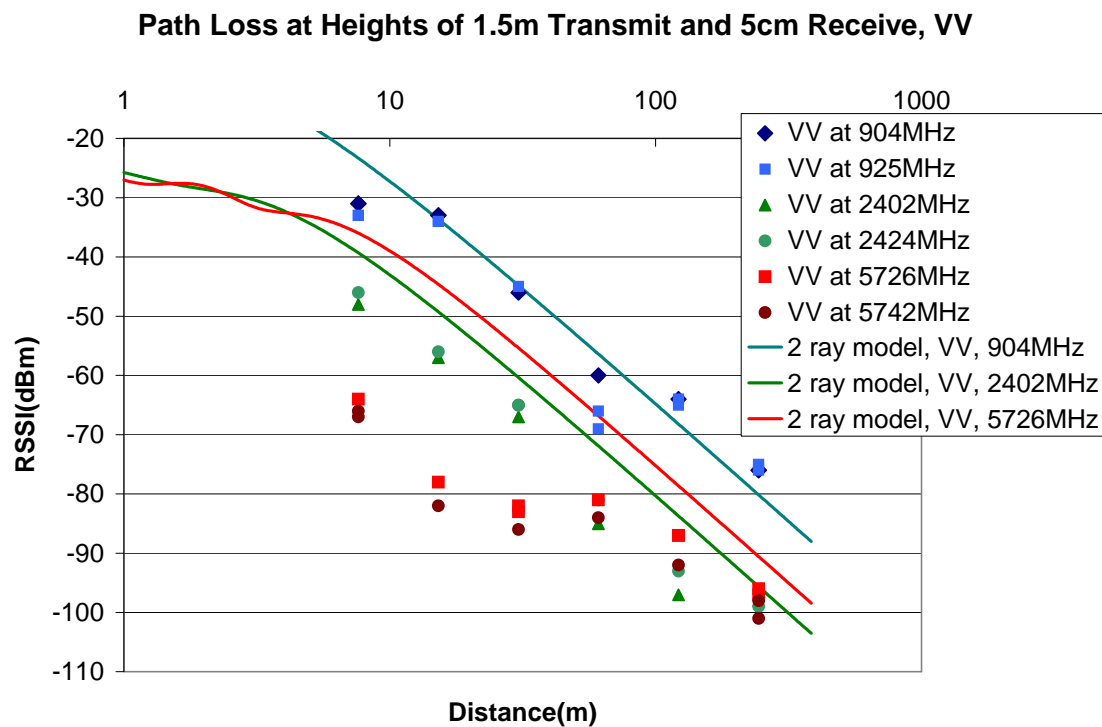


**Figure 248: Propagation as a different transmit and receive heights on the beach, VV.**
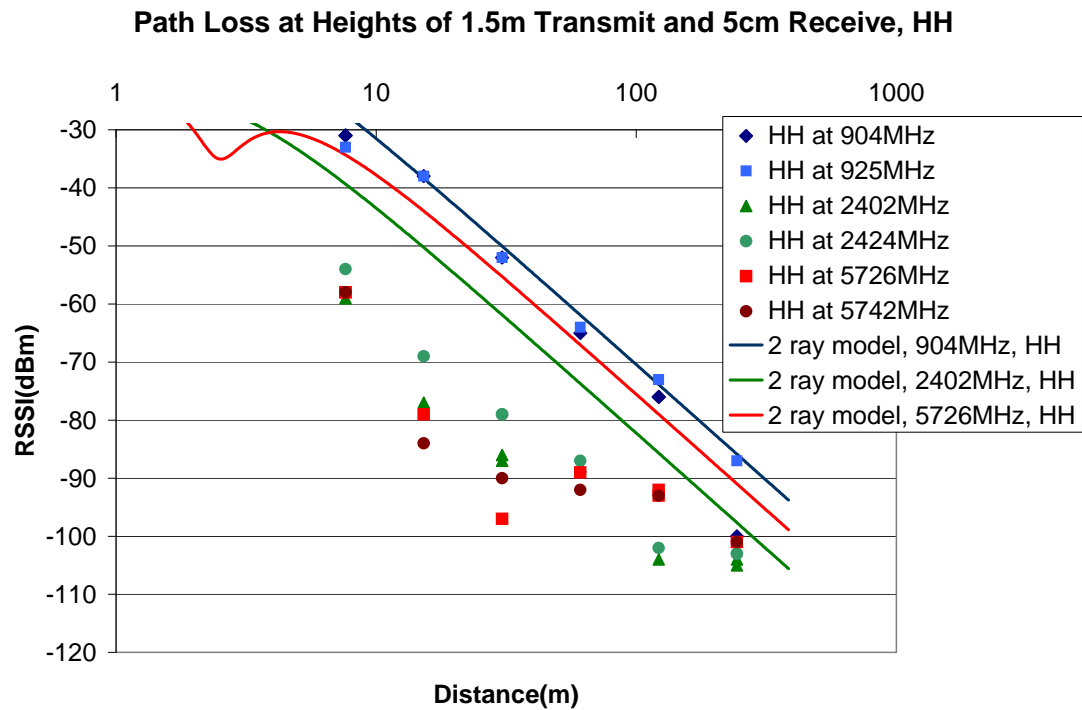
**Figure 249: Propagation as a different transmit and receive heights on the beach, HH.**
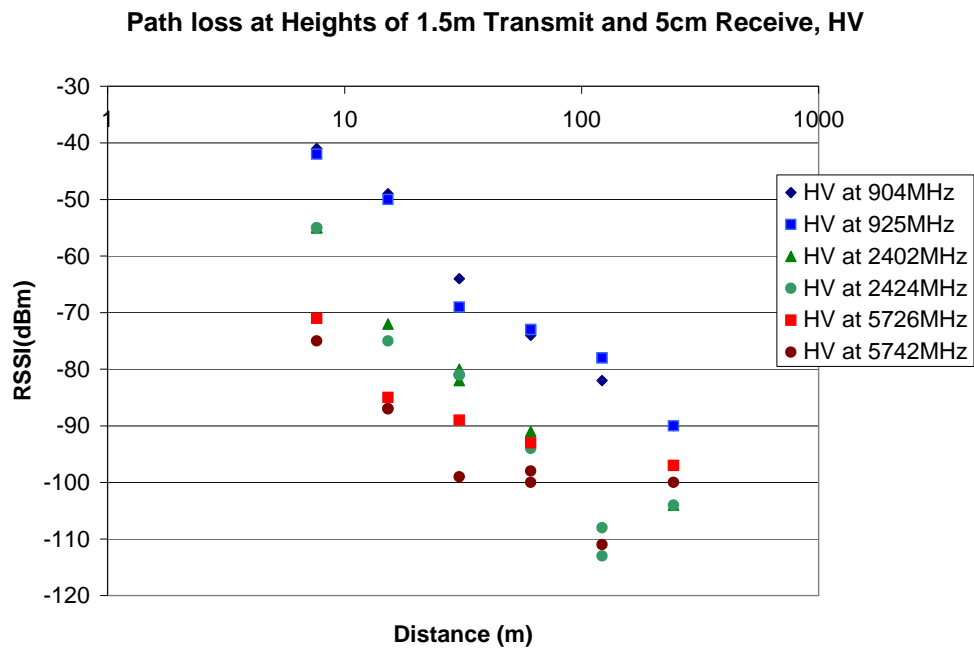


**Figure 250: Propagation as a different transmit and receive heights on the beach, HV.**

To provide an indication of the impact of individual scatterers, and groups of scatterers a number of measurements were taken in the mid size parking garage roof (of figure 62) with the receiver on and inside a car and the transmitter at a distance of 50ft from the car. Results are shown in figures 251-254.

**Near Vehicle Fading at VV, 5cm Tranmsit Height at 15.24m**
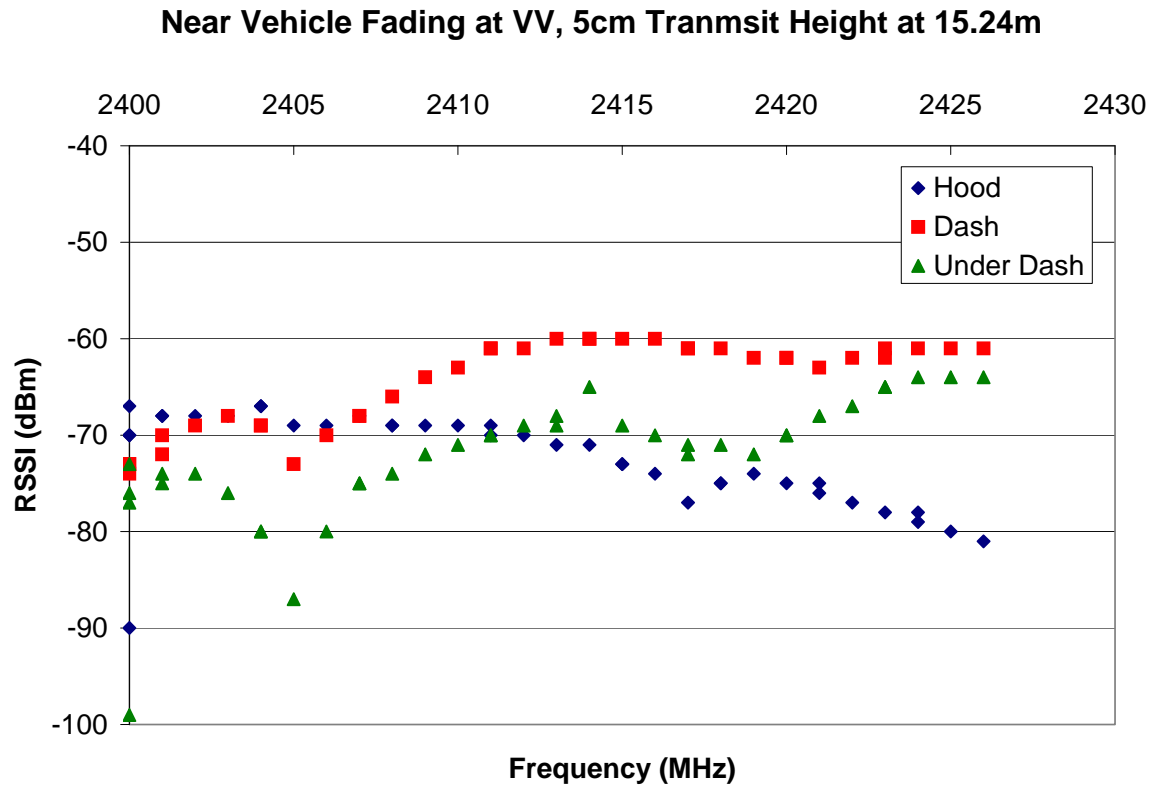


**Figure 251: Fading near a vehicle, on a parking garage roof, VV.**

**Near Vehicle Fading at VV, 5cm Tranmsit Height at 15.24m**
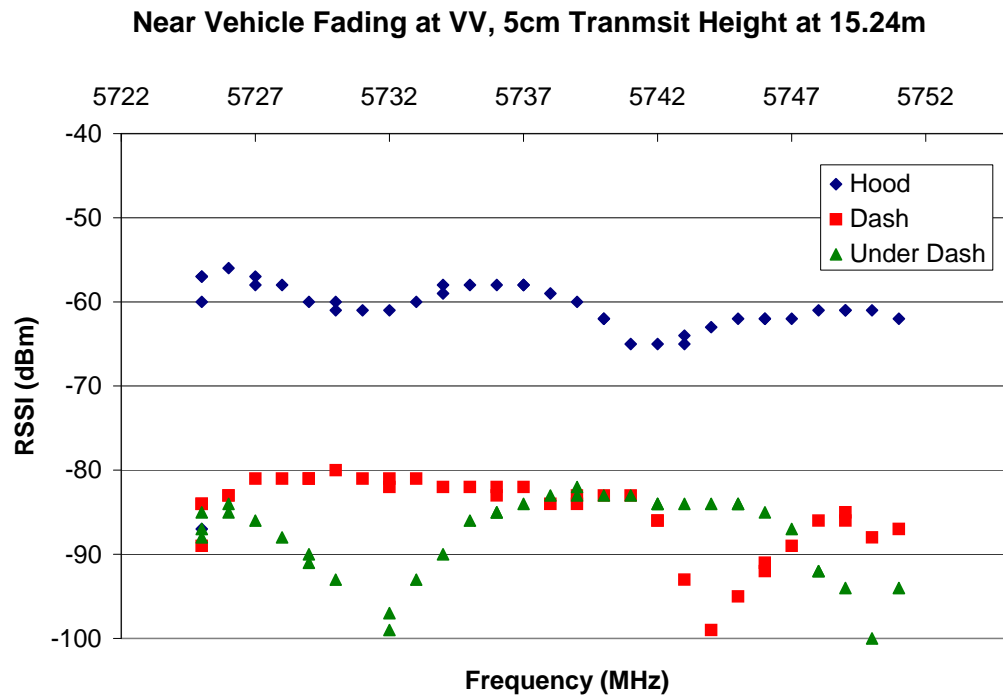
**Figure 252: Fading near a vehicle, on a parking garage roof, VV.**



**Near Vehicle Fading at HV, 5cm Tranmsit Height at 15.24m**
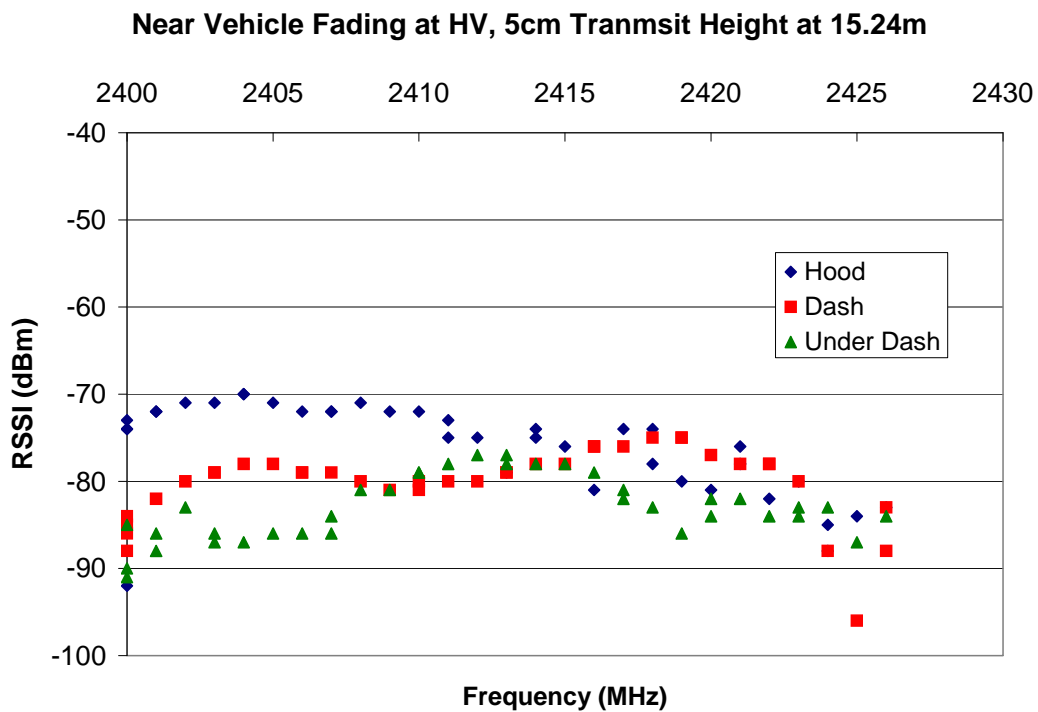
**Figure 253: Fading near a vehicle, on a parking garage roof, HV.**

141

**Near Vehicle Fading at HV, 5cm Tranmsit Height at 15.24m**
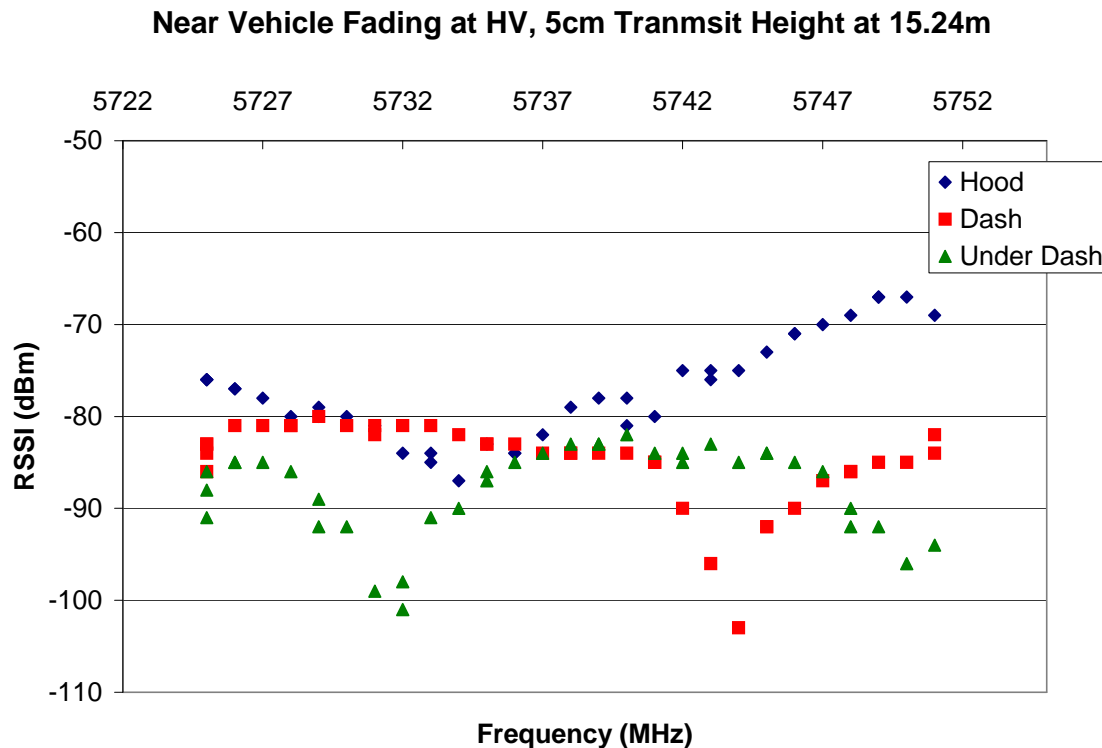
**Figure 254: Fading near a vehicle, on a parking garage roof, HV.**

<h2 style="text-align:center">PROPAGATION STUDY DISCUSSION</h2>

The data presented in the previous section provides a comparison of short-range wireless propagation in nineteen environments ranging from relatively open to substantially cluttered areas. This data quantifies the impact of the signals polarization, the amount of scattering (through both characterization of the cross-polarization-in conjunction with the antenna parameters and the fading level seen in each environment), and the dependence of the environment and antenna location on the signal range.

FADING

In the scatterer free environments of the open fields (the open field park had no scatterers nearby at the 15m distance only at larger distances) and the open parking lot shown in figure 63 similar fading levels (within 5dB across each frequency band) are seen. As environments with more scatterers are considered, the fluctuation with frequency is more pronounced. For example the two parking garage roofs show increased scattering (10dB to 20dB range in the fading seen depending on frequency) due to the proximity of light poles and railing in the smaller parking garage case, and to parked cars in the larger garage roof. Similarly environments with more vegetation and buildings also incorporate substantially more scattering. An anomaly observed in figures 79, 97, 105 is the reception of paging frequencies at 929MHz and 930MHz particularly at

the beach, as after the first four measurement environments (figures 59-62) the receive frequency range was tightened to only 902-928MHz to prevent picking up these errant readings.

Shown in table 3 is the average fading range for each of the environments across the first 27MHz of each of the ISM bands. In putting together this figure a number of aberrations in the plots were dropped such as the erroneous measurements at 929MHz and 930MHz due to reception of paging frequencies. In addition the occasional isolated low value seen in some of the plots (lower by 10dB or more) was not included as these are attributed to the unsynchronized nature of the receiver and transmitter, i.e. when the transmitter switches frequencies during a signal reception thus power is not received over the entire time slot at which each RSSI value is determined. The ranging of fading seen in these environments is easily seen in table 3 (from figures 79 to 132). The maximum fading seen in these outdoor areas is around 25 dB for co-polarized signals and 30dB for cross-polarized signals. In addition the fading appears to be dominated by the presences of scatterers as opposed to surface roughness. In this table in the open environments T. represents the turf farm, P. the open park, B, the beach. In the parking lots, L. represents the large parking garage roof, Rf. The medium size parking garage roof, and Lot the empty beach parking lot. In the flat vegetation areas 1 represents park 1, B, the area of dense bushes, and 2 represents park 2. In the rolling hills areas S. represents Schbarum Park, T the Topanga filed, and H. the Hahn park at the base of a hill not far from some playground equipment. In the Urban areas C. represents the measurements in the science court, K. the measurements along Kelton avenue, and B. the measurements along Bruin walk. In the rough vegetation T represents the Topanga hiking trail, W1 the first Will Rogers hiking trail, and W2 the second Will Rogers hiking trail. In a few of the environments data was not taken in the 5.7GHz band, for example the 5.7GHz equipment was not utilized in the open turf farm, and the data set was corrupted for the 5.7GHz data taken in the flat park 1 environment.

In the open environments the signal strength fading is consistently within ~5dB in the 900MHz band for the VV and HH polarizations (figures 79, and 97). The HV polarization in the open field exhibits more variation (up to 10dB at the beach, while still within ~5dB on the flat turf farm and open park). The variety of variation seen in these open environments apparently indicates the influence of the surface roughness to increase the variation in the cross polarized signals, and reduces the overall level of the received signal. This level of variation due to surface roughness appears to be consistent within the plus or minus 3-5dB seen in the Wireless Insight modeling described above.  For both the 900MHz band (figure 115) and the 2400MHz band (figure 121) HV measurements the cross polarization seen at the beach is markedly lower than at the turf farm or in the grassy park. While in looking at the 5725MHz band (figure 127) the park HV measurements actually drop below the beach measurements.

**Table 3: Approximate variation in fading with the first 27MHz of each ISM band.**

| Signal | Open | | | Parking Lots | | | Flat Vegetation | | | Rolling Hills | | | Urban | | | Rough Vegetation | | |
|---|---|---|---|---|---|---|---|---|---|---|---|---|---|---|---|---|---|---|
| | T. | P. | B. | L. | Rf | Lot | 1 | B. | 2 | S. | T. | H. | C. | K. | B. | T | W1 | W2 |
| VV 900 | 3 | 3 | 5 | 11 | 8 | 5 | 10 | 10 | 19 | 8 | 4 | 15 | 20 | 20 | 20 | 20 | 15 | 25 |
| VV 2.4 | 4 | 4 | 7 | 10 | 10 | 7 | 16 | 5 | 17 | 18 | 10 | 15 | 20 | 12 | 15 | 25 | 10 | 8 |
| VV 5.7 | | 3 | 8 | 5 | 5 | 6 | | 15 | 15 | 5 | 6 | 12 | 7 | 9 | 18 | 9 | 11 | 6 |
| HH 900 | 6 | 4 | 5 | 22 | 11 | 4 | 18 | 10 | 12 | 14 | 3 | 20 | 15 | 13 | 20 | 20 | 12 | 20 |
| HH 2.4 | 5 | 4 | 8 | 15 | 15 | 10 | 15 | 3 | 14 | 5 | 7 | 15 | 18 | 20 | 12 | 15 | 11 | 20 |
| HH 5.7 | | 6 | 15 | 20 | 7 | 10 | 21 | 7 | 18 | 3 | 5 | 22 | 10 | 24 | 18 | 22 | 10 | 12 |
| HV 900 | 6 | 5 | 10 | 14 | 15 | 15 | 25 | 12 | 12 | 5 | 14 | 30 | 21 | 15 | 15 | 25 | 20 | 20 |
| HV 2.4 | 9 | 5 | 16 | 14 | 17 | 20 | 17 | 6 | 15 | 10 | 20 | 25 | 15 | 18 | 17 | 7 | 13 | 10 |
| HV 5.7 | | 12 | 15 | 20 | 10 | 10 | 15 | 10 | 15 | 10 | 20 | 15 | 15 | 15 | 19 | 14 | 10 | 10 |

In general for the VV fading measurements in the 900MHz band most surface roughness is limited in electrical size. In those environments without substantial additional scatterers the fading within the band is limited to less than about 8dB. For example in figures 79, 80, and 82, the turf, the open park, the beach, the roof, the parking lot, Schbarum park, and Topanga measurements all are within 8dB variation across the band and for example for the turf farm and the open park this variation is within about 3dB. This 3dB may be attributed to variations due to scattering off the antenna tripod and due to measurement uncertainty within 1dB. The limited variation seen at higher frequencies as well appears to indicate that the influence of the equipment is limited to less than 3dB for VV polarization. In the 900MHz band the influence of moderate surface roughness (seen at the beach and in the rolling hills environments) appears to be within 5-8dB, specifically since the Hahn rolling hill environment (fading shown in figure 82) included a number of scatterers as well as the sloping hillside off to one side. This is consistent with the surface roughness simulations described above. Upon incorporating scatterers into the environments the influence on VV fading is substantial, increasing from ranging over 10dB for the widely separated trees of the park 1 area (fading in figure 81) up to 20dB for the three outdoor urban environments and to a variation of 25db for the roughest vegetation of the 2<sup>nd</sup> Will Rogers hiking trail.

The VV fading measurements in the 2400MHz band (figures 85 to 90) generally provide about the same level of variation seen in the 900MHz band, with some variations between specific environments. The open environments of the turf farm, the open park, and the parking

lot, all vary within about 7dB over the frequencies from 2400MHz to 2427MHz. Increased fading is seen in the other open environments due to the surface roughness at the beach (about 10dB), due to the sloping hills and tall grass at the Topanga rolling hills (about 10dB), the sloping hills and surrounding trees of Schbarum park (18dB), the cars and light poles on the large roof (10dB), the light poles and railing on the smaller roof (10dB).  As for the 900MHz response the addition of scatterers increases the variation substantially, across ~15dB for the trees in park 1 and park 2 areas, across 15dB for the Hahn rolling hills surrounding trees, hill and play ground equipment, and again over up to 20dB for the urban environments. In increasing the frequency the level of fading seen in the bushes and in the two Will Rogers hiking trail (rough vegetation areas) actually decreases. This may be attributed to the increasing number of substantial scatterers in the vegetation (effectively reducing the degree of nulls in the coherent cancellation of the multipath signals) as the frequency is increased.

The VV fading measurements from 5725MHz to 5752MHz (figures 91 to 96) also exhibits similar behavior to the first two frequency bands, exhibiting the same trends seen in comparing the 2.4GHz and 900MHz band. Again fading is low in the generally open environments, within 8dB in the open park, the beach, the large roof, the roof, the parking lot, Schbarum Park, the Topanga rolling hills, the Court of sciences area, and even the second Will Rogers hiking trails. In fact in many cases the level of fading seen in the 5.7GHz band is decreased over that in the other two bands, for example within 11dB for all the hiking trails (figure 96) and within 9dB for two of the urban environments (figure 95). The only environment in which substantially increased fading is seen in comparison with the other bands is the dense bushes environment in which fading is shown in figure 93. This environment appears to have the largest frequency dependence at the 50ft distance considered as the fading changes from gradual, to limited to much more apparently discontinuous or incoherent. At the distance for which fading is shown (about 15m) most of these environments provide a clear line-of-sight path between antennas. The two that do not are the bush environment and the second Will Rogers hiking trail. Both of these environments have their line of sight path blocked by substantial vegetation. However in both these environments substantially different fading is observed in the 5.7GHz band compared with the other frequencies, very limited (within 5dB) in the second Will Rogers hiking trail, and substantial (~20dB) within the dense bushes. From the comparison of the VV fading in the three frequency bands for these two environments the scale of the scatterers appears to be much larger (long tall grass rather than dense bushes) in the second Will Rogers hiking trail.

The HH polarization fading in the 900MHz band seen in figures 97 to 102 is very similar to the VV polarization fading. Fading in the open environments of the turf farm, the open park, the parking lot, and the Topanga rolling hills are all within 6dB in the 900MHz band. Substantially more fading is seen in the second Will Rogers hiking trail (20dB), and in the large and small roofs (22 and 11dB). More substantial fading is also seen in environments with more scatterers in the in the first Will Rogers hiking trail (12dB) and the Topanga hiking trail (20dB), in the urban environments (15-20dB), in the Hahn rolling hills scenario (~20dB), in the park 2 trees (~12dB), and in the bushes (10dB).

Figures 103 to 132 provide similar details on the HH and HV polarization in the three frequency bands. In particular as seen in the open environments the cross-polarization (HV) fading variation is higher than either of the two co-polarized polarizations. This can be attributed

specifically to the surface roughness and any scatterers that are present as these are the mechanisms for cross coupling form the horizontal to vertical polarization.

Also shown in figure 133 to 135 are the fading levels seen in the field at the Fort Leonard Wood test site. These are consistent with the previous open field measurements taken, and this environment fits into the classification used for the other areas as a rolling hills environment. Limited fading is seen in this environment, and the figures provide an alternative viewpoint comparing the fading of each polarization within each frequency band.  In general the levels of HH and VV fading are similar in each band with increased variation for the HV signals, with the interesting effect that the cross-polarized signals in the 5.7GHz band approach the signal strength levels of the other two polarizations. This is attributed to increased cross polarization at higher frequencies due to the measurement equipment, to the roughness of the field surface on the electrical scale of 5.7GHz, and to the dense grass and brush in the field.

Within the data collected the frequency dependent fading can be simplistically separated into environments with a few dominant large individual scatterers (within the short-ranges considered, and into environments with a large number of influential scatterers In general in both these environments large amount of fading can occur. fading, however to separate the two the continuous nature (or effective coherence length) of the fading can be used. At lower frequencies (the 900MHz band) environments such as the two parks with sparse trees and the parking garages appear to provide a few distinct dominant scatterers and as a result a slow variation, with frequency, can been seen in the fading. While at higher frequencies for all of the denser environments a large number of scatterers appear to provide much more discontinuous fading. This is apparently a result of the larger numbers and variety of types of scatterers as the frequency is increased, since the effective phase length increments are the same in all three bands (1MHz steps or a phase change of 20.9 mrad or 1.2° per meter of changed path length). One anomaly observed is in the dense bush environment more scatterers are present, yet in the 900MHz band the fading appears to indicate one or a few dominant scatterers are producing a coherent phase center for the scatterers. At higher frequencies the bush environment with its large number of scatterers over the signal path (corresponding to the data in the higher two frequency bands) appears to more closely correlate with prior modeling of urban and rural scenarios over multiple kilometers where many scatterers are assumed over the transmission path, rather than a clustered group of scatterers representing a single tree, or light post. In general from the fading plots of figures 79 to 132, it appears that the presence of a few "clumps" of scatterers in short-range measurements can significantly influence the fading variability seen within the ISM band. This is reasonable in a ray interpretation, as the coherent interaction of a small group of rays can provides significant variation as the rays electronic path length is changed (i.e. frequency is changed). In addition the abrupt fading that appears to have a much shorter coherence length possibly due to larger numbers of scatterers, is also observed particularly at higher frequencies. In general the fading levels seen appear to be less than 10dB in must "uncluttered" open environments, and up to variation over 25dB in outdoor cluttered environments in which a LOS path or near LOS path exists at short ranges.

PATH LOSS AT ANTENNA HEIGHTS OF FIVE CENTIMETERS

The fading shown in figures 79 to 135 is attributed to the presence of scatterers within the

environment (providing up to 25dB variation over a frequency band when scatterers dominate). In addition figures 136 to 192 demonstrate the influence of scatterers on the signal power decay with distance. This analysis focuses on VV polarization at antenna heights of 5cm. In general within each environment type the trend in the power fall-off corresponded roughly to the two ray model predictions of equation (2) for antenna heights of 5cm. For a power law fit the two ray model at 5cm antenna heights and the distances of 1m to 250m corresponds to a fourth power fall off of signal power with distance. Thus a comparison of the power law trend with a fourth power fall off is provided in each figure by the two-ray model. In general, all the environments appear to generally follow this fourth power trend.

The clearest environments correspond the closest to the prediction of the two-ray model. In figures 136, 137, 154, 155, 172, and 173 the turf farm, the open park, and the beach all follow the trend of the two-ray model closely, particularly at distances of less than 30m. The values of the measurements in the 2.4GHz band and the 5.7GHz band are lower than the model's prediction since the predictions do not incorporate the system cable and connector loss. In addition in the open park beyond about 50m a couple of small trees were near to the line of measurement, resulting in the reduced path loss seen at distances of larger than 50m as scattered signals enhanced the propagation. This trend is consistent across all polarizations, and in fact the HV polarizations shown in figures 138, 156, and 174 follow a similar trend as the HH and VV polarizations. All of these open fields present an improved performance over the two-ray model at distances approaching 100m, this is attributed to the influence of additional scatterers becoming more influential as the strength of the direct and ground bounce rays decrease. In addition the equipment noise floor was reached around -115dBm, although in most cases the breakpoint observed is at levels higher than this.

As the propagation distance is increased past a few dominant scatterers the logarithmic slope of the power decay appears to decrease. This corresponds in a ray model interpretation to the strength of the LOS and ground bounce ray combination decreasing to the point that other scattered rays (traveling over a longer path and incorporating scattering) may make significant contributions to the received signal. The open park environment provides a striking example of this as at approximately 70m a group of trees stood along the line on which measurements were taken. The influence of these trees to provide additional scattering above the LOS and ground bounce paths is clearly seen in figures 154 and 172. The lack of this change in behavior in the 900MHz measurements represents the frequency dependent nature of scattering from the trees, i.e. scattering from individual leaves and branches increases, as they are a larger fraction of wavelength. Generally, at 900MHz (free space wavelength of 33cm) scattering from a tree's branches and trunk may be substantial, although not as large as at higher frequencies as demonstrated in the figures 154 and 172. The general breakpoint seen, from a fourth power fall off (i.e. the two ray model prediction) to a more gradual slope is attributed to the influence of elevated scatterers providing substantial additional power at the receiver through the non-direct paths. This trend can be seen in most of the environments, for all the polarizations For example in the 900MHz band the open clear turf, beach, parking lot, the rolling hills environments, and the Fort Leonard Wood test site fit the trend of the two-ray model well, with the smaller parking garage roof showing the most variation, while the more cluttered urban, flat vegetation and rough vegetation environments generally provide reduced path loss over the two ray model predictions. In fact the smaller parking lot and the dense bushes provide the only environments in which

147

substantial cancellation is seen (below the two-ray model predictions). On the parking garage roof this can be certainly attributed to a clustered large scatterer, a metal railing nearby with an attached light post, resulting in a null in the field at short distances. However in general the other environments at 900MHz as well as 2.4GHz and 5.7GHz as shown in figures 136 to 192 either provide a similar path loss to the two-ray model, or depending on the location and type of scatterers provide an improvement over those predictions at mid range distances.

The influence of this scattering at short ranges in the measurements taken tends to decrease the over all path loss as opposed to the common breakpoint seen in cellular systems [5], where at antenna heights of a few to tens of meters as the distance is increased the angle of each ground bounce ray approaches ninety degrees from the surface normal, providing more complete cancellation at longer distances and a decay to a fourth power law trend. Here at least at the short distances observed the predominance of large scatterers at a higher elevation than either the transmit or receive antennas can increase the received signal over that expected from the two ray model. In a ray analysis each scattered ray undergoes a spherical wave-front reduction at each scattering providing the expectation of at least a fourth power loss, however for large and/or specular scatterers the energy scattered may be large enough and directional enough to provide more power than the interaction of the LOS and ground bounce rays. In general the signal path loss observed appears to follow the two-ray model at short distances (within 10-20m in most environments) with slight improvements over those predictions in LOS areas at moderate ranges out to a hundred meters or so. In some cases the resultant fall off is worse than the two-ray model prediction, however in these cases the fading with frequency is generally substantial so frequency-spreading schemes can compensate somewhat for this loss, or the environment contains substantial multiple scattering such as in the brush filled field. It is interesting to observe in the cluttered environments of the rough vegetation areas, at larger distances beyond 100m or so the measured values start to fall back down to the fourth power loss predicted by the two-ray model (figures 151, 152, 169, 170, 187, and 188). This can be understood as analogous to the dense bushes environment, where the impact of multiple scattering starts to attenuate the signal, resulting in fall off analogous to prior longer range cellular studies.

In the figures the two ray model for each surface permittivity type are shown based on the values in table 2. These values provide rough estimates of the soil permittivity, however as can be seen in the figures, even with widely different permittivity and conductivity values, at the ground bounce angles considered, substantial variations in the predictions are not observed.

ANTENNA HEIGHT INFLUENCE ON PATH LOSS AT A DISTANCE OF FIFTEEN METERS

Figures 193 to 247 present the power received as a function of antenna height within each environment for VV, HH, and HV polarized signals at a distance of about 15m between transmitter and receiver. All measurements are at distance of 50ft or 15.2m except those taken on the turf farm and on top of the small parking garage, which were taken at a distance of 45 feet or 13.7m, those taken at Schbarum park at a distance of 70 ft (21.3m) and those taken in the second Will Rogers hiking trail at a distance of 60ft (18.3m). Also shown are comparisons of the two-ray models prediction of path loss as a function of antenna height. In the open environments in the 902-928MHz ISM band the predictions correspond to the measurements very well. However in the other environments and the other ISM bands the comparison tend to be less favorable. In

addition as the frequency is increased the correspondence of the model and the predictions is much less accurate. This may be influenced by less accurate soil permittivity and conductivity values (table 2) as well as the additional cable and connector loss in the system, not incorporated into the 2-ray predicted path loss. However even with these adjustments the errors appear more pronounced at higher frequencies. Surface roughness may also influence the accuracy of the predictions, particularly at higher frequencies. In most open environments the trend predicted by the two-ray model of increased performance with height is seen (figures 193-198, 211-216, 229-231, and 247. However in most of the environments with substantial scattering (figures 199-210, 217-228, and 232-246), the reduction of path loss with increasing height is much less pronounced. This is attributed to the abundance of elevated scatterers in the environment, and may indicate the relative unimportance of the LOS and ground bounce rays in this environment. The influence of frequency dependent scattering is seen in these comparisons particularly in the 5.7GHz band in the parking lot environments as the increased scattering reduces the path loss seen at the lowest heights. In general in the environments measured, increasing the antenna heights to an elevation of 50cm improves the signal range up to tens of dB, with the more cluttered the environment the less benefit provided. Increasing the height beyond 50cm at the distance of 15m and frequencies considered does not substantially improve performance. However at longer distances this transition height will be higher, with the expectation of a similar distance to height ratio of 30 providing best-case performance, corresponding to the break point in the Fresnel reflection.

PATH LOSS AS A FUNCTION OF DISTANCE FOR DIFFERENT TRANSMITTER AND RECEIVER HEIGHTS

All of the path loss measurements at different antenna heights discussed in the previous section were taken for peer-to-peer systems with the same transmit and receive antenna heights. In addition limited testing was conducted on the beach with different transmit and receive antenna heights. Measurements were taken with a receiver height of 5cm and transmitter heights of 5cm, 9cm, 15cm, 50cm, and 150cm at distances of 7m to 243m. Shown in figures 248-250 is the power fall of with distances for a transmitter height of 1.5m and a receiver height of 5cm in the beach environment. At these heights and distances the data correlates best with the two-ray model in the 900MHz band, shows a similar trend in the 2.4GHz band, and shows an interesting dip in the trend in the 5.7GHz band. This dip is attributed to the beach surface roughness on an electrical scale, since it is the most significant in the 5.7GHz band. In general these measurements support the use of the two-ray model in simulating alternate transmitter receiver scenarios other than the peer-to-peer (equal transmit and receive heights) focused on above. For example to provide a path loss model for a man portable, or remotely deployed jammer expected to operate at short distances.

MEASUREMENTS OF PROAPGATION IN THE PRESENCE OF A VEHICLE

Figures 251-254 demonstrate the fading level seen near a car in the mid size parking garage roof environment. These figures compare with data for the roof in figures 86, 92, 121, and 128, taken in the same area although at a different receive antenna height (5cm instead of on or in the Toyota Corolla used for measurements). The fading levels seen in figures 251-254 are substantially larger than those seen in the environment without the car, particularly the

149

measurements taken inside the car on its dashboard, or below the dash in front of the front seat. These measurements provide a first look at the level of fading due to the car, ~10dB external to the car and on the dash, and about 20dB from internal to the car to external to it. In addition the fading seen in the car appears to vary slowly with frequency, apparently indicating the presence of a few dominant scatterers such as the hood and roof, unlike many of the cluttered environments where the fading was much more scattered across the fading range.

# DEVELOPMENT OF PICOWINS TAGS: METHODS FOR EXTENDING COMMUNICATION RANGE

The analytical and empirical propagation study of short-range wireless communication demonstrates the severe energy requirements of near ground communications. As the PicoWINS tags are battery operated this power limitation of range provides the severest requirements to a tags wireless operation. As a result within the PicoWINS feasibility investigation the possibilities for optimizing the tag-to-tag, tag-to-gateway, and tag-to-munition link were investigated.

### CHANNEL CODING METHODS FOR INCREASED RANGE

Measurements with 2.4GHz frequency hopped spread spectrum radios operating in the 2.4GHz to 2.485GHz band displayed ranges with a minimum of approximately 15 to 20m in outdoor scenarios with 100mW of transmitted power. These measurements were conducted in rugged vegetation obstructed terrain shown in figure 255, with both the radiating and transmitting elements in close proximity to the ground. The 15 to 20m minimum range is viable for a multi-hop communication scenario given a high density of Tags, such as seen in the tactical Tags of PicoWINS. However, increased redundancy, less stringent placement requirements, and enhanced network robustness will be achieved by extending this range. Towards that end a number of possibilities are investigated.



**Figure 255: An example of the terrain in which 2.4GHz transmission range of 15m was achieved at 100mW.**

In order to extend the range of the wireless systems more power must be allocated in the channel's link budget than is presently the case. Since the PicoWINS networks are expected to

operate in a variety of environments the worst case $R^4$ signal propagation fall off is a design constraint. In addition, since individual Tags should be inconspicuous, increased antenna height is not desired. This leaves only a few other avenues of approach. First, increasing the transmitted power. Second, increasing the antenna gain, i.e. focusing the transmitted power only in the desired directions. Third, encoding the signal to reduce the power needed at reception given the constraints of the propagation channel.

Increased range may be achieved simply, by increasing the power radiated. However, given $R^4$ fall off, a doubling in reception distance requires a drastic power increase. Within the power constraints imposed by battery size, particularly at the tactical Tag level in PicoWINS this is unfeasible. While possibly an option for more complex nodes or gateways interspersed throughout the Tag network, on the Tag level increased transmission power beyond 100mW is not viable. Instead the alternative range extending techniques considered here may in certain situation be desired to reduce power transmission requirements on individual Tags, rather than to increase range.

PicoWINS Tags will be deployed approximately in two-dimensional networks on the earth's surface. In a few instances, such as indoor deployment or very rough terrain, three-dimensional networks on multiple building floors could be imagined, however in the majority of cases Tag placement can be approximated well with a perturbed flat plane. As a result power radiated from the Tags both overhead and into the ground is generally wasted. Ideally the antenna element on each Tag may be designed to focus energy along the ground enhancing the communication range along the surface of the earth. Two-dimensionally omni-directional antennas are commercially available at 2.4GHz in the form of long dipole antennas oriented normal to the ground. In order to increase antenna directivity the generally the size of the antenna must be increased. In addition since the directivity is desired to remain isotropic in the plane of the network, rotational symmetry is often utilized. For example a commercially available dipole with 9dBi of gain at 2.4GHz is 23 inches long oriented perpendicular to the ground. This is much larger than the form factor desired for the tactical Tags, in addition to providing a conspicuous breakable package. Patch antenna elements would be better suited for these applications, however achieving high directivity patch end-fire radiation (along the surface of the patch) omni-directionally in two-dimensions is difficult.

Shown in figure 256 is a radiation power pattern for a coax fed, stack of two end-fire triangular patches. In this figure the patches are oriented in the $\phi$=90 degree plane. Even in this case however, which has nulls in the radiation pattern that are oriented perpendicular to the patch, very little gain is achieved along end-fire, that is along grazing to the earth. To enhance the directivity along grazing in conventional patch configurations requires either a substantial area, or thickness increase, beyond that desired for most PicoWINS applications.
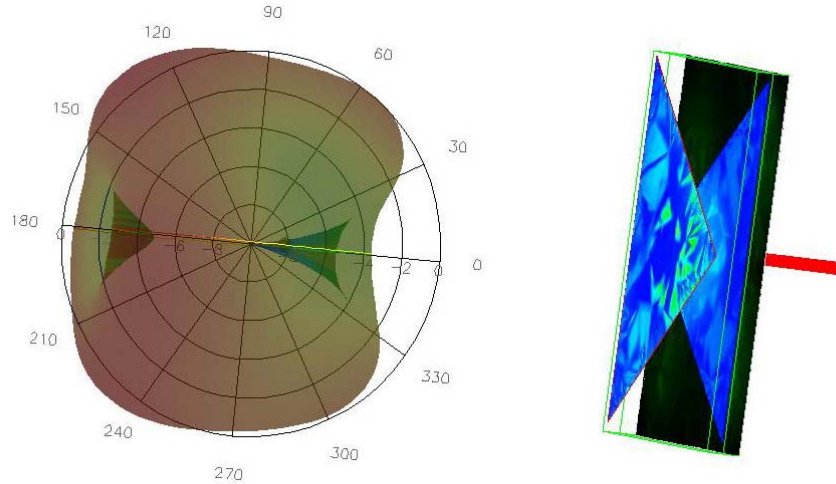
**Figure 256: Radiation pattern and geometry of a stacked two-dimensionally omni-directional patch antenna (substrate dimensions are 2.8 by 2.8 by 0.25 inches at 2.4GHz – larger than desired for a Tag, but feasible for a larger gateway).**

The most promising range enhancing technology is to increase the receiver sensitivity through signal coding and noise reduction in the radio. The theoretical limit on the allowable signal to noise ratio may be specified by the Shannon-Hartley capacity theorem under the assumption of additive white Gaussian noise (AWGN) in the channel. This theorem relates the channels capacity C, the bandwidth, BW, of the channel, and the allowable signal to noise ratio (SNR):

$$C = BW \log_2 (1 + SNR)$$

The Shannon limit states that this capacity is the minimum signal transmission rate at which it is possible with improved coding to achieve arbitrarily small probability of error at reception. It is based on the assumption of an Additive White Gaussian Noise (AWGN) channel and does not indicate an optimal coding scenario, however it does provide an ideal for comparison with the 2.4GHz wireless channel.

The PicoWINS 2.4GHz radios used for propagation measurements provides a sensitivity of –93dBm. This provides, for 100mW transmission, –113dB of loss in the transmission channel. Due to fading in the communication channel, with the frequency hopped spread spectrum system to reduce multi-path, reception was generally achieved out to –85dBm at a maximum range of greater than 15m. In order to analyze the performance of the 2.4GHz radios presently used, thermal noise is first assumed to provide the dominant noise component. In this case assuming room temperature the noise floor at room temperature is:

$$P_N = kT(BW) = -115.1dBm$$

This value assumes a temperature slightly higher than room temperature (T=300 K), and a bandwidth of 750 kHz as specified for each frequency hopped channel in the radios. The radios utilized in the prior PicoWINS measurements have a channel capacity of 460Kbps and a channel

bandwidth of 750kHz (per frequency hop), thus in order to allow the possibility of error free transmission requires a signal to noise ratio of –2.76dB according to the Shannon-Hartley capacity theorem. Between the thermal noise floor of –115.1dBm and the receiver sensitivity there is a 22.1dB difference. Therefore, in conjunction with the minimum SNR this provides a theoretically possible gain (assuming only thermal noise) of 24.86dB through signal coding. This value does not consider other noise sources, such as multi-path or other 2.4GHz radiators, in addition to assuming the noise figure of all the components is zero, and so is a best-case estimate. However it does provide an indication of the possible increase in range at room temperature (24dB corresponds to a range increase of a factor of 8 or a minimum range of 120m) both through improved signal coding-to take advantage of the channel noise statistics, and the use of lower noise components in the radio itself. This analysis assumes that the transmission rate of 460Kbps and the channel bandwidth of 750KHz (per frequency hop) used in the present radios are held constant. Alternatively reducing the radio transmission rate in conjunction with reducing the bandwidth used would provide a reduction in the noise floor and possibly required minimum SNR. The noise factor due to components within the radio will increase the noise floor above the –115.1dBm example considered here. However the SNR values required for reception for the present radios are well above the theoretical minimum of –2.76dB. As a result the largest increase in range appears to be through the use of sufficiently complicated coding scheme that allows a reduction in error probability at reception closer to the –2.76dB SNR limit.

The frequency hopped (FH) radios currently used enable signal reception at longer ranges by sweeping the carrier frequency through the entire 75 channels of the 2.4GHz to 2.485GHz band. Thus even if only a single channel had a noise floor low enough to allow an SNR of –2.76dB, then with the proper signal coding within this FH scheme a transmission rate of 460Kpbs/(75 channels)=6.13Kbps could still be achieved. In other words improvements due to signal coding can be considered independently of the frequency hopping since improved signal coding within each channel will enable a reduction in the SNR down to that which according to the Shannon limit still allows an arbitrary reduction in the bit error rate at reception. Frequency hopping does increase the signal overhead somewhat due, and hence reduce the true channel capacity, however the hand-shaking overhead necessary to implement the frequency scheme does not substantially add to the necessary channel capacity and so will not result in a large change in the above calculations. Improved signal coding within the frequency-hopped scheme (i.e. an improved radio in PicoWINS) allows an increase in the transmission range, by reducing the required SNR within each channel.

**RF MODEM PERFORMANCE EXTENSION WITH RADIOS USED FOR EARLY PROPAGATION MEASUREMENTS**

In order to further explore the possibilities of extending PicoWINS Tag transmission range, the range extensions possible by improving the characteristics of the radios used for testing are explored. The frequency hopped spread spectrum radios tested have a specified sensitivity limit of -93dBm and transmit with a bandwidth of 750kHz per hopping channel at a channel capacity of 460bps. Changing any of these characteristics may improve the radios range.

Improving the sensitivity of the radios will directly impact the range by increasing the

dynamic range allocated to propagation loss. Shown in figure 257 is the predicted range achievable by changing the sensitivity of the radio used with all other characteristics kept constant. In this figure five different measurement environments are considered. In each of these environments the maximum range achieved, and error bounds on that range, are shown as points at the radio sensitivity level of –93dBm. In addition, the measurements in each environment were used to calculate the signal fall off as a power law fit. The five environments in which measurements were conducted are:

First, measurements indoors at our current office building located on the third (top) floor of a business park.. This office space consists of a 4000 square foot facility with cubicle partitions preventing a line of sight between most of the measured points. The maximum range in this case included transmission through interior walls, as well as cubicle partitions. The indoor measurements presented a signal power fall of approximately $R^3$, however in all other cases, due to the both the transmitting and receiving antennas proximity to the ground, approximate $R^4$ propagation loss was seen.

The second case considered consisted of measurements on a flat unobstructed beach a hundred yards above the waterline. In this case each antenna was approximately 10cm above the sand, and so a line of sight path was available between both antennas at all times.

The fourth environment was an empty parking lot in which measurements were made along the asphalt across a seventy-foot gap between a parking structure and our three-story office building. In these measurements both the receiving and transmitting antenna were placed about 10cm above the asphalt.

The fifth environment consisted of measurements made along a hiking trail through dense shrubs and small trees over uneven ground. In these measurements both antennas were within 10cm of the ground and line of site was blocked at most times by either vegetation, the uneven ground, or both. In all cases increased receiver sensitivity provides increased range by reducing the noise threshold, however due to the $R^4$ propagation loss in the four latter cases (and due to the $R^3$ loss in the first case), substantial sensitivity improvements must be made for incremental improvements in range.

**System range versus Receiver Sensitivity**
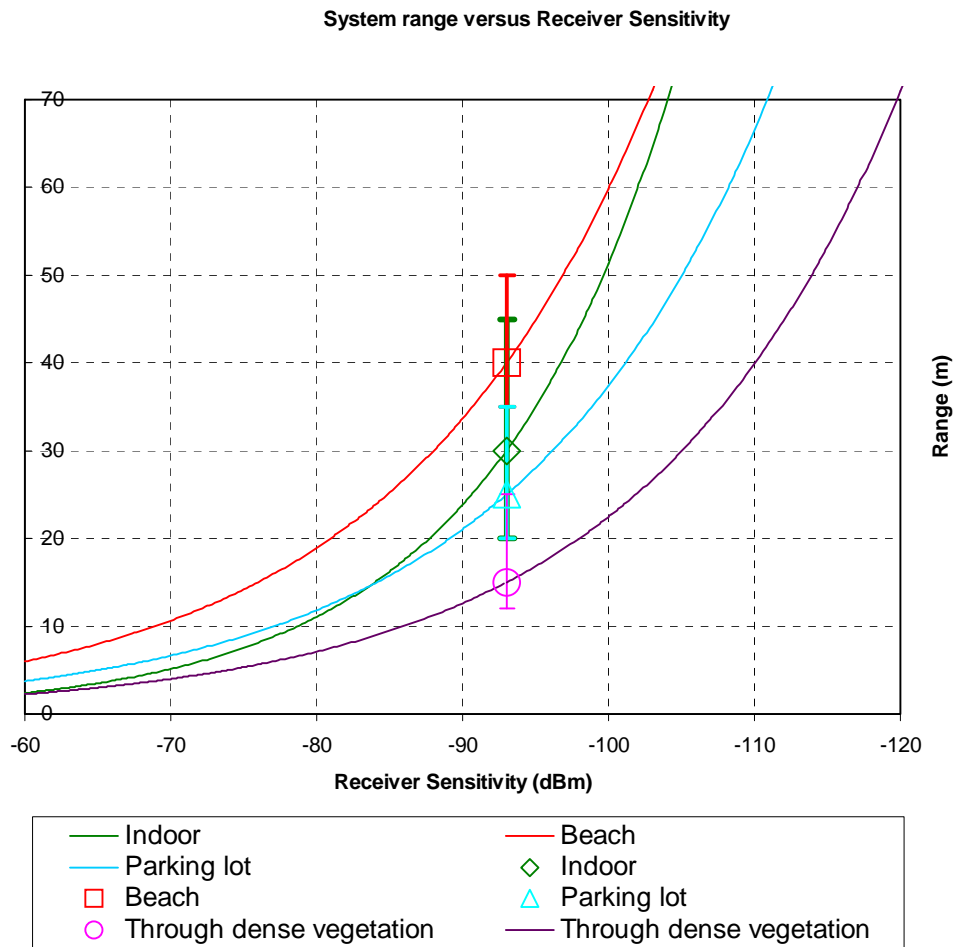


**Figure 257: Range versus receiver sensitivity, normalized to various measurement environments.**

The Shannon-Hartley capacity theorem relates the signal-to-noise ratio dictated by the Shannon limit (at which it is theoretically possible to achieve an arbitrarily small bit error rate through coding) to a channels throughput capacity and available bandwidth. This theorem describes the theoretical optimum case. The radios used for measurements are not near this optimum, as a result using these measured points for normalization of the Shannon-Hartley predictions provides a reasonable description of the trade off between channel capacity, channel bandwidth, and signal to noise ratio (SNR). In order to relate the SNR to the radios range thermal noise is assumed to be the dominant noise contribution. The trade off in range versus bandwidth, and versus channel capacity is then shown in figures 258 and 259, respectively for the five environments considered. In all cases the thermal noise floor was assumed to be at room temperature, and the measured points for the 460kpbs capacity and 750kHz bandwidth FHSS radios are shown on the curves. It is easily seen that the most substantial improvements in range can be accomplished by reducing the channel capacity (or necessary throughput) such as by

increased signal redundancy. For the PicoWINS Tags normal operations this does not provide a severe problem, as most messaging will consist of status codes, or low speed sensor data. Using the measured data points to normalize the range phase space provides a realistic basis, which incorporates the channel characteristics implicitly. For example since the maximum range was not achieved at –93dBm in each case due to the different fading characteristics of each channel (for example the minimum received signal strength was approximately –85dBm in the indoor case), normalizing to the achievable maximum range, but using the radio characteristics as a baseline, allows us to provide predictions for how a radio with improved characteristics (relative to our current radio) will operate in a variety of channels.

**Constant Channel Capacity of 460kbps**
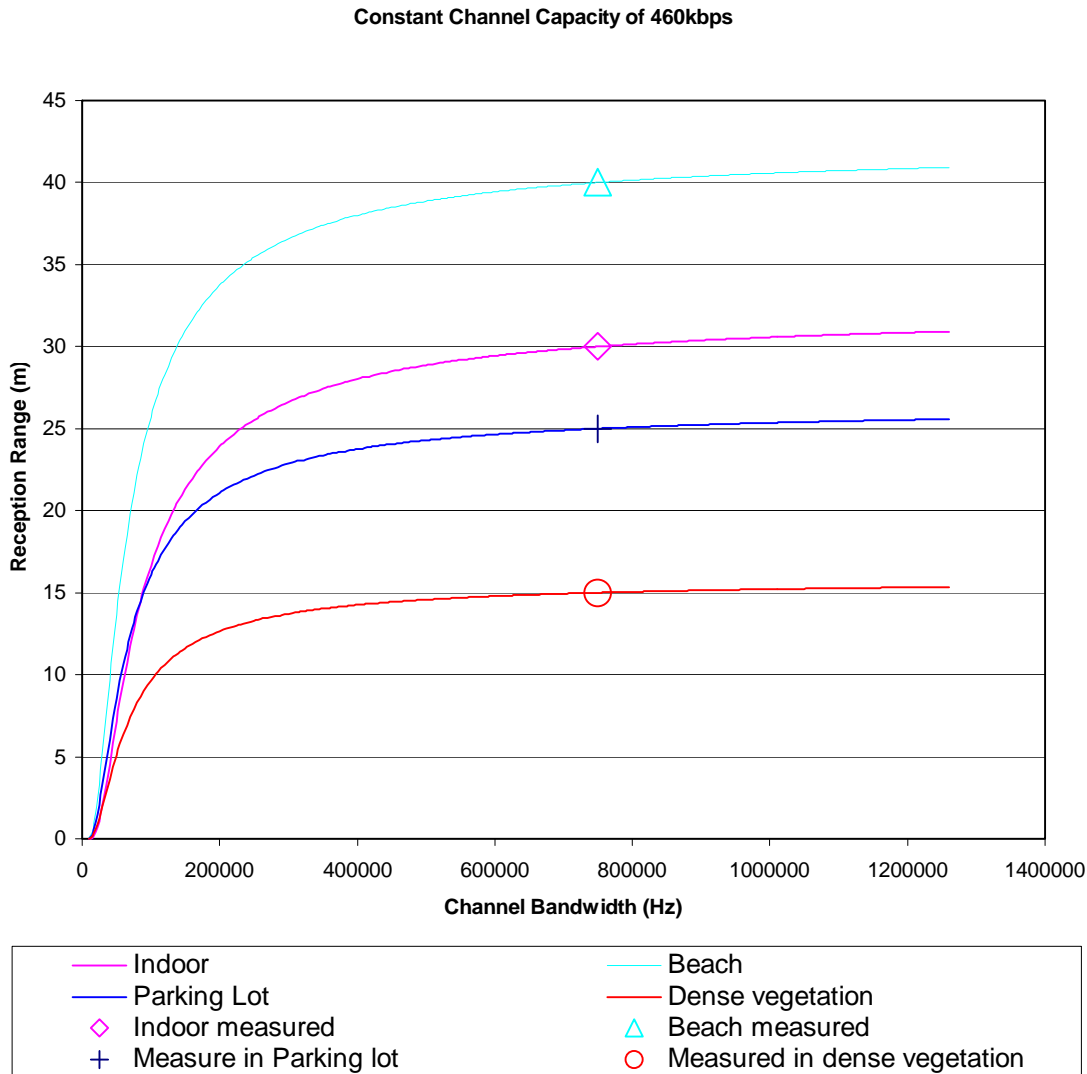


**Figure 258: Radio range versus channel bandwidth according to the Shannon-Hartley theorem with thermal noise the dominant contribution, normalized to a variety of measurements.**

**Constant Channel Bandwidth of 750kHz**
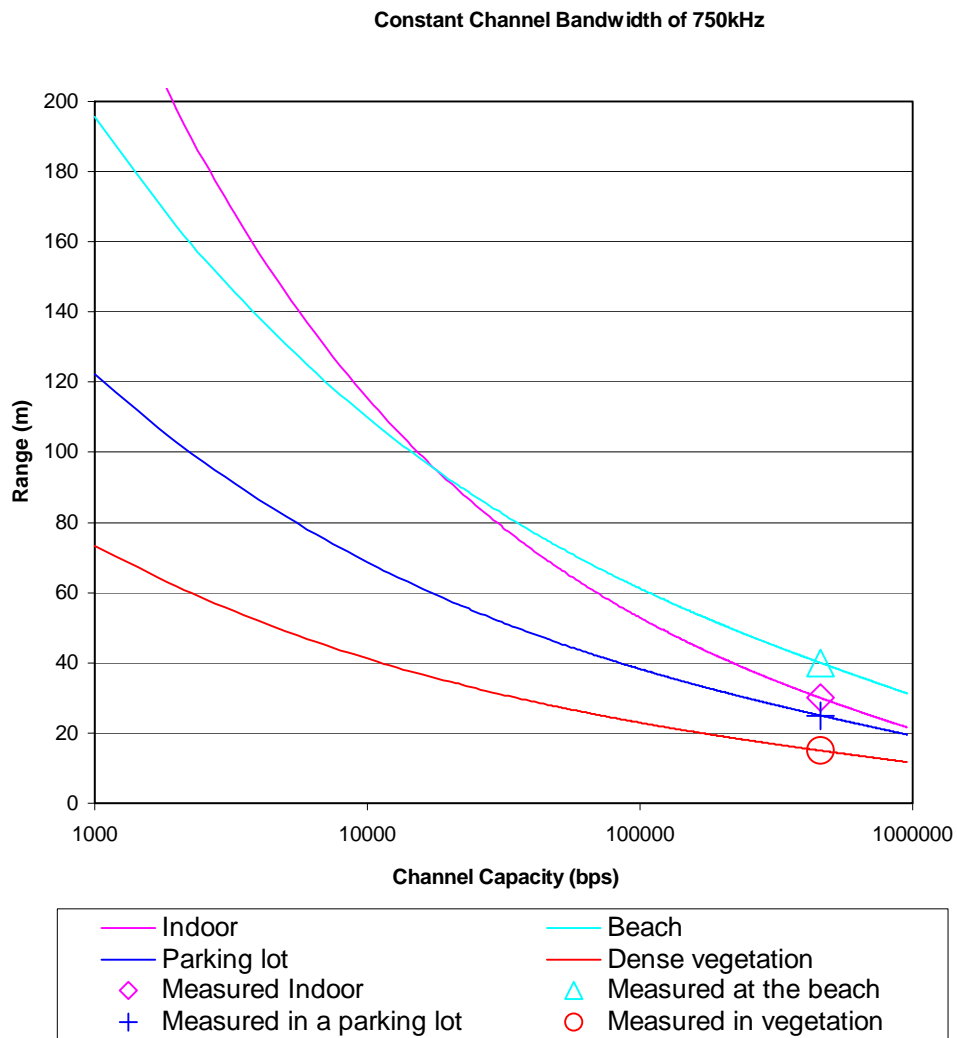


**Figure 259: Radio range versus channel capacity according to the Shannon-Hartley theorem with thermal noise the dominant contribution, normalized to a variety of measurements.**

# SUMMARY OF ANNULAR RING PATCH CHARACTERISTICS

A tag replacement for landmines requires a small compact antenna that is insensitive to the environments in which it is deployed. Due to their strong field confinement patch antennas were considered in order to limit the detuning of the tag antenna by variation in the antenna near field. An investigation of possible patch and non-resonant antenna configurations to provide the minimum size resulted in selection of the printed annular ring patch antenna for investigation. The lowest order transverse magnetic ($TM_{11}$) mode of the annular ring patch antenna provides a small resonant antenna structure. This structure can be further reduced in size with an appropriate matching circuit or by incorporating inductive slots and shorting planes within the antenna. First however an investigation of the unperturbed annular ring $TM_{11}$ mode has been conducted. A few of the key characteristics of this antenna, along with the properties that make it appropriate for placement on a small tag include:

Field concentrated under the ring (E field strongest at edges between ring and ground plane) as shown in the field strength plot of figure 260. Incorporating electronics in the center of the patch should only perturb the antenna's radiation without substantially influencing this dominant mode.

The small resonant size comes at the price of higher input impedance, requiring a transition to 50Ω line, implemented with a small parasitic patch, or designs for a high input impedance antenna. An example matching geometry is discussed further below.

High radiation efficiency associated with resonant antenna elements, as compared with sub-resonant sized antennas.
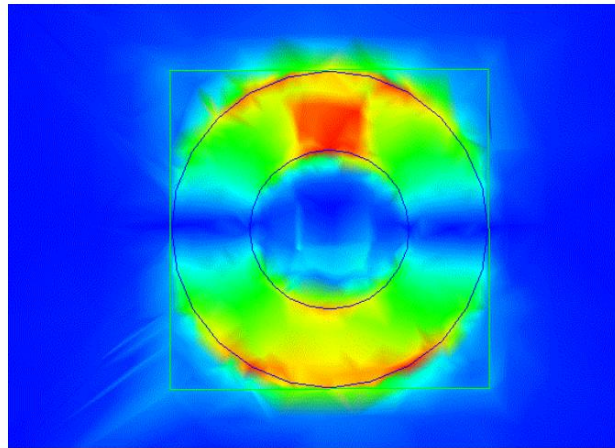


**Figure 260: Field distribution of $TM_{11}$ mode.**

The annular ring is characterized by the antenna inner ring radius a, the outer ring radius b, the substrate thickness d, the substrate permittivity ε, and substrate loss tangent tanδ. A simulated preliminary antenna design operating over the 5.8GHz ISM band on ceramic loaded Teflon, ε=10.2 and tanδ=0.003, consisted of the approximate dimensions of b=3.7mm, a=1.8mm,

and d=0.7mm for a total volume of $0.3cm^3$. General trade offs in the rings $TM_{11}$ resonant size versus these parameters are listed below.

The linear size of the antenna approximately scales with the square root of the dielectric constant. Increasing the dielectric constant reduces size, but also tends to reduce antenna efficiency by increasing dielectric loss.

Reducing the ratio of b/a increases the necessary linear size of the antenna for resonance, although with a gentle slope.

Increasing dielectric thickness increases the antenna efficiency if $\lambda_0/\sqrt{\varepsilon} < 1/8$.

Even moderate changes in geometric parameters require a new optimization of the antenna design with the feeding network, in order to match to a $50\Omega$ input line.

Size reductions well beyond the size of resonant antennas are possible, however these can cause substantial reductions in efficiency. The efficiency is related to antenna loss resistance and radiation resistance. For a small dipole the radiation resistance $R_{rad}$ scales as $(l/\lambda_0)^2$ while for a small loop $R_{rad}$ scales as $(C/\lambda_0)^4$, where the dipole is of length l and the loop is of circumference C. Thus, once the antenna losses surpass radiation, and assuming the antenna loss only slowly varies with frequency, **the antenna efficiency is approximately proportional to at best the antennas linear size over wavelength squared**. Thus a factor of 10-size reduction reduces efficiency by at least 20dB. This is not even considering the difficulty in matching to low input impedance. The reduction in efficiency as $f^2$ is only asymptotically approached once the losses increase, however the required matching circuitry generally limits the use of sub-resonant sized elements. As a result the focus here is on the resonant annular ring patch antenna.

Annular ring patch antennas provide a compact radiating structure in their $TM_{11}$ mode. Annular ring elements have been widely investigated over the last 20 years [19-23,25-27] and due to their compact nature have often been considered as array elements. However, the compact resonant size of the lowest order $TM_{11}$ and $TM_{21}$ modes comes at the price of input impedance larger than the conventional $50\Omega$ coaxial feed. In the past large matching networks and proximity coupled feeds [23,25-27] have been used to reduce the input impedance of small resonant rings.

In our research we have considered input impedance matching to an annular ring by feeding a $50\Omega$ coax line through a short micro-strip line that is proximity coupled to the antenna. Designs were implemented using the HFSS software package. Measured $S_{11}$ results are presented for designs in both the 2.4GHz and 5.8GHz ISM bands. These antennas are designed for a minimum area, and hence in each case a single ring is considered over a truncated square ground plane. These antennas are intended for low profile compact applications appropriate for local wireless networks of interconnected low cost sensors.

An annular ring antenna may be modeled to first order as a resonating circular cavity with perfectly electrically conducting top and bottom and perfectly magnetically conducting

cylindrical walls. The resonance is then dictated by the cylindrical wave equation solutions, and radiation is considered a perturbation of this canonical problem [23]. Numerous analytical, numerical, and experimental solutions for the annular ring patch have been conducted [19-23, 25-27] and will not be repeated here. In all cases the input impedance of the antenna, when fed with a coax was an order of magnitude higher than $50\Omega$ at resonance for the lowest order, $TM_{11}$, mode. In order to create a modular antenna package that may be integrated into a variety of radios for either the 2.4GHz or 5.8GHz ISM bands in order to test system concepts, here a compact proximity coupled feeding network is optimized.

Based on the resonant ring model $TM_{11}$ resonant ring antenna designs for the 2.4GHz and 5.8GHz ISM bands were created on a Rogers 4005 substrate. To compensate for the high input impedance of these antennas when coax fed a transition patch is used to proximity couple to the antenna. This transition may be thought of as a truncated microstrip line, i.e. a truncation of the conventional proximity coupling feed [26,27]. Alternatively, the transition may be considered as a capacitive coupled patch due to its sub-resonant size [25]. The truncated microstrip, as seen in figure 260, leverages planar printed circuit board technology while creating a reduced impedance for the antenna as seen from a coax connector. Considering the transition as proximity coupled microstrip line provides a starting point for numerical optimization based on well-known design equations.

**Numerical Optimization**

To design small low profile ring antennas appropriate for the 2.4GHz and 5.8GHz ISM bands the HFSS finite element software package was used. With HFSS the length (l), width (w), coax feed point (t), microstrip transition offset (c), and ring resonance may all be optimized in a full wave simulation. The ring geometry is shown in figure 261. In this picture the ring is located on the top of a substrate of total thickness $d_1+h+d_2$. The microstrip transition is located $d_1+h$ below the annular ring, which is a distance $d_2$ above a truncated square ground plane of linear size g. Three layers were used to fabricate the antenna on Rogers 4005 circuit board using a commercial PCB prototype manufacturer. Layers $d_1$ and $d_2$ are made up of Rogers 4005 ($\varepsilon=3.38$, tan $\delta=0.002$) and are each 32mils thick while layer h is a 7 mil thick FR4 bonding material ($\varepsilon=4.2$, tan$\delta=0.02$) .

To optimize a single annular ring antenna on a truncated substrate and ground plane to operate within the 2.4-2.4835 GHz ISM band the geometry of figure 261 was utilized with the layer thickness given above and $b/a\approx2$. After a number of HFSS simulations a ring geometry of a=315mils, b=625mils, g=1260mils, w=233mils, l=562mils, c=95mils, t=15mils, x=50mils was selected. These simulations optimized the design for operation within the ISM band when fed with a $50\Omega$ coax line. Within HFSS a $TM_{11}$ field resonance is seen within the patch as shown in the field magnitude along a substrate cross-section 32mils beneath the ring of figure 262. Figure 262 also shows the radiation pattern of the patch antenna above the truncated ground plane according to HFSS. Both plots of figure 262 are at 2.44GHz where HFSS predicted an efficiency of 52% and a directivity of 4.7dB, the end of the antenna's -3dB return loss band.

In the 5.8GHz band the HFSS simulations resulted in a ring geometry of a=130mils, b=267mils, g=560mils, w=143mils, l=310mils, c=100mils, t=185mils, x=0mils. Using a coax line feed within HFSS the 5.8GHz antenna had an efficiency of 51% and a gain of 1.7dB at 5.51GHz, the start of the antenna's -3dB $S_{11}$ bandwidth. The electric field 32mils under the antenna and radiation pattern are shown in figure 263.

**Experimental Comparison with HFSS Designs**

The ring antennas were manufactured for both the 2.4GHz and 5.8GHz ISM bands. To provide the coax input a via connected the transition microstrip to a circular aperture in the ground plane. An SMA connector was then soldered to this aperture. The 2.4GHz and 5.8GHz band antennas with SMA connectors are shown in figure 261.

One-port $S_{11}$ measurements of these antennas were made using an HP 8510 network analyzer. A comparison of return loss measurements with HFSS simulation for the 2.4GHz antenna of the previous section is shown in figure 264. A simulation error in the resonance location of 2.2% is observed, although the 50MHz bandwidth and resonance depth are consistent. A similar shift down of 4% in the bandwidth location was observed in the 5.8GHz antenna with less consistency in the resonance depth predictions. The difference in the simulated and measured results may be attributed to manufacturing tolerances however the consistently low predictions seem to indicate a systematic error, for example in the permittivity values used, due to assumption of infinitesimally thin perfect conducting elements in HFSS, or due to parasitics in the SMA connectors used for measurements. To compensate for these shifts slightly smaller annular rings were measured, and the return loss is shown in figures 265 and 266 for the 2.4GHz and 5.8GHz antennas respectively. Shown in figure 265 are measurements of two prototypes of the same antenna. The measurements show the variability introduced from soldering the SMA connectors to the via and ground plane. The antenna of figure 265 has the properties b=595mils, a=305mils, g=1260mils, w=233mils, l=562mils, c=95mils, t=15mils, x=50mils. The antenna of figure 266 has the properties b=255mils, a=125mils, g=580mils, w=143mils, l=310mils, c=100mils, t=185mils, x=0mils. The 5.8GHz antenna of figure 266 demonstrates a wide 540MHz -3dB bandwidth as a result of the electrically large substrate thickness ($0.065\lambda_0$) and interaction with the capacitive transition element to create a resonance with a positive antenna input reactance slope, (resulting in a reduced slope at resonance).

**Antenna Design Conclusions**

Designs for coax fed compact ring antennas operating in the lowest order $TM_{11}$ mode were demonstrated using a truncated microstrip transition. These designs demonstrate a size order for resonant antennas, however substantial reductions of at least a factor of two are further possible using increased dielectric constant substrates and inductive slots and grounding posts to reduce size. Simulated and experimental results for the designed antennas were shown demonstrating the size and depth of the resonance. HFSS modeled the antennas qualitatively, but the resonance location was off in all cases by at least a few percent. A 2.4GHz antenna was shown encompassing half the commercial ISM band, while the 5.8GHz antenna provided a larger than needed bandwidth. These antennas demonstrated the use of a combined coax to proximity coupled, or capacitive coupled microstrip element in order to use the compact nature of the $TM_{11}$ annular ring resonance with a conventional 50Ω coaxial feed line. In order to be used for tactical tags, the size of the antennas must be further reduced. Options for this include using shorting

posts to cut the size of the antenna in half; this would require an additional optimization of the antenna feed. Further size reduction on the order of 30% can also be achieved using inductive slots on the edges of the annular ring, in addition to increasing the dielectric constant reducing both size and environmental antenna decoupling, but also reducing the antenna radiation efficiency. This investigation provides an idea of the size of resonant antennas; the antenna input impedance, as well as some sample designs appropriate for a first implementation of a tactical tag.
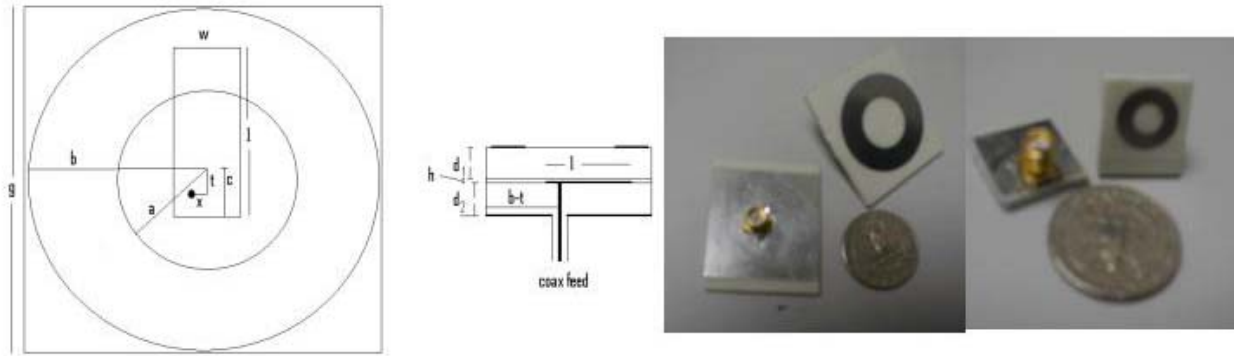


**Figure 261: Ring and proximity transition geometry and fabricated 2.4GHz and 5.8GHz samples.**
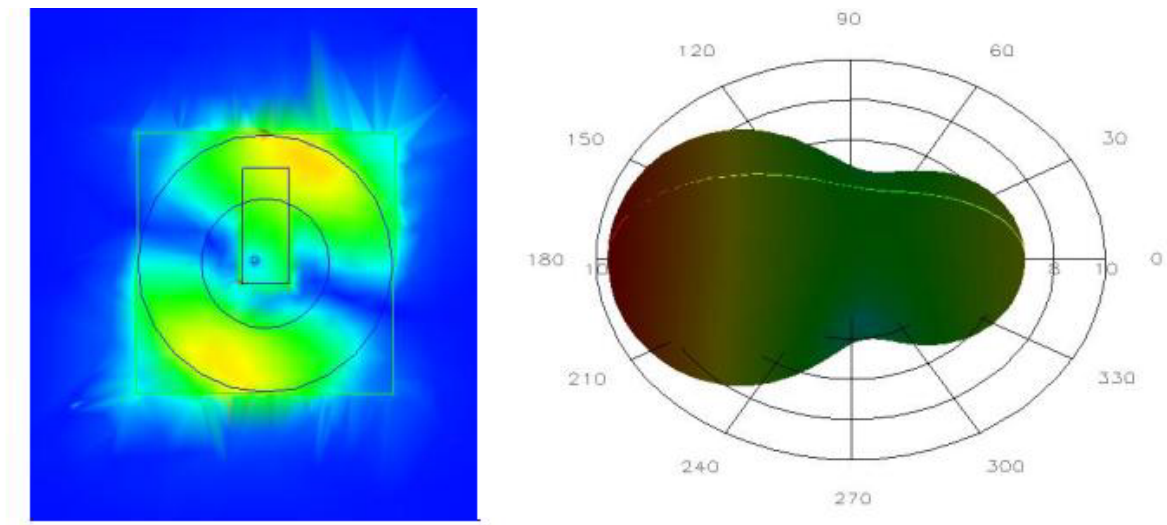


**Figure 262: 2.4GHz electric field magnitude and far field pattern predicted with HFSS.**
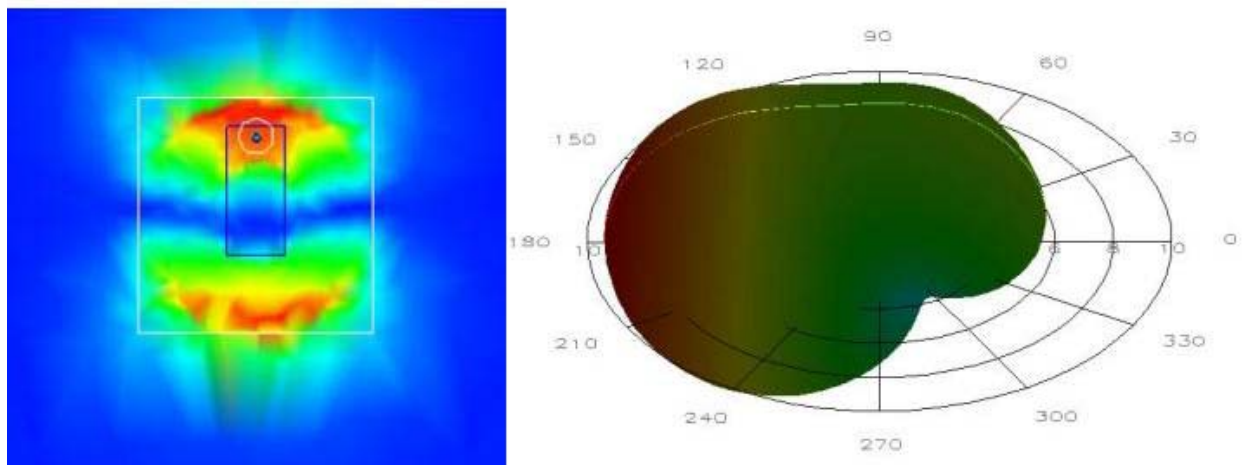
**Figure 263: 5.8GHz electric field magnitude and far field pattern predicted with HFSS.**
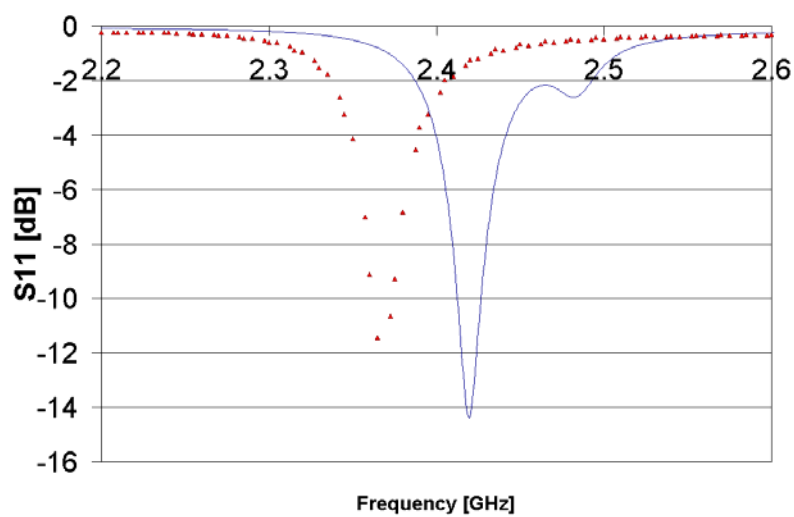


**Figure 264: HFSS optimized antenna, measured and simulated results.**
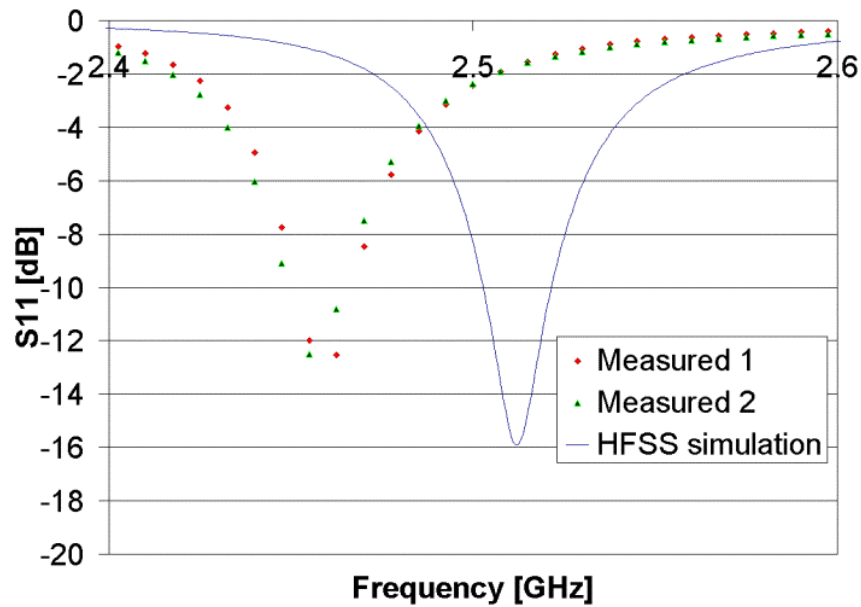
**Figure 265: Perturbed 2.4GHz antenna.**
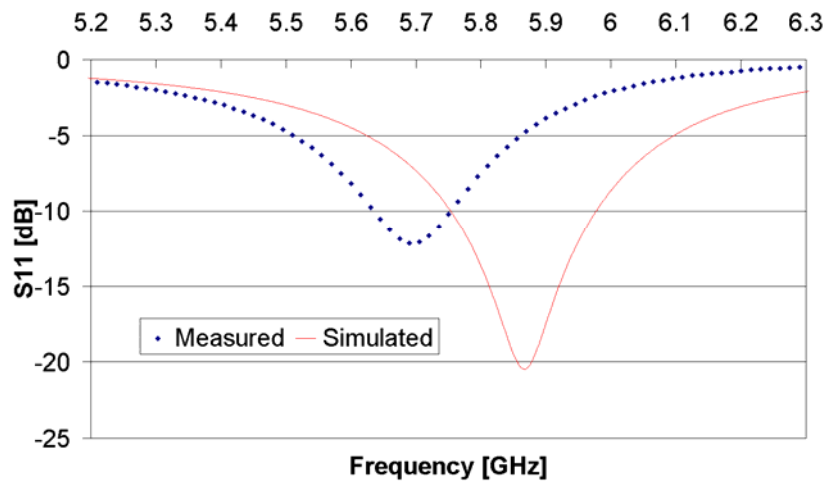


**Figure 266: Perturbed 5.8GHz antenna.**

# PICOWINS CONCLUSIONS

This report presents a summary of the work done by Sensoria Corporation in both analyzing the fundamental limits on tactical tag design, and in designing prototype PicoWINS systems. Focus was given to hardware demonstration, exploring ranging options to locate the tags, to quantifying the propagation environment seen by tags, and to optimizing a tags antenna and communication within the constraints of a surface-to-surface, low-power wireless link. Substantial modeling and measurement of propagation in a variety of environments was

discussed. Particular focus was given to the 900MHz, 2.4GHz and 5.8GHz ISM bands as they provide a high bandwidth, worldwide available wireless link, and cover a wide swath of frequencies. The substantial influence of the ground at propagation paths near ground grazing incidence was demonstrated. In addition the validity of modeling propagation in semi-uncluttered environments using a simple ray-optics approach was demonstrated. For more cluttered environments empirical power law fits were shown to be appropriate with in all cases measured worst-case fourth power attenuation. The requirements of a small environmentally insensitive antenna were also discussed as appropriate for the wireless links considered. A general analysis indicated the appropriateness of using a resonant annular ring patch antenna, and preliminary designs for both the 2.4GHz and 5.8GHz ISM bands were developed and experimentally tested.

Within the propagation study component of the PicoWINS contract Short-range wireless propagation near the ground was considered experimentally in the three ISM frequency bands, 902-928MHz, 2.4-2.4835GHz, and 5725-2875GHz. Results were provided for the fading in each frequency band for vertical-to-vertical (VV) polarization, for horizontal-to-vertical (HV) polarization, and for horizontal-to-horizontal (HH) polarization. In addition propagation fall off as a function of distance and antenna height was explored for all three polarizations in each frequency band. In general the presence of a few "clumps" of scatterers in short-range measurements appeared to significantly influence the fading variability seen within the ISM band, over that seen in environments with widely distributed, or no scatterers. In addition large numbers of scatterers tended to provide substantial quick variation over the frequency band, rather than a smoother variation with frequency expected with only a few dominant coherent contributions to the signal. Scatterers tended to have a more substantial impact on the path loss than the ground surface roughness, both in looking empirically at undulating environments, and in modeling random roughness on a limited scale, the fluctuation tended to be with ±3-5dB or so, compared with fluctuations up to 25dB due to dense scatterers. The signal path loss observed appeared to follow a two-ray LOS and ground bounce model at short distances (within 10-20m in most environments) with slight decreases in the predicted path loss compared with those predictions at moderate ranges out to a hundred meters, as additional scattered rays from higher elevated scatterers improved received signal performance. In addition limited indications of a path loss drop off in highly cluttered environments at distances beyond 100m was observed. Also while the signal strength as a function of antenna height correlated well with the two-ray model for open environments at the lower frequencies, decreased accuracy was seen as the number of scatterers increased and as the frequency increased. In addition a significant reduction in the increased path loss of lower antenna heights was observed as the density of scatterers in each environment increased. Overall the short-range wireless near ground propagation in open to semi-cluttered areas appears to be modeled reasonably well with a simple two ray model, with anomalies observed as the number of scatterers is increased, both in fading, range and height dependence. These anomalies tended to decrease the path loss at distances of less than 100m. In general the two ray model appears to provide a lower bound in open environments on system performance with scattering at short ranges (less than a few hundred meters) often improving the signal strength, particularly for systems operating at capacities of less than a few Mbps where the short dispersion spread does not degrade the signal reception substantially.

# REFERENCES

1. Arnold Sommerfeld, Partial Differential Equations in Physics, Academic Press, New York, 1949, pp. 236-289.

2. K. A. Norton, "The Calculation of Ground-Wave Field Intensity over a Finitely Conducting Spherical Earth", Proceedings of the I.R.E, December 1941, pp. 23-39.

3. James R. Wait, "The Ancient and Modern History of EM Ground-Wave Propagation", IEEE Antennas and Propagation Magazine, Vol. 40, No. 5, Oct. 1998, pp. 7-24.

4. S. R. Saunders, Antennas and Propagation for Wireless Communication Systems, John Wiley & Sons, New York, 1999, pp. 85-321.

5. H. Masui, K. Takahashi, S. Takahashi, K. Kage, and T. Kobayashi, "Difference of Path-Loss Characteristics due to Mobile Antenna Heights in Microwave Urban Propagation", IEICE Trans. Fundamentals, Vol. E82-A, No. 7, July1999, pp. 1144-1150.

6. N. Patwari, G. D. Durgin, T. S. Rappaport, and R. J. Boyle, "Peer-to-Peer low antenna outdoor radio wave propagation at 1.8GHz", IEEE 49th Vehicular Technology Conference, Houston TX, May, 1999.

7. K. Sohrabi, B. Manriquez, and G. J. Pottie, "Near Ground Wideband Measurement in 800-1000MHz", IEEE 49th Vehicular Technology Conference, Houston TX, May, 1999.

8. C. A. Balanis, "Antenna Theory Analysis and Design", Second Edition, John Wiley & Sons, Inc., New York, pp. 86-87, 1997.

9. G. J. Gaskin and J. D. Miller, "Measurement of Soil Water Content Using a Simplified Impedance Measuring Technique", *J. Agric. Engng. Res.*, Vol. 63, 1996, pp. 153-160.

10. F. L. Teixeira, W. C. Chew, M. Straka, M. L. Oristaglio, and T. Wang, "Finite-Difference Time-Domain Simulation of Ground Penetrating Radar on Dispersive, Inhomogeneous, and Conductive Soils", *IEEE Trans. Geo. and Rem. Sens.*, vol 36, no. 6, Nov. 1998, pp. 1928-1937.

11. R..E. Diaz, W. M. Merrill, and N. G. Alexopoulos, " Analytic Framework for the modeling of Effective Media", *Journal of Applied Physics*, vol. 84, no. 12, Dec. 15, 1998, pp. 6815-6826.

12. ThetaProbe Soil Moisture Sensor Type ML2x Users Manual ML2x-UM-1.21

13. J. E. Hipp, "Soil Electromagnetic Parameters as Functions of Frequency, Soil Density, and Soil Moisture", *Proceedings of the IEEE*, vol. 62, no. 1, Jan. 1974, pp. 98-103.

14.  K. Pokkuluri, *Effect of Admixtures, Chlorides, and Moisture on Dielectric Prperties of Portland Cement Concrete in the Low Microwave Frequency Range,* Master's Thesis, Virginia Polytechnic Institute and State University, 1998.

15. G. D. Durgin, V. Kukshya, and T. S. Rappaport, "Joint Angle and Delay Spread Statistics for 1920 MHz Peer-to-Peer Wireless Channels", 2001 *IEEE AP-S International Symposium,* Boston, MA, July 8-13, 2001.

16. James R. Wait, Electromagnetic Waves in Stratified Media, Pergamon Press, New York, 1970, pp.35-45.

17. Weng Cho Chew, Waves and Fields in Inhomogeneous Media, Van Nostrand Reinhold, New York, 1990, pp. 71-101.

18. Jan T. Hvid, Jorgen Bach Andersen, Jorn, Toftgard, and Jprgen Bojer, "Terrain-Based Propagation Model for Rural Area - An Integral Equation Approach", IEEE Transactions on Antennas and Propagation, Vol. 43, No. 1, January 1995, pp. 41-46.

19.  S. M. Ali, W. C. Chew, and J. A. Kong, "Vector Hankel Transform Analysis of Annular-Ring Microstrip Antenna", *IEEE Trans. on Ant. and Prop.* Vol. AP-30, No. 4, July 1982, pp. 637-644.

20.  W. C. Chew, "A Broad-Band Annular-Ring Microstrip Antenna", *IEEE Trans. on Ant. and Prop.*  Vol. AP-30, No. 5, September 1982, pp. 918-922.

21. J. S. Dahele and K. F. Lee, "Characteristics of Annular-Ring Microstrip Antenna", *Electronics Letters,* Vol. 18, No. 24, Nov. 25, 1982, pp. 1051-1052.

22. A. K. Bhattacharyya and R. Garg, "Input Impedance of Annular Ring Microstrip Antenna Using Circuit Theory Approach", *IEEE Trans. AP* Vol. AP-33, No. 4, April 1985, pp. 369-374.

23. K. F. Lee and J. S. Dahele, "Handbook of Microstrip Antennas," Edited by J. R. James and P. S. Hall, Chapter 3, Peters Peregrinus Ltd., London, 1989.

24. G. A. E. Vandenbosch and A. R.  Van de Capelle, **"**Study of the Capacitively Fed Microstrip Antenna Element", *IEEE Trans. AP,* Vol. 42, No. 12, Dec. 1994, pp. 1648-1652.

25. M. J. Tsai and N. G. Alexopoulos, "Electromagnetically coupled microstrip ring-type antennas of arbitrary shape", *IEEE AP-S Int. Symp.* Vol. 1, pp. 684-687, Newport Beach, CA, June 1995.

26.  R. R. Ramirez and N. G. Alexopoulos, "Single Feed Circularly Polarized Microstrip Ring Antenna and Arrays," *IEEE AP-S Int. Symp.* Vol. 3, pp 1364-67, Atlanta, GA, June 1998.

27. D. M. Kokotoff, J. T. Aberle, and R.B. Waterhouse, "Rigorous Analysis of Probe-Fed Printed Annular Ring Antennas", *IEEE Trans. AP* Vol. 47, No. 2, Feb. 1999, pp. 384